N68-18656

Surveyor Spacecraft System

SURVEYOR I FLIGHT PERFORMANCE

FINAL REPORT

Volume III of III

JPL Contract 950056 / October 1966

SSD 68223R

J.D. CLOUD
Manager
System Engineering and Analysis Laboratory

K.C. BEALL
Director
Surveyor I Post Flight Evaluation

R.H. LEUSCHNER
Head
Post Flight Analysis Section

HUGHES

HUGHES AIRCRAFT COMPANY
SPACE SYSTEMS DIVISION

CONTENTS

ILLUSTRATIONS

TABLES

5.7 VERNIER ENGINE SUBSYSTEM

5.7.1 INTRODUCTION

5.7.1.1 System Description

The Surveyor vernier propulsion system (VPS) is a bipropellant, variable thrust, liquid rocket system utilizing an oxidizer composed of 90 percent nitrogen tetroxide and 10 percent nitric oxide (Mon 10) and a fuel composed of 72 percent monomethyl hydrazine and 28 percent water (Figure 5.7-1). The VPS consists of three regeneratively cooled thrust chambers (TCAs) with radiation cooled expansion cones. Each TCA has a variable thrust range from 30 to 104 pounds vacuum thrust.

Propellant is supplied to the TCAs from six tanks employing positive expulsion bladders. One fuel tank and one oxidizer tank supply each TCA and are located adjacent to the TCA near each of the three spacecraft landing legs.

Propellant expulsion is accomplished by pressurizing the propellant tanks on the gas side of the bladders with helium gas. The helium is stored under high pressure in a spherical pressure vessel. The helium tank, together with the pressure regulator, dual check and relief valves, and servicing connections, is mounted outboard of the spaceframe between landing legs 2 and 3.

Thermal control of the VPS is both active and passive. Electric heaters are installed on two oxidizer tanks, one fuel tank, and on all propellant feedlines to the TCAs. Passive thermal control consists of the application of black and white paint and vapor-deposited aluminum to selected portions of the VPS together with super insulation applied to the propellant tanks. The feedlines are wrapped with aluminum foil to deter heat loss.

5.7.1.2 System Purpose

The VPS has three main functions during a Surveyor lunar landing mission:

1) Midcourse velocity correction and attitude control

2) Attitude control during retro phase
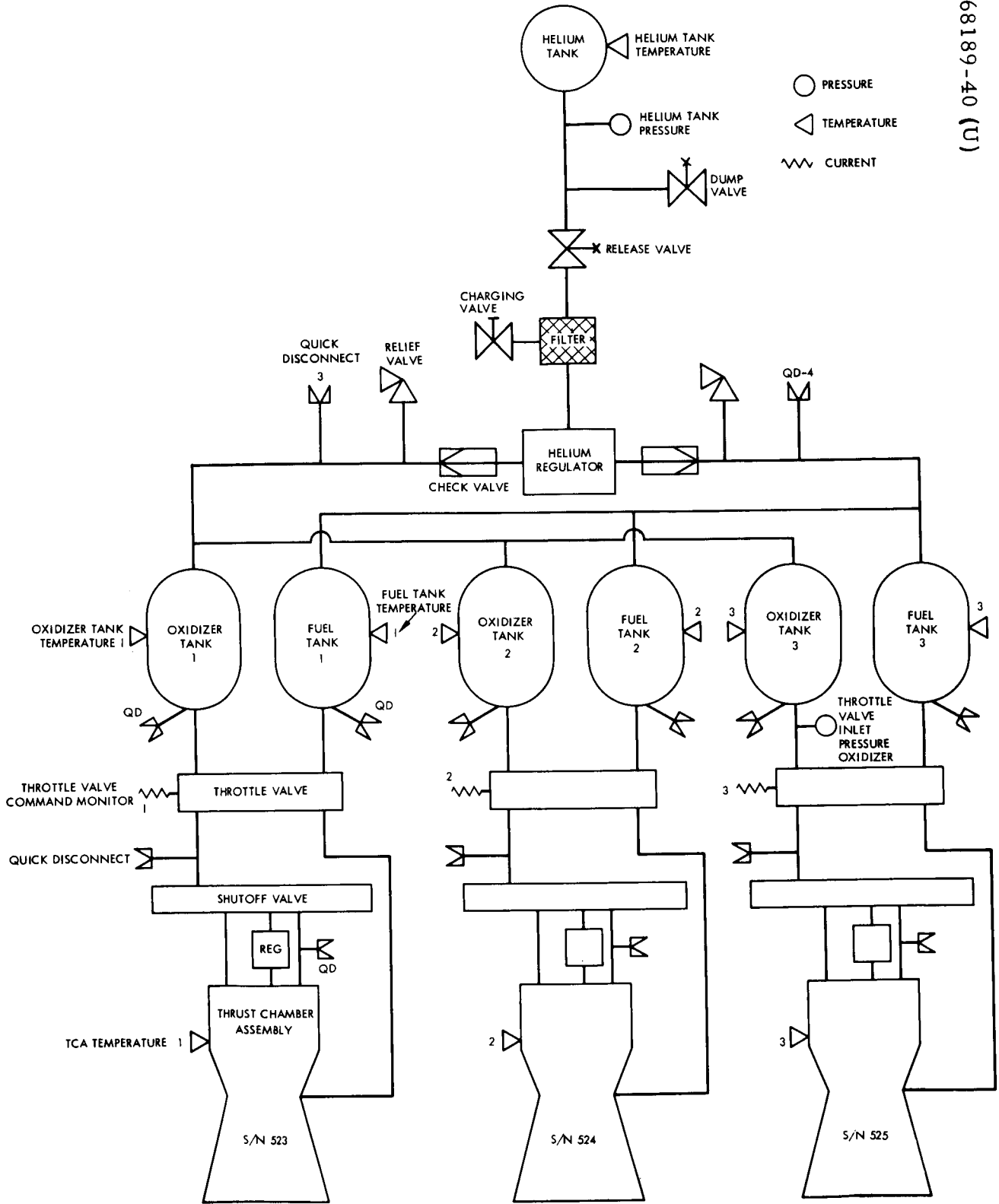
Figure 5.7-1.   Vernier Propulsion System Schematic

3) Attitude control and velocity correction during the final descent maneuver

The midcourse velocity correction may be required to correct initial launching and injection errors. The Surveyor VPS has the capability of providing velocity corrections up to 50 m/sec with sufficient propellant remaining to successfully land the spacecraft on the moon. The required correction is transmitted to the spacecraft in the form of a desired burn time at constant acceleration of 0.1 g which results in a thrust level of approximately 70 pounds for each of the three VPS TCAs. In addition to providing the required velocity change, the VPS also provides spacecraft attitude control during the maneuver.

Attitude control during firing of the spacecraft retro motor is provided by the VPS. The VPS is ignited approximately 1.1 seconds prior to retro ignition. Attitude control by the VPS is biased around a total vernier thrust level of either 150 or 195 pounds, depending on predictions of spacecraft attitude and velocity at retro burnout. The desired vernier thrust level is transmitted to the spacecraft several minutes prior to initiation of the retro maneuver sequence. Following retro burnout, the vernier thrust level is increased to 267 pounds total thrust to further slow the spacecraft to allow the ejected retro motor case to fall clear.

Following retro motor ejection, the VPS is throttled to approximately 110 pounds total thrust under radar control. When the spacecraft intersects the first "descent segment," the VPS, operating in the closed-loop mode with the radar system, "acquires" the predetermined altitude-velocity profile and keeps the spacecraft on the profile. Each succeeding segment of the profile is acquired in a similar manner. At an altitude of 13 feet, the VPS is shut down and the spacecraft free falls to the lunar surface.

5.7.1.3 General Performance Summary

The vernier engine system performed in an essentially nominal manner, meeting or exceeding all of its transit and landing requirements. There were no anomalies or unexpected failures in any part of the vernier engines, fuel storage and distribution, or fuel pressurization equipment.

5.7.2 MAJOR VERNIER SYSTEM EVENTS

Table 5.7-1 lists the time of occurrence of the major events concerning or influencing the vernier engine system.

5.7.3 SUMMARY OF RESULTS

A summary of the vernier engine system performance parameters as determined from postflight analysis is given in Table 5.7-2 along with the predicted values.

TABLE 5.7-1. SC-1 PROPULSION EVENTS

Event	GMT	Mission Time, hr:min:sec	Command
Pressurize VPS	151:06:19:09	L + 15:38:8	0607
M/C ignition	151:06:45:04	L + 16:4:03	0721
M/C shutdown	151:06:45:24.75	L + 16:4:23.75	
T/D ignition	153:06:14:47.6	L + 63:43:46.6	
T/D shutdown	153:06:17:34.2	L + 63:46:33.2	
Helium dump	153:06:26:31	T/D + 00:08:57	0610

5.7.4 ANOMALY DESCRIPTION

There were no anomalies evident throughout the vernier engine system during its designed transit and landing life. However after 105 hours of postlanding lunar operations, the oxidizer pressure relief valve vented (for the ninth time) and failed to properly reseat. This occurred at a relief valve temperature estimated to be approximately 200°F or higher which is considerably above the upper specified temperature for the valve. Thus this is not considered to be a hardware failure and is predicted from preflight vernier pressurization system qualification tests. This anomaly is discussed in detail in subsection 5.7.6.1.

5.7.5 CONCLUSIONS AND RECOMMENDATIONS

5.7.5.1 Conclusions

The Surveyor vernier propulsion system successfully met all requirements of the SC-1 transit mission and survived almost 2 lunar days and a night while being subjected to a thermal environment that exceeded specification requirements for almost every component.

Some of the specific conclusions that can be reached as a result of the successful SC-1 mission are as follows:

1) The performance of the vernier propulsion system was well within specification limits through all phases of Mission A as expected.

2) The propellant loading procedures utilized at ETR for SC-1 are satisfactory both from the standpoint of propellant weight distribution between tanks and that no discernable gas was left inside

TABLE 5.7-2. MISSION PARAMETERS – PREDICTED AND ACTUAL

	Predicted	Actual
Squib release helium ΔP	178 psia	188 psia
Midcourse helium consumption	375 psia	383 psia
Touchdown helium consumption	2221 psia	2122 psia
VPS midcourse thrust	219.5 pounds	219.5 pounds
Midcourse startup impulse dispersion		
Leg 1	-0.613 lb-sec[*]	-0.08 lb-sec[**]
Leg 2	-0.013 lb-sec[*]	-0.232 lb-sec[**]
Leg 3	+0.627 lb-sec[*]	+0.312 lb-sec[**]
Midcourse shutdown impulse dispersion		
Leg 1	-0.20 lb-sec[*]	+0.27 lb-sec
Leg 2	-0.22 lb-sec[*]	-0.37 lb-sec
Leg 3	+0.42 lb-sec[*]	+0.10 lb-sec
VPS retro phase thrust	194 pounds	197 pounds[***]
VPS retro eject thrust	282 pounds	285 pounds[***]
Touchdown startup impulse dispersion		
Leg 1	-0.613 lb-sec[*]	-0.02 lb-sec[**]
Leg 2	-0.013 lb-sec[*]	+0.22 lb-sec[**]
Leg 3	+0.627 lb-sec[*]	-0.20 lb-sec[**]
Touchdown shutdown impulse dispersion		
Leg 1	-0.20 lb-sec[*]	+0.19 lb-sec[**]
Leg 2	-0.22 lb-sec[*]	-0.26 lb-sec[**]
Leg 3	+0.42 lb-sec[*]	+0.07 lb-sec[**]
Midcourse propellant used	16.8 pounds[‡]	16.50 pounds
Terminal descent propellant used	120.5 pounds[‡]	122.5 pounds

[*]From TCA FAT data.

[**]See Section 5.6.

[***]Reference 4.

[‡]See Section 5.15.

the propellant bladders as a result of loading. The latter conclusion is arrived at by the absence of uncommanded thrust transients from the SC-1 flight data.

3) The helium supply is adequate to expel all usable propellant as was expected. See "Expulsion of SC-1 Landed Propellant."

4) High pressure helium system leakage is below the telemetry system sensing accuracy as was expected (see subsections 5.7.6.3 and 5.7.6.4).

5) Dissolved helium coming out of solution and causing uncommanded thrust transients was, as expected, not evident on SC-1.

6) Strain gages presently installed on the TCA mounting brackets performed their primary function of positively indicating vernier ignition and shut down, but, as expected, they are not suitable for quantitative thrust analysis (see subsection 5.7.7.6).

5.7.6 SUBSYSTEM PERFORMANCE ANALYSIS

5.7.6.1 Mission Oriented Performance Description

Prelaunch

Final propulsion preparations for the SC-1 launch were begun on 14 May 1966 when propellant loading of the vernier subsystem was initiated. A total of 183.96 pounds was loaded, of which 73.92 pounds of fuel and 107.92 pounds of oxidizer are usable (Reference 1). Preloading calculations of the SC-1 propellant capacity (see subsection 5.7.6.2) indicate a total load of 183.98 pounds of which 108.04 pounds of oxidizer and 73.80 pounds of fuel are usable. The slight differences noted are well within the specified loading tolerance from Reference 1.

The helium tank was charged on 24 May 1966 to a pressure of 5225 psig at 72° F. Telemetry readings of the tank temperature and pressure were taken on 26, 27, 28, and 30 May (see Table 5.7-3). Based on these telemetry checks, an "on pad" leak rate of 346 standard cc/hr was calculated (see subsection 5.7.6.3). This is equivalent to 6.8 psi/day as compared with 5.2 psi/day measured during joint flight acceptance composite test (J-FACT) at ETR. It should be pointed out that the verified accuracy of the helium tank pressure transducer is ±133 psi (Reference 2) and that the pressure differences noted in Table 5.7-3 are well below the verified transducer accuracy. Accordingly, the difference between J-FACT and on-pad leakage is not significant.

Thermal conditioning of the spacecraft prior to launch was maintained at 75° F. Two hours prior to launch, the shroud temperature was increased to 85° F. Table 5.7-4 compares the predicted propulsion temperatures with

TABLE 5.7-3. SC-1 TELEMETRY CHECK PROPULSION DATA

(Propulsion Data from ETR)

Date	Time, GMT	P1, Helium Pressure, psig	P2, Manifold Pressure, psig	P17, Helium Tank Temperature Sensor, °F	Mode
5/26	0239		261.7		2
	0259	5186			2
	0433			73.04	4
	0459	5174	260.7		2
	1321	5279	269.8		6
	1355	5285			5
5/27	2116			74.8	5
	2144	5262			5
	2147			82.72	5
	2152		261.7		5
5/28	2320	5578			6
5/30	0602	5148	254.6		2
	0640			72.16	4
	1342			88.01	5
	1348	5303			6
	1354		264.7		5

the actual stabilized values just prior to increasing the shroud temperature to 85° F. All temperatures were within the shroud temperature tolerance and all propulsion parameters appeared normal at liftoff.

Coast 1 (L + 30 Minutes to L + 14 Hours 30 Minutes

The initial postinjection spacecraft interrogation indicated that all propulsion parameters were normal. Indication of heater operation on the leg 2 propellant line was noted at L + 1 hour 17 minutes. Heater operation was between 21 and 26° F. The leg 3 propellant line heater started operation between 21 and 27° F at L + 1 hour 59 minutes. The leg 1 propellant line heater appeared to actuate once at L + 9 hours 11 minutes and then stabilized at 23° F.

Helium pressure decreased from 5191 psia at 72° F at L - 2 hours 20 minutes to 5103 psia at 58° F at L + 15 hours 05 minutes (Figure 5.7-2). Leakage calculations (see subsection 5.7.6.4) during this period indicated a negative leak rate, confirming the fact that the helium leak rates encountered on the SC-1 flight were below the accuracy level of the instrumentation. Additionally, the helium tank temperature measurement is not truly representative of the bulk gas temperature except under stabilized conditions.

TABLE 5.7-4. ACTUAL VERSUS PREDICTED TEMPERATUES

Temperature Sensor	Prelaunch		Midcourse		Terminal Descent	
	Actual, degrees	Predicted, degrees	Actual, degrees	Predicted, degrees	Actual, degrees	Predicted, degrees
P4, leg 2 line	73.8	75	24.9	20-27	21.4	20-27
P5, leg 2 fuel tank	73	75	49	64	35.4	37
P6, leg 3 oxygen tank	72.2	75	51.2	67	39.9	46
P7, leg 1 TCA	69.1	75	57.7	76	59.4	76
P8, leg 1 line	74.5	75	31.0	35	23.9	35
P9, leg 3 line	74.0	75	23.9	30	23.9	30
P10, leg 2 TCA	72.4	75	73.2	82	72.4	82
P11, leg 3 TCA	72.7	75	58.6	72	59.5	72
P13, leg 1 fuel tank	71.5	75	56.5	67	51.3	52
P14, leg 3 fuel tank	72.1	75	58.0	67	52.7	51
P15, leg 1 oxygen tank	71.9	75	58.8	67	41.4	51
P16, leg 2 oxygen tank	71.4	75	42.4	63	24.0	30
P17, helium tank	73.4	75	58.4	75	60.2	75
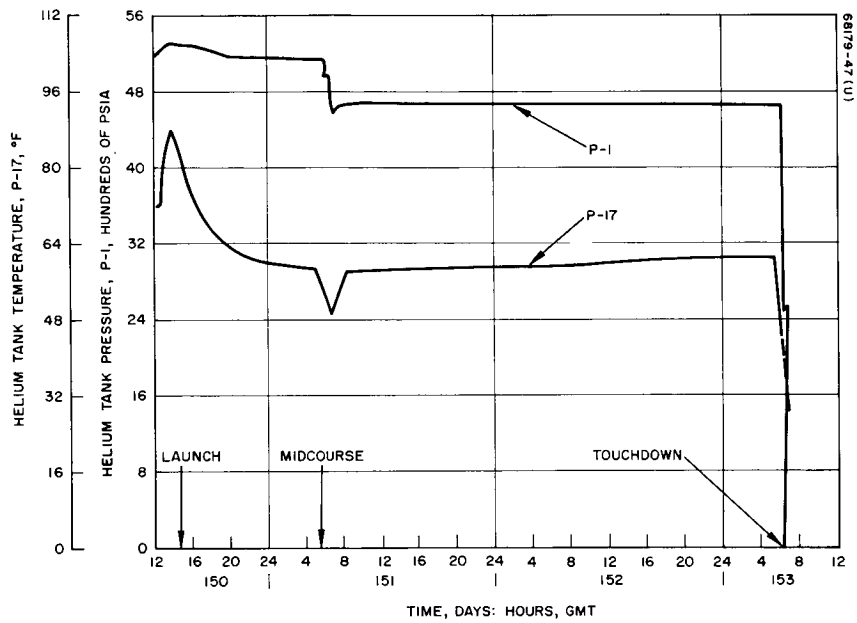
Figure 5.7-2.   SC-1 Helium Tank Pressure
and Temperature Flight History

Helium pressure at vernier ignition was 4850 psia (mode 1); helium pressure at cutoff was 4467 psia. Actual pressure drop was 383 psi. Computed pressure drop based on a polytropic exponent of 1.45 was 375 psi (see "Predicted Midcourse Helium Consumption" and Table 5.7-4).

Propellant consumption during midcourse was computed by the Systems Analysis Group (see Section 5.14) to be 16.50 pounds (see Table 5.7-4). This agrees well with the preignition prediction of 16.8 pounds.

Interrogation of the spacecraft following the midcourse correction indicated that the propellant tank and feedline temperatures had risen. This presumably is due to temperature gradients existing in the propellant tanks. Propellant from the middle of the tank is 10 to 15 degrees warmer than the propellant at the bottom of the tank in contact with the temperature sensor. When propellant is utilized during firing, warmer propellant comes in contact with the tank and propellant line sensors, increasing their temperature. Peak temperatures noted on the TCAs after shutdown were 322, 281, and 252° F on the leg 1, 2, and 3 TCAs, respectively. It should be noted that cool-down times were slightly longer than predicted and, consequently, the constraint on TCA refiring has been changed to a minimum of 1 hour between firings with the second firing delayed until all three TCAs are at a temperature of no more than 165° F.

Coast II (L + 17 Hours to L + 62 Hours)

Following the midcourse firing and reacquisition of sun and star, the propulsion system temperatures began following the predicted temperature profiles, although in some cases with shifts owing to the temperature changes described in the previous section. Gyro drift checks conducted during the period perturbated the leg 2 TCA temperature as in the Coast I period. The propellant tank heaters on oxidizer tanks 1 and 2 and fuel tank 2 were enabled at L + 46 hours as per the standard operating sequence.

After the midcourse correction, the regulator locked up at a corrected value of 772 ± 18.5 psia and maintained this value until initiation of terminal descent.

The helium tank pressure remained constant at the value established following midcourse stabilization from about L + 21 hours to L + 50 hours. This indicates that leakage of the propellant system was slight and, furthermore, that not much additional helium went into the propellant as a result of the increased system pressure subsequent to the squib release. From L + 50 hours to L + 56 hours, the helium tank pressure dropped 18 psi and then stabilized until the initiation of the terminal descent sequence. The helium tank pressure transducer manufacturer quotes 0.35 percent of full scale or 21 psi for a 6000 psi range, the minimum resolution attainable on this transducer. It should be noted that the indicated 18 psi drop was within this band.

The oxidizer system pressure as indicated by the leg 3 oxidizer transducer dropped from 256 psia at L - 2 hours 20 minutes to 245 psia prior to squib release at L + 15 hours 38 minutes (Figure 5.7-3). Concurrent with the 11 psi pressure drop, the average oxidizer tank temperature dropped from 75 to 50° F, causing both a decrease in tank ullage temperature and an increase of tank ullage volume owing to propellant density increase.

Deviations from the nominal spacecraft attitude with respect to the sun during gyro drift measurements resulted in temperature changes of as much as 18° F on the leg 2 TCA. The attitude deviations altered the shadow patterns on the TCA, causing the temperature changes.

Midcourse Operations (L + 14 Hours 30 Minutes to L + 17 Hours)

Propulsion system condition just prior to the midcourse correction was nominal. All temperatures were within the predictability range of the thermal analysis (see Table 5.7-4). The maximum deviations of approximately 20° F were noted on the helium tank temperature sensor and the leg 1 TCA temperature sensor. It should be noted that both parameters were well within their operating range.

The helium release squib was actuated at L + 15 hours 38 minutes 8 seconds, and the propellant tank pressure increased from 245 psia to 779 psia immediately and remained at 779 psia until just prior to midcourse ignition at which time the value was 780 psia. Corrections to this figure indicate a lockup pressure of 765 ± 18.5 psi (see subsection 5.7.6.6). This compares favorably with 762 to 777 psia during regulator flight acceptance test (FAT).

Ignition of all three engines was smooth and well controlled. Thrust control during the midcourse correction was 219.5 pounds, corresponding to a spacecraft acceleration of 0.1005 g (see Section 5.6 and Table 5.7-2).

Startup impulse dispersions are shown in Table 5.7-2. A maximum variation of 0.544 lb-sec is indicated. This is well below the specification requirement of Reference 3. It is also concluded that all three TCAs were producing controlled thrust at 0.150 second.

Peak gyro angles at shutdown were less than 2 degrees, and the shutdown impulse dispersions shown in Table 5.7-2 are also well within the requirements of Reference 3.
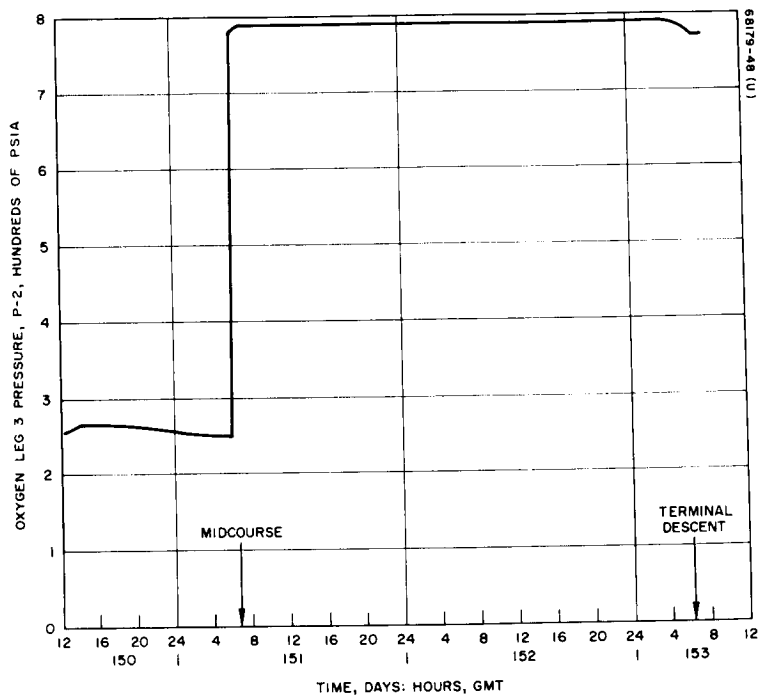
Figure 5. 7-3. Oxygen Pressure During Flight

Terminal Descent (L + 62 Hours to L + 63 Hours

Prior to retro ignition, all propulsion temperatures were normal. Maximum deviation from the predicted nominal was -15° F for the helium tank sensor and the leg 1 TCA sensor.

Vernier ignition was indicated at 06:14:47 GMT and appeared smooth. Shortly after retro ignition, the leg 1 TCA throttled to a higher thrust level and then returned to the commanded level. The leg 2 and 3 TCAs throttled down and returned to the commanded thrust level. Possibly omnidirectional antenna A was extended at this time, causing a momentary attitude transient and a small center of gravity shift.

Startup impulse dispersions at vernier ignition are shown in Table 5.7-2. A maximum variation of 0.24 lb-sec is indicated. This is well below the specification requirement of Reference 3. Shutdown impulse variations are also indicated in Table 5.7-2. The maximum variation is 0.45 lb-sec, well within specification.

Steady-state thrust during retro burning was approximately 197 pounds as compared with the 194 pounds required. The retro eject thrust level was approximately 285 pounds as compared with the 282 required.

Thrust levels varied between 30 and 90 pounds during RADVS-controlled descent. Vernier cutoff was signaled by the 13-foot mark, and the spacecraft touched down on the lunar surface at 153:06:17:35.6 GMT.

Propellant consumption, from terminal descent trajectory considerations (see Section 5.15), was computed to be 122.55 pounds for the entire descent phase. The spacecraft landed with 42.79 pounds of usable propellant.

Helium consumption during the terminal descent phase was 2122 psi as shown in Table 5.7-2. The predicted consumption based on a polytropic exponent of 1.22 was 2221 psi (see "Predicted Touchdown Helium Consumption"). There is some uncertainty in the touchdown helium pressure as the signal was not available until 2 minutes after touchdown, and some heating occurred with a resulting pressure increase. It is thought any differences would be less than 50 psi (see Figure 5.7-4).

A calculation of helium required to expel the landed propellant indicated that the minimum regulator inlet pressure with 100 percent usable propellant expelled was 1518 psia. This was above the regulator requirement of 900 psia minimum (see Reference 5).

Lunar Period Touchdown —(End of First Lunar Day)

The spacecraft touched down at 153:06:17:35 GMT. Approximately 9 minutes after touchdown, dumping of the high pressure helium was initiated with dumping from an initial pressure of 2500 psia to 0 taking about 3 minutes.
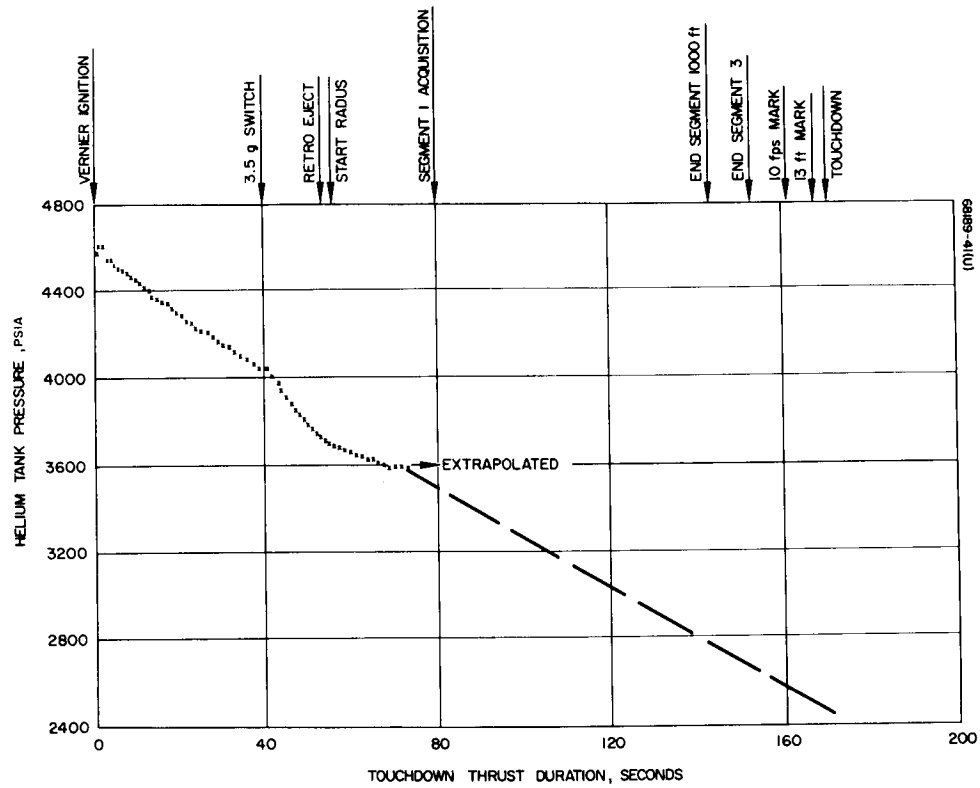
Figure 5.7-4. Helium Tank Pressure
During Terminal Descent

The spacecraft attitude with respect to the sun was such that leg 1 pointed directly away from the sun at an angle of 29 degrees above the horizon. In this attitude, the leg 1 propellant tanks and TCA were shaded with the leg 2 and 3 propellant tanks, lines, TCAs, and the helium tank illuminated. As the sun rose and set, this situation was reversed. The propulsion thermal history for the first 100 hours is shown in Figure 5.7-5 and is discussed in Table 5.7-5.

At touchdown the oxidizer manifold pressure indicated 770 psia. Approximately 22 hours after touchdown, the oxidizer pressure had risen to 832 psia. At this same time, the oxidizer relief valve vented, and the pressure decreased over a 3-hour period to 817 psia. Over the next 78 hours, to T/D + 105 hours, the oxidizer relief valve appeared to cycle nine times. On the ninth cycle, the valve relieved at 865 psia and failed to reseat. Over a period of 8 hours, the oxidizer system pressure dropped to 130 psia (see Figure 5.7-6). Concurrent with the pressure drop in the oxidizer system was a 20 to 25° F drop in temperature for all three oxidizer tanks. As the pressure in the oxidizer system decreased, the bladder in each tank slowly expanded to completely fill the tank. Decreasing the pressure on the oxidizer remaining in the tank caused some of it to flash into vapor, thus cooling the tank.

The oxidizer relief valve opened at pressures from 825 to 865 psia and reseated between 817 and 825 psia. The FAT records for this relief valve indicate a crack of 827 psig and a reseat of 810 psig. Helium tank temperature, as indicated by the thermal sensor located in the lower, shaded hemisphere of the tank, reached 140° F. It is anticipated that the temperature of the relief valves, located on the top of the tank in the sun and isolated from the mass of the tank shell through a threaded connection, was many degrees hotter than the sensor indicated.

Following venting of the oxidizer relief valve, the oxidizer system pressure stabilized at 130 psia. The computed vapor pressure of the leg 3 oxidizer tank was 110 psia, which agrees very well, demonstrating that the bladder remained intact and that all subsequent readings of the oxidizer system pressure were indicative of propellant vapor pressure in the No. 3 oxidizer tank (Figure 5.7-7).

During the second lunar day, oxidizer tank pressure still corresponded to the vapor pressure, which is evidence that the relief valve reseated at the lower pressure in the system. If the valve had not reseated, oxidizer would have permeated through the bladder and vented through the unseated relief valve until the tank was emptied; the tanks would then register zero pressure.

On 6 June 1966, the feasibility of firing the vernier propulsion system to aid in determining lunar soil bearing strength was investigated. At this time, the leg 1, 2, and 3 TCAs were at temperatures of 204, 221, and 208° F, respectively. The propellant lines were at temperatures between 150 and 189° F. From this data, it was evident that all three TCAs and lines were filled with oxidizer vapor because the oxidizer vapor pressure exceeded the
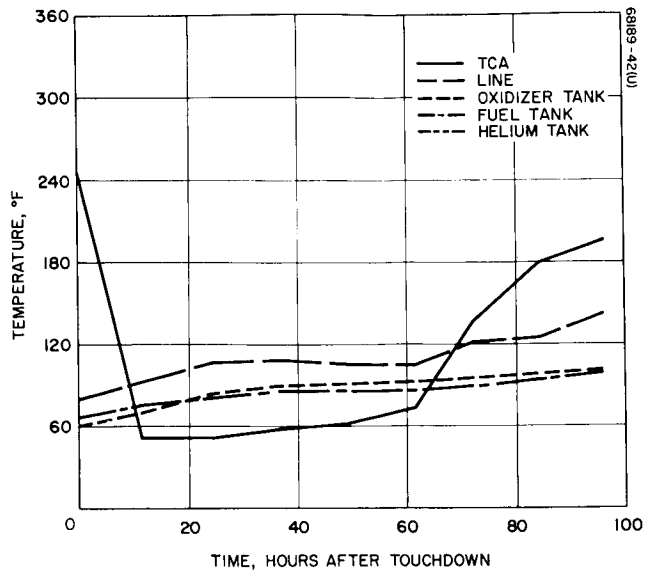
a) Leg 1
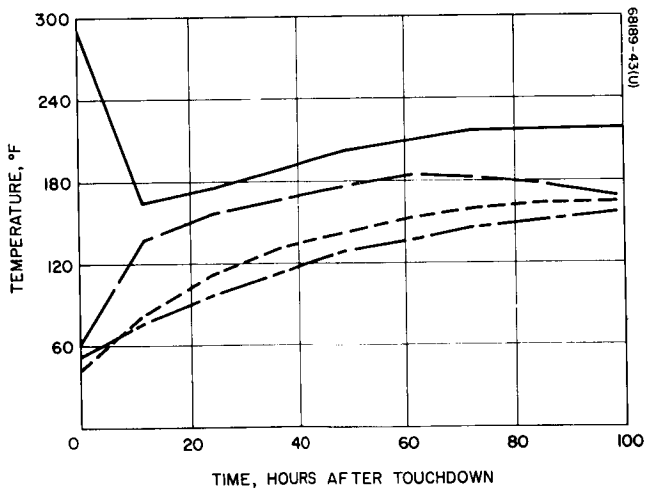
b) Leg 2
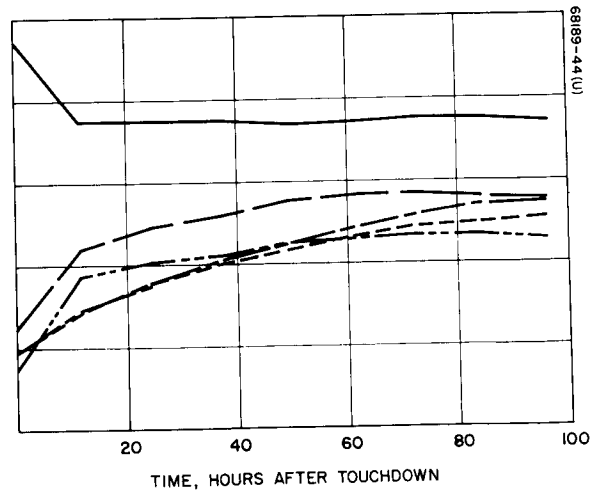
c) Leg 3

Figure 5.7-5. SC-1 Post-touchdown Temperatures

TABLE 5.7-5.   VERNIER PROPULSION SYSTEM MAXIMUM
TEMPERATURE DURING FIRST LUNAR DAY

	Touchdown Temperature, °F	Maximum Temperature, °F
TCAs		
1	383 ⎫	245
2	355 ⎬ Postshutdown temperatures	228
3	314 ⎭	224
Lines		
1	79.5	221
2	62.2	201
3	75.8	185
Fuel tanks		
1	66.2	190
2	51.8	164
3	67.7	171
Oxidizer tanks		
1	59.7	174
2	43.2	166
3	57.3	154
Helium tank	44.3	140

system pressure and only below-specification thrust levels could be obtained.
A requirement for ignition was that sufficient fuel pressure, 325 or more,
must be available to actuate the TCA propellant valves. There are no pres-
sure sensors on the fuel side of the system, and pressure there could only be
inferred by the fact that the fuel tanks had not undergone any temperature
drops such as were indicated on the oxidizer side of the system when the
oxidizer relief valve vented. It was decided not to attempt to fire the vernier
system at that time owing to the risk of depositing dust on the spacecraft
thermal finishes.

An attempt was made to fire the vernier system on the second lunar
day but, because of an electrical interlock failure, power could not be applied
to the TCA shutoff valve solenoids. The attempt was consequently terminated.
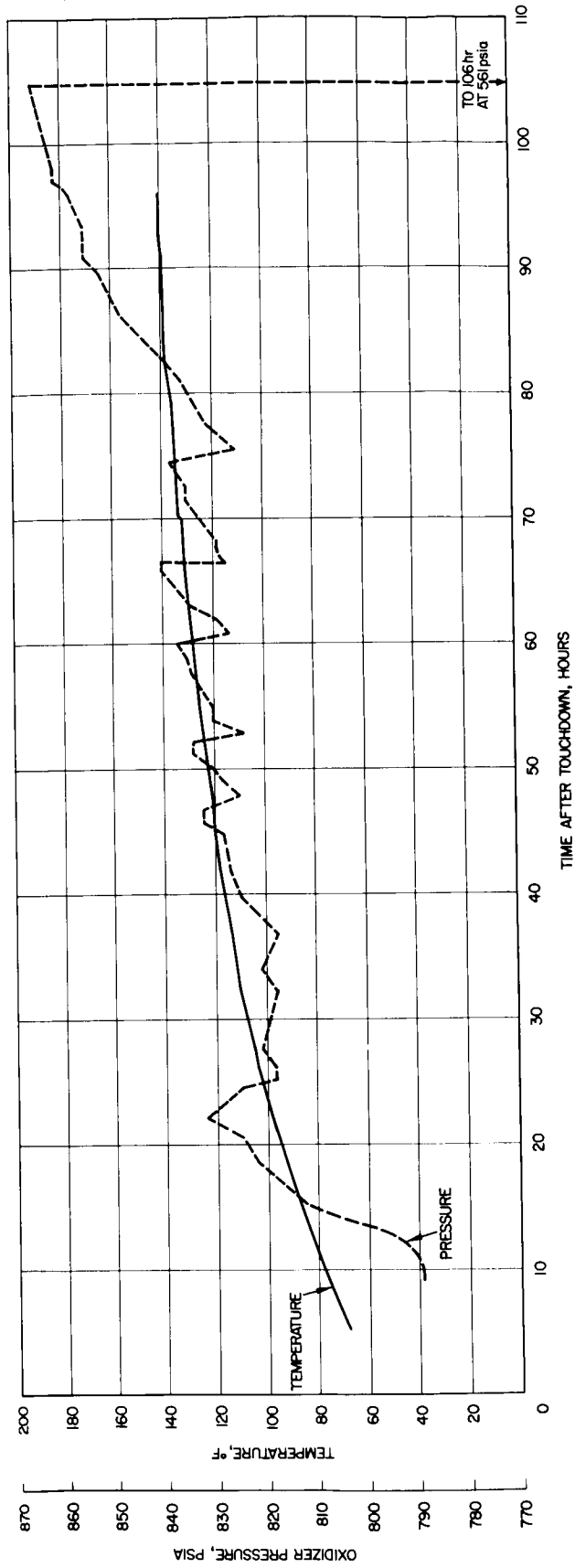
Figure 5.7-6. Average Oxidizer Tank Temperature and
Leg 3 Oxidizer Pressure Versus Time
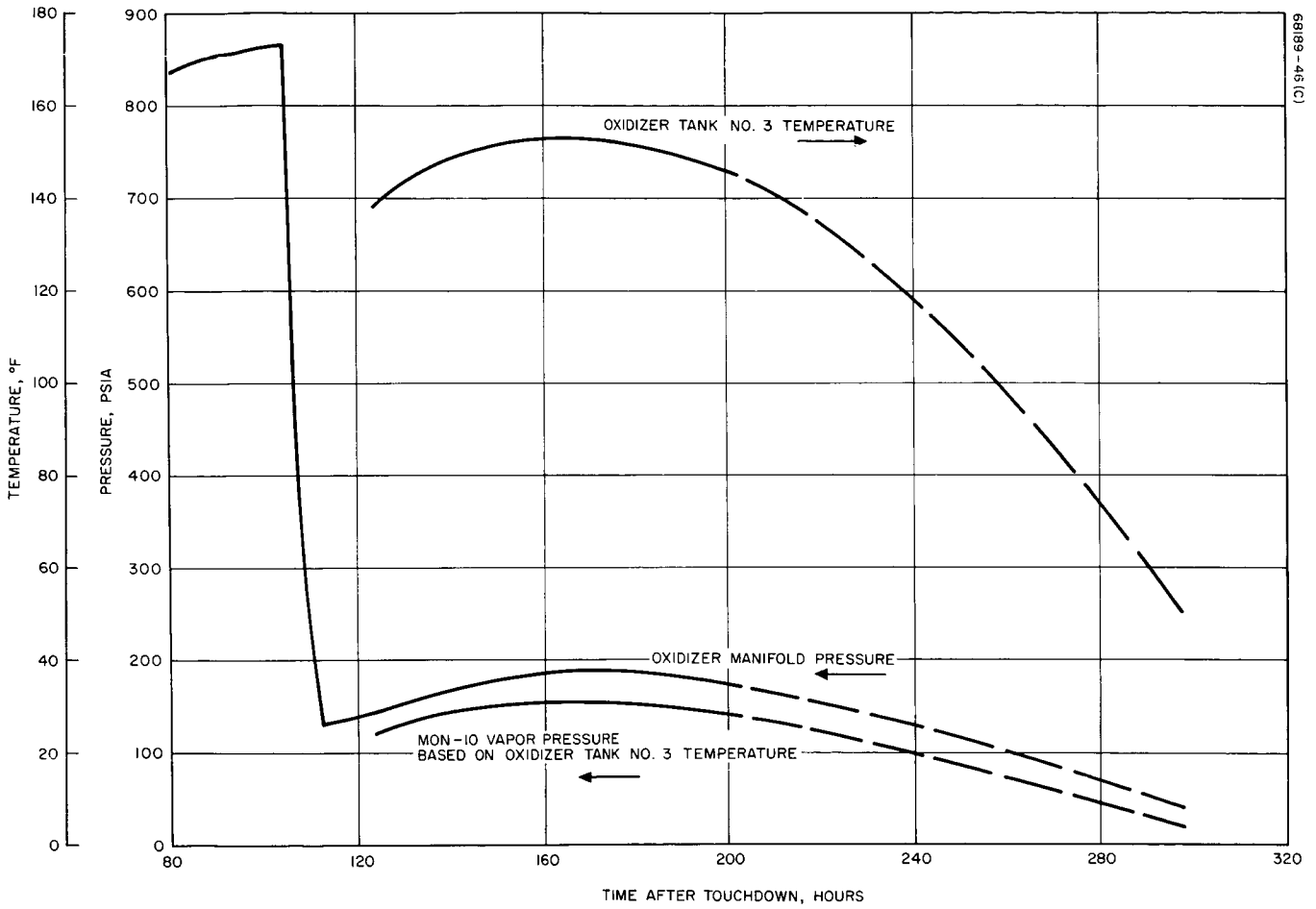
Figure 5.7-7. Leg 3 Oxidizer Pressure and Oxidizer Tank
Temperature and Indicated Vapor Pressure
Versus Time — Lunar Period

All indications are that the vernier propulsion system satisfactorily survived two lunar days and one lunar night under conditions exceeding specification limits for almost the entire system.

5.7.6.2 Propellant Loading Calculations

Predicted SC-1 Propellant Loads

Oxidizer System.

SC-1 oxidizer system total volume (using smallest tank)

$$= V_{tot} = 2225.1 \text{ in}^3 \text{ (References 6 and 7)}$$

Unusable volume trapped in lines and TCAs

$$= V_{TR} = 12.6 \text{ in}^3 \text{ (Reference 8)}$$

Unusable volume due to bladder inefficiency

$$= V_e = 11.1 \text{ in}^3 \text{ (Reference 8)}$$

Loading tolerance = 0.75 pound

$$V_{usable} = V_{tot} - V_{TR} - V_e$$

For worst-case conditions, the weight of unusable propellant is calculated at 0°F, the minimum expected temperature. Loading is based on zero ullage at 105°F, the maximum expected temperature. A -3 σ loading tolerance is also included.

$$W_{usable} = V_{tot}(\rho_{105°F}) - V_{TR}(\rho_{0°F}) - V_e(\rho_{0°F}) - 0.75$$

$$= (2225.1)(0.04947) - 12.6(0.05437) - 11.1(0.05437) - 0.75$$

$$= 108.037 \text{ pounds}$$

Fuel System.

SC-1 fuel system total volume

$$= V_{tot} = 2229.0 \text{ in}^3 \text{ (References 6 and 7)}$$

Unusable volume trapped in lines and TCAs

$$= V_{TR} = 12.9 \text{ in}^3 \text{ (Reference 8)}$$

Unusable volume due to bladder inefficiency

$$= V_e = 11.1 \text{ in}^3 \text{ (Reference 8).}$$

$$V_{usable} = V_{tot} - V_{TR} - V_e$$

Using the same assumptions for the fuel system as for the oxidizer system,

$$W_{usable} = V_{tot}(\rho_{105°F}) - V_{TR}(\rho_{0°F}) - V_e(\rho_{0°F}) - 0.75$$

$$= (2229.0)(0.03383) - 12.9(0.03586) - V_e(0.03586) - 0.75$$

$$= 73.796 \text{ pounds}$$

For a comparison of predicted versus actual SC-1 loading, see Table 5.7-6.

5.7.6.3   Helium Leakage on Pad

Using mode 2 data from SC-1 telemetry checks (Table 5.7-3),

$$PV = WZRT$$

where

$\quad$ P = helium tank pressure, psia

$\quad$ T = helium tank temperature, °R

$\quad$ V = helium tank volume, in^3

$\quad$ Z = helium compressibility factor

$\quad$ R = helium gas constraint

$$\ell nP + \ell nV = \ell nW + \ell nZ + \ell nR + \ell nT$$

Differentiating and rearranging, dV, dZ, and dR = 0

$$\frac{dW}{W} = \frac{dP}{P} - \frac{dT}{T}$$

TABLE 5.7-6. ACTUAL VERSUS PREDICTED SC-1 PROPELLANT LOADING

	SC-1 Predicted at 105°F		SC-1 Predicted at 70°F		SC-1 Act at 70°F	
	Oxidizer	Fuel	Oxidizer	Fuel	Oxidizer	Fuel
Total loaded gross, pounds	110.076	75.407	113.680	76.901	115.95	76.13
3 σ loading tolerance, pounds	0.75	0.75	0.75	0.75	0.75	0.75
Offload, pounds	0	0	3.604	1.494	6.01	0.610
Total loaded net, pounds	109.326	74.657	109.326	74.657	109.19	74.77
Unusable − 0°F, pounds	1.289	0.861	1.289	0.861	1.28	0.84
Total usable, pounds	108.037	73.796	108.037	73.796	107.92	73.92

Dividing by t, time

$$\frac{dW}{dt} = \frac{W}{P}\frac{dP}{dt} - \frac{W}{T}\frac{dT}{dt}$$

GMT 146:02:59 P_1 = 5186 psia

GMT 150:06:02 P_2 = 5148 psia

GMT 146:04:33 T_1 = 533°R

GMT 150:06:40 T_2 = 532°R

P_{aug} = 5162

T_{aug} = 532.5

Z = 1.166 (Reference 9), V_{HB} = 1300 in^3 based on expansion data of burst tanks

$$W_{av} = \frac{PV}{ZRT} = \frac{(5162)(1300)}{(1.166)(386.2)(532.5)(12)} = 2.332 \text{ pounds}$$

$$\frac{dP}{dt} = \frac{(5148 - 5186)}{99} = -0.3838 \text{ psi/hr}$$

$$\frac{dT}{dt} = \frac{532 - 533}{98} = -0.0102°\text{R/hr}$$

$$\frac{dW}{dt} = \frac{2.332(-0.3838)}{5162} - \frac{2.332(-0.0102)}{532.5} = -0.000173 + 0.00004424$$

$$\frac{dW}{dt} = -0.0001287 \text{ lb/hr}$$

$$\rho_{std} = \frac{P}{ZRT} = \frac{(14.696)(144)}{(1)(386.2)(520)} = 0.01054 \text{ lb/std ft}^3$$

$$\frac{dW}{dt} -0.0122 \text{ ft}^3/\text{hr } 1728 \text{ in}^3/\text{ft}^3 \quad 16.4 \text{ cc/in}^3 \quad \text{std/cc-hr} = 346 \text{ std cc/hr}$$

5.7.6.4 Helium Leakage During Coast I

Using mode 5 data from SC-1 TTY,

$$PV = WZRT$$

where

  P = helium tank pressure, psia

  T = helium tank temperature, °R

  V = helium tank volume, in^3

  R = helium gas constant

  Z = helium compressibility factor

$$\ell nP + \ell nV = \ell nW + \ell nZ + \ell nR + \ell nT$$

Differentiating and rearranging dV, dZ, dR = 0

$$\frac{dW}{W} = \frac{dP}{P} - \frac{dT}{T} \text{ dividing by dt}$$

$$\frac{dW}{dt} = \frac{W}{P}\frac{dP}{dt} - \frac{W}{T}\frac{dT}{dt}$$

GMT 150:12:25 P_1 = 5191 psia

GMT 150:12:25 T_1 = 532.4°R

GMT 151:05:40 P_2 = 5103 psia

GMT 151:05:40 T_2 = 518.4°R

$$P_{aug} = 5147 \text{ psia}$$

$$T_{aug} = 525.4°R$$

$$Z = 1.166 \text{ (Reference 9)} \qquad V_{HB} = 1300 \text{ in}^3 \text{ based on expansion data of burst tanks}$$

$$W_{aug} = \frac{PV}{ZRT} = \frac{(5147)(1300)}{(1.166)(386.2)(525.4)(12)} = 2.357 \text{ pounds}$$

$$\frac{dP}{dt} = \frac{5103 - 5191}{17.25} = -5.191 \text{ psi/hr}$$

$$\frac{dt}{dt} = \frac{518.4 - 532.4}{17.25} = -0.812°R/hr$$

$$\frac{dW}{dt} = \frac{2.357(-5.101)}{5147} - \frac{2.357(-0.812)}{525.4} = -0.002335 + 0.003642$$

$$\frac{dW}{dt} = +0.001307 \text{ lb/hr}$$

Any leakage is below the telemetry sensing capability.

5.7.6.5   SC-1 Helium Consumption

Helium Consumption — Squib Release

Following the method outlined in Reference 10:

The initial gas weight is: (460 + 58.6 = 518.6°R)

$$W_{H.T._1} = \frac{5038(1291)}{1.172(386)\ 12(518.6)} = 2.31 \text{ pounds}$$

The gas volume in the propellant tanks (downstream of the squib) is:

$$V_{P.T.} = 2227.1 + 2232.0 - \frac{109.19}{0.05202} - \frac{74.27}{0.03484}$$

$$= 4459.1 - 2099.0 - 2131.7 = 228.4 \text{ in}^3$$

The initial propellant tank gas weight is then:

$$W_{P.T._1} = W_{OT_1} + W_{FT_1} = \frac{245(128.1)}{1(386)(12)(510)} + \frac{260(100.3)}{1(386)(12)(514)} = 0.0133 + 0.01095$$

$$= 0.0243 \text{ pound}$$

Propellant tank gas weight after helium release is:

$$W_{P.T._2} = \frac{776(228.4)}{1.028(386)(12)(518.6)} = 0.0718 \text{ pound}$$

The amount of helium transferred is then:

$$W = 0.0718 - 0.0243 = 0.0475 \text{ pound}$$

The corresponding postrelease helium tank stabilized pressure at 58.6°F is:

$$P_{H.T._2} = 5038 \left(\frac{2.31 - 0.0475}{2.31} \right) = 5038 \left(\frac{2.26}{2.31} \right) = 4930 \text{ psia}$$

The prestabilization pressure is found from:

$$P_1 \theta_1^n = P_2 \theta_2^n = P_1 \left(\frac{V}{W} \right)_1^n = P_2 \left(\frac{V}{W} \right)_2^n$$

or (since $V_1 = V_2$)

$$P_2 = P_1 \left(\frac{W_2}{W_1} \right)^n = 5038 \left(\frac{2.26}{2.31} \right)^{1.65} = 5038 \, (0.978)^{1.65}$$

$$= 5038(0.9639) = 4860 \text{ psia versus } 4850 \text{ psia recorded}$$

Predicted Midcourse Helium Consumption

$$P_f = P_1 \left(1 - \frac{P_{op} \, n \, Z_1 \, \dot{Q}\Delta t_b}{P_1 \, V_{HB}} \right) \quad \text{(Reference 10)}$$

where

$\quad P_1$ = initial helium tank pressure, psia

$\quad P_f$ = final helium tank pressure, psia

$\quad P_{op}$ = propellant tank operating pressure, psia

$\quad \dot{Q}\Delta t_b$ = volume of propellant expelled, in^3

V_{HB} = helium bottle volume

n = polytropic exponent

Z = helium compressibility factor

$$T_{oxidizer\ average} = \frac{58 + 42 + 50}{3} = 50°F \qquad \text{(flight data)}$$

$$T_{fuel\ average} = \frac{56 + 50 + 57}{3} = 54°F \qquad \text{(flight data)}$$

Oxidizer density = ρ_{ox} = 0.0521 lb/in^3 at 50°F   (Reference 11)

Fuel density = ρ_f = 0.0348 lb/in^3 at 54°F   (Reference 11)

$$\rho_{mixture} = \frac{1}{\frac{0.6}{0.0521} + \frac{0.4}{0.0348}} = 0.0435\ lb/in^3$$

$W_{propellant}$ = 16.504 pounds (from Table 5.7-2)

$$\dot{Q}\Delta t = \frac{W_p}{\rho_{mix}} = \frac{16.504}{0.0435} = 379\ in^3$$

$$P_f = P_1 \left(1 - \frac{P_{op}\ n\ Z\ \dot{Q}\Delta t_b}{P_1\ V_{HB}}\right)$$

P_1 = 4850 psia   (flight data)

P_{op} = 760 psia   (flight data)

n = 1.45   (Reference 10)

Z = 1.166   (Reference 9)

V_{HB} = 1300 in^3 from tank expansion data on burst tanks

$$P_f = 4850 \left[1 - \frac{(760)(1.45)(1.166)(379)}{4850(1300)} \right]$$

$$P_f = 4850 (1 - 0.07724) = 4475 \text{ psia}$$

$$P_{f \text{ pred}} = 4475$$

$$P_{f \text{ actual}} = 4467$$

Pressure Recovery Due to Temperature Stabilization
_____

$$\frac{T_2}{T_1} = \left(\frac{P_2}{P_1} \right)^{n-1/n}$$

where

T_2 and P_2 are postshutdown conditions

T_1 and P_1 are preignition conditions

$$\frac{T_2}{518} = \left(\frac{4467}{4850} \right)^{0.3105}$$

where

$$T_2 = 505°R$$

$$\frac{P_2}{T_2} = \frac{P_3}{T_3}$$

where T_3 and P_3 are transit stabilized conditions.

$$P_3 = \frac{518(4467)}{505} = 4590 \text{ psia} \qquad \Delta P = 4590 - 4467 = 123 \text{ psia}$$

Actual $\Delta P = 4593 - 4461 = 132 \text{ psia}$

Predicted Touchdown Helium Consumption

$$P_f = P_1 \left(1 - \frac{P_{op} \, n \, Z_1 \, \dot{Q}\Delta t_b}{P_1 \, V_{HB}} \right) \qquad \text{(Reference 10)}$$

where

P_1 = initial helium tank pressure, psia

P_f = final helium tank pressure, psia

P_{op} = propellant tank operating pressure

$\dot{Q}\Delta t_b$ = volume of propellants expelled, in^3

n = polytropic exponent

Z = helium compressibility factor

$$T_{\text{oxidizer average}} = \frac{41.4 + 24.0 + 39.9}{3} = 35°F \qquad \text{(TTY data)}$$

$$T_{\text{fuel average}} = \frac{51.3 + 35.0 + 52.7}{3} = 46°F \qquad \text{(TTY data)}$$

Oxidizer density = ρ_{ox} = 0.5292 lb/in^3 at 35°F $\qquad$ (Reference 11)

Fuel density = ρ_f = 0.03507 lb/in^3 at 46°F $\qquad$ (Reference 11)

$$\rho_{\text{mixture}} = \frac{1}{\dfrac{0.6}{0.05292} + \dfrac{0.4}{0.03507}} = 0.0440 \; lb/in^3$$

W_{prop} for T/D = 122.546 $\qquad$ (Table 5.7-4)

$$Q\Delta t_b = \frac{W_p \, T/D}{\rho_{mix}} = \frac{122.546}{0.0440} \; in^3 = 2788 \; in^3$$

$$P_f = P_1 \left(1 - \frac{P_{op} \, n \, Z_1 \, \dot{Q}\Delta t_b}{P_1 \, V_{HB}} \right)$$

$P_1 = 4579$ psia   (flight data)

$P_{op} = 760$ psia   (flight data)

$n = 1.22$ (Reference 10)

$Z = 1.117$ (Reference 9)

$Q\Delta t_b = 2788$ in^3

$V_{HB} = 1300$ in^3 from expansion data on burst tanks

$$P_f = 4579 \left[1 - \frac{(760)(1.22)(1.117)(2788)}{(4579)(1300)} \right]$$

$$= 4579 \, (1 - 0.48507) = 2358 \text{ psia}$$

$P_{f_{pred}} = 2358$ psia

$P_{f_{actual}} = 2457$ psia or less

Expulsion Capability of SC-1 Landed Propellant

$$P_f = P_1 \left[1 - \frac{P_{op} \, n \, Z \, V_{prop}}{P_1 \, V_{HB}} \right] \quad \text{(Reference 10)}$$

where

$P_1 = $ SC-1 T/D helium tank pressure, psia

$P_f = $ helium tank pressure remaining after expelling usable landed propellant, psia

$P_{op} = $ propellant tank operating pressure

$V_{prop} = $ SC-1 landed usable propellant

$V_{HB} = $ helium bottle volume

$n = $ polytropic exponent

$Z = $ helium compressibility factor

propellant average density $\rho_{mix} = 0.0440 \, lb/in^3$ (See "Predicted Touchdown Helium Consumption.")

From Table 5.7-2

$$
\begin{array}{cccc}
 & \text{Loaded} & & \\
 & \text{Usable} & \text{M/C} & \text{T/D} \\
\end{array}
$$

$$W_{prop \ usable \ at \ T/D} = 181.84 - 16.50 - 122.55 = 42.79 \text{ pounds}$$

$$V_{prop} = \frac{W_{prop}}{\rho_{mix}} = \frac{42.79}{0.0440} = 973 \text{ in}^3$$

$$P_f = P_1 \left[1 - \frac{P_{op} \ n \ Z \ V_{prop}}{P_1 \ V_{HB}} \right]$$

where

$P_1 = 2457 \text{ psia}$ (flight data)

$P_{op} = 760 \text{ psia}$ (flight data)

$n = 1.22$ (Reference 10)

$Z = 1.07$ (Reference 9)

$V_{HB} = 1300 \text{ in}^3$ from expansion data on burst tanks

$$P_f = 2457 \left[1 - \frac{(760)(1.22)(1.07)(973)}{(2457)(1300)} \right]$$

$$= 2457 \, (1 - 0.30222) = 1714 \text{ psia}$$

Under worst case conditions assuming n = 1.65 (isentropic process)

$$P_f = 2457 \left[1 - \frac{(760)(1.65)(1.07)(973)}{(1300)(2457)} \right]$$

$$= 2457 \, (1 - 0.38199) = 1518 \text{ psia}$$

Allowing 200 psi for telemetry inaccuracies, this value is still in excess of that specified in Reference 5.

5.7.6.6 Regulator Lockup Determination

GMT 151:02:41:55 P_2 lockup = 780 psia = 776 BCD, mode 1

mode 2 = 776 BCD

$$S_1 = 1002 \text{ BCD}$$
$$S_2 = 1 \text{ BCD}$$
$$S_5 = 135 \text{ BCD}$$
B/P Format 18

$$TM_{corr} = TM_{ind} + \delta_{LD} + \delta_{A/D} + \delta_I + \delta_E \qquad \text{(Reference 2)}$$

$$\delta_I = \frac{I_{unbalance}(R_1 + R_2)(TM_{ref} - TM_{ind})TM_{ind}}{\left(TM_{ref}\right)^2} \qquad \text{(Reference 2)}$$

$$I = 135 \text{ BCD} = -3\mu a$$

$$\delta_I = (-3 \times 10^{-6})(2 \times 10^3) \frac{(1002 - 776)\ 776}{(1002)(1002)}$$

$$= -6 \times 10^{-3} \frac{(226)(776)}{(1002)(1002)} = -1.049 \times 10^{-3} \text{ volts}$$

$$4.88 \frac{MV}{BCD} \quad \text{so} = -0.214 \text{ BCD}$$

$$\delta_E = \frac{TM_{ind}}{TM_{ref}}(993 - TM_{ref}) = \frac{776}{1002}\left[993 - (1002 - 1)\right] = -\frac{776(8)}{1002}$$

$$= -6.19 \text{ BCD}$$

$$\delta_{A/D} = +0.5 \text{ BCD} \qquad \delta_{LD} = -1 \text{ BCD} \qquad \text{(Reference 2)}$$

$$P2_{corr} = 776 - 0.2 - 6.2 + 0.5 - 1 = 769 \text{ BCD}$$

$$P_2 = 769 \text{ BCD} = 765 \text{ psia}$$

FAT data indicates lockup at 4950 psia inlet = 777 psia

at 4000 psia inlet = 762 psia

5.7.6.7 Strain Gage Evaluation

A comparison of leg 2 and 3 corrected strain gage readings with corrected thrust command readings for the SC-1 retro phase is shown in Tables 5.7-7 and 5.7-8.

The retro phase was selected because the most accurate thrust command data of the flight was available for that period (Reference 4). Also during the mission, a comparison of strain gage and thrust command data was made for the midcourse maneuver, and that data from the propulsion flight log book is reproduced as Table 5.7-9.

It was also decided not to use the leg 1 strain gage data as the calibration data on that parameter was questionable, and, within the time available for data reduction, the leg 2 and 3 strain data would be sufficient to illustrate the utility of these channels.

An inertia correction and a zero shift correction were applied to the strain gage readings. The inertia correction arises because bending of the TCA at a fixed thrust level varies with the local acceleration field. This bending results in a strain gage output variation with acceleration. The data for applying this correction is taken from Reference 12. The zero shift correction was corrected for inertia effects as the preignition zero was at zero g, and the postshutdown zero was at 1 lunar g. The corrected correction was distributed linearly for the entire burning time, although strain gage information is only available for the first 74 seconds of vernier burn.

Early in the retro phase at GMT 06:14:52, inspection of the reduced data indicated a difference of 9 to 10 pounds between the corrected strain gage reading and the thrust command for the leg 2 TCA. At GMT 06:15:22, the same difference for the leg 2 TCA is 22 pounds. During the retro eject phase at GMT 06:15:38, the difference between strain gage reading and thrust command is 37 pounds. During the minimum acceleration phase at GMT 06:15:55, the difference is 25 pounds. In all cases, the strain gage indication is below the commanded thrust level. Similar results are indicated on the leg 3 TCA strain gage versus commanded thrust data.

It is evident that the data does not correlate well. A possible explanation for this fact is that the assumption of a linearly distributed zero shift is not valid. A more probable explanation is discussed in Reference 13, which noted that unsymmetrical heat flow in the bracket during thrusting could cause shifts in strain gage output.

TABLE 5.7-7.   LEG 2 RETRO PHASE STRAIN GAGE SUMMARY (P19)

Time, hr:min:sec	BCD	Uncorrected Thrust, pounds	Zero Shift Correction, pounds (-0.097 lb/sec)	FC-32 Acceleration Level, g	Inertia Correction, pounds	Corrected Thrust, pounds	FC-25 Commanded Thrust, pounds
06:14:40	268	10.2	-2.1	0.000562	-8.15	-0.05	
	268	10.2	-2.1	0.000562	-8.15	-0.05	
42	268	10.2	-2.1	0.000562	-8.15	-0.05	
	268	10.2	-2.1	0.000562	-8.15	-0.05	
44	268	10.2	-2.1	0.000562	-8.15	-0.05	
	268	10.2	-2.1	0.000562	-8.15	-0.05	
46	268	10.2	-2.1	0.000562	-8.15	-0.05	
	268	10.2	-2.1	0.000562	-8.15	0	
48	268	10.2	-2.1	0.000562	-8.15	-0.05	
	558	59.6	-2.197	3.74	22.3	79.70	64.3
50	352	*	-2.294	3.74	22.3		
	407	34.0	-2.391	3.94	24.0	55.61	64.3
52	396	32.1	-2.488	4.04	24.8	54.41	64.5
	384	*	-2.585	4.17			
54	380	29.4	-2.682	4.34	27.2	53.92	65.4
	365	*	-2.779	4.54			
56	355	25.1	-2.876	4.68	30.0	52.22	65.4
	340	22.5	-2.976	4.79	30.9	50.42	64.7
58	333	21.3	-3.070	4.85	31.4	49.63	64.7
	326	20.1	-3.167	4.98	32.4	49.33	65.4
06:15:0	315	*	-3.264	5.08			
	307	16.9	-3.361	5.20	34.2	47.74	66.0
2	300	15.7	-3.458	5.31	35.1	47.34	65.4
	295	14.8	-3.555	5.43	36.1	47.35	65.4
4	287	13.4	-3.652	5.62	37.7	47.45	65.6
	280	*	-3.749	5.75			
6	276	11.6	-3.846	5.87	39.7	47.45	65.4
	269	10.4	-3.943	6.07	41.3	47.76	65.4
8	259	8.6	-4.040	6.31	43.3	47.86	65.4
	248	6.7	-4.137	6.68	46.3	48.86	64.7
10	235	*	-4.234	6.88			
	224	*	-4.331	7.03			
12	223	2.4	-4.428	7.19	50.4	48.37	65.6
	207	-0.2	-4.525	7.36	51.8	47.08	65.3
14	199	*	-4.622	7.60			
	189	-3.3	-4.719	7.79	55.3	47.28	65.6
16	177	-5.4	-4.816	8.02	57.2	46.98	64.7
	167	-7.1	-4.913	8.13	58.1	46.09	64.7
18	158	-8.6	-5.010	8.36	60.0	46.39	65.4
	145	*	-5.107	8.67			
20	133	-12.9	-5.204	8.87	64.2	46.10	65.7
	126	-14.1	-5.301	9.02	65.4	46.00	64.7
22	111	-16.7	-5.398	9.14	66.3	44.20	65.3

Table 5.7-7 (continued)

Time, hr:min:sec	BCD	Uncorrected Thrust, pounds	Zero Shift Correction, pounds (-0.097 lb/sec)	FC-32 Acceleration Level, g	Inertia Correction, pounds	Corrected Thrust, pounds	FC-25 Commanded Thrust, pounds
06:15:22	103	-18.0	-5.495	9.30	67.6	44.11	66.0
24	98	*	-5.592	9.46			
	95	-19.4	-5.689	9.46	68.9	43.81	66.0
26	98	-18.9	-5.786	8.01	57.1	32.41	66.9
	111	-16.7	-5.883	3.86	23.3	0.72	65.6
28	226	*	-5.980	2.19			
	352	*	-6.077	1.40			
30	544	*	-6.174	0.923			
	568	*	-6.271	0.689			
32	588	64.6	-6.368	0.527	-3.9	54.33	93.4
	596	*	-6.465	0.469			
34	608	68.0	-6.562	0.352	-5.3	56.14	93.8
	613	68.8	-6.659	0.352	-5.3	56.84	93.8
36	615	69.1	-6.756	0.352	-5.3	57.04	93.8
	614	69.0	-6.853	0.352	-5.3	56.85	93.8
38	612	68.6	-6.950	0.352	-5.3	56.35	93.8
	613	68.8	-7.047	0.352	-5.3	56.45	93.8
40	614	69.0	-7.144	0.352	-5.3	56.56	93.8
	608	68.0	-7.241	0.352	-5.3	55.46	93.8
42	611	68.5	-7.338	0.176	-6.7	54.46	93.8
	611	68.5	-7.435	0.117	-7.2	53.87	34.3
44	344	23.2	-7.532	0.117	-7.2	8.47	34.0
	569	61.4	-7.629	0.117	-7.2	46.57	38.3
46	387	30.6	-7.726	0.117	-7.2	15.67	27.1
	333	21.3	-7.823	0.117	-7.2	6.28	39.8
48	359	*	-7.920	0.117	-7.2		
	356	25.3	-8.017	0.117	-7.2	10.08	34.1
50	356	25.3	-8.114	0.117	-7.2	9.99	30.6
	365	26.8	-8.211	0.117	-7.2	11.39	35.1
52	375	28.5	-8.308	0.117	-7.2	12.99	33.3
	369	27.5	-8.405	0.117	-7.2	11.90	29.6
54	374	28.4	-8.502	0.117	-7.2	12.70	35.6
	361	26.1	-8.599	0.117	-7.2	10.30	34.9
56	352	24.6	-8.696	0.117	-7.2	8.70	37.5
	368	27.3	-8.793	0.117	-7.2	11.31	36.6
58	379	29.2	-8.890	0.117	-7.2	13.11	34.3
	368	27.3	-8.987	0.117	-7.2	11.11	33.5
06:16:00	359	25.8	-9.084		-7.2	9.52	35.1
1	377	*	-9.181				

*Data not reduced for these points.

5.7-34

TABLE 5.7-8.   LEG 3 RETRO PHASE STRAIN GAGE SUMMARY (P20)

Time, hr:min:sec	BCD	Uncorrected Thrust, pounds	Zero Shift Correction, pounds (-0.135 lb/sec)	FC-32 Acceleration Level, g	Inertia Correction, pounds	Corrected Thrust, pounds	FC-25 Commanded Thrust, pounds
06:14:40	229	3.8	4.4	0.000562	-8.15	0	
	229	3.8	4.4	0.000562	-8.15	0	
42	229	3.8	4.4	0.000562	-8.15	0	
	229	3.8	4.4	0.000562	-8.15	0	
44	229	3.8	4.4	0.000562	-8.15	0	
	229	3.8	4.4	0.000562	-8.15	0	
46	229	3.8	4.4	0.000562	-8.15	0	
	230	4.0	4.4	0.000562	-8.15	0	
48	229	3.8	4.4	0.000562	-8.15	0	
	554	62.2	4.265	3.74	+22.3	88.77	65.1
50	381	*	4.130	3.74			
	379	31.7	3.995	3.94	24.0	59.70	65.5
52	378	31.5	3.860	4.04	24.8	60.16	66.1
	375	*	3.725	4.17			
54	365	29.1	3.590	4.34	27.2	59.89	66.1
	355	*	3.455	4.54			
56	340	24.5	3.320	4.68	30.0	57.82	66.1
	329	22.4	3.185	4.79	30.9	56.49	66.1
58	313	19.4	3.050	4.85	31.4	53.85	66.1
	302	17.4	2.915	4.98	32.4	52.72	66.1
06:15:0	297	*	2.780	5.08			
	287	14.6	2.645	5.20	34.2	51.45	66.1
2	273	12.0	2.510	5.31	35.1	49.61	66.1
	264	10.3	2.375	5.43	36.1	48.78	66.1
4	257	9.0	2.240	5.62	37.7	48.94	66.1
	243	*	2.105	5.75			
6	232	4.3	1.970	5.87	39.7	45.97	66.1
	228	3.6	1.835	6.07	41.3	46.74	66.1
8	217	1.5	1.700	6.31	43.3	46.50	67.5
	211	0.4	1.565	6.68	46.3	48.27	67.5
10	200	*	1.430	6.88			
	195	*	1.295	7.03			
12	184	-4.5	1.160	7.19	50.4	47.06	67.5
	177	-5.8	1.025	7.36	51.8	47.03	67.5
14	169	*	0.890	7.60			
	160	-9.0	0.755	7.79	55.3	47.6	67.9
16	152	-10.5	0.620	8.02	57.2	47.32	67.5
	144	-12.0	0.485	8.13	58.1	46.59	67.5
18	137	-13.3	0.350	8.36	60.0	47.05	67.0
	124	*	0.215	8.67			
20	116	-17.2	0.080	8.87	64.2	47.08	67.5
	103	-19.6	-0.055	9.02	65.4	45.75	67.5
22	94	-21.3	-0.190	9.14	66.3	44.81	67.0
	84	-23.1	-0.325	9.30	67.6	44.18	66.1

Table 5.7-8 (continued)

Time, hr:min:sec	BCD	Uncorrected Thrust, pounds	Zero Shift Correction, pounds (-0.135 lb/sec)	FC-32 Acceleration Level, g	Inertia Correction, pounds	Corrected Thrust, pounds	FC-25 Commanded Thrust, pounds
06:15:24	78	*	-0.460	9.46			
	76	-24.6	-0.595	9.46	68.9	43.71	65.8
26	72	-25.3	-0.730	8.01	57.1 .	31.07	64.9
	113	-17.7	-0.865	3.86	23.3	4.74	64.9
28	300	*	-1.000	2.19			
	509	*	-1.135	1.40			
30	539	*	-1.270	0.923			
	551	*	-1.405	0.689			
32	561	65.3	-1.540	0.527	-3.9	59.86	94.4
	567	*	-1.675	0.469			
34	574	67.7	-1.810	0.352	-5.3	60.59	93.5
	574	67.7	-1.945	0.352	-5.3	60.46	93.5
36	569	66.8	-2.080	0.352	-5.3	59.42	94.4
	570	67.0	-2.215	0.352	-5.3	59.49	94.4
38	569	66.8	-2.350	0.352	-5.3	59.15	93.5
	569	66.8	-2.485	0.352	-5.3	59.02	94.3
40	568	66.6	-2.620	0.352	-5.3	58.68	93.5
	570	67.0	-2.755	0.352	-5.3	58.95	94.4
42	564	66.8	-2.890	0.176	-6.7	57.21	94.4
	287	*	-3.025	0.117			
44	309	18.7	-3.160	0.117	-7.2	8.34	32.6
	344	25.2	-3.295	0.117	-7.2	17.71	49.5
46	276	12.5	-3.430	0.117	-7.2	1.87	27.8
	307	18.3	-3.565	0.117	-7.2	7.54	36.6
48	312	*	-3.700	0.117			
49	313	*	-3.835	0.117			
50	313	19.4	-3.970	0.117	-7.2	8.23	30.8
	307	18.3	-4.105	0.117	-7.2	7.00	30.1
52	309	18.7	-4.240	0.117	-7.2	7.26	31.0
	307	18.3	-4.375	0.117	-7.2	6.73	31.8
54	297	16.5	-4.510	0.117	-7.2	4.79	32.6
	303	17.6	-4.645	0.117	-7.2	5.76	34.2
56	295	16.1	-4.780	0.117	-7.2	4.12	32.4
	307	*	-4.915	0.117	-7.2		
58	295	16.1	-5.050	0.117	-7.2	3.85	31.0
	305	17.9	-5.185	0.117	-7.2	5.52	32.4
06:16:00	310	18.9	-5.320		-7.2	6.38	28.5
1	248	*	-5.455				

*Data not reduced for these points.

5.7-36

TABLE 5.7-9. SC-1 PROPULSION LOGBOOK MIDCOURSE DATE SUMMARY (From Bulk Printer Format 18)

	Engine 1				Engine 2				Engine 3			
	FC-25		P-18		FC-26		P-19		FC-27		P-20	
GMT	Indicated Value, pounds	Corrected Value,* pounds	Indicated Value, pounds	Corrected Value,* pounds	Indicated Value, pounds	Corrected Value,* pounds	Indicated Value, pounds	Corrected Value,* pounds	Indicated Value, pounds	Corrected Value,* pounds	Indicated Value, pounds	Corrected Value,* pounds
064504 (before M/C)	70.5	64.2	5.4	0	71.2	67.0	8.1	0	71.8	66.8	-0.2	0
064505	81.7	77.2	72.7	68.7	81.0	78.0	68.6	61.3	80.6	76.7	70.6	71.7
064511	79.2	74.5	65.7	65.0	78.1	74.9	63.8	56.2	78.4	74.3	67.3	68.8
064515	79.2	74.5	60.2	61.8	77.3	74.0	60.9	53.1	78.6	74.5	62.0	63.8
064520	79.0	74.3	55.9	60.3	76.7	73.3	57.0	48.9	78.2	74.1	57.8	60.0
064523	78.7	74.0	55.3	61.4	76.3	72.9	55.9	47.7	78.2	74.1	55.9	58.3
064527 (after M/C)	70.3	64.0	-7.5	0	71.1	66.9	9.2	0	71.4	66.4	-1.9	0
Zero shift	-0.2		-12.9		-0.1		1.1		-0.4		-1.7	

*Corrected values use proper calibration curves for FC-25, -26, -27, linearly distributed zero shift (with time), and acceleration correction on P-18, -19, -20.

5.7.7 REFERENCES

1. R. Costello to R. Gunter, W. McCandless, K. Beall, and G. Kerster, "Results of SC-1 Propellant Loading," Ref. 22-53-ETR-28, 17 May 1966.

2. L. Gee to K. Beall, "SC-1 TM Verification," Ref. 2253.1/580, 24 February 1966.

3. "Interface Document Surveyor Vernier Propulsion Thrust Chamber Assembly TD 339 Flight Model," Hughes Aircraft Company Specification 287015A, 27 July 1966.

4. R. Breshears and J. Stockey, JPL Data Reduction of FC25, 26, and 27.

5. "Vernier Propulsion System Regulator, Pneumatic Pressure," Power and Propulsion Systems Procurement Specification, Hughes Aircraft Company Specification 262665A, 1 December 1964.

6. R.A. Laird to Distribution, "VPS Propellant Tank Capacities of S-6, SC-1 and SC-2," Ref. IDC 2227.1/1543, 13 April 1966.

7. R.A. Laird to Distribution, "Unmanifolded Surveyor Vernier Propulsion System Propellant Inventory," Ref. IDC 2227.1/761, 2 June 1965.

8.   R. Laird to Distribution, "A21 and A21A/114 Vernier Propulsion System Propellant Inventory," Ref. IDC 2227.1/1110, 29 September 1966.

9.   "Hydrogen Handbook," AFFTC, TR-60-19.

10. G. F. Pasley to Distribution, "Surveyor Vernier System Helium Utilization as Determined by the S-6 TAT Program," Ref. IDC 2227.1/1125, 6 October 1965.

11. "Technical Manual, Operating and Maintenance Instructions — Qualification Thrust Chamber Assembly, Model TD-339," Publication No. 8984 — H2A, Thiokol Chemical Corporation, Reaction Motors Division, Denville, New Jersey, 15 December 1965.

12. J. Stockey to A. Briglio, "Strain Gage Readings of SC-1," Ref. SP/SA No. 70, 17 May 1966.

13. T. B. Shoebotham to Distribution, "Expected Flight Strain Gage Performance based on Test Results of S-6 and S-7 TAT Programs," Ref. IDC 2227.1/1132, 12 October 1965.

5.7.8   ACKNOWLEDGEMENTS

5.8 PROPULSION — MAIN RETRO

5.8.1 INTRODUCTION

The main retro-rocket, which performs the major portion of the deceleration of the spacecraft during terminal descent, is a spherical, solid propellant unit with a partially submerged nozzle.

The unit is attached at three points to the spacecraft near the landing leg hinges, with explosive nut disconnects for postfiring ejection. Friction clips around the main retro-rocket engine nozzle flange provide attachment points for the altitude marking radar. The igniter gas pressure ejects the altitude marking radar when the retro firing sequence is initiated. The main retro-rocket engine ignition squibs and retro release explosive nuts operate from a pulsed, 19-ampere, constant-current source. Commands are initiated by the flight control system.

The nozzle is partially submerged to minimize overall length. The nozzle has a graphite throat insert backed up by laminates of carbon cloth phenolic with a fiberglass exit cone lined with bulk carbon phenolic. The case is of high strength steel and insulated with asbestos and inorganic fiber filled buna-N rubber to maintain the case at a low temperature level during burning.

The main retro-rocket engine with propellant weighs approximately 1386 pounds. The engine utilizes an aluminum, ammonium perchlorate, polyhydrocarbon, case-bonded composite-type propellant and conventional grain geometry. The engine thrust may vary between 8000 to 10,000 pounds over the temperature range of 50 to 70°F.

Two thermal sensors are installed on the main retro-rocket engine case for telemetering engine temperature during transit. One thermal sensor is installed for monitoring nozzle temperature during transit.

The main retro-rocket engine employs a safe and arm device that has dual firing, single bridgewire squibs for the engine igniter. In addition, provisions for local and remote safe and actuation and remote indication of inadvertent firing of the squibs are included. Both mechanical and electrical isolation exists between squib initiator and pyrogen igniter in the safe condition.

5.8.2 LIST OF ITEMS CONSTITUTING ANALYSIS EFFORT

1) Reconstruction of thrust versus time curve from accelerometer and doppler data (Figure 5.8-1)

2) Calculation of engine specific impulse

3) Determination of thrust vector excursions and roll moments generated by the retro engine

4) Determination of T3500

5.8.3 MAJOR EVENTS AND TIMES

Table 5.8-1 gives the major events and times associated with the firing of the retro engine.

TABLE 5.8-1. MAJOR EVENTS AND TIMES FOR RETRO FIRING

Event	GMT	Maximum Error, second
Vernier ignition	day 153, 06:14:47.558	0.05
Retro ignition	14:48.658	0.05
3500-pound thrust level	15:27.515	0.1
"Actual" 3.5 g	15:27.665	0.1
3.5 g switch	15:27.943	0.015
Retro ejection signal	15:39.943	0.015
Retro ejected signal	15:40.066	0.5

5.8.4. SUMMARY OF RESULTS

Table 5.8-2 is a summary of main retro performance parameters.

5.8.5 ANOMALY DESCRIPTION

No anomalies were noted.

5.8.6 CONCLUSIONS AND RECOMMENDATIONS

The SC-1 main retro-rocket engine operated well within all required tolerances. No changes to the SC-2 retro-rocket engine or to the engine performance prediction models are recommended.

5.8.7 ANALYSIS

5.8.7.1 Thrust Versus Time

The technique used in the reconstruction of the thrust versus time trace from both accelerometer and doppler data is discussed later
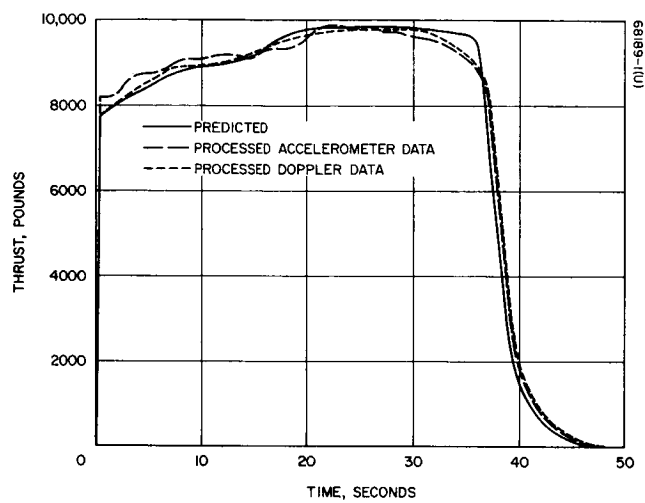
Figure 5.8-1. SC-1 Main
Retro Engine

Thrust versus time

TABLE 5.8-2. SUMMARY OF MAIN RETRO
PERFORMANCE PARAMETERS

Parameter	Predicted Main Retro Value	Required Main Retro Value and Tolerance	Actual Value	Uncertainty
Bulk temperature °F	55	±15	54	±5
T3500, seconds	38.5	±0.4	38.9	±0.1
Maximum thrust, pounds	9800	<10,000	9850	±100
Total impulse, lb-sec	359,924	±3600	358,556	±1800
Specific impulse, seconds	289.5	±3	288.4	±1.5
Center of gravity excursion, inch	—	<0.030		
Thrust vector excursion			0.013*	±0.001
Displacement, inch	—	<0.040		
Angular, degree	—	<0.2		
Roll torque, in-lb	—	<80	18*	±6

*Total value from all sources.

(subsection 5.15.6.2). This reconstructed trace varies from the predicted trace as shown in Figure 5.8-1. The maximum difference is 7 percent and it occurs at 36 seconds. This, however, is in the area of maximum error for both the accelerometer and doppler data since the spacecraft passes through maximum deceleration at this point, and the spacecraft weight uncertainty is at its highest as a result of the uncertainty in propellant weight at that point.

5.8.7.2 Specific Impulse

The main retro-rocket engine specific impulse was obtained by correcting the predicted nominal specific impulse used in the preflight descent trajectory computer program by the velocity at retro burnout measured on SC-1. The difference between the actual and predicted burnout velocities, 428 and 392 fps, respectively, amounts to 0.43 percent. This difference was then assumed to be due entirely to the main retro-rocket engine and thus its specific impulse was found to be 0.43 percent low versus the 1 percent allowed. This approach is conservative from the retro-rocket engine point of view since the velocity difference is actually due to a number of sources in addition to the main retro-rocket engine. Some of these other sources are as follows:

1) Uncertainty in vernier engine specific impulse

2) Uncertainty in vernier engine thrust level

3) Uncertainty in vernier engine weight versus time

4) Uncertainty in retro-rocket engine specific impulse versus time

5) Uncertainty in retro-rocket engine weight versus time

6) Uncertainty in doppler data

5.8.7.3 Retro Disturbance Torques

1) Following retro ignition, all three vernier engines settled almost precisely at their midthrust condition. This indicates that retro disturbance torques owing to thrust vector to center of gravity offset was virtually nonexistent compared with the expected values of 100 ft-lb.

2) At about 10 seconds prior to the 3.5 g point, differential thrusting of engines 1 and 3 produced 10 ft-lb of corrective torque. This implies that a maximum thrust vector to center of gravity offset of 0.013 inch was experienced, whereas a total of 0.18 inch offset is allowed. This value is a combination of the following factors:

   a) Retro nozzle to attachment plane alignment

   b) Spacecraft to retro engine alignment

   c) Retro engine and spacecraft center of gravity

   d) Retro engine thrust vector lateral and angular excursions during burning

   e) Retro engine center of gravity excursions during burning

   Because of the very low maximum total value experienced, no attempt was made to separate these effects.

3) The maximum required corrective roll torque produced by the vernier engine was 18 in.-lb. Assuming all this torque was produced by the main retro engine, 18 in.-lb is well below the maximum of 80 in.-lb allowed the retro engine.

4) No attitude disturbance was noted at case ejection.

5.8.7.4 T3500

The T3500 (time from ignition to the time when thrust decays to 3500 pounds) prediction was apparently marginal. The total error of 1 percent equals the tolerance for the prediction; however, this total error is the result of the actual engine temperature gradient uncertainty, the error in calculating the bulk temperature corresponding to that gradient, telemetry error, and prediction error. Since these errors cannot be evaluated fully and since they can combine in a random manner, it is not clear that the 1 percent prediction error tolerance was met.

5.8.8 REFERENCES

1. "Surveyor Spacecraft A21 Model Description," Hughes Aircraft Company, Document No. 224847B, 1 March 1965.

2. "Surveyor Main Retro Engine A21-26 Support Documentation," Thiokol Chemical Corporation.

3. "Surveyor I Flight Performance Quick Look Report," 17 June 1966.

4. "SC-1 Event Times from Teltab," Hughes Aircraft Company, IDC 2253.2/616, 11 July 1966.

5.8.9 ACKNOWLEDGEMENTS

The following people contributed to the main retro analysis:

L. M. Spicer, coordinator

D. Bender (System Analysis)

L. H. Davids (System Analysis)

H. D. Marbach (Flight Control)

5.9   ALTITUDE MARKING RADAR

5.9.1   INTRODUCTION

The altitude marking radar (AMR) is a conventional pulsed radar operating at X band.   It employs an early/late gate detection scheme for identifying the centroid of the lunar reflected signal.   It is installed in the exhaust cone of the main retro engine and its sole purpose is to automatically initiate the terminal descent at precisely the correct slant range from the lunar surface.

The SC-1 AMR functioned normally in all respects.   The true altitude mark was generated at the expected time and initiated the automatic terminal descent sequence at the nominal altitude.   (Routine emergency mark backup command transmission was received by SC-1 after the on-board mark had been generated.)   AMR AGC indicated essentially the nominal predicted signal strength throughout the operating time, confirming both the design and the Muhleman reflectivity model for that approach angle.   The AMR late gate signal was normal, confirming the presence of RF return signal and detected video within the gate at the proper time relative to the mark.

5.9.2   MAJOR EVENT TIMES

The times associated with the major AMR events are summarized in Table 5.9-1.   The times listed are the GMT times indicated at DSIF 11 when the event was recorded.   The actual event occurred at the spacecraft either 1.23 seconds later for commands or 1.23 seconds earlier for telemetered spacecraft events.

5.9.3   SUMMARY OF RESULTS

A summary of the achieved AMR performance parameters and the corresponding predicted or required values is presented in Table 5.9-2.

5.9.4   ANOMALY DESCRIPTION

There were no anomalies detected in the performance of the AMR.

TABLE 5.9-1. MAJOR AMR EVENT TIMES

Event	Source	Day	Hr	Min	Sec	Tol	Comments
				DSIF 11 GMT,			
AMR power on command	DSIF CDC command printer	153	06	09	57.5	±0.5	
AMR on telemetry	DSIF 11 magnetic tape	153	06	10	0.07	±0.5	
AMR enable command	ETR command decoding and signal line printer	153	06	12	57.68	±0.01	
AMR enable telemetry	DSIF 11 magnetic tape	153	06	13	0.070	±0.5	Warmup time was 180 seconds
AMR backup command	ETR command decoding and signal line printer	153	06	14	39.514	±0.01	At spacecraft
AMR mark telemetry	DSIF 11 magnetic tape	153	06	14	38.463	±0.05	At spacecraft; enabled time was 99.6 seconds
Vernier engine ignition telemetry	DSIF 11 magnetic tape	153	06	14	47.533	±0.02	Ignition delay was 7.83 ± 0.07 second. Commanded delay was 7.85 seconds
Retro engine ignition telemetry	DSIF 11 magnetic tape	153	06	14	48.758	±0.20	

TABLE 5.9-2. AMR PERFORMANCE SUMMARY

Parameter	Required or Predicted Value	Actual Value
AMR warmup time	280 ± 10 seconds	280 ± 1 second
AMR enable time	100 ± 10 seconds	99.6 ± 0.7 second
AMR mark accuracy	0.3 mile at 0 degree	Not determinable *
Received signal at mark	> -93.0 dbm required ≈ -59.7 dbm predicted	-59.7 dbm

*No independent source of marking range exists with accuracy even approaching that of AMR.

5.9.5 CONCLUSIONS AND RECOMMENDATIONS

Continued use of the AMR on future spacecraft is required for proper margin in terminal descent. Generation of the backup command is also worthwhile as long as it is certain that the AMR will never be pre-empted.

5.9.6 PERFORMANCE ANALYSES

5.9.6.1 AMR Timing Sequence

The nominal time sequence was observed·meticulously by the space flight operations facility (SFOF). The specified time to turn on AMR prime power is 280 $\neq$ 10 seconds before the predicted time of mark; the SC-1 value was about 279.7 seconds. The specified time to enable the AMR(which turns on high voltage and enables the video circuitry) is 100 $\neq$ 10 seconds before the predicted time of mark; the SC-1 value was about 99.7 seconds. The optimum warmup interval of 180 seconds between these two commands was observed exactly.

The SFOF routine procedure of emergency mark backup command transmission was effective 1.04 ± 0.15 seconds after the on-board generation of the true altitude mark. This can be demonstrated since telemetry discrete signal FC-64 (AMR mark) is generated only if the AMR starts the retro sequence of events, but not if the sequence was initiated by the backup command. Since FC-64 was received at the DSIF at 06:14:39.958 GMT (+0, -0.4 second), the AMR mark must have begun the sequence.

The exact times of mark generation and backup command receipt can be accurately determined by considering related events. Propagation time between earth and spacecraft at that time was 1.245 seconds. The emergency AMR command was transmitted at 14:38.269, reaching the spacecraft at 14:39.514. The command enable signal was observed at 14:41.538, indicating that it occurred at the spacecraft between 14:39.29 and 14:40.29.[*] This falls within the enable signal generation interval, and it is not possible to get a closer value.

For the AMR mark time, counting of the magnitude register (initiated by the mark) can be used to get a precise value. Two register values and times at DSIF were as follows:

06:14:40.008	151 counts
06:14:41.008	131 counts

These verify the accuracy of the nominal 20 counts/second rate, and thus it is easy to extrapolate back to the latest time that the register had 157 counts, the preset value of preretro sequence delay:

06:14:39.708	157 counts

---

[*]Since the command reached the spacecraft within this interval, this demonstrates proper occurrence of the command enable signal, but it is not possible to time this event more closely.

This earth-receipt time must be translated back to the spacecraft, and thus the AMR mark occurred at 06: 14: 38. 463 ± 0. 05 second (at spacecraft).

Since the AMR mark was effective, retro burnout occurred when the spacecraft was still 10,000 feet above the programmed descent profile. If, however, the backup command was the effective agent (1. 04 seconds later) burnout would have been only 500 feet above the profile. Considering the tolerance on the command time, a worst-case condition of 500 feet below the profile could have been encountered. In other words, reliance on the manually-sent command could have changed the remarkably nominal Surveyor descent to one which was marginal at best.

5. 9. 6. 2   Altitude Marking Accuracy

Preflight AMR analyses predicted marking ranges of 59. 63 statute miles for a vertical approach and 59. 57 miles for a 25-degree approach, with 3σ accuracies including predicted in-flight parameter drifts of $\neq$1068 feet and $\neq$1704 feet, respectively. Flight path analysis and command information indicates an SC-1 approach angle of about 6. 2 degrees, with an approach velocity of 8565 ft/sec. The predicted SC-1 marking range would therefore be about 59. 62 miles $\neq$ about 1200 feet (3σ). While these accuracies exceed those of independent data that might be used for confirmation, there are several indications of nominal performance, notably the very close to nominal retro burnout conditions. These, with nominal conditions during retro burning, especially the quite low lateral velocities, can be expected only from essentially nominal ignition conditions.

5. 9. 6. 3   Received Signal Strength and Lunar Reflectivity

The preflight measurement of SC-1 AMR transmitted pulse length was 3. 3 microseconds, corresponding to a round-trip resolution of 0. 307 mile along axis. Even at only 6. 2 degrees off vertical incidence, however, range variation across the effective beamwidth is 0. 286 mile, stretching the returned pulse by an additional 2. 74 microseconds, for an effective received pulse length of 6. 0 microseconds. With the approach velocity of 1. 623 miles per second, the video pulse closing rate was 17. 48 microseconds per second. The video late gate measured before launch as 19. 8 microseconds (20. 0 ± 1. 0, required) should therefore produce output within 3 db of peak for 1. 186 seconds, ensuring that some one of the once-per-second telemetry samples of late gate signal should be close to peak amplitude. In SC-1, this sample occurred at 06: 14: 39. 2, with an amplitude corresponding with calibrated saturation of the detector circuit. Since this was within 1 second of the actual mark time, presence of proper radar return is confirmed. Figure 5. 9-1 shows this signal from SC-1 telemetry channel R-29 (AMR late gate). All AMR telemetry channels go full scale as the AMR itself is forcibly jettisoned at retro ignition.

The Surveyor AMR is always beamwidth-limited in azimuth, with a required maximum equivalent rectangular beamwidth of 0. 0465 radian; the preflight measured SC-1 AMR value was 0. 0397 radian. The AMR is also pulse-length limited in elevation for significant approach angles, corresponding
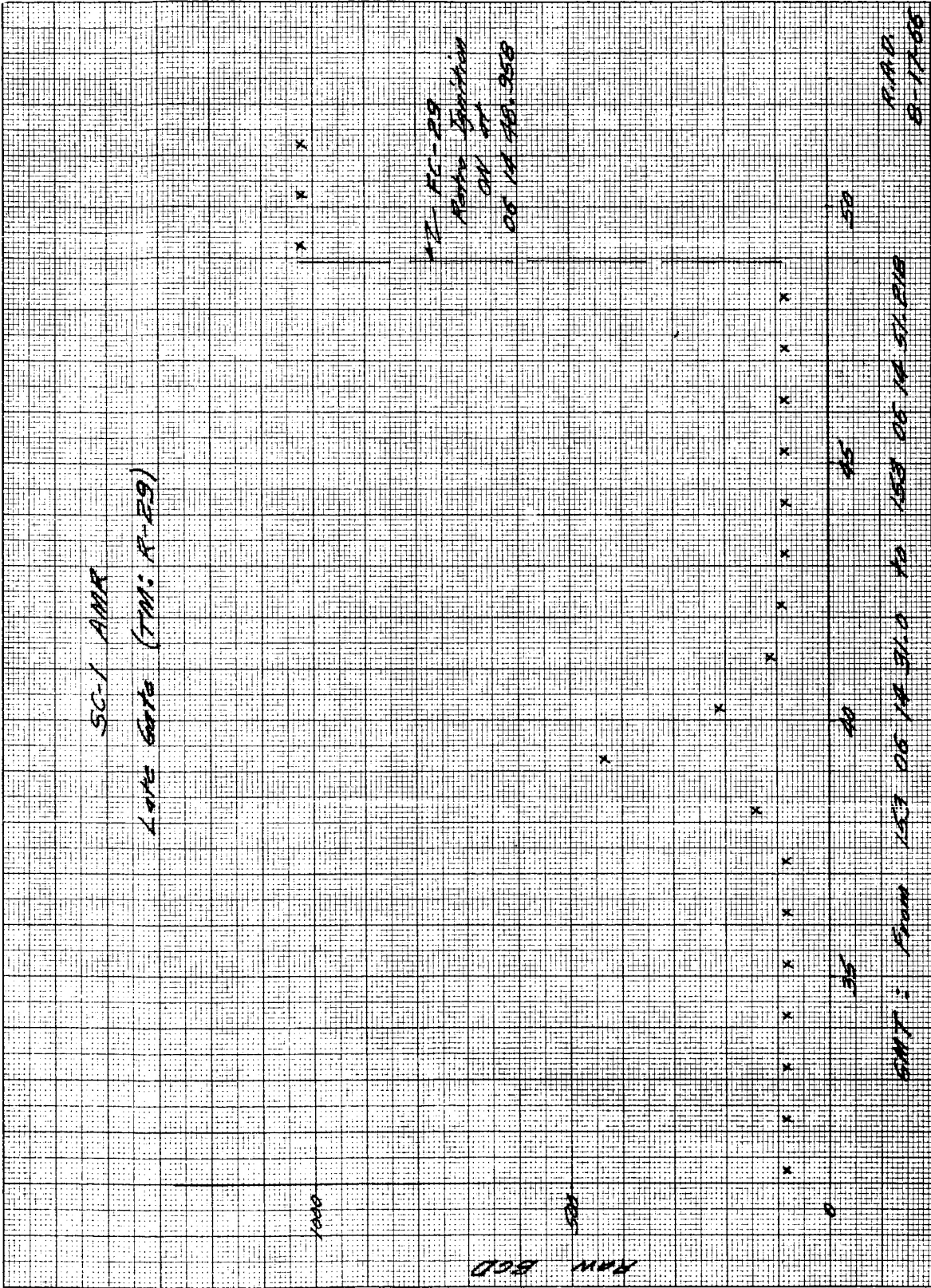
Figure 5.9-1. AMR Late Gate (R-29)

with an inverse-cubed range dependence. Near the vertical, however, it becomes beamwidth-limited in elevation as well as in azimuth, producing an inverse-squared range dependence. The latter proved to be the case in SC-1 at 6.2 degrees. The pulse-length resolution at this angle is 2.83 miles, while the beamwidth dimension at the expected marking range is 2.36 miles; both referred to the lunar surface. At the AMR frequency of 9300 megacycles, the total amplitude factor in the nominal Muhleman reflectivity model is -0.55 db, the mean-slope parameter is 0.36, and the angle-dependent function is -3.36 db at 6.2 degrees, for a total power reflection coefficient of -3.91 db at 6.2-degree incidence. Preflight SC-1 AMR test data included a transmitted power of +62.37 dbm peak and a peak one-way antenna gain over isotropic of +36.3 db. Using the beamwidth-limited range equation, with inverse-squared range dependence, the predicted nominal received peak signal strength is -59.71 dbm at the expected marking range.

Predicted signal at longer ranges has been extrapolated backward from this value, at the rate of -6 db per octave of range, at the velocity of 1.623 miles per second, as shown in Figure 5.9-2. Plotted on this same graph are the corrected dbm equivalents of the unbiased values of telemetry channel R-14 (AMR automatic gain control), using calibration data for 3.0 microsecond pulses, the nearest value for which calibration is made, and a -3.0 db correction for the 6.0 microsecond stretched pulses actually received. Flight data appears to be virtually on the nominal prediction, thus confirming both the AMR design and the nominal Muhleman reflectivity model at the SC-1 approach angle.

The required AMR threshold for 0.999 cumulative probability of proper marking is -96.0 $\neq$ 3.0 dbm with 3.0 microsecond pulses. The preflight SC-1 AMR 3.0-microsecond threshold was measured as -93.6 dbm, corresponding with a 6.0-microsecond threshold at -96.6 dbm. Hence, at the time of the in-flight mark, SC-1 had essentially a +37 db margin above its 0.999 probability threshold.

5.9.7 ACKNOWLEDGEMENTS
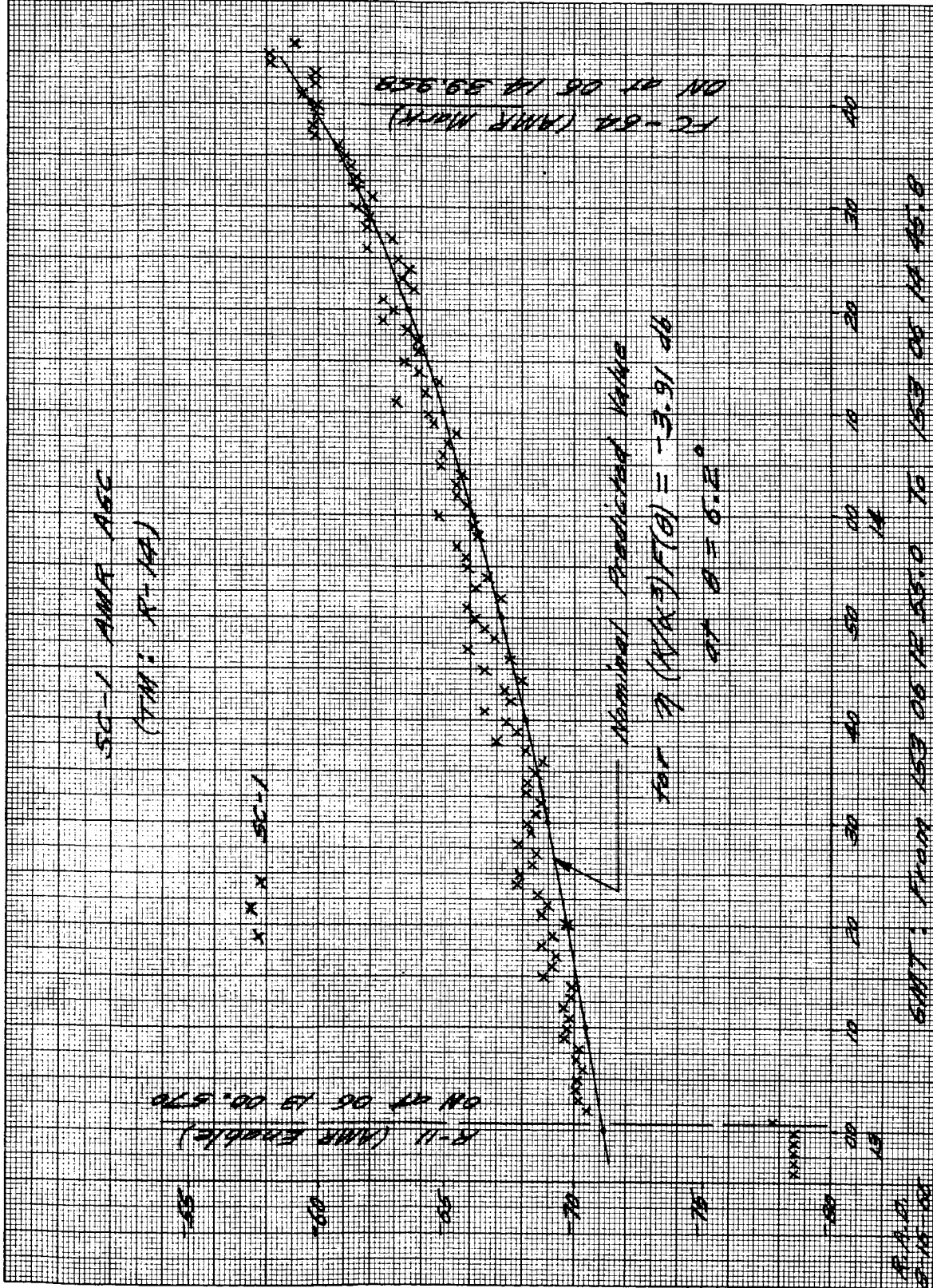
Figure 5.9-2. AMR Automatic Gain Control (R-14)

5.10   RADAR ALTIMETER AND DOPPLER VELOCITY SENSOR (RADVS)

5.10.1   INTRODUCTION

The RADVS is an integrated radar system that will measure slant range to the lunar surface and three spacecraft orthogonal velocity components with respect to the moon. These measurements will be supplied to the flight control electronics to allow continuous control of spacecraft flight parameters during vernier descent.

The doppler velocity sensor receiver circuits sample the energy radiated by the transmitter for comparison with the energy reflected from the lunar surface. The energy returning from the lunar surface will exhibit doppler frequency shifts proportional to the relative velocity along each beam axis. Since the three beam axes each contain velocity components proportional to velocities along more than one of the spacecraft orthogonal axes, it is necessary to combine the velocities so that an output will be obtained which will be a velocity vector meaningful in the spacecraft coordinate system. The horizontal components of velocity thus obtained (V_x and V_y) are used to align the thrust axis with the velocity vector during the lunar approach. The vertical velocity component obtained (V_z) is used in the altitude-velocity control system during the lunar approach.

RADVS performed normally throughout the descent. The only unexpected event was a minimum interval unlock of RADVS beam 3, attributed to passage of the main retro engine case just after its separation from the spacecraft. This was not a radar anomaly, since its operation was normal under such conditions. Mission A demonstrated the capability for an automatic terminal descent with the desired soft landing well within design values. This was accomplished by the entire flight control system using the radars as on-board sensors.

Surveyor Mission A provided the first high resolution radar data available on lunar reflectivity. While the first of a series of engineering models, it is felt that this first mission is not without significant value. Confirmation of the Muhleman reflectivity model with nominal coefficients, even at the limited number of incidence angles involved, is considered of major importance. For this reason, additional material has been included to clarify the model used, so that conclusions may be drawn in proper context of the definitions used. Both AMR automatic gain control and RADVS reflectivity signals provided useful data for evaluation of the model.

5.10.2   RADAR DISCRETE EVENTS

The time sequence of discrete events associated with radar operation is shown in Table 5.10-1. All times shown are GMT of receipt of telemetry data at DSIF 11 Goldstone. Only where necessary will times at the spacecraft be used. Significant events and time intervals will be noted in the discussion; the balance of those shown are included for reference. Accuracy of event time determination is limited by the telemetry sampling rate for the digital words involved. This was once per second for most signals while in telemetry mode 2 above the descent profile. In telemetry mode 3, effective just before profile capture, not only is the frame rate doubled, but also selected signals were sampled many times per frame. Critical events were then sampled 18 times per second, the highest rate used at the 11 bits/sec basic telecommunications rate throughout the descent.

5.10.3   ANOMALY DESCRIPTION

The only RADVS event that appeared initially to be an anomaly was a brief dropout on beam 3. Subsection 5.10.5.5 shows that this is probably caused by passage of the ejected retro case through the RADVS beam, in which case this performance would be normal.

5.10.4   PERFORMANCE ANALYSES

5.10.4.1   RADVS Turnon

RADVS on (prime power) occurred properly, essentially at retro ignition. Since high voltage is not required for this, the altimeter search function appeared on the analog range output, telemetry channel FC-35, during warmup. High voltage time-in is not observed directly in flight, but measured 24 seconds, typically, in flight acceptance test. Acquisition by every velocity beam, plus RODVS (reliable velocities), appeared within about 1 second of each other, the combination appearing at about 30 seconds after power on, typically 6 seconds after time-in. Altimeter beam acquisition, plus RORA (reliable range), appeared 9.0 seconds later, or about 39 seconds after retro ignition. This was just prior to retro thrust decay to 3.5 g, or 14 seconds prior to retro separation.

5.10.4.2   Conditions at Reliable Velocities (RODVS)

From main retro engine characteristics, flight conditions at RODVS are estimated as 55,000 feet altitude and 3280 fps velocity. With the spacecraft aligned with the total velocity, the latter value is equivalent to the maximum required doppler velocity sensor (DVS) capability of 3000 fps on each beam. The corresponding doppler frequency is 81.0 kHz, the nominal upper limit of the DVS wide-band search sweep. Nominal predicted signal strength at 55,000 feet with vertical attitude is -93.5 dbm, or 17.9 db above the -111.4 dbm nominal DVS wide-band tracker sensitivity at 81.0 kHz.

TABLE 5.10-1   SC-1 RADAR DISCRETE EVENTS

GMT (DSIF 11)	Signal	Event
153 06 10 00.073	R-1	AMR on
06 13 00.070	R-11	AMR enable
06 14 39.708	FC-64	AMR mark
06 14 47.558	FC-28	Vernier engine ignition
06 14 48.958	FC-29	Retro engine ignition
06 14 49.15	R-28	RADVS on
06 15 13	—	(Estimated RADVS high voltage time-in)
06 15 17.667	R-15, R-16	D1 lock, D2 lock
06 15 18.567	R-17	D3 lock
06 15 18.547	FC-34	RODVS (reliable velocities)
06 15 27.2	R-18	D4 (R) lock
06 15 27.547	FC-33	RORA (reliable range)
06 15 27.957	FC-30	Retro burnout
06 15 28.547	FC-63	Inertia switch
06 15 39.956	FC-31	Retro eject on
06 15 40.566	V-4	Retro ejected
06 15 42.4	FC-62, FC-42	Retro sequence off, RADVS descent on
06 15 42.566	$\overline{R\text{-}17}$	D3 unlock
06 15 42.356	$\overline{FC\text{-}34}$, $\overline{FC\text{-}33}$	RODVS off, RORA off
06 15 44.566	R-17	D3 lock
06 15 44.546	FC-34, FC-33	RODVS, RORA
06 16 06	(V_z data)	Segment acquisition
06 17 10.552	FC-37	1000-foot mark
06 17 28.754	FC-36	10 fps
06 17 34.203	FC-38	14-foot mark
06 17 35.74	—	Retro accelerometer indicates touchdown
06 17 35.651	K-13	Leg 2 touchdown
35.659	(strain gages)	Leg 1 touchdown
35.67		Leg 3 touchdown

From flight path analysis and command, the flight path angle at retro ignition was actually 6.2 degrees off the local lunar vertical, and the roll orientation placed beam 1 closer to vertical and beams 2 and 3 farther away. Telemetered reflectivity signal strengths at initial acquisition were -92.9, -96.2, and -95.5 dbm on beams 1, 2, and 3, respectively. It appears that each DVS beam acquired as soon as its velocity component decreased to the upper acquisition limit, with essentially nominal signal strength margin at that moment.

The sweeping range pattern on the analog range output during altimeter search disappeared at RODVS. With the appearance of velocity values, the entire altimeter search effect was depressed below the analog zero range level by the heavily negative V_z compensation to the altimeter converter during such high velocities. As V_z decreased, however, the still sweeping altimeter search function began to rise above zero, as confirmed by the indicated range output. This performance is entirely normal and did not represent an altimeter "false lock." At RORA, the indicated range values became reliable.

5.10.4.3   Conditions at Range Reliable (RORA)

From main retro engine characteristics, flight conditions at RORA are estimated as 36,000 feet altitude and 690 fps velocity. Correlation with telemetered values appears reasonable, recognizing that velocity was just coming out of telemetry saturation. Nominal predicted radar altimeter signal strength at 36,000 feet, with vertical attitude, is -87.8 dbm, or 27.1 db above the -114.9 dbm nominal radar altimeter wide-band tracker sensitivity at 80.0 kHz. Telemetered reflectivity signal strength at RORA was -96.0 dbm. A fraction of this difference may be attributed to attitude still slightly off vertical; the balance might indicate a few db attenuation by the still burning main retro plume (parallel with the radar altimeter beam), but this is rather conjectural. The estimated retro characteristics at RORA would produce a composite altimeter frequency of 76.6 kHz. Ryan says the upper RA sweep limit was above requirement, actually at 91.0 kHz in wide band. Since estimated retro characteristics are still changing rapidly in this region (230 fps decrease in velocity in the previous 1 second), and since the analog velocity was just coming out of telemetry saturation at the first correct analog range indication, it is highly probable that the altimeter beam first acquired as soon as the composite frequency (sum of scaled R_z plus scaled V_z) decreased to the upper acquisition limit, with about 19 db signal strength margin at that moment.

5.10.4.4   Operation During Retro Burn

There is no evidence yet available to contradict the conclusion that the RADVS was operating properly in the wide-band mode during retro engine burn (although not used for flight control at this time), and also that it switched to narrow band after retro burnout without loss of any beam and with no noticeable effect on any of its prime analog outputs: V_x, V_y, V_z, and R_z. The relatively small lateral velocities of about +70 fps for V_x and about -6 fps for V_y during retro tend strongly to confirm proper lock to the lunar

surface reflections and not to any spurious frequencies that might have been generated in the high vibrational environment of the main retro engine. Further, these lateral values were essentially constant as R_z and V_z varied smoothly through the region of retro burnout, and telemetry indicates continuity of all tracker locks and both reliable signals.

5.10.4.5 Loss of Lock After Retro Separation

With only one exception, this continuity of lock and reliable signals appears constant from first lock to touchdown. This exception is apparent from the analog traces. V_x is uninterrupted, but simultaneously there is a large positive excursion of V_y (which is normal for those conditions), a drop of V_z to essentially half its previous value, and a small increase in R_z caused by the V_z compensation effect. These occur together for about 2 seconds, after which all values are restored and continue properly. These are the necessary and sufficient indications of a brief dropout of beam 3. This was confirmed by the discrete events from digital words in telemetry, with proper concurrent off conditions of both reliable signals, preventing flight control utilization during that interval. Beam 3 relock and proper concurrent restoration of both reliable signals were also indicated.

Since this was the only unexpected radar event in the SC-1, it warrants further explanation. Telemetry signal FC-63 (inertia switch) is generated by sensing retro thrust decay below 3.5 g (earth g). An on-board delay of 12.0 seconds produces FC-31 (retro eject on), and an additional on-board delay of 2.15 seconds produces FC-42 (start RADVS descent). FC-42 defines the earliest instant of flight control switch to RADVS-sensed quantities, and then only if the reliable signals are also present. FC-42 plus FC-34 (RODVS) will switch attitude steering from inertial to RADVS V_x and V_y (lateral velocities). FC-42 plus FC-33 (RORA) will switch acceleration (thrust-sum) control to RADVS V_z and R_z (axial velocity and range). The time sequence indicates that retro passage through or nearly through beam 3 caused sufficient shadowing of the normal lunar signal path to cause beam 3 unlock in the interval from 2.0 to 4.0 seconds after retro separation. No false lock occurred, and all analog outputs were normal for the equivalent of CRO-DVS operation with beam 3 out. RODVS went off as it should, however, because its Conditional Reliable Operate (CRO) generation had been inhibited by more than 1 second of previous fully reliable DVS. RORA off is normal for an unlock of any one or more of beams 1, 3, 4, regardless of prior condition. Reappearance of both RODVS and RORA was normal with relock of beam 3. Since V_x is unaffected by beam 3, the essentially constant +70 fps value through this interval confirms that there was no spacecraft steering until after the beam 3 relock, indicating further that RODVS was off when FC-42 came on. Velocity data after relock indicates that steering was initiated upon restoration of RODVS and was completed within about 2 seconds. With RORA, acceleration command was maintained at 0.9 g (lunar g), because the sensed R_z and V_z values were above the descent segments.

5.10.4.6 Telemetry Signal Bias Corrections

Telemetry bias corrections were derived from post-touchdown readings. Table 5.10-2 shows the 130-millivolt value applicable to R_z, V_z, and the reflectivity signals. Table 5.10-3 shows biases of 583 3/4 bcd on V_x and 579 bcd on V_y. Table 5.10-4 shows corrected velocity data above the profile, including the beam 3 unlock interval. Table 5.10-5 shows corrected R_z, V_z data on the descent profile. Table 5.10-6 shows lateral velocity noise calculations.

TABLE 5.10-2.   SC-1 RADVS POSTLANDING BIAS IN R_z AND V_z

Time, GMT	Doppler Velocity V_z, FC-41, bcd
06:1744	29
	28
	28
	28
1745	29
	28
1746	29
	27
1748	29
	28
1749	29
	27
1750	29
	28
1751	29
	28
1753	29
	28
1754	30
	28
1755	30
	27
1756	30
	29
1758	30
	28
	28.538

TABLE 5.10-3. SC-1 RADVS LATERAL VELOCITIES

Time, GMT	Doppler Velocity V_x, FC-39, bcd	Doppler Velocity V_y, FC-40, bcd	Computed Biases			
			V_x, bcd	V_y, bcd	V_x, fps	V_y, fps
06 1616	584	576	+0 1/4	-3	+0.15	-1.76
1618	579	578	-4 3/4	-1	-2.78	-0.59
1619	584	581	+0 1/4	+2	+0.15	+1.17
1620	584	576	+0 1/4	-3	+0.15	-1.76
1621	585	579	+1 1/4	0	+0.73	0
1623	582	584	-1 3/4	+5	-1.03	+2.93
1624	579	579	-4 3/4	0	-2.78	0
1636	583	576	-0 3/4	-3	-0.44	-1.76
1638	583	578	-0 3/4	-1	-0.44	-0.59
1639	582	583	-1 3/4	+4	-1.03	+2.34
1640	582	582	-1 3/4	+3	-1.03	+1.76
1641	582	579	-1 3/4	0	-1.03	0
1643	583	578	-0 3/4	-1	-0.44	-0.59
1644	579	579	-4 3/4	0	-2.78	0
1645	582	578	-1 3/4	-1	-1.03	-0.59
1648	582	577	-1 3/4	-2	-1.03	-1.17
1649	582	579	-1 3/4	0	-1.03	0
1650	583	579	-0 3/4	0	-0.44	0
1651	583	579	-0 3/4	0	-0.44	0
1653	582	582	-1 3/4	+3	-1.03	+1.76
1654	583	577	-0 3/4	-2	-0.44	-1.17
1655	582	577	-1 3/4	-2	-1.03	-1.17
1656	583	579	-0 3/4	0	-0.44	0
1658	582	577	-1 3/4	-2	-1.03	-1.17
1659	582	582	-1 3/4	+3	-1.03	+1.76
06 1700	580	580	-3 3/4	+1	-2.20	+0.59

Table 5.10-3 (continued)

Time, GMT	Doppler Velocity V_x, FC-39, bcd	Doppler Velocity V_y, FC-40, bcd	Computed Biases			
			V_x, bcd	V_y, bcd	V_x, fps	V_y, fps
06 1710	581	580	-2 3/4	+1	-1.61	+0.59
1711	584	577	+0 1/4	-2	+0.15	-1.17
1713	583	576	-0 3/4	-3	-0.44	-1.76
1714	583	579	-0 3/4	0	-0.44	0
1715	583	579	-0 3/4	0	-0.44	0
1716	585	575	+1 1/4	-4	+0.73	-2.34
1718	582	577	-1 3/4	-2	-1.03	-1.17
1719	583	577	-0 3/4	-2	-0.44	-1.17
1721	583	579	-0 3/4	0	-0.44	0
1723	581	577	-2 3/4	-2	-1.61	-1.17
1724	583	579	-0 3/4	0	-0.44	0
1725	583	580	-0 3/4	+1	-0.44	+0.59
1726	583	577	-0 3/4	-2	-0.44	-1.17
1728	583	579	-0 3/4	0	-0.44	0
1729	583	577	-0 3/4	-2	-0.44	-1.17
1730	577	585	-6 3/4	+6	-3.96	+3.52
1731	585	575	+1 1/4	-4	+0.73	-2.34
1733	583	579	-0 3/4	0	-0.44	0
1734	581	579	-2 3/4	0	-1.61	0
1744	584	579				
1745	584	579				
1746	583	579				
1748	584	579				
1749	584	579				
1750	584	579				
1751	584	579				
1753	583	579				
1754	584	579				
1755	583	579				
1756	584	579				
1758	584	579				
Average	583 3/4	579				

TABLE 5.10-4. ADDITIONAL VELOCITY DATA RECOVERED
FROM RAW DATA TAPES*

Time, GMT	V_x, bcd	V_y, bcd	V_z, bcd	V_x, fps	V_y, fps	V_z, fps
06 1525	686	568	1023	+60.0	-6.4	779
1526	691	572	1023	+62.9	-4.1	779
1527	702	568	1023	+69.3	-6.4	779
1528	702	568	1023	+69.3	-6.4	779
1529	696	568	960	+65.8	-6.4	729
1530	696	572	830	+65.8	-4.1	628
1531	700	572	758	+68.1	-4.1	571
1532	696	574	710	+65.8	-2.9	534
1533	696	574	679	+65.8	-2.9	509
1534	694	575	655	+64.6	-2.3	491
1535	703	567	643	+69.9	-7.0	481
1536	697	572	633	+66.4	-4.1	473
1537	702	569	624	+69.3	-5.9	466
1538	702	574	620	+69.3	-2.9	463
1539	700	572	608	+68.1	-4.1	454
1540	703	574	604	+69.9	-2.9	450
1541	704	569	596	+70.5	-5.9	445
1542	709	564	587	+73.4	-8.8	438
	709	564	583	+73.4	-8.8	434
1543	703	597	578	+69.9	Region of beam 3 dropout, in which correct V_x, high V_y, low V_z, and high R_z values are all normal.	
	704	767	468	+70.5		
1544	707	1023	319	+72.2		
1545	707	1023	315	+72.2		
1546	638	548	572	+31.8	-18.2	426
1547	582	574	580	-1.0	-2.9	432
1548	583	582	579	-0.4	+1.8	431
1549	584	579	582	+0.1	0	434
1601	581	585	585	-1.6	+3.5	436

*Corrected for post-touchdown observed biases of 583 3/4 bcd on V_x, 579 bcd on V_y, and 20.8 fps on V_z.

TABLE 5.10-5. SC-1 RADVS BIAS-CORRECTED R_z AND V_z
WITHOUT COMMUTATION-CYCLE TIME CORRECTION

Time, GMT	R_z, feet	V_z, fps
06 1616	13304	392.7
1618	12448	382.5
1619	12056	375.4
1620	11704	367.5
1621	11352	361.2
1623	10648	346.3
1624	10256	338.4
1636	6736	253
1638	6232	240
1639	5992	231
1640	5800	223
1641	5528	217
1643	5136	204
1644	4896	200
1645	4704	197
1648	4120	181
1649	3960	176
1650	3768	173
1651	3568	169
1653	3256	160.7
1654	3104	157.5
1655	2944	152.9
1656	2784	149.8
1658	2372	142.0
1659	2360	138.8
06 1700	2240	134.9

Table 5.10-5   (continued)

Time, GMT	R_z, feet	V_z, fps (First Word Only)
06 1710	992 (low deviation)	106.4
1711	776.8 (high deviation)	105.0
1713	768.8	93.3
1714	690.8	86.2
1715	602.8	80.8
1716	518.8	75.4
1718	378.0	64.4
1719	315.2	59.7
1721	211.6	45.7
1723	137.6	30.1
1724	110.0	23.8
1725	90.4	15.9
1726	70.8	15.9 (14.4, second word)
1728	47.6	9.7
1729	39.6	8.1
1730	34.0	3.4 (4.2, second word)
1731	32.0	4.2 (3.4, second word)
1733	20.0	5.0 (5.0, second word)
06 1734	12.4	3.4 (3.4, second word)

Table 5.10-5 (continued)

Time, GMT	FC-35, volts dc		R_z, feet	FC-41, fps	
	Biased	Unbiased		Biased	Unbiased
06 1600	2.712	2.582	20,656	440	438
1604	2.419	2.289	18,312	440	438
1605	2.360	2.230	17,840	442	440
1606	2.311	2.181	17,448	442	440
1607	2.262	2.132	17,056	439	437
1609	2.150	2.020	16,160	429	427
1610	2.096	1.966	15,728	423	421
1611	2.038	1.908	15,264	418	416
1613	1.935	1.805	14,440	409	407
1614	1.881	1.751	14,008	404	402
1615	1.837	1.707	13,656	399	397
1625	1.378	1.248	9,984	332	330
1626	1.334	1.204	9,632	325	323
1628	1.251	1.121	8,968	310	308
1629	1.212	1.082	8,656	303	301
1631	1.133	1.003	8,024	288	286
1633	1.070	0.940	7,520	275	273
1634	1.031	0.901	7,208	265	263
1635	1.006	0.876	7,008	258	256
1701	0.391	0.261	2,088	134	132
1704	0.342	0.212	1,696	125	123
1705	0.327	0.197	1,576	122	120
1706	0.312	0.182	1,456	119	117
1708	0.283	0.153	1,224	113	111
1709	0.268	0.138	1,104	111	109

TABLE 5.10-6. ESTIMATED NOISE ON V_x AND V_y

Time, GMT	V_x', bcd	$V_x-\bar{V}_x'$, bcd	$(V_x-\bar{V}_x)^2$, bcd	V_y', bcd	$V_y-\bar{V}_y'$, bcd	$(V_y-\bar{V}_y)^2$, bcd
06 1616	+0 1/4	+1.8	3.24	-3	-3	9
1618	-4 3/4	-3.2	10.24	-1	-1	1
1619	+0 1/4	+1.8	3.24	+2	+2	4
1620	+0 1/4	+1.8	3.24	-3	-3	9
1621	+1 1/4	+2.8	7.84	0	0	0
1623	-1 3/4	-0.2	0.04	+5	+5	25
1624	-4 3/4	-3.2	10.24	0	0	0
1636	-0 3/4	+0.8	0.64	-3	-3	9
1638	-0 3/4	+0.8	0.64	-1	-1	1
1639	-1 3/4	-0.2	0.04	+4	+4	16
1640	-1 3/4	-0.2	0.04	+3	+3	9
1641	-1 3/4	-0.2	0.04	0	0	0
1643	-0 3/4	+0.8	0.64	-1	-1	1
1644	-4 3/4	-3.2	10.24	0	0	0
1645	-1 3/4	-0.2	0.04	-1	-1	1
1648	-1 3/4	-0.2	0.04	-2	-2	4
1649	-1 3/4	-0.2	0.04	0	0	0
1650	-0 3/4	+0.8	0.64	0	0	0
1651	-0 3/4	+0.8	0.64	0	0	0
1653	-1 3/4	-0.2	0.04	+3	+3	9
1654	-0 3/4	+0.8	0.64	-2	-2	4
1655	-1 3/4	-0.2	0.04	-2	-2	4
1656	-0 3/4	+0.8	0.64	0	0	0
1658	-1 3/4	-0.2	0.04	-2	-2	4
1659	-1 3/4	-0.2	0.04	+3	+3	9
06 1700	-3 3/4	-2.2	4.84	+1	+1	1
Σ	-40 1/2	-0.2*	58.04	0	0	120
$\times \frac{1}{26}$	-1.558	-0.077*	2.23	0	0	4.62
rms, bcd			1.49			2.15
rms, fps			1.16			1.68
06 1710	-2 3/4	-1.58	2.50	+1	+1.8	3.24
1711	+0 1/4	+1.42	2.02	-2	-1.2	1.44
1713	-0 3/4	+0.42	0.18	-3	-2.2	4.84
1714	-0 3/4	+0.42	0.18	0	+0.8	0.64
1715	-0 3/4	+0.42	0.18	0	+0.8	0.64
1716	+1 1/4	+2.42	5.86	-4	-3.2	10.24
1718	-1 3/4	-0.58	0.34	-2	-1.2	1.44
1719	-0 3/4	+0.42	0.18	-2	-1.2	1.44
1721	-0 3/4	+0.42	0.18	0	+0.8	0.64
1723	-2 3/4	-1.58	2.50	-2	-1.2	1.44
1724	-0 3/4	+0.42	0.18	0	+0.8	0.64
1725	-0 3/4	+0.42	0.18	+1	+1.8	3.24
1726	-0 3/4	+0.42	0.18	-2	-1.2	1.44
1728	-0 3/4	+0.42	0.18	0	+0.8	0.64
1729	-0 3/4	+0.42	0.18	-2	-1.2	1.44
1730	-6 3/4	-5.58	31.2	+6	+6.8	46.24
1731	+1 1/4	+2.42	5.86	-4	-3.2	10.24
1733	-0 3/4	+0.42	0.18	0	+0.8	0.64
06 1734	-2 3/4	-1.58	2.50	0	+0.8	0.64
Σ	-22 1/4	-0.02*	55.06	-15	+0.2*	91.16
$\times \frac{1}{19}$	-1.171		2.90	-0.790		4.80
rms, bcd			1.703			2.19
rms, fps			1.33			1.71

*Residual error in approximate calculations.

The following calculations apply to the RADVS postlanding bias in R_z and V_z (see Table 5.10-2):

$$28.54 \text{ bcd} = 22.3 \text{ fps}$$

but

$$V_z = +1.5 \text{ fps with trackers unlocked}$$

$$= 1.92 \text{ bcd}$$

$$\text{Bias} = +20.8 \text{ fps } (V_z)$$

$$= +52.0 \text{ feet } (R_z < 1000)$$

$$= +1040 \text{ feet } (R_z > 1000)$$

$$\text{Bias} = +0.130 \text{ volt on } R_z, V_z, \text{ and all reflectivity signals}$$

(Correction to raw data is -0.130 volts dc)

5.10.4.7 Descent Profile

Acquisition of the stored descent profile occurred at 153:06:16:06. The remainder of the descent was almost perfectly nominal. Noise on all four RADVS primary outputs has been evaluated by flight control analog simulation and determined to be within the preflight noise model values. Range and velocity values, corrected only for telemetry bias as above, are plotted in Figure 5.10-1 against the preflight computer-predicted descent profile. The performance was excellent. The last range value just prior to the 1000-foot range mark was 996 feet. The scale factor change caused by this mark accounts for the predicted lag in the telemetry conditioning circuit of the range values just under 1000 feet. Even the approach to each linearized descent segment from an acceleration saturated state followed exactly the computed flight control performance for the SC-1 configuration.

5.10.4.8 Touchdown

Unambiguous and precise cutoff and touchdown values for all parameters are complicated by both telemetry sampling granularity and the mutual dependence of variables. The cutoff mark was off at 06:17:34.147, and was on at 06:17:34.203. Taking the average of the three strain gage indications as touchdown at 06:17:35.55, the free-fall time was between 1.35 and 1.41 seconds, versus a nominal of 1.38; V_z at cutoff was lower than the nominal 5.0 fps (but well within the ±1.5 fps system tolerance). Best estimates, not only fitting all data but also well within all system requirements are as follows: cutoff at 4 fps, R_z of 14 feet, and h_o of 12 feet; 1.5-second fall; and 12 fps at touchdown. No error can be found in the altimeter readings; hence, no radar evidence of effects attributable to lunar dust can be found in the SC-1 data.
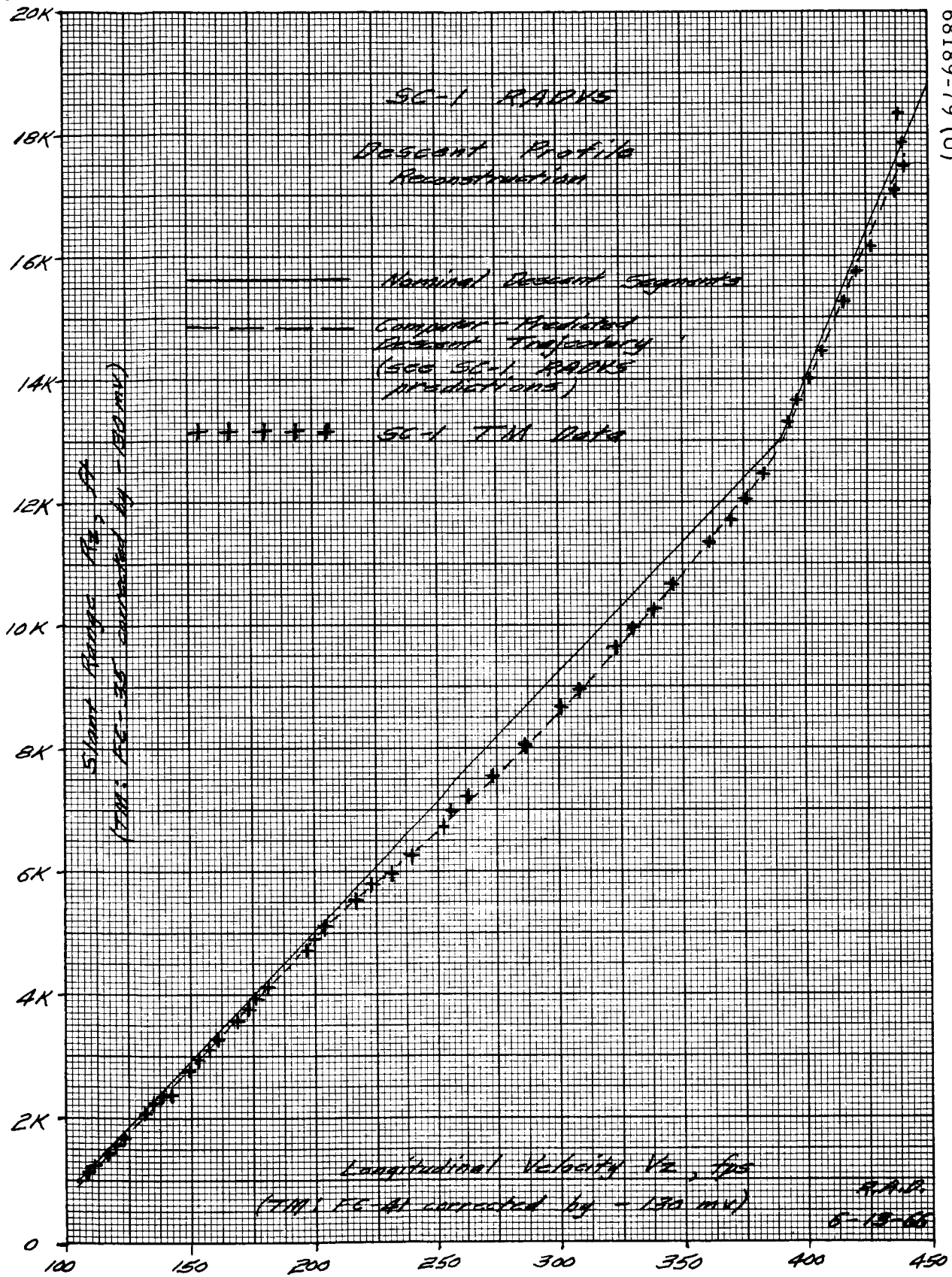
a) Above 1700 Feet

Figure 5.10-1. RADVS Descent Profile Reconstruction
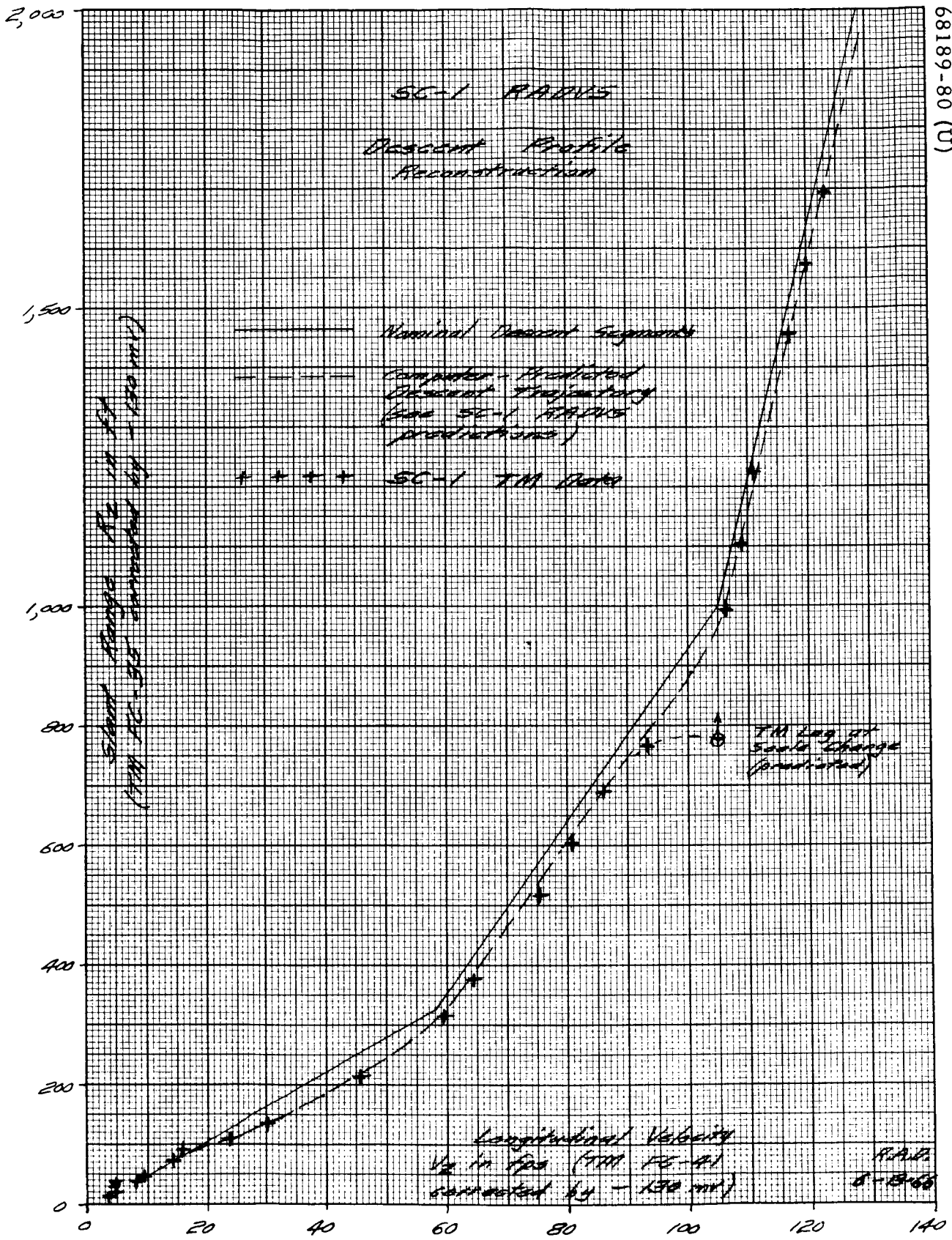
b) Below 1700 Feet

Figure 5. 10-1 (continued). RADVS Descent
Profile Reconstruction

5.10.4.9 Radar Reflectivity Analysis

RADVS gain-switching events and reflectivity signal amplitudes for the Muhleman reflectivity model with nominal coefficient were derived, described, and presented in a succession of radar description and SC-1 prediction packages. The unusual difference in frequency responses seen by the signal circuits and by the gain-switching threshold circuits was treated in detail, with predictions of unusually high gain states at very low altitudes, confirmed by the SC-1 data. Mid-gain states were predicted on all beams prior to the descent profile. SC-1 also verified these predictions, except that beam 4 had frequent switching in and out of the mid-gain state. This is characteristic of higher scintillation on the vertical, which was expected but not predicted quantitatively. Low-gain state predictions were followed rather well, as were brief returns to mid-gain during about the last 10 seconds, with predicted reflectivity saturation actually occurring in this interval on the DVS beams. Beam 4 was more irregular, again being essentially on the vertical.

The most useful portion of the data for RADVS reflectivity evaluation is from profile acquisition (just under 18,000 feet in SC-1) down to about 1000 feet. In this region, all DVS beams were in a quite stable gain-state condition, and beam 4 gain-switching was less frequent. Spacecraft attitude is essentially vertical after profile acquisition, allowing the assumption of knowledge of beam incidence angles without a precise nine-dimensional trajectory reconstruction. Also, once on the profile, range and velocity are directly related in predictable fashion. This relationship permits direct prediction of power and velocity as functions of range, frequency as a function of velocity (and of range also, for the altimeter beam only), preamplifier rolloff correction as a function of frequency, and reflectivity signal amplitude as a function of power, rolloff, and reflectivity calibration test data, all related explicitly to real-time remaining to touchdown for the predicted descent. Confirmation that this profile was indeed followed by the SC-1 permitted direct application of these predictions to the SC-1 RADVS reflectivity signal evaluation.

In evaluating test data on SC-2, a long-standing test procedure error of 4.2 db was discovered. It has been established that this error existed in all SC-1 Hughes test data on RADVS sensitivity and reflectivity calibrations. As a result, all previous reflectivity predictions have been revised to account for this difference. This correction explains most or all of the original appearance of signal strengths from 4 to 6 db below nominal, placing them now in the region within about 0 to 2 db below nominal. Beams 1 and 2 (Figures 5.10-2a and b) appear very close to nominal, if the few gain-switching transients are ignored, with minor scintillation suggestive of Rayleigh scattering. Beam 3 (Figure 5.10-2c) is very similar except that its average is about 2 db below nominal in the region above 1000 feet, while almost nominal below 1000 feet, possibly correlating with terrain to the northeast.
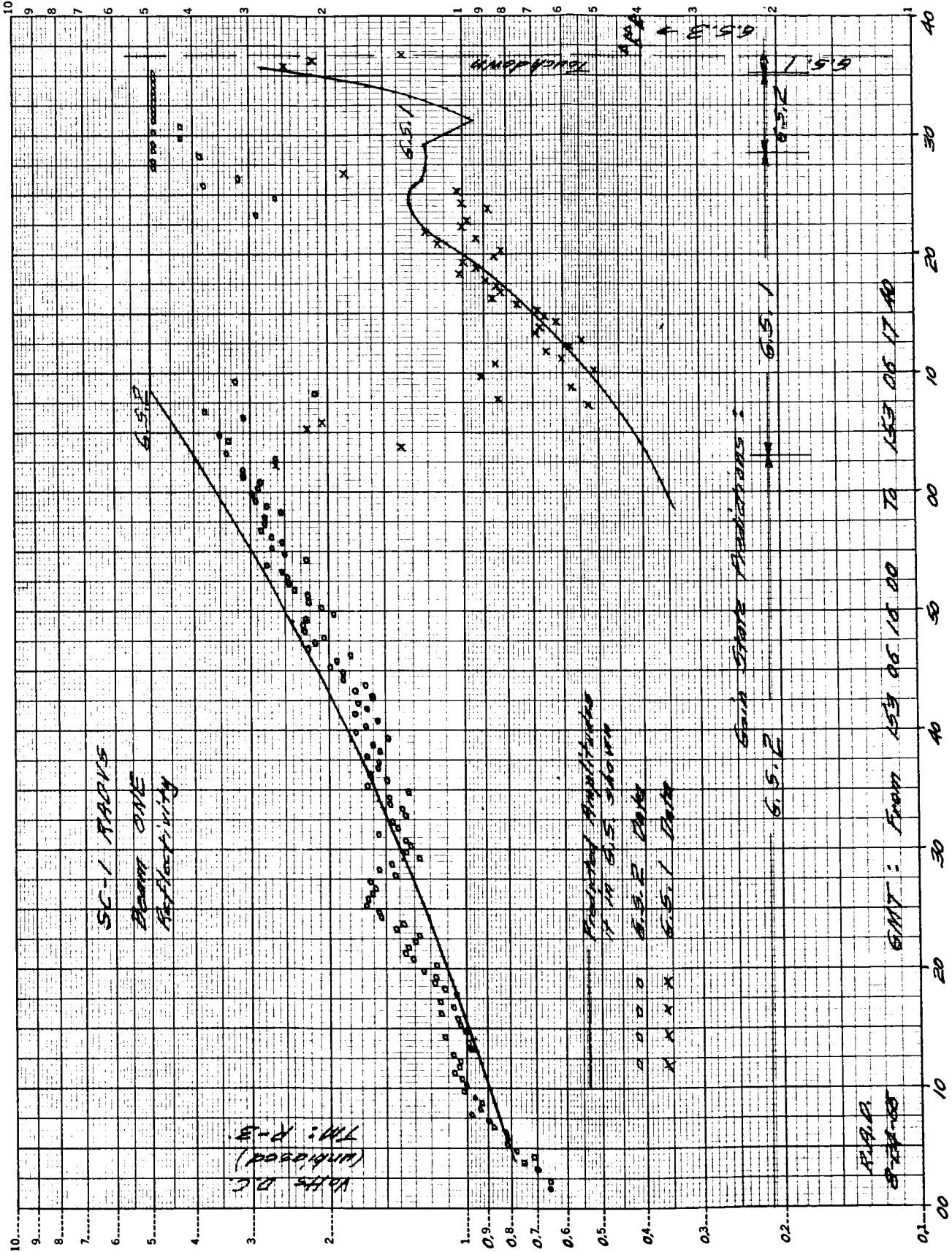
a) Beam 1

Figure 5.10-2. RADVS Reflectivity
Telemetry volts

b) Beam 2

Figure 5.10-2 (continued). RADVS Reflectivity
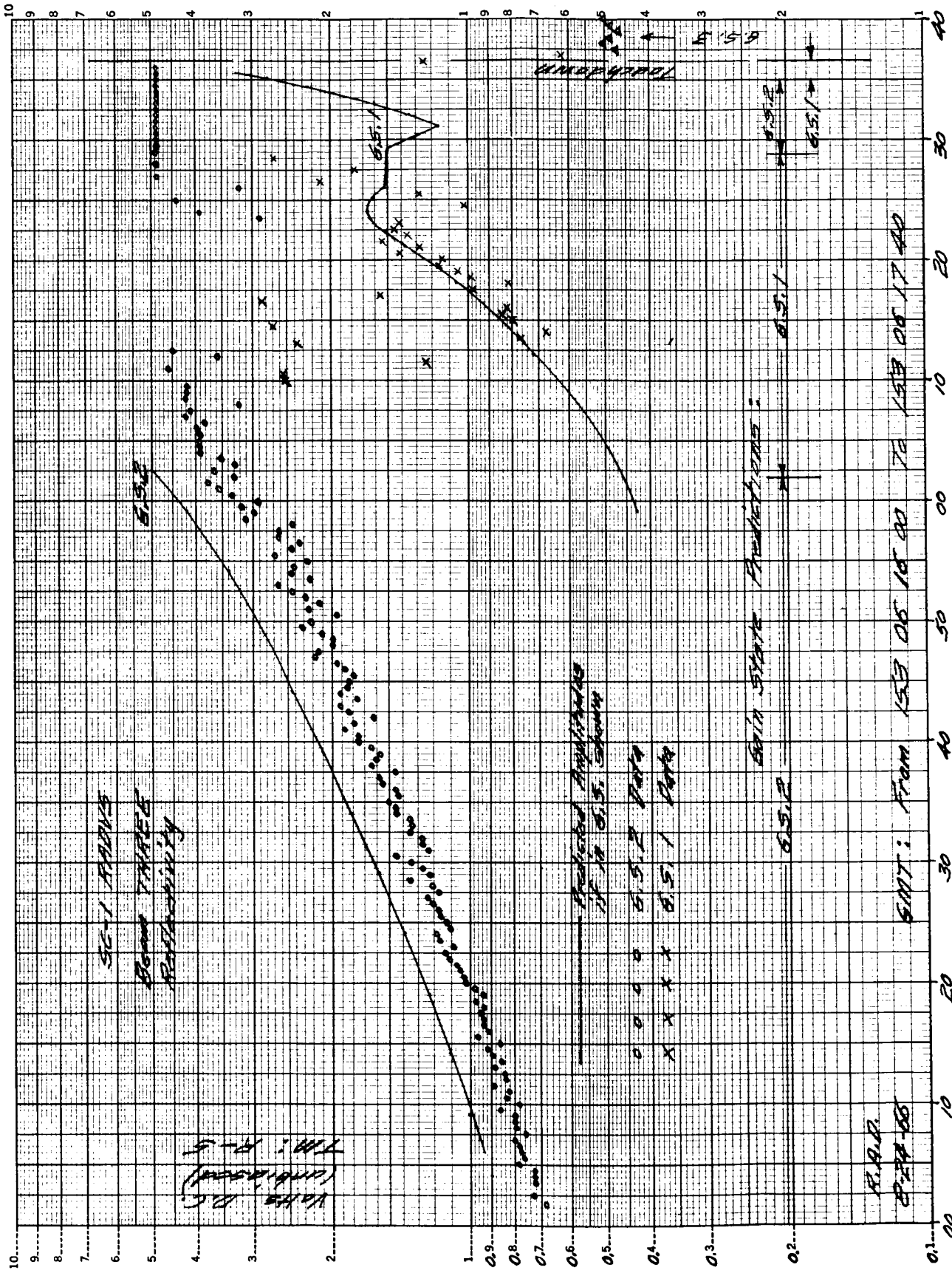
Telemetry volts

c) Beam 3

Figure 5.10-2 (continued). RADVS Reflectivity
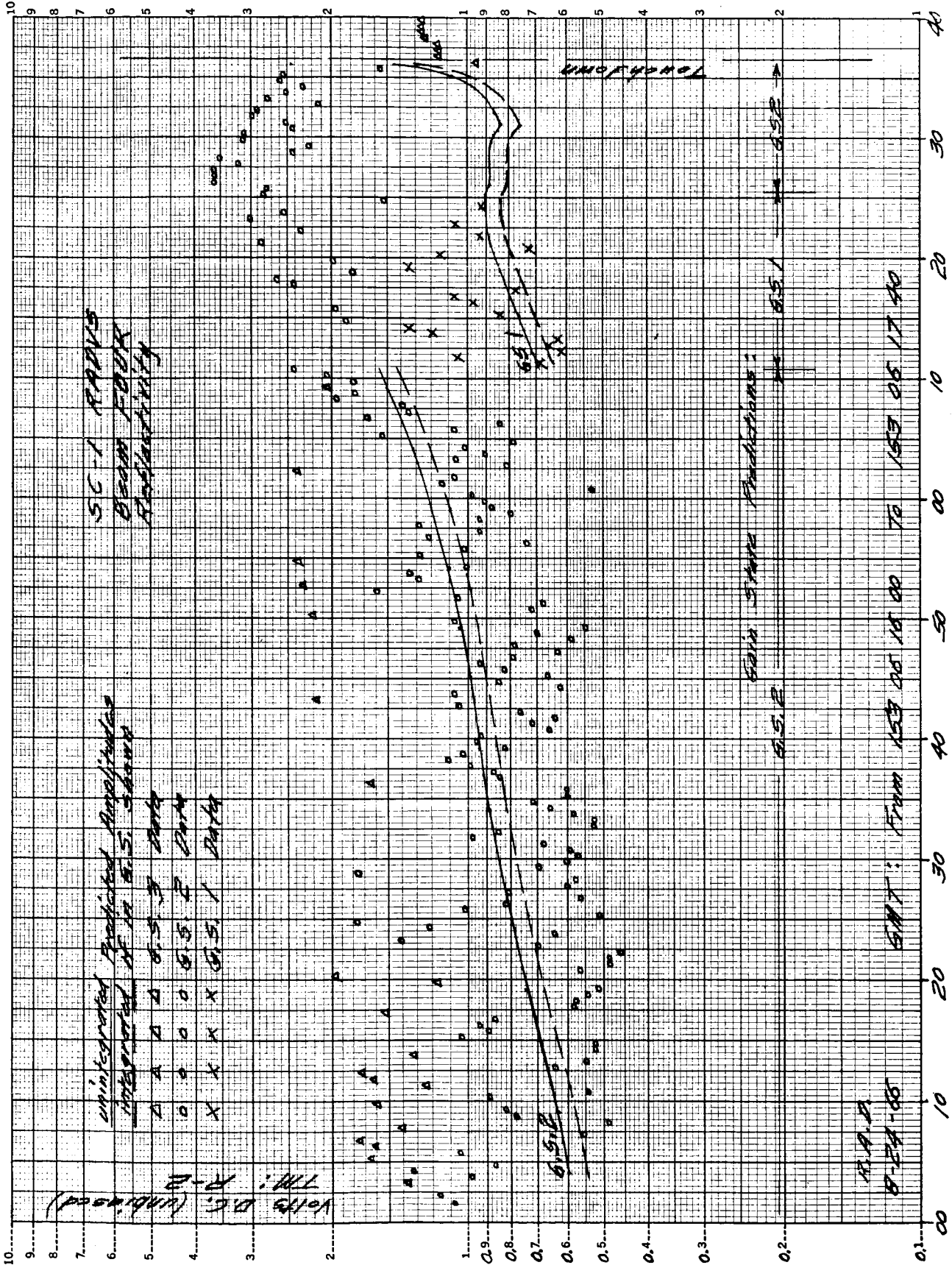
Telemetry volts

Figure 5.10-2 (continued). RADVS Reflectivity

d) Beam 4

If only the mid-gain state data is considered on beam 4 (Figure 5.10-2d), it averages about 2 db below nominal, with apparent scintillation of about ±5 db. Including the other gain states suggests an average 2 to 3 db below nominal, with apparent scintillation of ±6 or 7 db. Further work is required to account quantitatively for noise limiting at low analog voltages and/or minor nonlinearity at the higher voltages, which may have actually compressed the scatter of real data on beam 4 in particular. One advantage of plotting the analog voltage itself, as in Figure 5.10-2, is to show the response of the circuit involved. Conversion to dbm, through the calibration data, has also been performed as shown in Figures 5.10-3 and 5.10-4. In these plots, any compression on the analog voltage scale, especially of an artificially large separation of dbm values in adjacent gain states. JPL (W. E. Brown, Jr.) is also precessing all this data in several ways, including amplitude distribution functions and their effects upon data as it would be telemetered.

Figures 5.10-2 through 5.10-4 are adequate justification for the following conclusions:

1) Average values are from 0 to 2 db below nominal, suggesting no basis for present modification of the expected nominal coefficient.

2) All DVS beams were consistent while in a gain-state, showing minor variations which may correlate with terrain features, but otherwise having only a db or two of scintillation suggestive of Rayleigh scattering.

3) Higher scintillation on the vertical (altimeter) beam is not unexpected, but might include some minor plume interaction.

5.10.4.10 Reflectivity Model

The reflectivity model used by Hughes and approved by JPL for design evaluation of both Surveyor radars was developed by Dr. Duane O. Muhleman, then of JPL, now at Cornell and still active on the Surveyor scientific evaluation team's electrical working group. Based upon total hemispheric return to earth-based radars, the surface backscatter function (identical with the impulse response of a spherical surface), after convolution with pulse shape and determination of a single wavelength-dependent parameter (the mean slope at the radar wavelength) provided excellent fit of complete pulsed return time responses observed from earth without the artificiality of earlier specular-plus-diffuse models. The angular dependence function of the Muhleman model was therefore not only physically logical in its assumptions and mathematically rigorous in its derivation but also experimentally justified for earth-based observation.
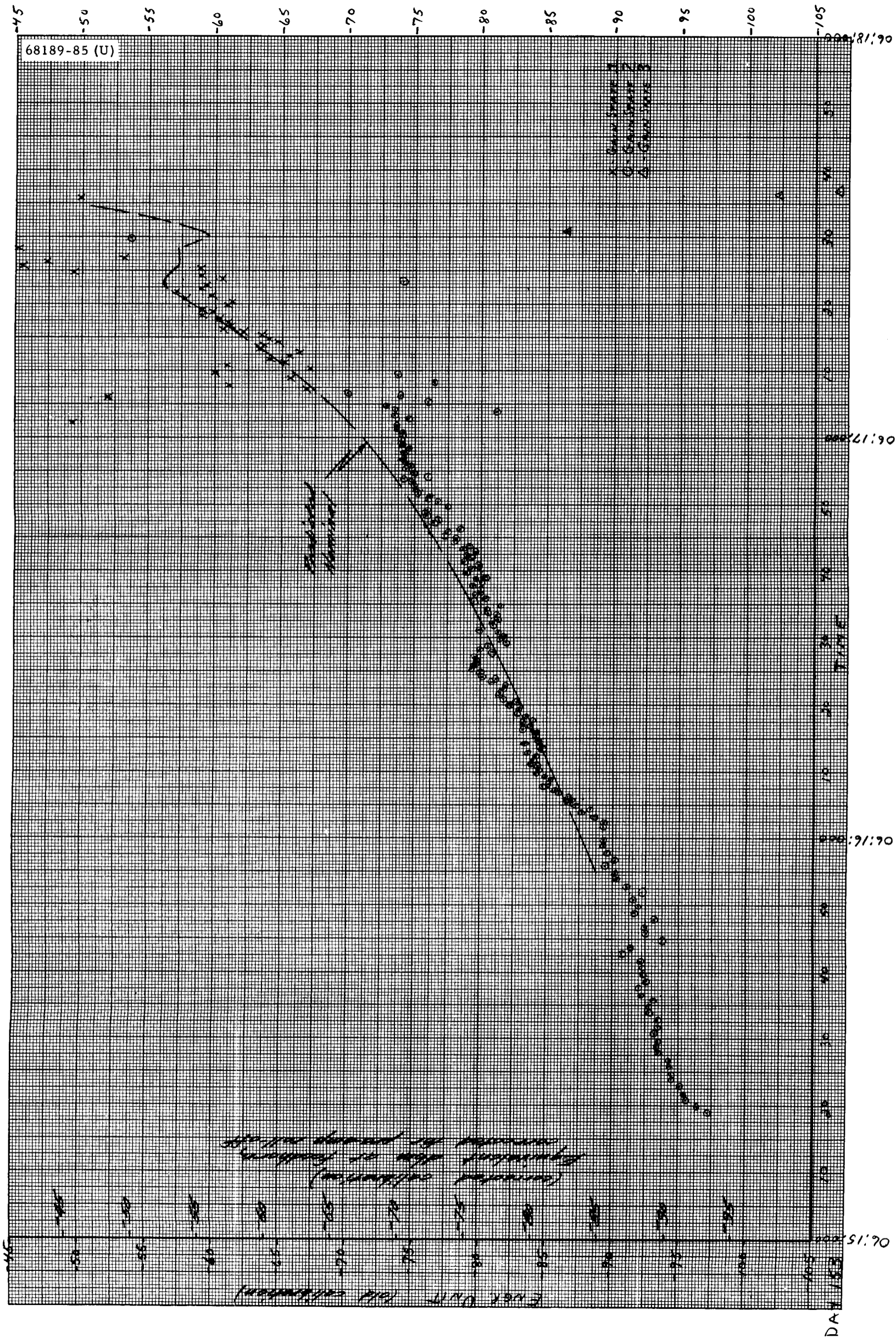
a) Beam 1

Figure 5.10-3. RADVS Reflectivity
Corrected dbm at feedhorn

5.10-23

68189-85 (U)

5·10·24
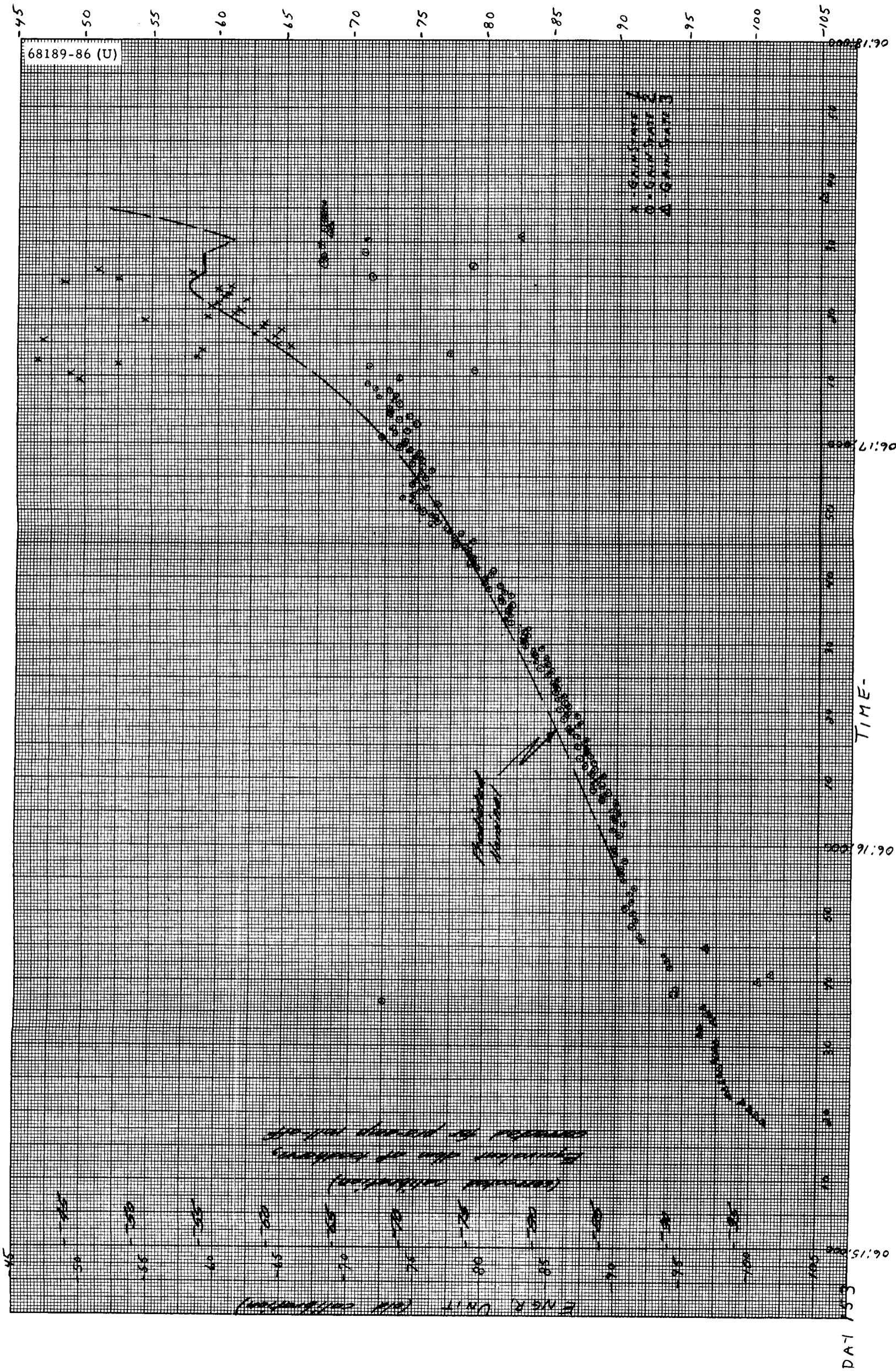
b) Beam 2

Figure 5.10-3 (continued). RADVS Reflectivity
Corrected dbm at feedhorn

5.10-25

TIME

ENGR UNIT
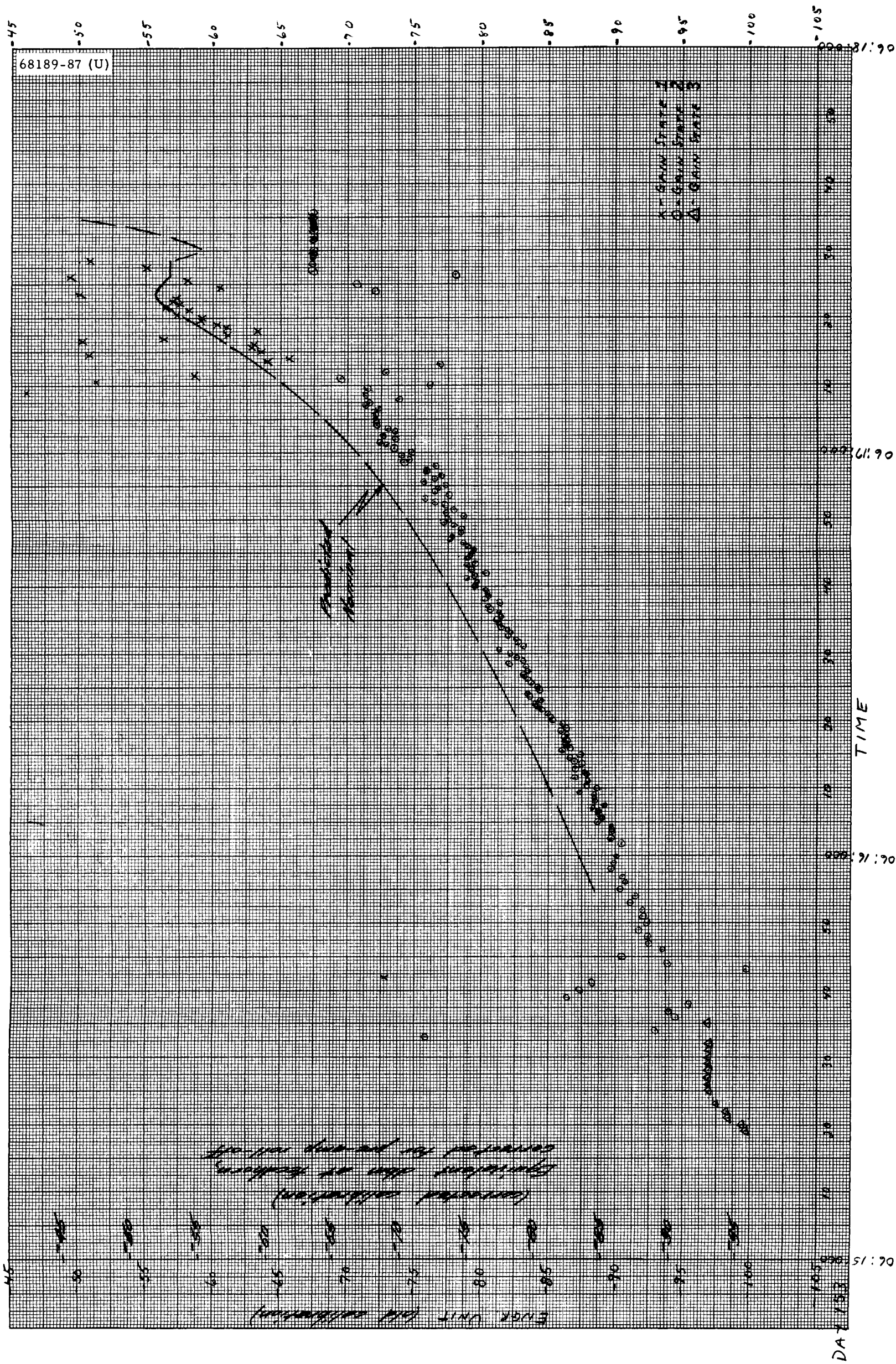
c) Beam 3

Figure 5.10-3 (continued).   RADVS Reflectivity

Corrected dbm at feedhorn

5.10-27

5.10-28
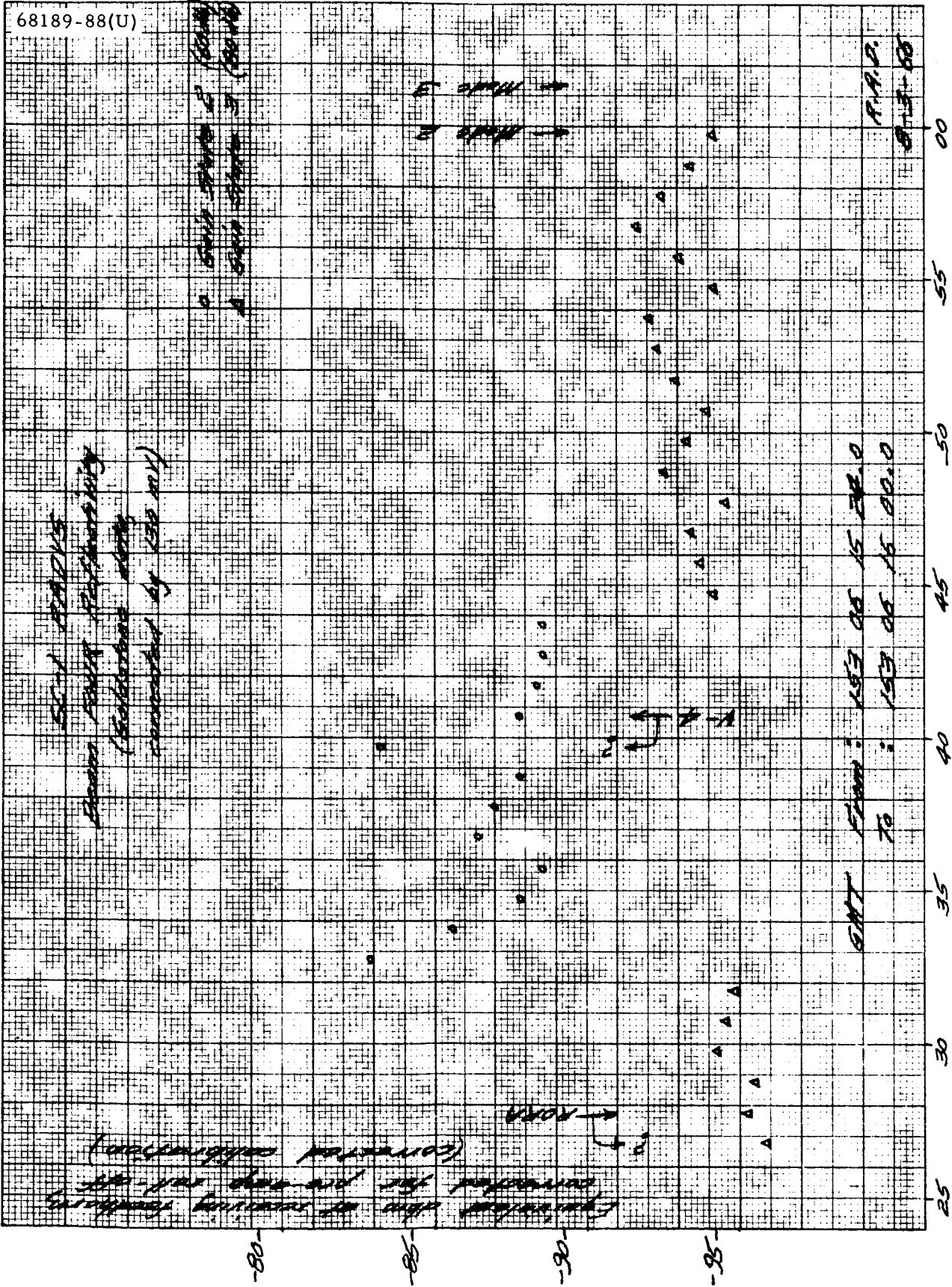
68189-88(U)

a) From 06:15:24 to 06:16:00 GMT

Figure 5.10-4. RADVS Beam 4 Reflectivity
Corrected dbm at feedhorn
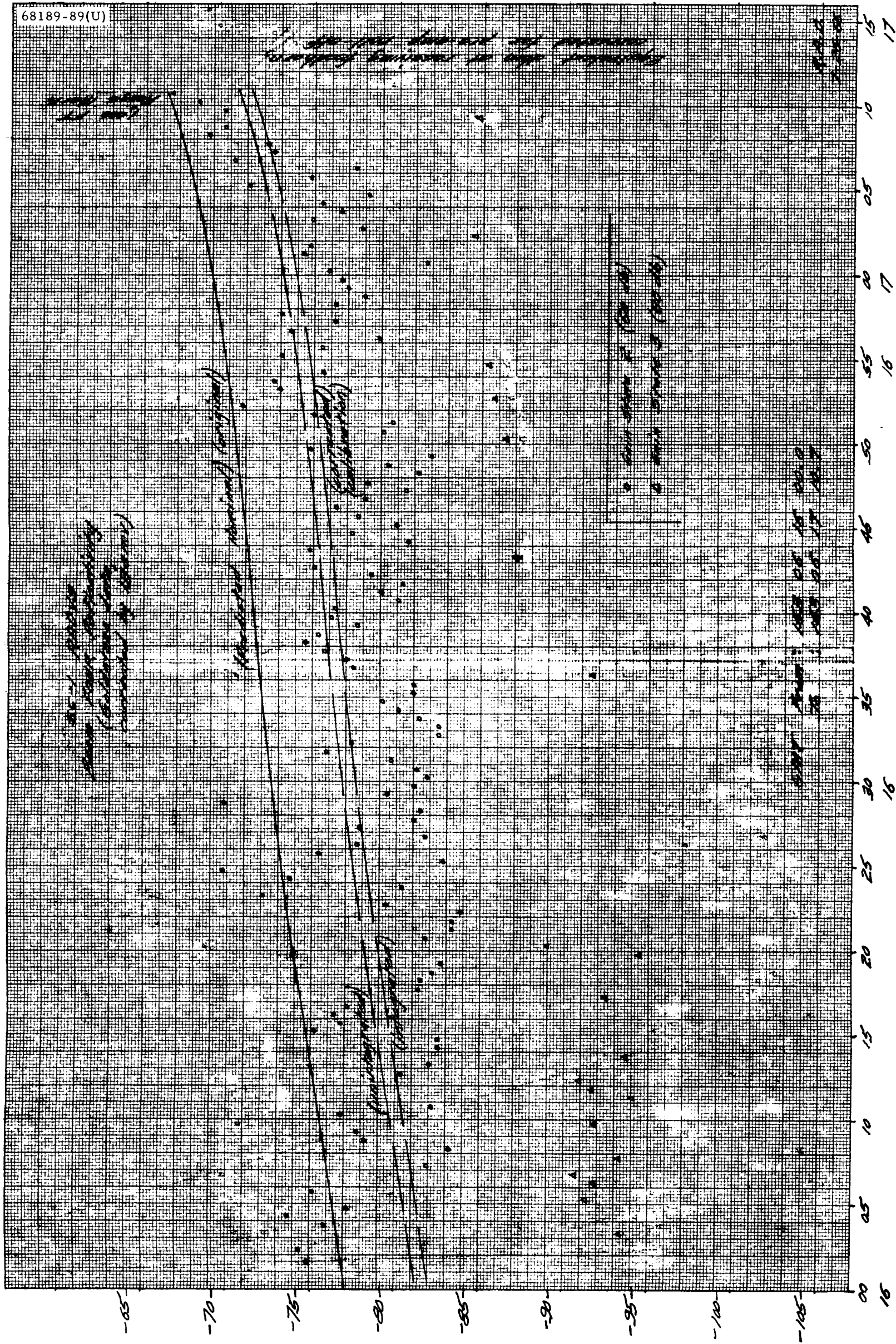
b) From 06:16:00 to 06:17:10 GMT

Figure 5.10-4 (continued). RADVS Beam 4 Reflectivity
Corrected dbm at feedhorn

5.10-31

5-10-32
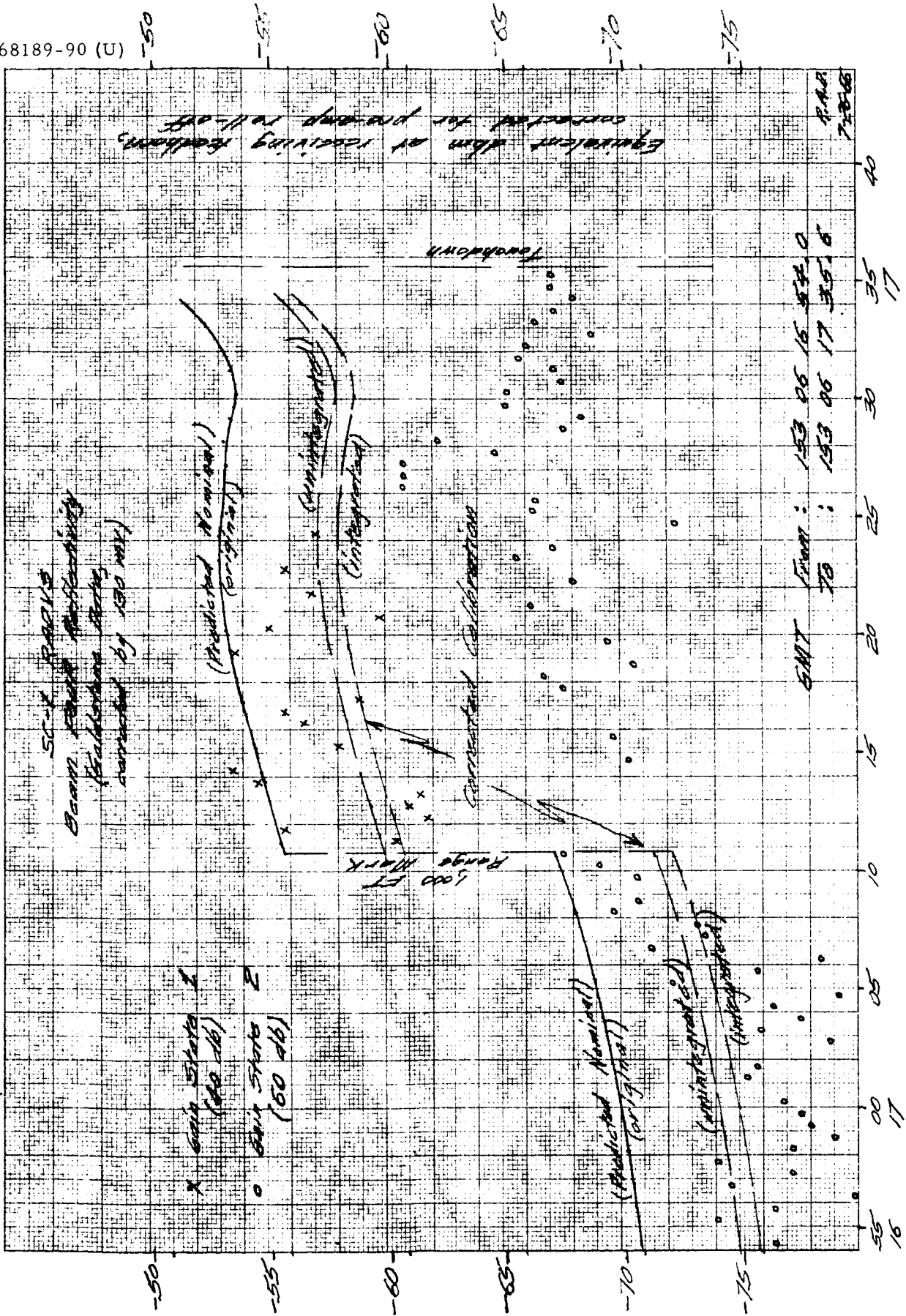
c) From 06:17:00 to touchdown, GMT

Figure 5.10-4 (continued). RADVS Beam 4 Reflectivity
Corrected dmb at feedhorn

Two major questions remained, however. Discrepancies of a few decibels among the numerous workers in the field, plus basic uncertainties in absolute calibration of such data, made the total amplitude coefficient more difficult to define with certainty. The value 0.075, or -11.25 db, was agreed to among JPL, Hughes, and Ryan as the most probable dimensionless coefficient — the ratio of actual radar cross section to that of a lossless and isotropic sphere of lunar radius, where the latter is simply the area of the projected lunar disc. The capability to operate at 6 db (required) or at 10 db (desired) below nominal reflectivity was made a functional requirement for Surveyor radars. This requirement is being retained as insurance against local terrain variation effects.

Muhleman's derivation permitted rigorous treatment of density functions for orientation of normals to ray-optic surface facets, without their size being specified or even appearing in the derivation. For earth observations this was not a conceptual obstacle, but its validity for high resolution at close ranges was really unknown. While certain questions still remain about scintillation on the vertical, both the nominal coefficient and high resolution applicability appear to have been confirmed by Surveyor Mission A for those incidence angles evaluated. It is hoped that later missions will succeed in augmenting this confirmation at other incidence angles.

The angular dependence derived by Muhleman is:

$$F(\theta) = \alpha^3 / (\sin \theta + \alpha \cos \theta)^3$$

where θ is the angle of incidence (off local lunar vertical) and α is a wavelength-dependent mean-slope parameter. Subjecting this function to a hemispheric integral normalization condition requires that it be multiplied by a factor (K/α^3). Pertinent values are:

AMR: $\quad \alpha = 0.36 \quad K/\alpha^3 = +10.70$ db

RADVS: $\quad \alpha = 0.39 \quad K/\alpha^3 = +10.15$ db

The total reflectivity factor is therefore:

$$\eta (K/\alpha^3) F(\theta)$$

where

$$\eta = 0.075$$

This total factor is essentially a power reflection coefficient of the lunar surface, normalized to a lossless and isotropic sphere. It may also be viewed as the effective radar cross section per unit of surface area, a dimensionless ratio. It is not the surface backscatter function, which is cosine θ times this factor.

Introduction of this factor into the radar range equation produces the following:

$$\frac{dP_r}{d\Omega} = \frac{P_t \lambda^2 G^2 g^2 \eta \, F(\theta)}{(4\pi)^3 r^4}$$

as the backscattered power density per unit solid angle subtended at the antenna of a monostatic, single beam CW lunar radar, where the one-way antenna power pattern has a peak gain g relative to isotropic and an angular dependence g normalized to unity maximum.

Separate derivation has shown that the CW power received by a gaussian model antenna pattern becomes:

$$P_r = \frac{P_t \lambda^2 (G/2) \eta \, (K/\alpha^3) \, F(\theta)}{(4\pi R)^2}$$

where R = slant range to the lunar surface along the direction of peak gain g. The factor 1/2 in (G/2) is the approximate result of integration, over the beamwidth, of the simultaneously varying slant range, incidence angle variation of $F(\theta)$, and the pattern factor g. For a gaussian pencil beam, this factor of 1/2 is exact within less than 0.10 db for angles beyond 10 degrees by a first order error analysis. Right on the vertical, however, because of the essentially exponential nature of $F(\theta)$ at small angles, integration over the beamwidth produces a received power 0.78 db less than indicated by the above range equation with the factor 1/2 and at $\theta = 0$ degree. (This beamwidth-limited integration is analogous to convolution of the sharp exponential with pulse length when considering pulsed return from the immediate vicinity of the sub-earth point.) Numerical evaluation of interest in SC-1 produces reflectivity factors of -3.91 db at 6.2 degrees for the AMR; -10.04 db at 25 degrees for RADVS; and -1.10 db unintegrated, or -1.88 db integrated, at 0 degree for RADVS.

The design features of both radars, all pertinent background material for performance analysis and evaluation, detailed description of postmission data forms and procedures for their evaluation, plus specific SC-1 test data affecting the interpretation, were detailed in "Post-Mission Analyses Involving Radar Data." Documents concerning predicted preamplifier signal strength and gain-switching behaviour of test model T-2 (5-20-66), a similar treatment of flight model A-21 (5-30-66), and a complete SC-1 prediction package (5-31-66) were also prepared. Although unpublished by Hughes, these documents were distributed in reproduced handwritten form to other members of both the SCAT and the scientific electrical group, prior to Mission A.

The predicted R_z, V_z values are shown in Figures 5.10-5 through 5.10-8. The nominal db-budget parameters are then indicated. Nominal signal calculations are shown in Tables 5.10-7 and 5.10-8, and are graphed in Figures 5.10-9 and 5.10-10. Individual beam parameters measured for SC-1 (subsection 5.10.4.12) are the basis for the calculations in Tables 5.10-9 through 5.10-12 in Figure 5.10-11. ETR calibration data (by W. T. Black) is shown in Tables 5.10-13 and 5.10-14. Reflectivity calibration curves are shown in Figures 5.10-12 through 5.10-15. All these were necessary to develop the nominal predictions in Figures 5.10-2 through 5.10-4.

5.10.4.11   Total Signal Power Calculations

The total signal power received on any one beam has been well documented as follows:

$$P_r = \frac{P_t \, (G/2) \, \lambda^2}{(4 \, \pi R)^2} \left[\eta \, (K/\alpha^3) \, F(\theta) \right]$$

where

$$F(\theta) = \alpha^3 \left[\sin \theta + \alpha \cos \theta \right]^{-3}$$

$$\alpha = 0.39$$

$$\eta \, (K/\alpha^3) = -1.10 \text{ db (nominal moon)}$$

The standard DVS db-budget for minimum margin hardware has consistently been (see page 5.10-62):
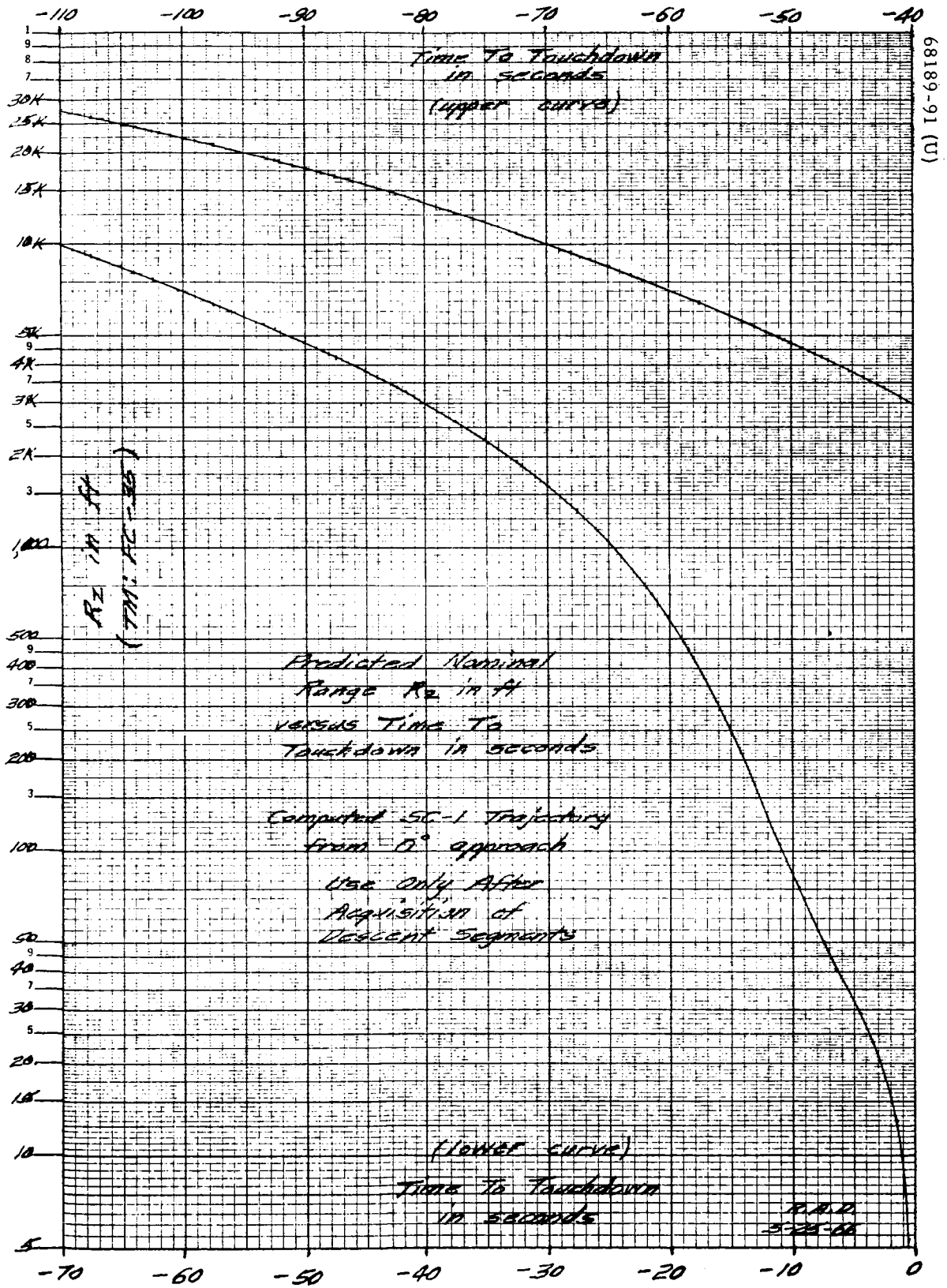
Figure 5.10-5. Predicted Nominal Range R_z
Versus Time (Acquisition to Touchdown)
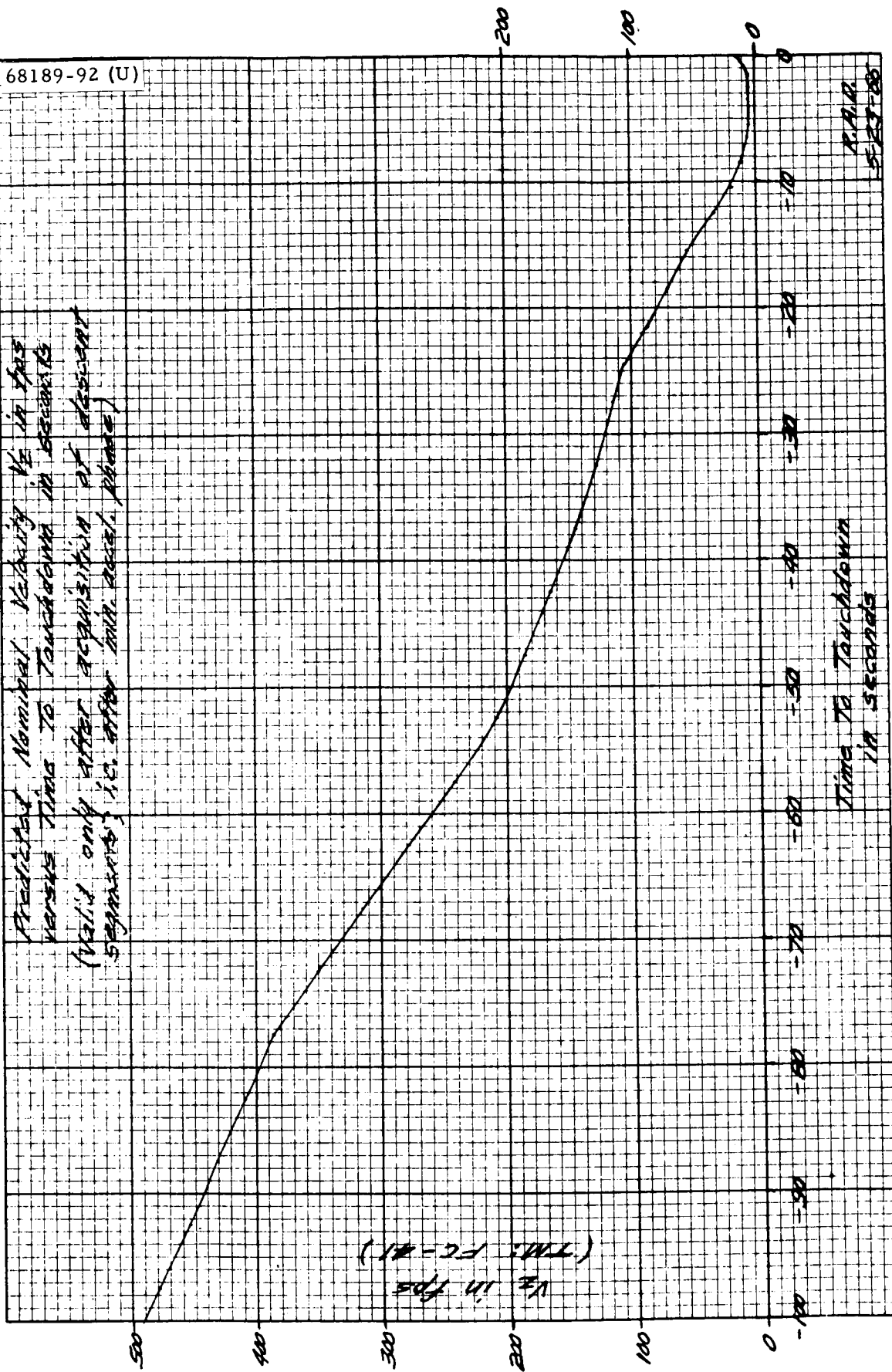
Figure 5.10-6. Predicted Nominal Velocity V_z Versus Time (Acquisition to Touchdown)

5.10-38
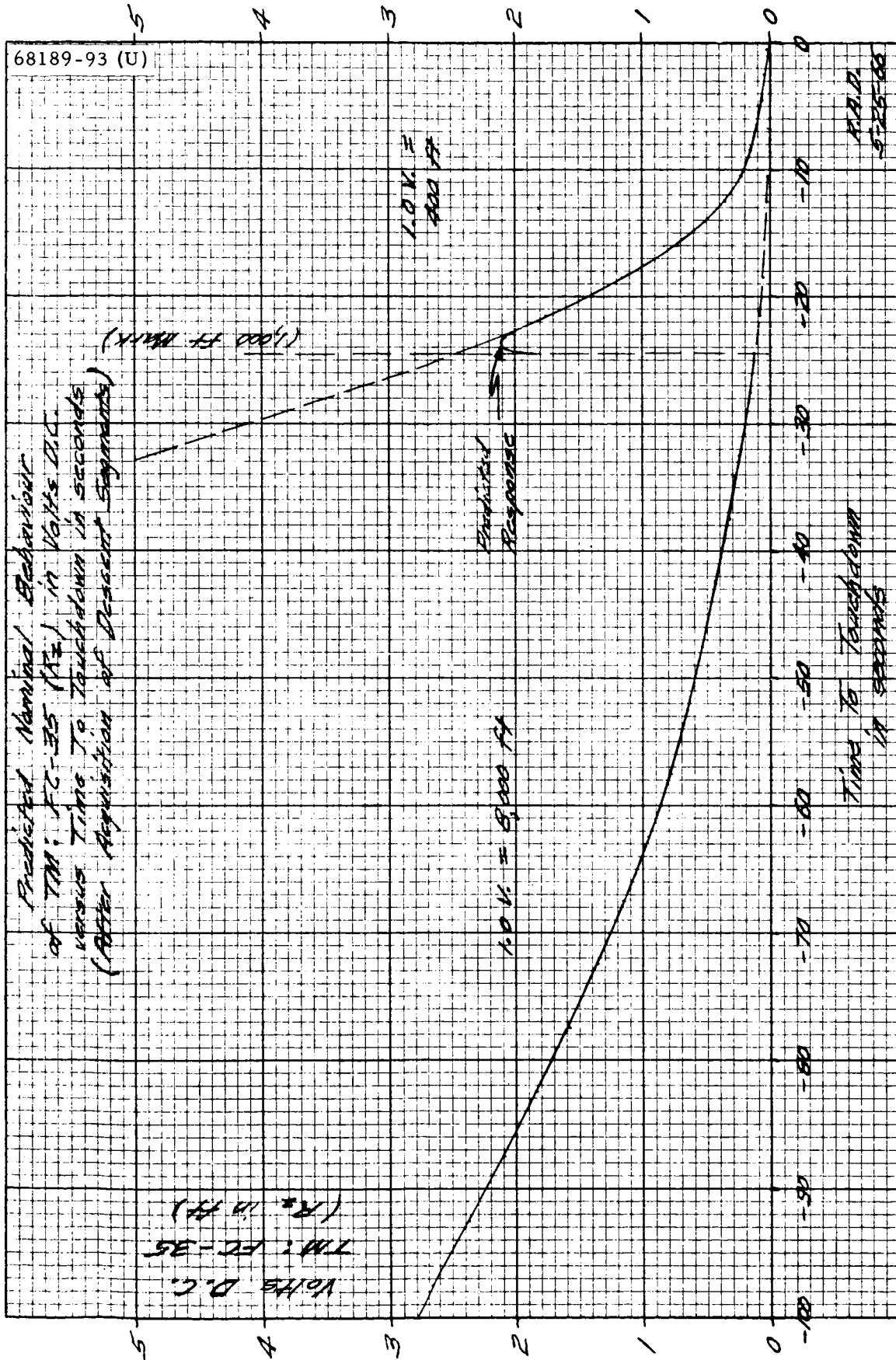
Figure 5.10-7. Predicted Nominal Behavior of R_z Versus Time (Acquisition to Touchdown)

5.10-39

1.0 V = 160 fps

Time To Touchdown in seconds
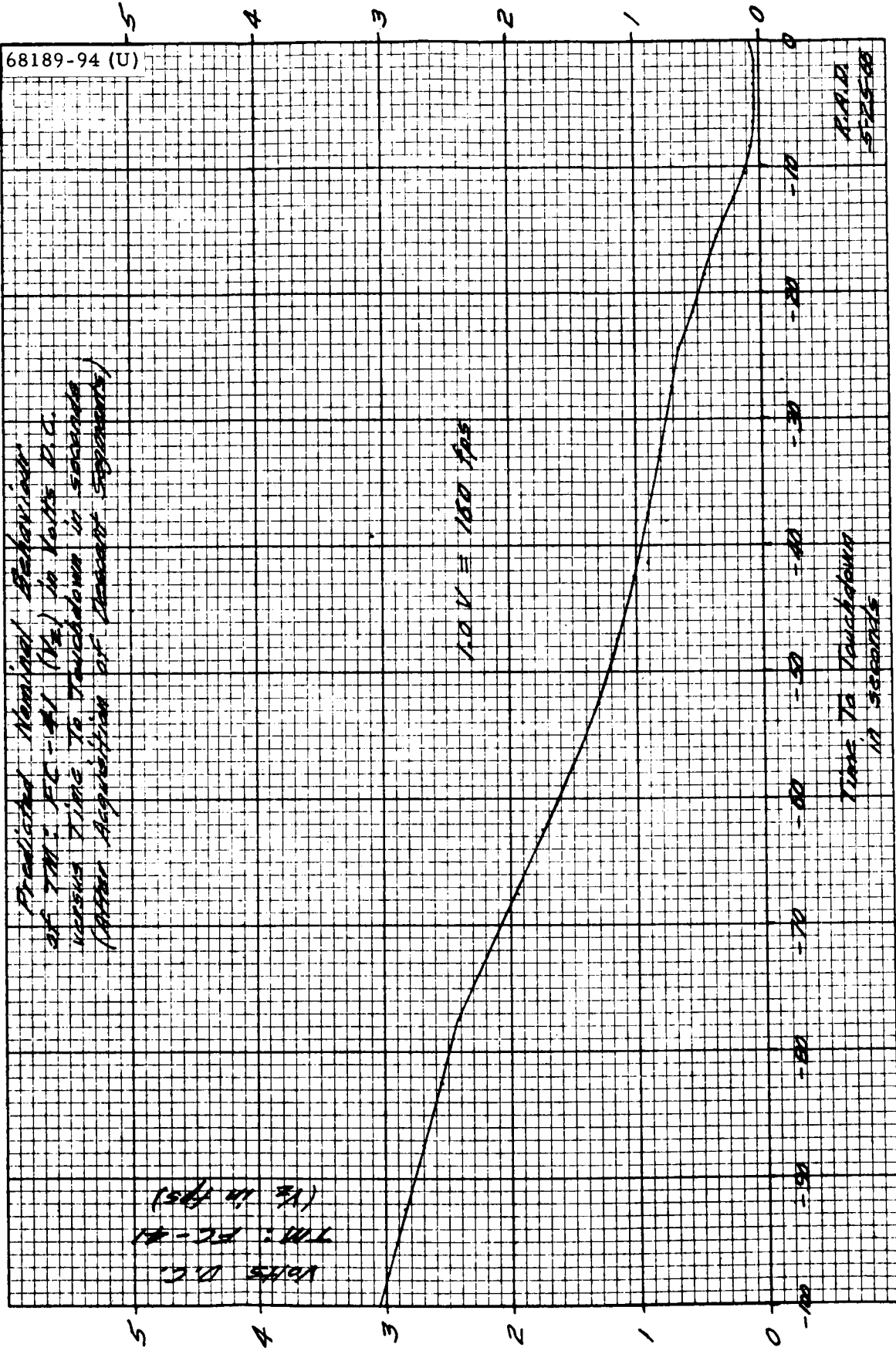
Figure 5.10-8. Predicted Nominal Behavior of V_z Versus Time (Acquisition to Touchdown)
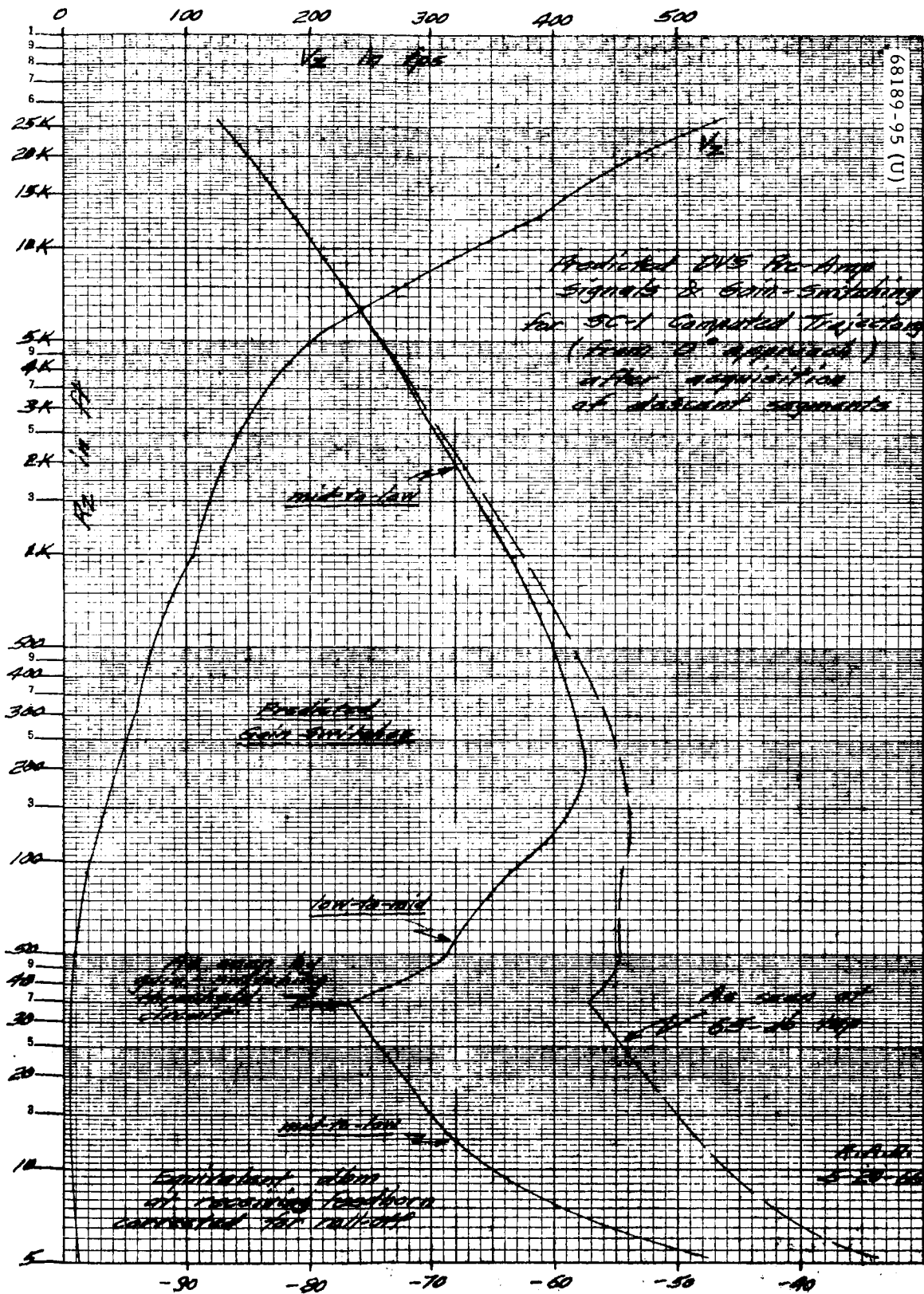
Figure 5.10-9. Predicted DVS Preamplifier
Signals and Gain-Switching
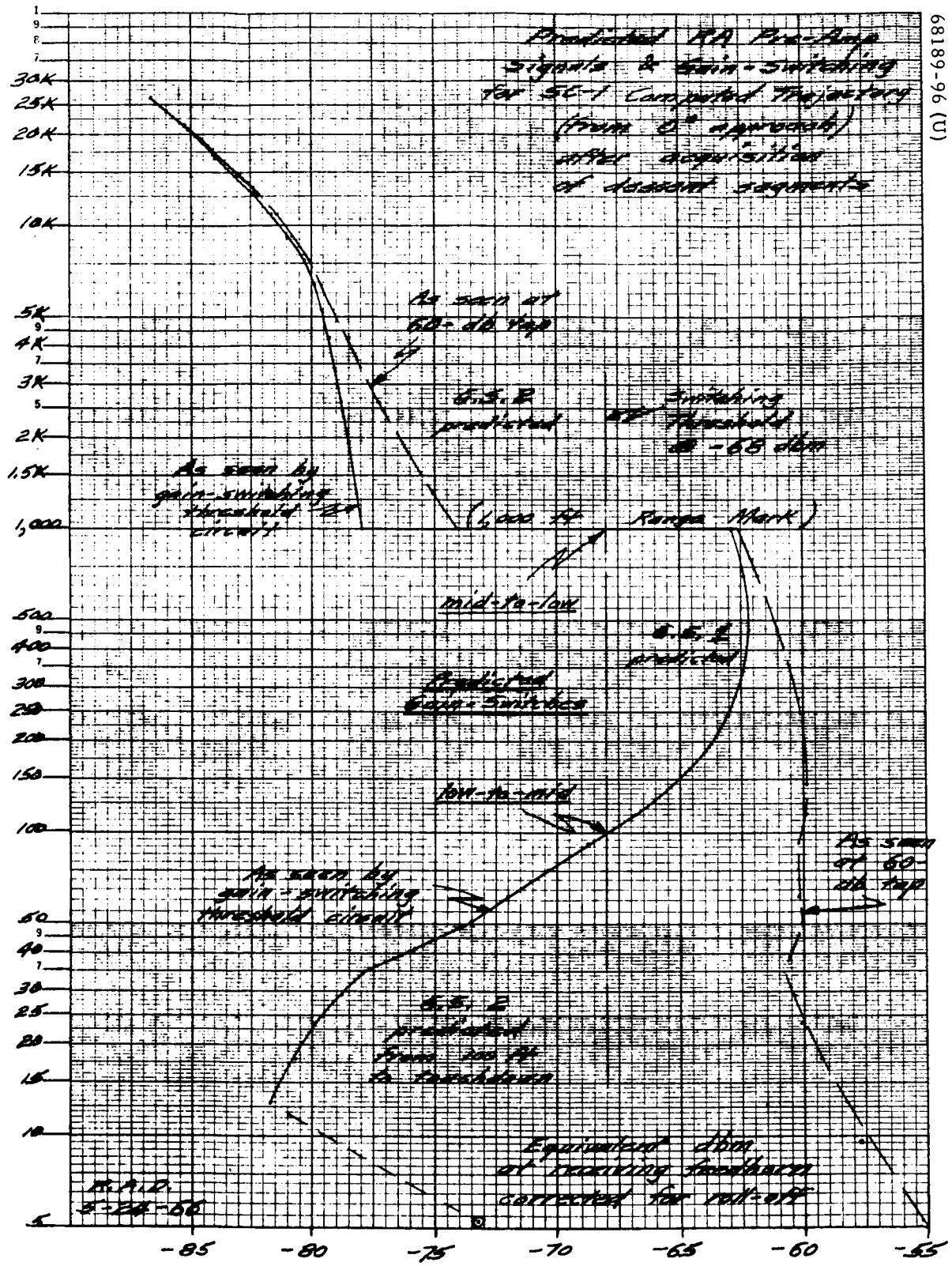
Figure 5.10-10. Predicted RA Preamplifier
Signals and Gain-Switching

SC-71 RADVS Beam ONE

Predicted Pre-Amp Signals
and Guid-Switching

after missed signal acquisition
& for nominal lunar reflectivity

As seen at
65-db top

As seen at
gain-switching
threshold circuit

(corrected)

(original)

Predicted
switching
Threshold

8-27-65
R.A.D.
5-30-66

Equivalent dbm at Feedhorn
corrected for roll-off

Time To Touchdown
in seconds
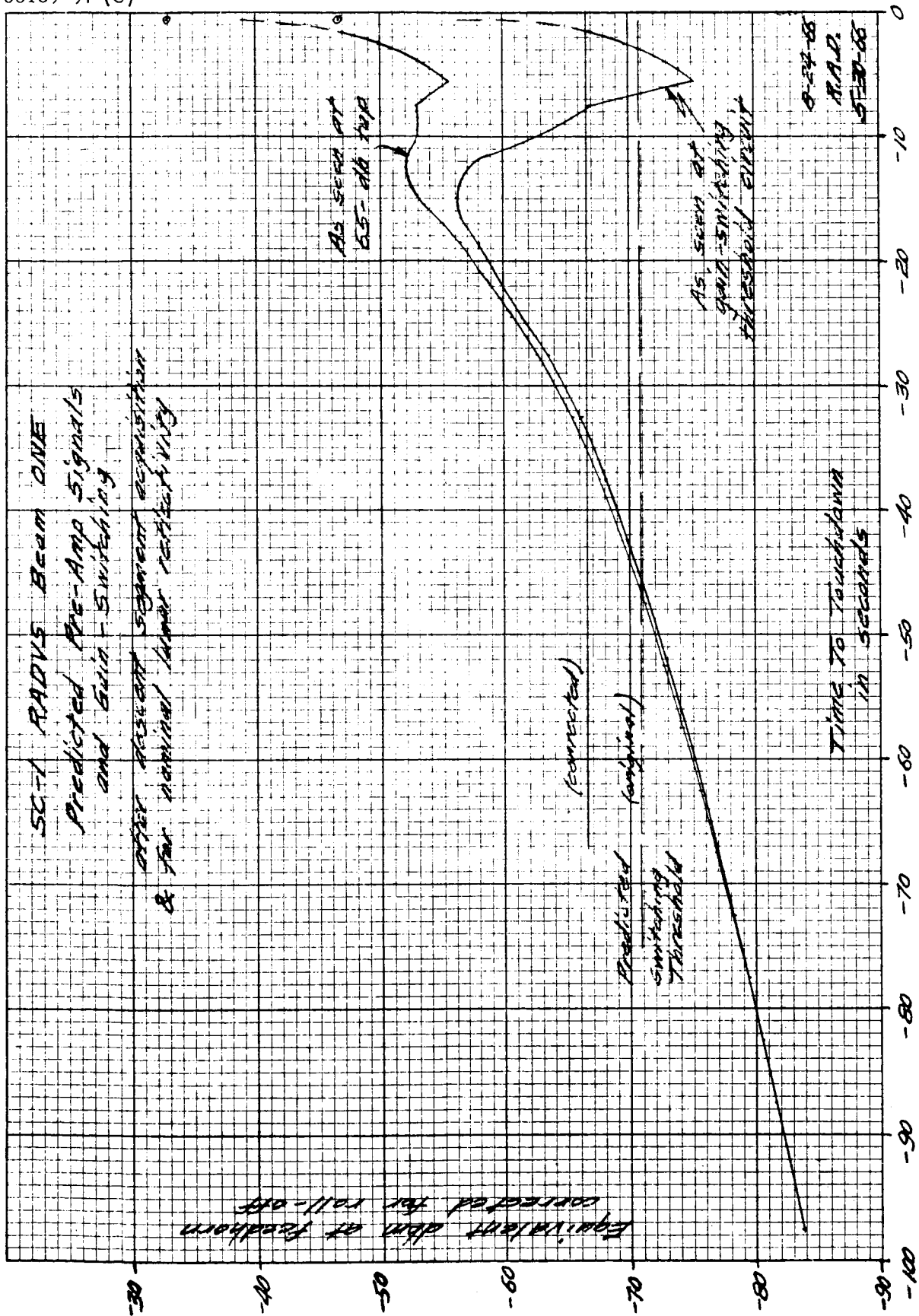
a) Beam 1

Figure 5.10-11. RADVS Predicted Preamp Output
in Corrected dbm at Feedhorn Versus
Time to Touchdown, seconds
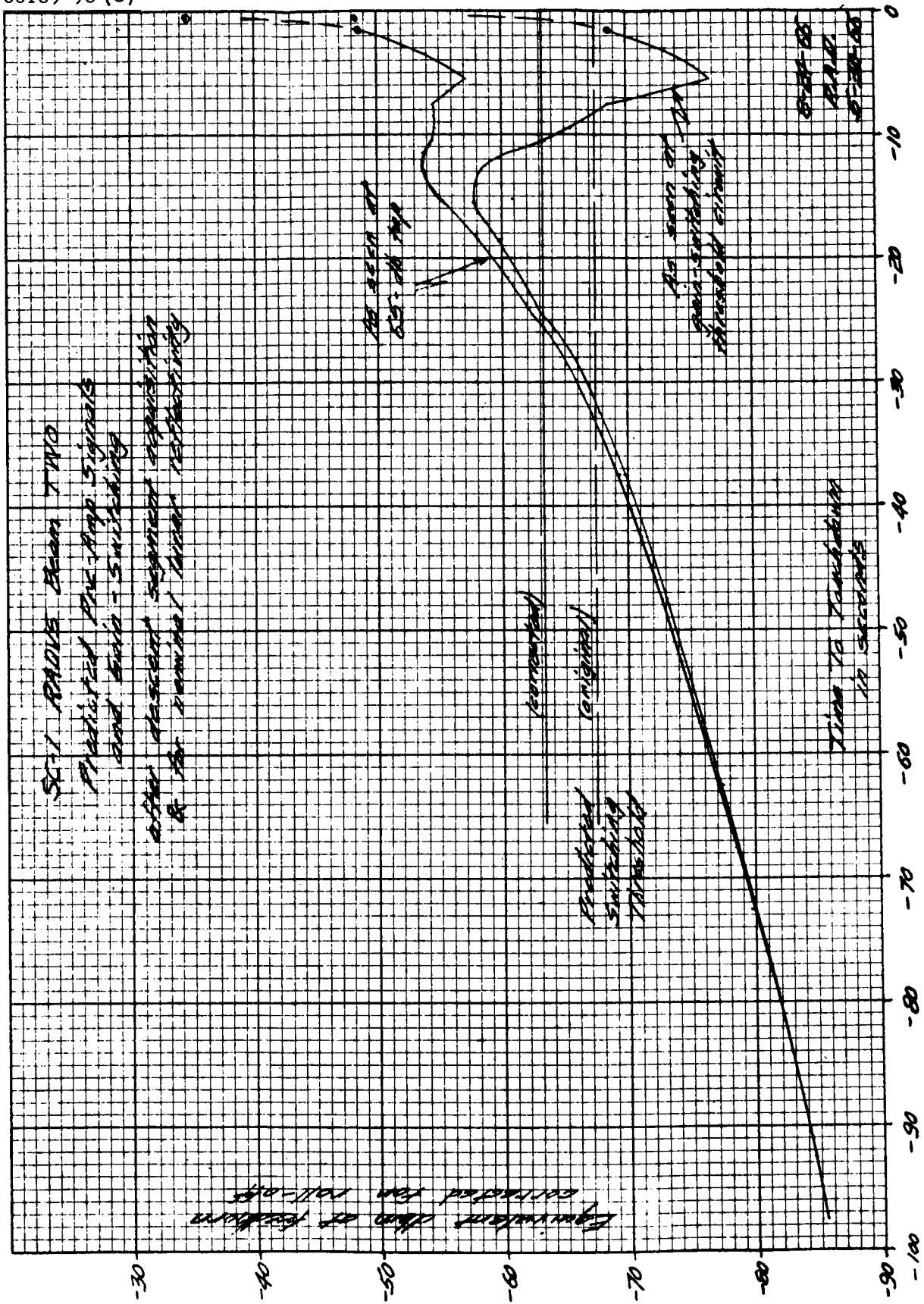
b) Beam 2

Figure 5.10-11 (continued). RADVS Predicted Preamp
Output in Corrected dbm at Feedhorn Versus
Time to Touchdown, seconds
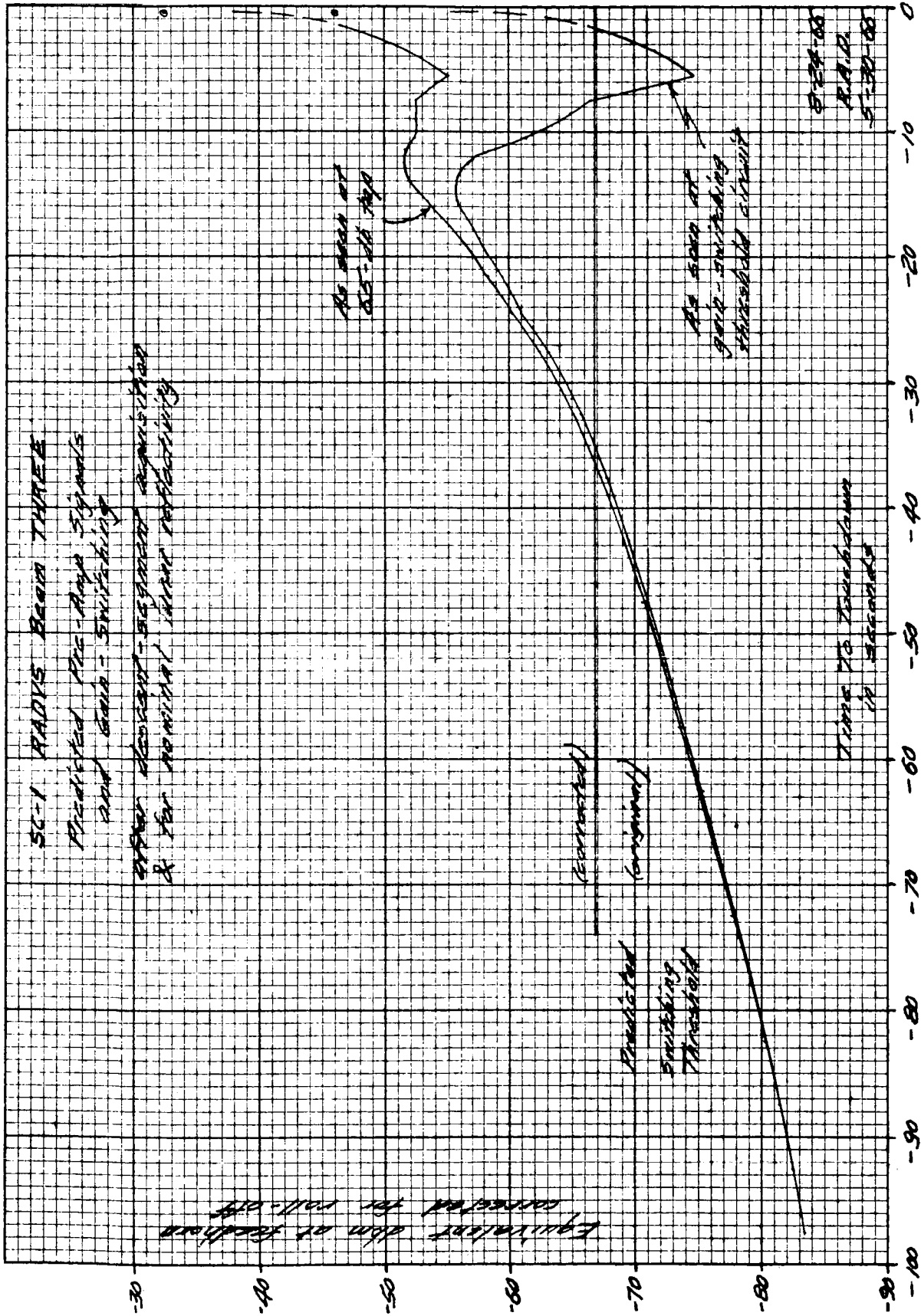
Figure 5.10-11 (continued). RADVS Predicted Preamp
Output in Corrected dbm at Feedhorn Versus
Time to Touchdown, seconds

c) Beam 3
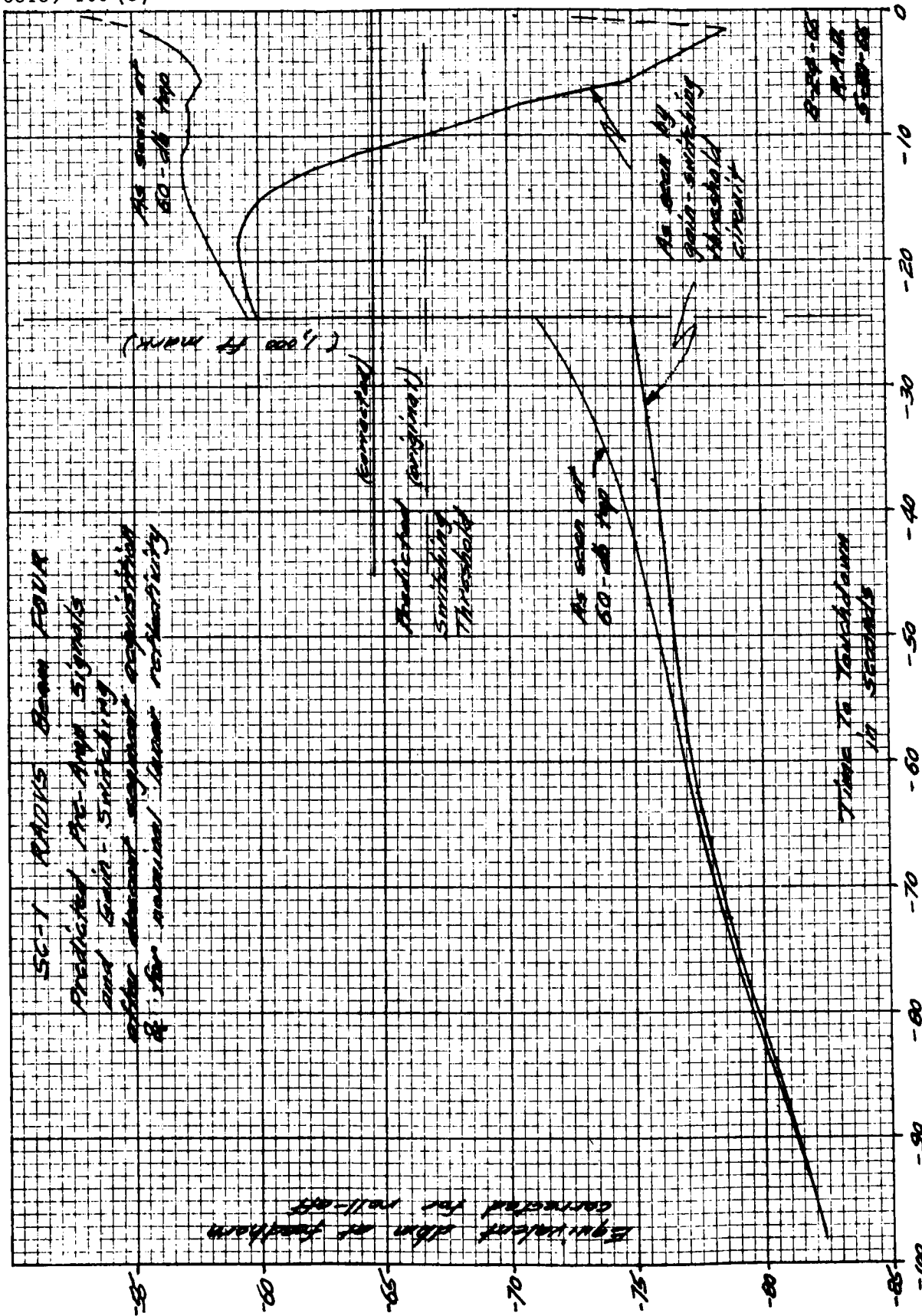
d) Beam 4

Figure 5.10-11 (continued). RADVS Predicted Preamp
Output in Corrected dbm at Feedhorn Versus
Time to Touchdown, seconds
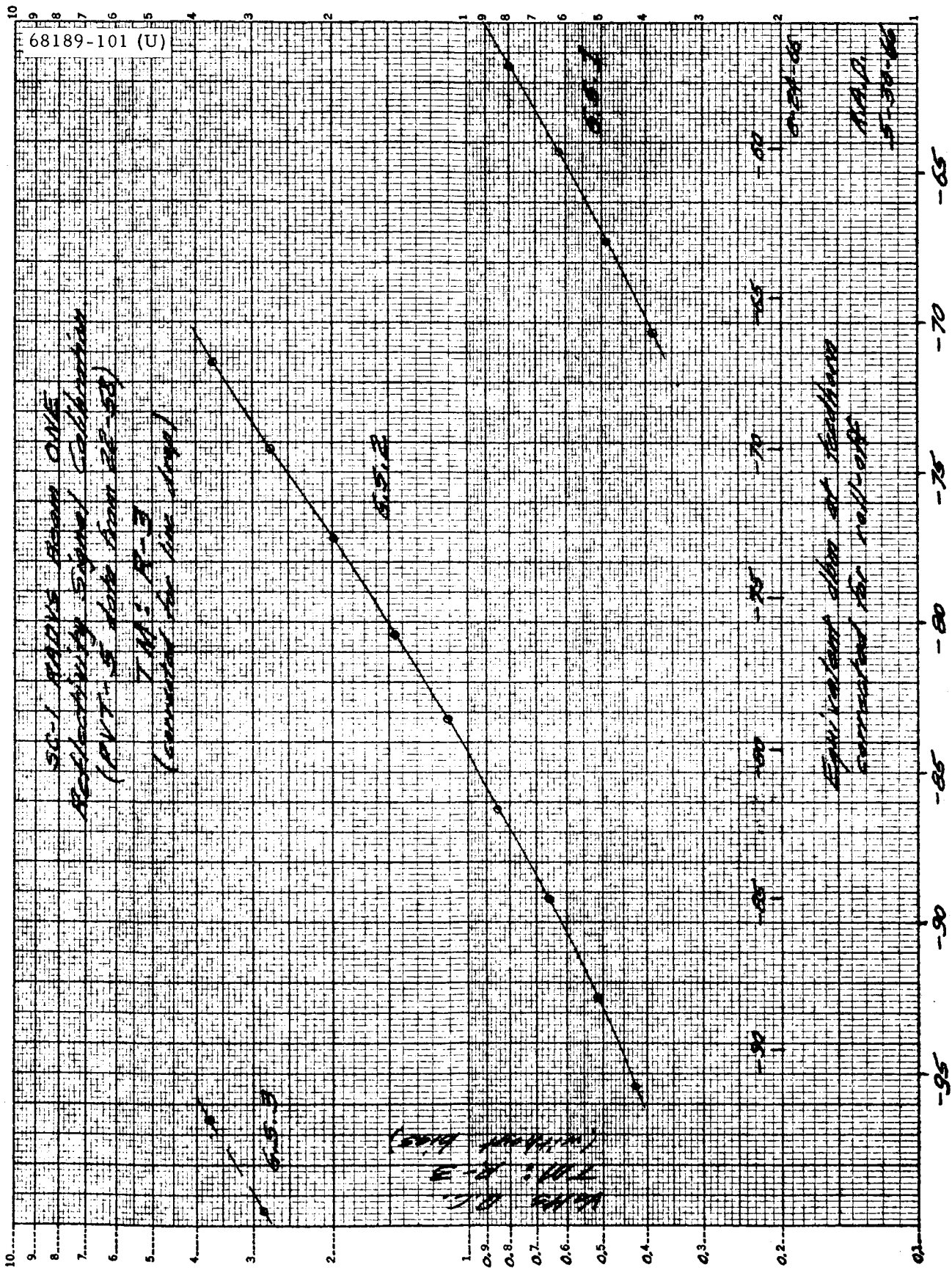
Figure 5.10-12. RADVS Beam 1 Reflectivity Signal Calibration,
Telemetry Volts Versus Corrected dbm at Feedhorn

a) 95 to 55 dbm

5.10-47

68189-102 (U)
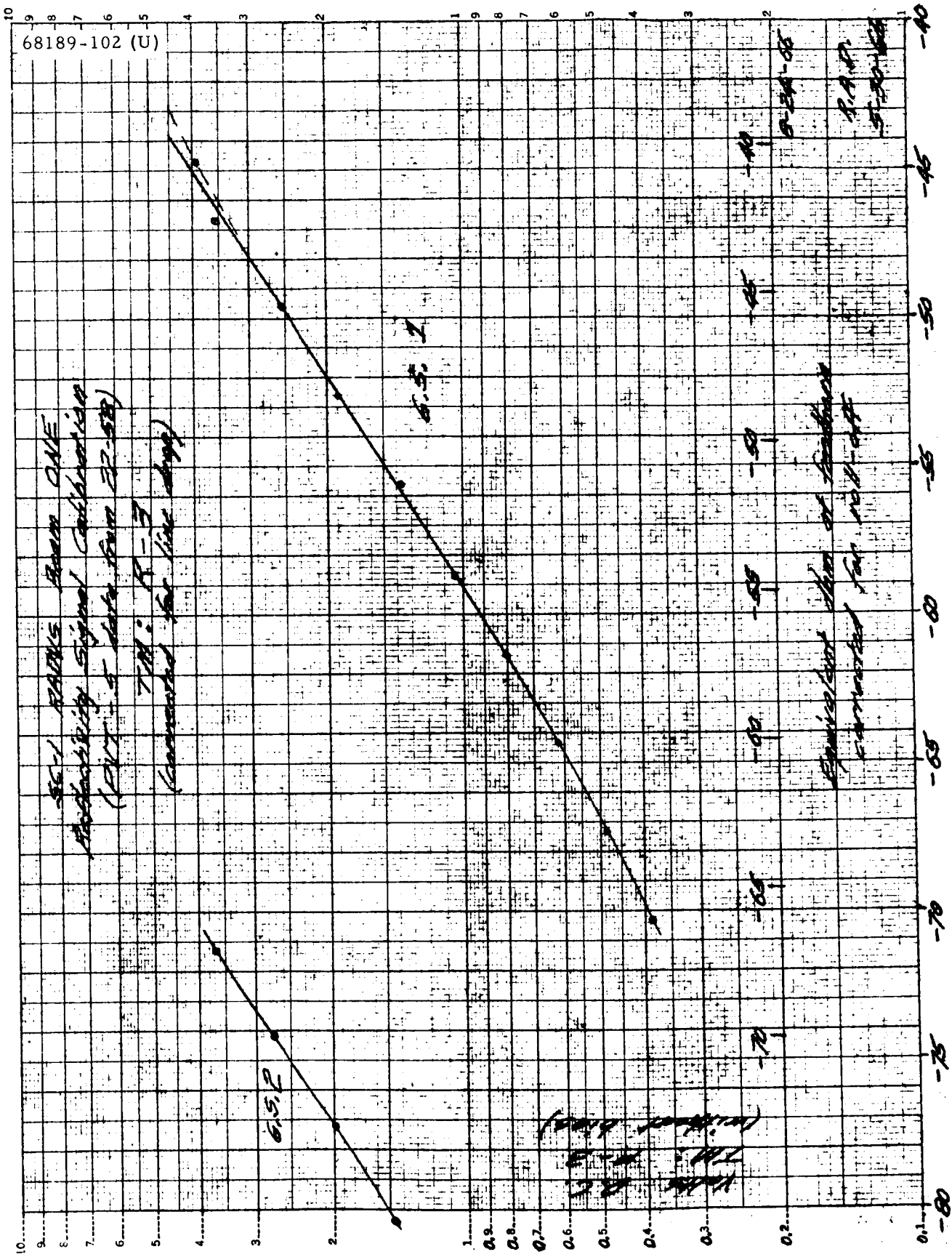
b) 75 to 40 dbm

Figure 5.10-12 (continued). RADVS Beam 1 Reflectivity Signal
Calibration, Telemetry Volts Versus
Corrected dbm at Feedhorn
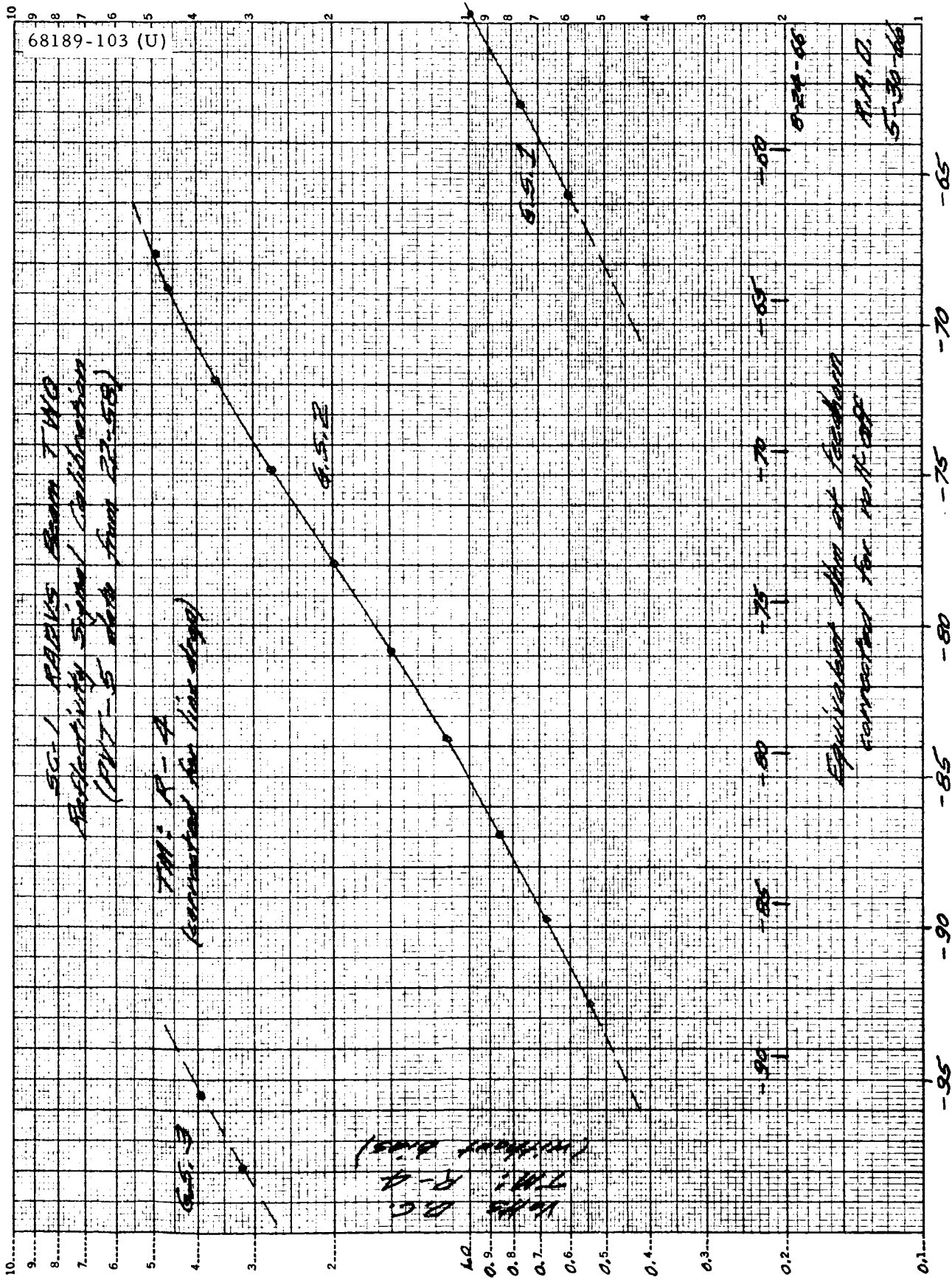
Figure 5.10-13. RADVS Beam 2 Reflectivity Signal Calibration, Telemetry Volts Versus Corrected dbm at Feedhorn

a) 95 to 55 dbm

68189-104 (U)
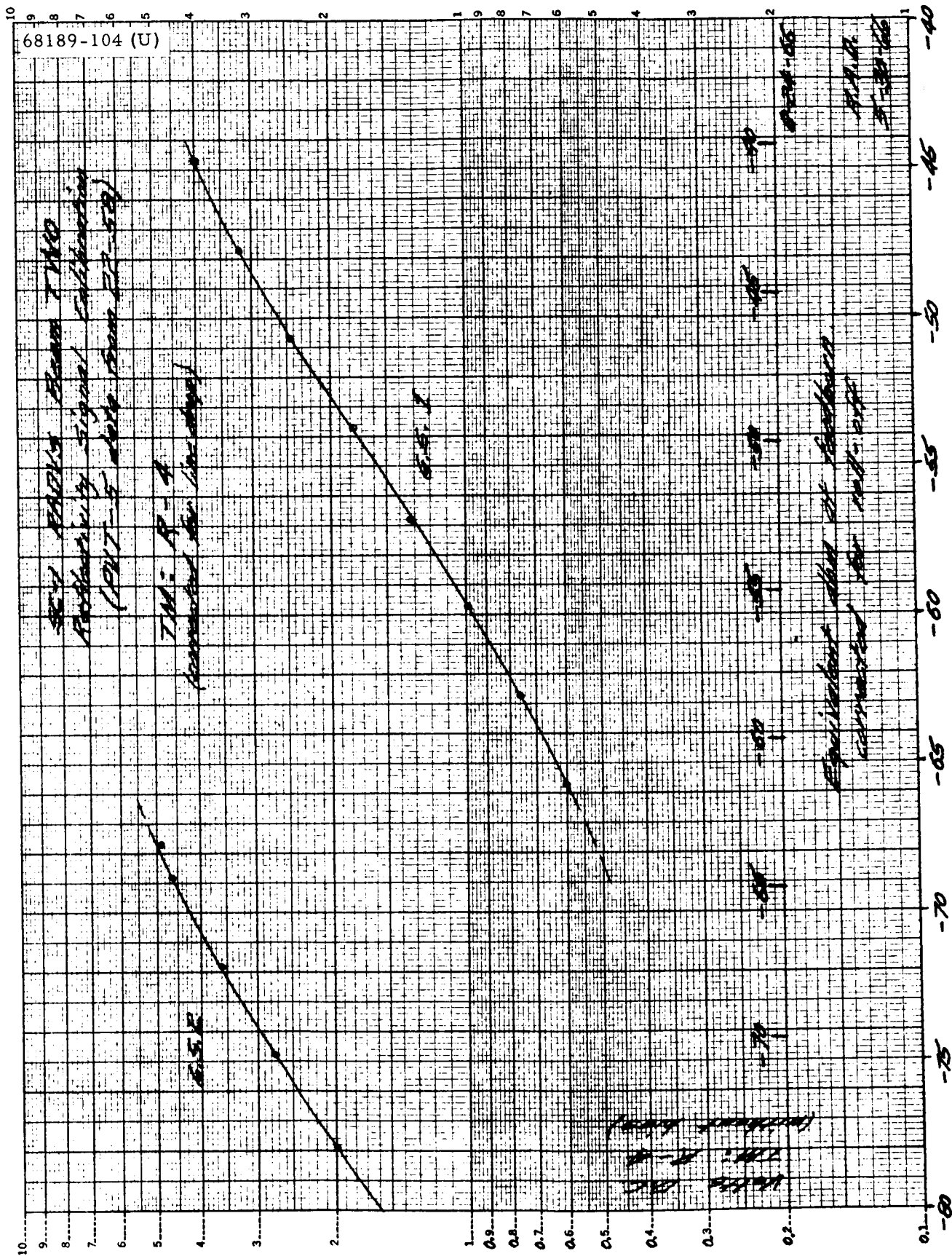
b) 75 to 40 dbm

Figure 5.10-13 (continued). RADVS Beam 2 Reflectivity Signal
Calibration, Telemetry Volts Versus
Corrected dbm at Feedhorn
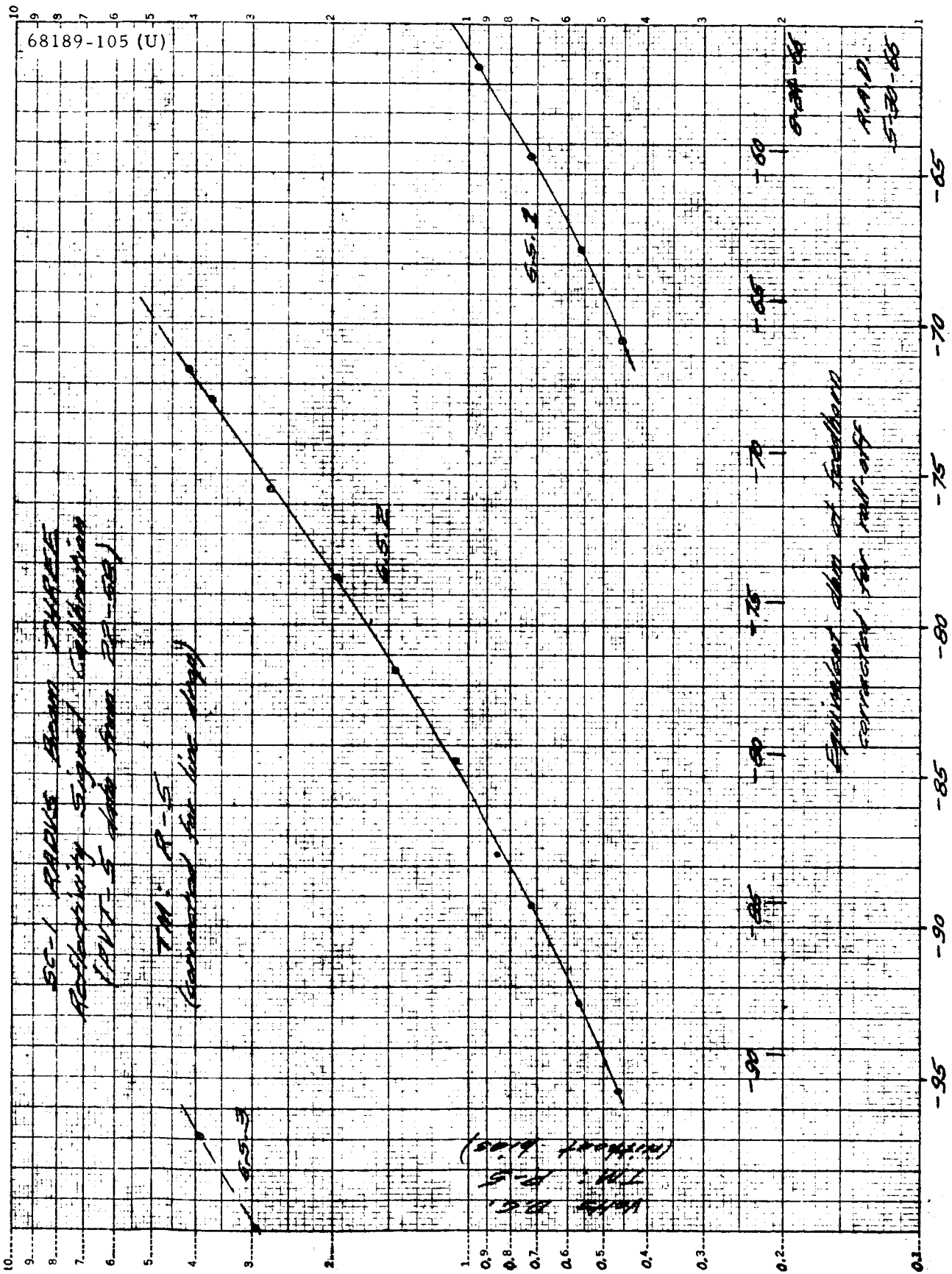
Figure 5.10-14. RADVS Beam 3 Reflectivity Signal Calibration,
Telemetry Volts Versus Corrected dbm at Feedhorn

a) 95 to 55 dbm

68189-106 (U)
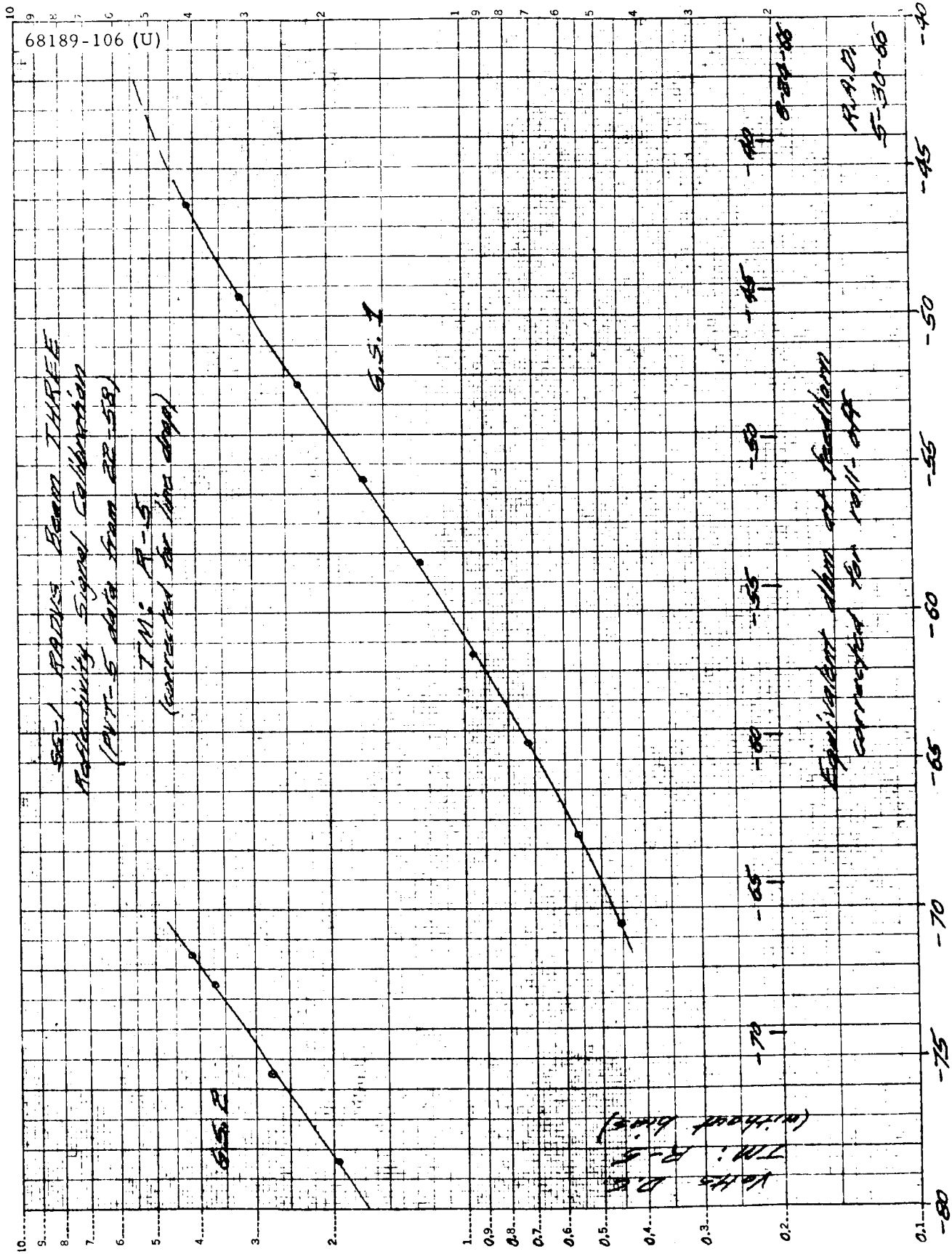
b) 75 to 40 dbm

Figure 5.10-14 (continued). RADVS Beam 3 Reflectivity Signal
Calibration, Telemetry Volts Versus
Corrected dbm at Feedhorn
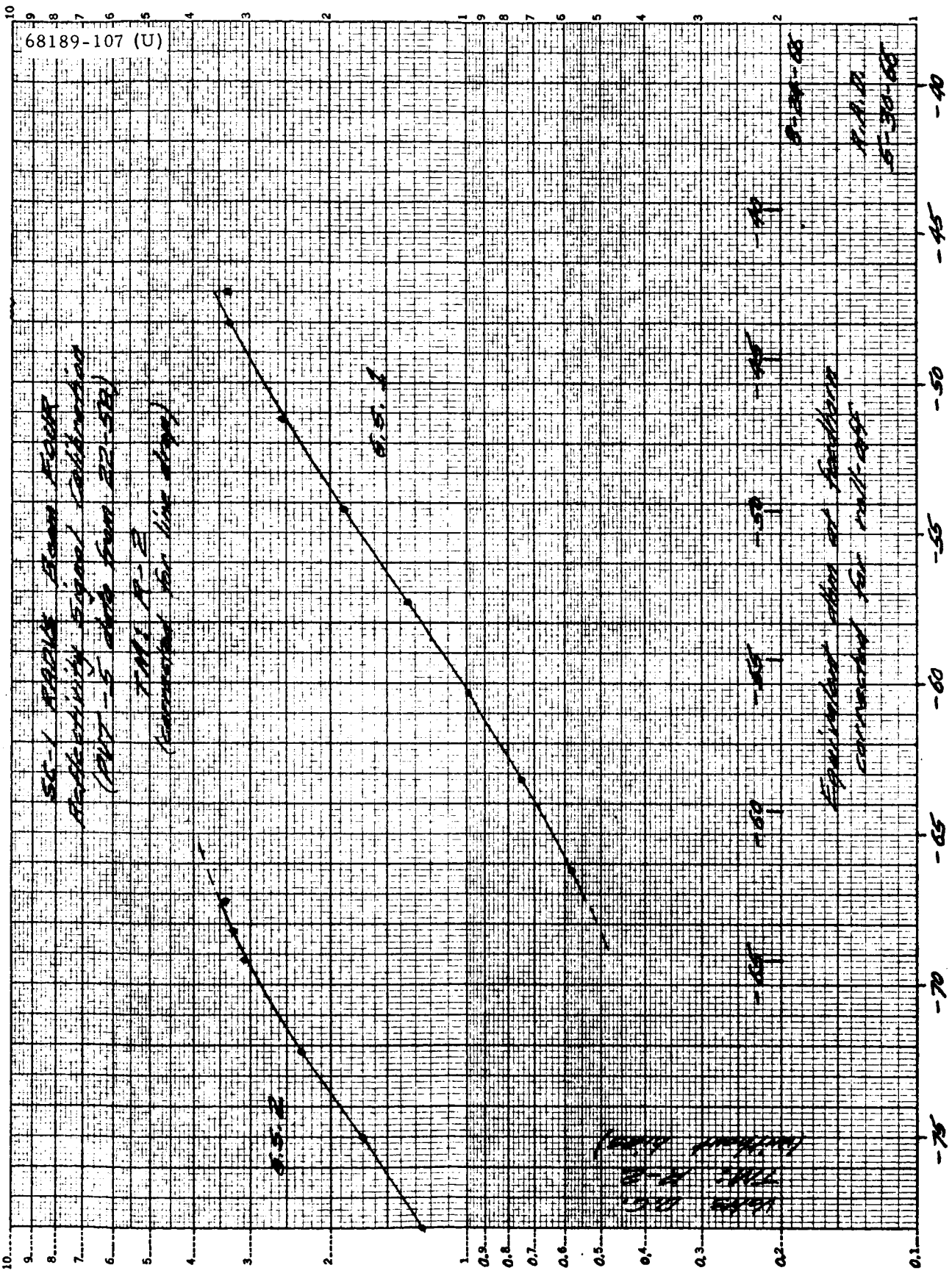
Figure 5.10-15. RADVS Beam 4 Reflectivity Signal Calibration,
Telemetry Volts Versus Corrected dbm at Feedhorn

a) 92 to 52 dbm
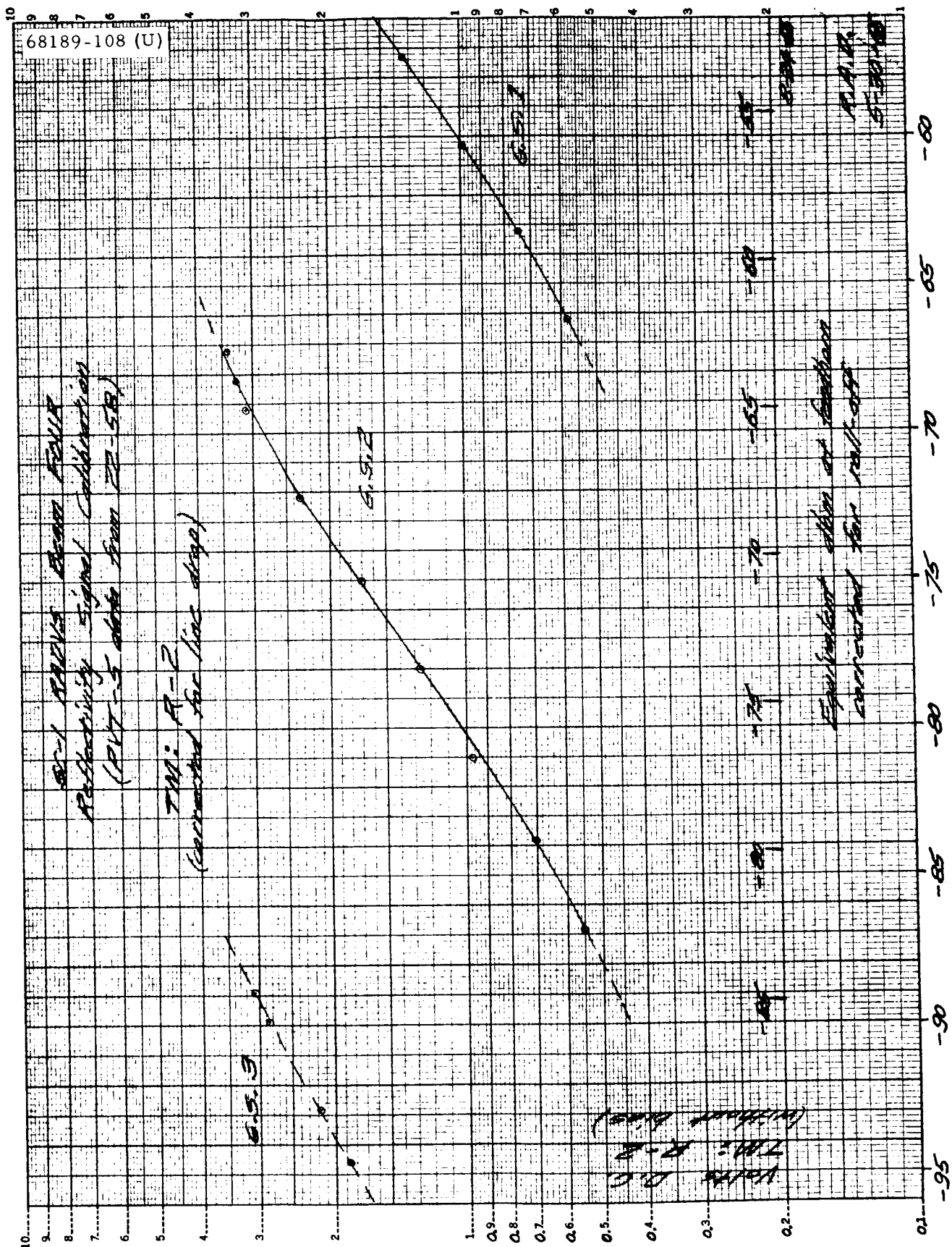
b) 74 to 43 dbm

Figure 5.10-15 (continued). RADVS Beam 4 Reflectivity Signal
Calibration, Telemetry Volts Versus
Corrected dbm at Feedhorn

TABLE 5.10-7. DVS PREAMPLIFIER SIGNAL CALCULATIONS FOR COMPUTED SC-1 TRAJECTORY FROM 0 DEGREE APPROACH

(Used only after descent-segment acquisition)

t, seconds	h, feet	V, fps	$D_{1,2,3}$, Hz	Rolloff, db		P_r, dbm		
				First	Both	Uncorrected	Corrected For Rolloff	
							First	Both
76	26,371	530.1	13,000	0.2	0.2	-87.18	-87.4	-87.4
81	23,780	504.4	12,350	0.2	0.2	-86.28	-86.5	-86.5
86	21,320	478.7	11,730	0.3	0.3	-85.33	-85.6	-85.6
91	18,985	454.3	11,120	0.3	0.3	-84.32	-84.6	-84.6
96	16,770	431.2	10,590	0.3	0.4	-83.24	-83.5	-83.6
101	14,665	409.2	10,010	0.3	0.4	-82.08	-82.4	-82.5
106	12,670	386.3	9,460	0.4	0.5	-80.82	-81.2	-81.3
111	10,825	350.2	8,590	0.5	0.6	-79.45	-79.9	-80.0
116	9,160	314.2	7,700	0.6	0.7	-78.00	-78.6	-78.7
121	7,676	278.2	6,810	0.8	1.0	-76.46	-77.3	-77.5
126	6,372	242.2	5,940	1.0	1.2	-74.84	-75.8	-76.0
131	5,246	208.0	5,100	1.3	1.5	-73.16	-74.5	-74.7
136	4,264	184.5	4,520	1.6	1.9	-71.36	-73.0	-73.3
141	3,392	163.6	4,000	1.9	2.3	-69.37	-71.3	-71.7
146	2,619	145.0	3,550	2.3	2.8	-67.12	-69.4	-69.9
151	1,933	128.6	3,150	2.8	3.5	-64.48	-67.3	-68.0
156	1,325	114.0	2,790	3.3	4.1	-61.21	-64.5	-65.3
159	994	106.1	2,600	3.7	4.5	-58.71	-62.4	-63.2
162	702	86.9	2,130	4.8	5.9	-55.69	-60.5	-61.6
165	466	69.9	1,712	6.1	7.8	-52.13	-58.2	-59.9
168	276	54.0	1,323	7.9	10.4	-47.58	-55.5	-58.0
171	144.4	32.5	796	11.8	16.9	-41.95	-53.8	-58.9
172	114.9	25.3	620	13.9	20.6	-39.97	-53.9	-60.6
173	92.5	18.50	453	16.5	25.5	-38.08	-54.6	-63.6
174	75.5	14.77	362	18.4	29.2	-36.32	-54.7	-65.5
175	61.7	12.09	296	20.2	32.6	-34.56	-54.8	-67.2
176	50.3	9.90	243	21.9	35.9	-32.79	-54.7	-68.7
177	41.0	7.04	172	24.9	44.8	-31.02	-55.9	-72.8
178	34.9	5.11	125	27.6	47.3	-29.62	-57.2	-76.9
179	29.2	5.00	122.5	27.8	47.7	-28.07	-55.9	-75.8
180	23.6	5.00	122.5	27.8	47.7	-26.22	-54.0	-73.9
181	18.0	5.00	122.5	27.8	47.7	-23.87	-51.7	-71.6
182	12.87	5.00	122.5	27.8	47.7	-20.95	-48.8	-68.7
183	5.25	10.32	253	21.5	35.2	-13.16	-34.7	-48.4
183.50	-0.625	12.98	—	—	—	—	—	—

TABLE 5.10-8. RADAR ALTIMETER PREAMPLIFIER SIGNAL CALCULATIONS FOR COMPUTED SC-1 TRAJECTORY FROM 0 DEGREE APPROACH

(Used only after descent-segment acquisition)

t, seconds	A_R R, kHz	0.026 V, kHz	$F_{R'}$ kHz	Rolloff, db		P_r, dbm		
				First	Both	Uncorrected	Corrected For Rolloff First	Both
76	42.9	13.8	56.7	1.1	1.1	-85.64	-86.7	-86.7
81	38.6	13.1	51.7	1.3	1.3	-84.74	-86.0	-86.0
86	34.6	12.4	47.0	1.5	1.5	-83.79	-85.3	-85.3
91	30.8	11.8	42.6	1.8	1.8	-82.78	-84.6	-84.6
96	27.2	11.2	38.4	2.1	2.2	-81.70	-83.8	-83.9
101	23.8	10.6	34.4	2.4	2.6	-80.54	-82.9	-83.1
106	20.6	10.0	30.6	2.9	3.1	-79.28	-82.2	-82.4
111	17.60	9.11	26.71	3.5	3.7	-77.91	-81.4	-81.6
116	14.90	8.17	23.07	4.3	4.5	-76.46	-80.8	-81.0
121	12.49	7.24	19.73	5.2	5.4	-74.92	-80.1	-80.3
126	10.37	6.30	16.67	6.3	6.6	-73.30	-79.6	-79.9
131	8.52	5.41	13.93	7.5	8.0	-71.62	-79.1	-79.6
136	6.94	4.80	11.74	8.7	9.5	-69.82	-78.5	-79.3
141	5.51	4.25	9.76	10.2	11.3	-67.83	-78.0	-79.1
146	4.26	3.77	8.03	11.7	13.2	-65.58	-77.3	-78.8
151	3.14	3.34	6.48	13.4	15.6	-62.94	-76.3	-78.5
156	2.15	2.96	5.11	15.4	18.5	-59.67	-75.1	-78.2
159	16.18	2.76	18.94	5.4	5.7	-57.17	-62.6	-62.9
162	11.42	2.26	13.68	7.6	8.2	-54.15	-61.8	-62.4
165	7.58	1.82	9.40	10.4	11.6	-50.59	-61.0	-62.2
168	4.49	1.40	5.89	14.2	16.8	-46.04	-60.2	-62.8
171	2.35	0.84	3.19	19.5	24.9	-40.41	-59.9	-65.3
172	1.869	0.658	2.527	21.5	28.4	-38.43	-59.9	-66.8
173	1.503	0.481	1.984	23.7	32.3	-36.54	-60.2	-68.8
174	1.228	0.384	1.612	25.4	35.6	-34.78	-60.2	-70.4
175	1.003	0.314	1.317	27.2	27.2	-39.0	-60.2	-72.0
176	0.817	0.258	1.075	28.9	42.3	-31.25	-60.1	-73.5
177	0.666	0.183	0.849	31.0	46.4	-29.48	-60.5	-75.9
178	0.567	0.133	0.700	32.7	49.8	-28.08	-60.8	-77.9
179	0.475	0.130	0.605	33.9	52.3	-26.53	-60.4	-78.8
180	0.384	0.130	0.514	35.4	55.2	-24.68	-60.1	-79.9
181	0.293	0.130	0.423	37.0	58.4	-22.33	-59.3	-80.7
182	0.209	0.130	0.339	38.9	62.3	-19.44	-58.3	-81.7
183	0.0854	0.268	0.353	38.6	61.6	-11.62	-50.2	-73.2
183.50	—	—	—	—	—	—	—	—

TABLE 5.10-9. SC-1 RADVS BEAM 1 PREAMPLIFIER AND REFLECTIVITY SIGNAL CALCULATIONS

Time, seconds	P_r, Minimum Margin, dbm	P_r, Beam 1, dbm			Telemetry Channel: R-3, volts dc	
		Uncorrected	Corrected For Rolloff		Gain-State 2	Gain-State 1
			First	Both		
107.45	-87.18	-85.39	-85.6	-85.6	0.628	
102.45	-86.28	-84.49	-84.7	-84.7	0.675	
97.45	-85.33	-83.54	-83.8	-83.8	0.725	
92.45	-84.32	-82.53	-82.8	-82.8	0.790	
87.45	-83.24	-81.45	-81.7	-81.8	0.87	
82.45	-82.08	-80.29	-80.6	-80.7	0.96	
77.45	-80.82	-79.03	-79.4	-79.5	1.08	
72.45	-79.45	-77.66	-78.2	-78.3	1.20	
67.45	-78.00	-76.21	-76.8	-76.9	1.38	
62.45	-76.46	-74.67	-75.5	-75.7	1.56	
57.45	-74.84	-73.05	-74.0	-74.2	1.80	
52.45	-73.16	-71.37	-72.7	-72.9	2.06	
47.45	-71.36	-69.57	-71.2	-71.5	2.40	
42.45	-69.37	-67.58	-69.5	-69.9	2.90	
37.45	-67.12	-65.33	-67.6	-68.1	3.50	0.347
32.45	-64.48	-62.69	-65.5	-66.2		0.405
27.45	-61.21	-59.42	-62.7	-63.5		0.500
24.45	-58.71	-56.92	-60.6	-61.4		0.595
21.45	-55.69	-53.90	-58.7	-59.8		0.700
18.45	-52.13	-50.34	-56.4	-58.1		0.87
15.45	-47.58	-45.79	-53.7	-56.2		1.13
12.45	-41.95	-40.16	-52.0	-57.1		1.32
11.45	-39.97	-38.18	-52.1	-58.8		1.31
10.45	-38.08	-36.29	-52.8	-61.8		1.22
9.45	-36.32	-34.53	-52.9	-63.7		1.21
8.45	-34.56	-32.77	-53.0	-65.4		1.20
7.45	-32.79	-31.00	-52.9	-66.9		1.21
6.45	-31.02	-29.23	-54.1	-71.0		1.08
5.45	-29.62	-27.83	-55.4	-75.1		0.95
4.45	-28.07	-26.28	-54.1	-74.0		1.08
3.45	-26.22	-24.43	-52.2	-72.1		1.30
2.45	-23.87	-22.08	-49.9	-69.8		1.62
1.45	-20.95	-19.16	-47.0	-66.9		2.16
0.45	-13.16	-11.37	-32.9	-46.6		>5

TABLE 5.10-10.   SC-1 RADVS BEAM 2 PREAMPLIFIER AND REFLECTIVITY SIGNAL CALCULATIONS

| Time, seconds | P_r, Minimum Margin, dbm | P_r, Beam 2, dbm | | | Telemetry Channel: R-4, volts dc | |
| | | Uncorrected | Corrected For Rolloff | | | |
			First	Both	Gain-State 2	Gain-State 1
107.45	-87.18	-87.04	-87.2	-87.2	0.595	
102.45	-86.28	-86.14	-86.3	-86.3	0.64	
97.45	-85.33	-85.19	-85.5	-85.5	0.68	
92.45	-84.32	-84.18	-84.5	-84.5	0.76	
87.45	-83.24	-83.10	-83.4	-83.5	0.81	
82.45	-82.08	-81.94	-82.2	-82.3	0.89	
77.45	-80.82	-80.68	-81.1	-81.2	0.98	
72.45	-79.45	-79.31	-79.8	-79.9	1.10	
67.45	-78.00	-77.86	-78.5	-78.6	1.24	
62.45	-76.46	-76.32	-77.1	-77.3	1.42	
57.45	-74.84	-74.70	-75.7	-75.9	1.64	
52.45	-73.16	-73.02	-74.3	-74.5	1.89	
47.45	-71.36	-71.22	-72.8	-73.1	2.19	
42.45	-69.37	-69.23	-71.1	-71.5	2.60	
37.45	-67.12	-66.98	-69.3	-69.8	3.11	
32.45	-64.48	-64.34	-67.1	-67.8	3.80	0.395
27.45	-61.21	-61.35	-64.7	-65.5		0.485
24.45	-58.71	-58.57	-62.3	-63.1		0.57
21.45	-55.69	-55.55	-60.4	-61.5		0.66
18.45	-52.13	-51.99	-58.1	-59.8		0.785
15.45	-47.58	-47.44	-55.3	-57.8		1.01
12.45	-41.95	-41.81	-53.6	-58.7		1.19
11.45	-39.97	-39.83	-53.7	-60.4		1.18
10.45	-38.08	-37.94	-54.4	-63.4		1.10
9.45	-36.32	-36.18	-54.6	-65.4		1.08
8.45	-34.56	-34.42	-54.6	-67.0		1.08
7.45	-32.79	-32.65	-54.5	-68.5		1.09
6.45	-31.02	-30.88	-55.8	-72.7		0.97
5.45	-29.62	-29.48	-57.1	-76.8		0.86
4.45	-28.07	-27.93	-55.7	-75.6		0.98
3.45	-26.22	-26.08	-53.9	-73.8		1.16
2.45	-23.87	-23.73	-51.5	-71.4		1.47
1.45	-20.95	-20.81	-48.6	-68.5		1.97
0.45	-13.16	-13.02	-34.5	-48.2		>5

TABLE 5.10-11. SC-1 RADVS BEAM 3 PREAMPLIFIER AND REFLECTIVITY SIGNAL CALCULATIONS

Time, seconds	P_r, Minimum Margin, dbm	P_r, Beam 3, dbm			Telemetry Channel: R-5, volts dc	
		Uncorrected	Corrected For Rolloff		Gain-State 2	Gain-State 1
			First	Both		
107.45	-87.18	-84.96	-85.2	-85.2	0.715	
102.45	-86.28	-84.06	-84.3	-84.3	0.77	
97.45	-85.33	-83.11	-83.4	-83.4	0.83	
92.45	-84.32	-82.10	-82.4	-82.4	0.90	
87.45	-83.24	-81.02	-81.3	-81.4	1.00	
82.45	-82.08	-79.86	-80.2	-80.3	1.10	
77.45	-80.82	-78.60	-79.0	-79.1	1.22	
72.45	-79.45	-77.23	-77.7	-77.8	1.39	
67.45	-78.00	-75.78	-76.4	-76.5	1.58	
62.45	-76.46	-74.24	-75.0	-75.2	1.81	
57.45	-74.84	-72.62	-73.6	-73.8	2.10	
52.45	-73.16	-70.94	-72.2	-72.4	2.44	
47.45	-71.36	-69.14	-70.7	-71.0	2.86	
42.45	-69.37	-67.15	-69.1	-69.5	3.40	
37.45	-67.12	-64.90	-67.2	-67.7	4.20	0.427
32.45	-64.48	-62.26	-65.1	-65.8		0.49
27.45	-61.21	-58.99	-62.3	-63.1		0.605
24.45	-58.71	-56.49	-60.2	-61.0		0.72
21.45	-55.69	-53.47	-58.3	-59.4		0.855
18.45	-52.13	-49.91	-56.0	-57.7		1.06
15.45	-47.58	-45.36	-53.3	-55.8		1.38
12.45	-41.95	-39.73	-51.5	-56.6		1.65
11.45	-39.97	-37.75	-51.7	-58.4		1.61
10.45	-38.08	-35.86	-52.4	-61.4		1.51
9.45	-36.32	-34.10	-52.5	-63.3		1.50
8.45	-34.56	-32.34	-52.5	-64.9		1.50
7.45	-32.79	-30.57	-52.5	-66.5		1.50
6.45	-31.02	-28.80	-53.7	-70.6		1.32
5.45	-29.62	-27.40	-55.0	-74.7		1.17
4.45	-28.07	-25.85	-53.6	-73.5		1.34
3.45	-26.22	-24.00	-51.8	-71.7		1.60
2.45	-23.87	-21.65	-49.4	-69.3		2.05
1.45	-20.95	-18.73	-46.5	-66.4		2.75
0.45	-13.16	-10.94	-32.4	-46.1		>5

TABLE 5.10-12. SC-1 RADVS BEAM 4 PREAMPLIFIER AND REFLECTIVITY SIGNAL CALCULATIONS

| Time, seconds | P_r, Minimum Margin, dbm | P_r, Beam 4, dbm | | | Telemetry Channel: R-2, volts dc | |
| | | Uncorrected | Corrected For Rolloff | | | |
			First	Both	Gain-State 2	Gain-State 1
107.45	-85.64	-82.69	-83.8	-83.8	0.50	
102.45	-84.74	-81.79	-83.1	-83.1	0.53	
97.45	-83.79	-80.84	-82.3	-82.3	0.565	
92.45	-82.78	-79.83	-81.6	-81.6	0.595	
87.45	-81.70	-78.75	-80.9	-81.0	0.63	
82.45	-80.54	-77.59	-80.0	-80.2	0.68	
77.45	-79.28	-76.33	-79.2	-79.4	0.735	
72.45	-77.91	-74.96	-78.5	-78.7	0.785	
67.45	-76.46	-73.51	-77.8	-78.0	0.84	
62.45	-74.92	-71.97	-77.2	-77.4	0.89	
57.45	-73.30	-70.35	-76.7	-77.0	0.94	
52.45	-71.62	-68.67	-76.2	-76.7	0.99	
47.45	-69.82	-66.87	-75.6	-76.4	1.04	
42.45	-67.83	-64.88	-75.1	-76.2	1.10	
37.45	-65.58	-62.63	-74.3	-75.8	1.20	
32.45	-62.94	-59.99	-73.4	-75.6	1.31	
27.45	-59.67	-56.72	-72.1	-75.2	1.50	
24.45	-57.17	-54.22	-59.6	-59.9		0.71
21.45	-54.15	-51.20	-58.8	-59.4		0.76
18.45	-50.59	-47.64	-58.0	-59.2		0.82
15.45	-46.04	-43.09	-57.3	-59.9		0.88
12.45	-40.41	-37.46	-57.0	-62.4		0.90
11.45	-38.43	-35.48	-57.0	-63.9		0.90
10.45	-36.54	-33.59	-57.3	-65.9		0.88
9.45	-34.78	-31.83	-57.2	-67.4		0.89
8.45	-33.02	-30.07	-57.3	-69.1		0.88
7.45	-31.25	-28.30	-57.2	-70.6		0.89
6.45	-29.48	-26.53	-57.5	-72.9		0.86
5.45	-28.08	-25.13	-57.8	-74.9		0.835
4.45	-26.53	-23.58	-57.5	-75.9		0.86
3.45	-24.68	-21.73	-57.1	-76.9		0.89
2.45	-22.33	-19.38	-56.4	-77.8		0.96
1.45	-19.41	-16.46	-55.4	-78.8		1.05
0.45	-11.62	- 8.67	-47.3	-70.3		2.42

TABLE 5.10-13. RANGE AND VELOCITY ANALOG OUTPUT CALIBRATION

System Test Condition	Parameter, fps and feet				Input Frequencies, cps				Telemetry Outputs, bcd			
	V_x	V_y	V_z	R	D1	D2	D3	FR	FC-39	FC-40	FC-41	FC-35*
2	-300	-300	560	40,000	8,875	13,721	18,567	79,725	0066	0063	743	1023
4	+300	+300	325	36,530	12,795	7,958	3,102	67,920	1023	1023	440	963
5a	0	0	700	14,000	17,155	17,155	17,155	41,047	583	580	920	385
5b	-200	+200	700	14,000	17,154	20,445	17,155	41,048	231	931	921	385
5c	+200	-200	700	14,000	17,154	13,918	17,155	41,040	927	239	921	385
6	0	0	67	2,000	1,638	1,639	1,639	4,991	583	582	111	076
7a	-50	+50	100	1,200	2,445	3,268	2,445	4,583	495	668	156	057
7b	-50	+50	100	900	2,445	3,268	2,445	17,265	496	668	1?2	519
8	0	0	38	300	931	931	931	5,875	583	579	072	207
9	+50	-50	54.5	240	1,327	532	1,329	5,334	670	496	094	178
10a	0	0	5	50	124	124	124	945	583	579	031	079
10b	(No signal in)			0	(Radar altimeter ranging on waveguide pipe length only — high deviation)							052

*All FC-35 data points include radar altimeter waveguide length component 55 feet greater than simulated value of R column.

TABLE 5.10-14. REFLECTIVITY ANALOG OUTPUT CALIBRATION

Beam 1				Beam 2				Beam 3				Beam 4			
Telemetry, volts	R3, bcd	Power, -dbm	Gain-State	Telemetry, volts	R4, bcd	Power, -dbm	Gain-State	Telemetry, volts	R5, bcd	Power, -dbm	Gain-State	Telemetry, volts	R2, bcd	Power, -dbm	Gain-State
												0.371	0076	121.2	3
0.850	0174	114.0	3	0.762	0156	116.0	3	0.859	0176	115.0	3	0.386	0079	118.4	
1.020	0209	111.2		0.899	0184	112.9		1.045	0214	112.0		0.430	0088	115.4	
1.284	0263	108.3		1.126	0231	109.5		1.323	0271	108.9		0.484	0099	112.3	
1.660	0340	105.6		1.441	0295	106.9		1.719	0352	105.3		0.577	0118	109.3	
2.207	0452	102.5		1.880	0385	104.0		2.246	0460	102.8		0.699	0143	106.5	
2.974	0609	99.5		2.525	0517	100.9		3.047	0624	99.9		0.874	0179	103.4	
3.882	0795	96.5		3.320	0680	97.9		4.043	0828	96.8		1.127	0231	100.6	
0.543	0111	95.4	2	4.058	0831	95.5		0.582	0119	95.4	2	1.499	0307	97.6	2
0.631	0129	92.5		0.660	0135	92.5	2	0.684	0140	92.3		1.987	0407	94.6	
0.777	0159	89.2		0.796	0163	89.7		0.840	0172	89.3		2.305	0472	92.8	
0.967	0198	86.2		0.972	0199	86.9		0.972	0199	87.6		2.964	0607	89.9	
1.226	0251	83.2		1.245	0255	83.7		1.187	0243	84.5		3.198	0655	88.9	
1.587	0325	80.4		1.607	0329	80.8		1.568	0321	81.5		0.670	0137	86.8	2
2.110	0432	77.2		2.110	0432	77.9		2.065	0423	78.4		0.820	0168	83.8	
2.847	0583	74.2		2.852	0584	74.8		2.847	0583	75.5		1.094	0224	81.0	
3.794	0777	71.3		3.730	0764	71.8		3.804	0780	72.5		1.387	0284	78.0	
0.504	0103	70.3	1	4.746	0972	68.8		4.253	0871	71.5		1.820	0374	75.0	
0.606	0124	67.3		4.995	1023	67.7		0.572	0117	70.5	1	2.437	0499	72.2	1
0.738	0151	64.3		0.719	0147	65.7	1	0.679	0139	67.5		3.218	0659	69.2	
0.918	0188	61.4		0.879	0180	62.7		0.840	0172	64.4		3.398	0696	68.2	
1.162	0238	58.7		1.109	0227	59.7		1.074	0220	61.4		3.525	0722	67.2	
1.499	0307	55.6		1.441	0295	56.8		1.367	0280	58.3		0.699	0143	66.2	
2.022	0414	52.6		1.904	0390	53.7		1.777	0364	55.5		0.864	0177	63.2	
												1.109	0227	60.3	
2.671	0547	49.6		2.554	0523	50.7		2.437	0499	52.3		1.465	0300	57.3	
3.472	0711	46.7		3.315	0679	47.7		3.296	0675	49.3		1.992	0408	54.2	
												2.651	0543	51.2	
4.058	0831	44.7		4.121	0844	44.7		4.238	0868	46.2		3.442	0705	48.0	
												3.471	0711	47.0	

Increase power levels by 4.2 db.

P_t	+31.76 dbm (1.5 watts/beam)
G	+28.0 db
1/2	- 3.01 db
λ^2	-22.64 db
$(4\pi)^{-2}$	-21.98 db
$\eta(K/\alpha^3)$	- 1.10 db
Without $\dfrac{F(\theta)}{R^2}$	+11.03 dbm
F(25 degrees)	- 8.94 db
$\cos^2 25$ degrees	- 0.86 db
Without R_z^{-2}	+ 1.23 dbm

Hence

Total DVS signal power per beam, with vertical spacecraft altitude, in dbm at receiving feedhorn is:

$$P_r = \left[+1.23 - 20 \log_{10} R_z \text{ (ft)} \right] \text{ dbm}$$

Similarly, the standard radar altimeter db-budget for minimum margin hardware has consistently been as follows:

P_t	+23.22 dbm (210 milliwatt minimum)
G	+28.0 db
1/2	- 3.01 db
λ^2	-22.36 db
$(4\pi)^{-2}$	-21.98 db
$\eta(K/\alpha^3)$	- 1.10 db
Without $\dfrac{F(\theta)}{R^2}$	+ 2.77 dbm

For vertical spacecraft attitude, F(0 degree) = 0 db, and the total radar altimeter signal power in dbm at the receiving feedhorn is as follows:

$$P_r = \left[+2.77 - 20 \log_{10} R_z \text{ (feet)} \right] \text{ dbm}$$

(It is noted that this is actually 1.54 db stronger than the equivalent DVS dbm at all altitudes, because of the spacecraft vertical attitude assumption.)

5.10.4.12   SC-1 RADVS Individual Beam Parameters

All variations in receiver parameters are accounted for by the individual calibration of each beam's reflectivity signal output versus the standardized form of RF input level — equivalent dbm at the receiving feedhorn, but corrected for preamplifier rolloff.

The only remaining db budget parameters affecting signal strength indications are P_t and G for each beam. The previous A-21 RADVS evaluation was for minimum margin performance. Therefore, each beam is adjusted as shown in Table 5.10-15, using PVT-5 data on the launch configuration for P_t and unit flight acceptance test data for g.

TABLE 5.10-15.   BEAM ADJUSTMENTS

	Beam 1	Beam 2	Beam 3	Beam 4
P_t, PVT-5, dbm	+33.55	+31.85	+33.43	+24.97
P_t, minimum margin, dbm	+31.76	+31.76	+31.76	+23.22
	+ 1.79	+ 0.09	+ 1.67	+ 1.75
G, unit flight acceptance test, db	+28.0	+28.05	+28.55	+29.2
G, minimum margin, db	+28.0	+28.0	+28.0	+28.0
Total, db	0	+ 0.05	+ 0.55	+ 1.2
Net, per beam, db	+ 1.79	+ 0.14	+ 2.22	+ 2.95

5.10.5   REFERENCES

1.   "Post-Mission Analyses Involving Radar Data," 25 March 1966 (unpublished).

2.   "Nominal Descent RADVS Signals and Gain-Switching," 20 May 1966 (unpublished IDC).

3.   "A-21 RADVS — Predicted Minimum Margin Performance," 30 May 1966 (unpublished IDC).

4.   "SC-1 RADVS — Real Time Predictions," 31 May 1966 (unpublished IDC).

5.   "Surveyor I Flight Performance Quick Look Report," 17 June 1966.

5.10.6   ACKNOWLEDGEMENTS

5.11 STRUCTURES AND MECHANICAL ENVIRONMENT

5.11.1 LANDING GEAR LEG POT READINGS (POST-TOUCHDOWN)

Leg angle potentiometer readings for each of the three legs were received periodically throughout the SC-1 flight and after touchdown. Table 5.11-1 lists the angles measured at various times during the mission (angle of zero degree means full leg extension).

The small nonzero readings obtained when the legs are fully extended are due to "set up" tolerances on the leg angle potentiometers. The change in the readings on the individual legs can be attributed mostly to the tolerances in the lock strut mechanism which allows the leg angle to vary by approximately 0.9 degree. The leg angle readings after touchdown indicate that all three shock absorbers reextended completely.

The leg angles remained nearly constant after touchdown. The small change in the angles between day 153 and day 158 could be due to signal error. It is impossible to tell from these readings whether or not the shock absorber squib locks performed their function because the leg angles will remain constant without lock pins if the shock absorbers function properly. Only if there were a significant change in leg angle could it be said that the landing gear lock had not functioned properly.

5.11.2 TOUCHDOWN ANALYSIS OF STRAIN GAGES

At SC-1 touchdown the real-time output of strain gages positioned on each of the three landing gear shock absorbers was obtained. Figure 5.11-1 shows a smoothed reproduction of the time history of the strain gage outputs as recorded through the Goldstone 210-foot antenna (the original unprocessed data may be seen in Figure 5.11-2). The excellent quality of the traces indicates that the landing gear, the strain gages, and associated electronics functioned in a "normal" fashion during touchdown.

It is necessary to note, however, that some uncertainty exists with regard to the preflight calibrations performed on the strain gage outputs. Initially shock absorbers S/N 4, 6, and 7 were placed on spacecraft legs 1, 2, and 3, respectively, and calibrations were made. A defect in shock absorber S/N 6 required its rejection for flight and, as a result, shock
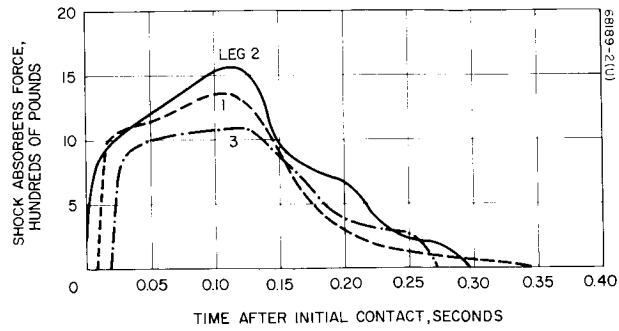
Figure 5.11-1. SC-1 Shock Absorber
Force-Time History Reduced
for 210-foot Dish Data
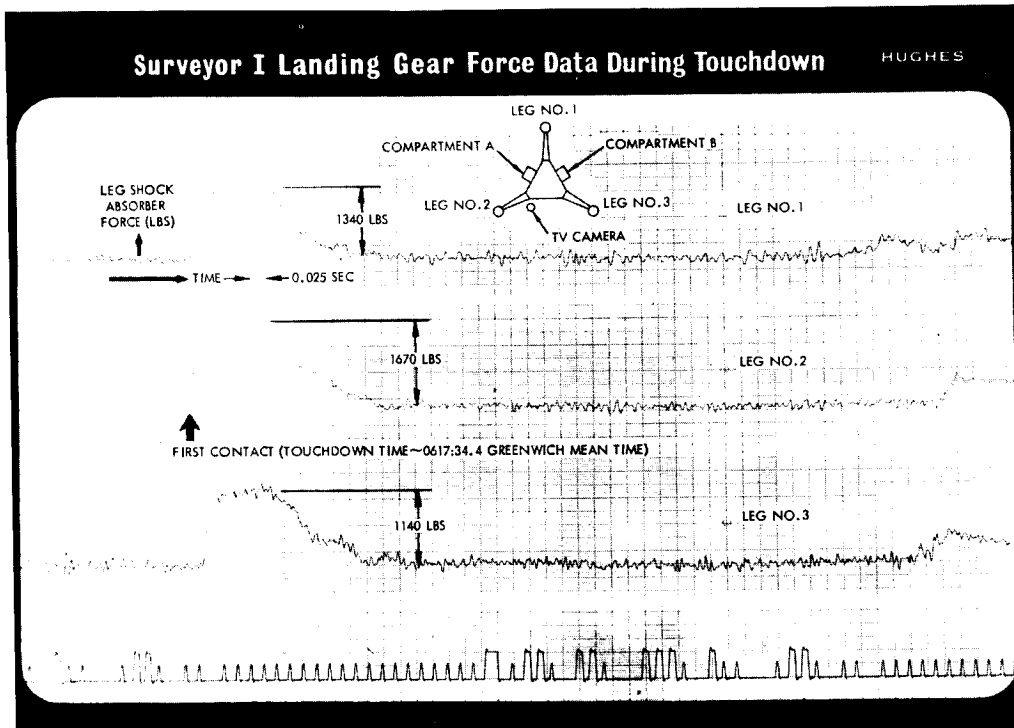
Figure 5.11-2. Unprocessed Oscillograph of Touchdown
Strain Gages from Goldstone 210-foot Antenna

Touchdown time is given at lunar surface
(preliminary value)

(Photo A15488)

TABLE 5.11-1. ANGLES MEASURED AT VARIOUS TIMES
DURING MISSION

Time	Leg Angles, degrees		
	Leg 1	Leg 2	Leg 3
Launch + 52 minutes	0.3	1.0	1.7
Retro — 1 hour 45 minutes	0.3	1.0	1.1
Retro — 10 minutes (day 153)	0.2	0.8	1.1
Touchdown + 3 minutes (prior to lock landing gear command)	0.8	1.8	1.8
Touchdown + 4 minutes (after lock landing gear command)	0.8	1.8	1.8
Day 154 4 hours 24 minutes	0.9	1.9	1.9
Day 158 1 hour 12 minutes	1.0	1.9	1.8

absorbers S/N 7 and 8 were positioned on legs 2 and 3, respectively. The change of shock absorber positions required an adjustment of less than 3 per-cent to the calibration curves.

It was further noticed that the calibration curve for the shock absorber on leg 3 differed considerably from the other two curves. This difference has not been completely explained, and, as a result, uncertainty exists with regard to the accuracy of the force time history reduced from the corresponding strain gage trace.

With regard to the traces plotted in Figure 5.11-1, therefore, it is concluded that apart from inherent inaccuracy of flight data reading and interpretations, the leg 1 trace involves no known inaccuracy, and leg 2 trace should be between 0 and 3 percent higher than shown. The accuracy of leg 3 trace is uncertain, as indicated above. It is felt, however, that since corre-lation between the flight data and analysis is very good, the inaccuracies of leg 3 trace cannot be excessively large.

It is apparent that surface contact of all three footpads was almost simultaneous, indicating that the spacecraft at touchdown was approximately normal to the surface. Footpad 2 impacted first, followed by footpad 1 at approximately 0.01 second and by footpad 3 at 0.02 second. The strain gage records show that following the primary impact the spacecraft rebounded clear of the surface and a secondary impact occurred approximately 1.0 second after initial impact, indicating that the footpads rebounded about

2-1/2 inches off the lunar surface. The maximum forces in the shock absorbers of leg 1, 2, and 3 were approximately 1350, 1600, and 1100 pounds. From these it can be shown that the maximum vertical load applied to the lunar surface was approximately 500 pounds. Conversion of this load into a surface dynamic pressure is a function of the footpad area in contact with the surface. The lower footpad is a truncated cone, and, based on the maximum load and the possible footpad contact areas, a maximum loading of between 6 and 10 psi was applied to the surface during impact.

Analytical simulations of the landing dynamics have been performed using the Hughes digital computer programs for touchdown on both hard and soft surfaces. The hard surface program has provided good correlation between measured and predicted force time histories and has been used to verify a vehicle rebound of 2-1/2 inches as indicated above. Figure 5.11-3 shows a typical analytical force time history for the initial impact phase. Good agreement is seen with the traces of Figure 5.11-1 with respect to pulse shape, force levels, and elapsed times between impacts. From the hard surface analysis it can be concluded that SC-1 landed at approximately 10 fps vertical velocity, 1 fps lateral velocity, and with an incidence relative to the lunar surface of about 1 degree. At this time a more extensive hard surface analysis, in an attempt to achieve improved correlation and better assessment of touchdown conditions, is unwarranted owing to inability of the Hughes program to incorporate individual shock absorber parameters in each leg assembly, and also because TV data indicates clearly that the surface of of the moon is not totally hard.

The Hughes soft surface two-dimensional landing computer program has been used in an attempt to arrive at soft surface characteristics. Because of present program limitations, simulated landings have been restricted to the three-point touchdown on a level surface with zero lateral velocity and angular motion. For this phase of the investigation, it is considered that this situation reasonably approximates the actual SC-1 touchdown conditions.

The soft surface representation in the Hughes computer program is a purely compressible surface in which the surface, at an initial density ρ_1, is compressed to a density ρ_2 by a penetrating object. Thus in the simple case of normal penetration (Figure 5.11-4), it can be shown that the force acting on the penetrating mass is

$$F = (p_o + b\,s)\,A + \frac{\rho_1\,\rho_2}{(\rho_2 - \rho_1)}\,A\,\dot{s}^2$$

where

p_o = surface static bearing pressure

s = depth of penetration

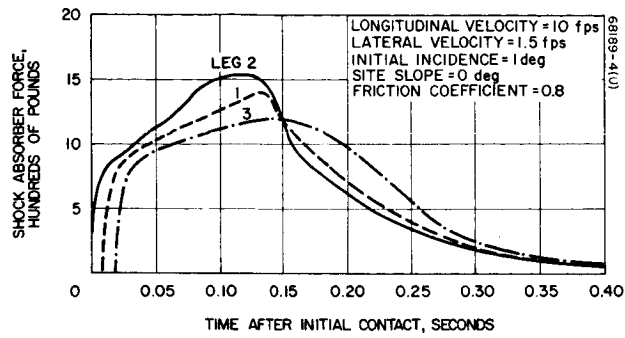b = frictional component

Figure 5.11-3. SC-1 Shock Absorber
Force-Time History From Mathe-
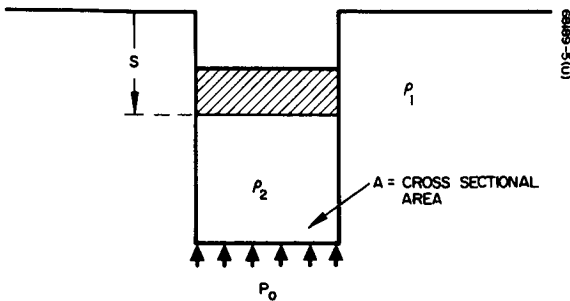matical Model Hard Surface

Figure 5.11-4. Soft Surface
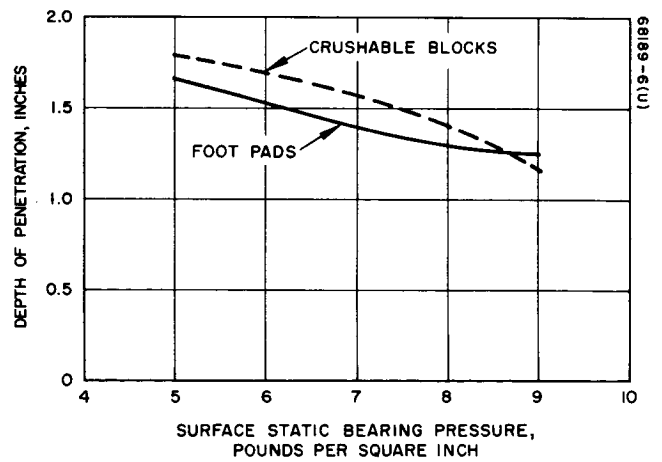Model for Penetration
Study

Figure 5.11-5. Penetration Versus
Surface Static Bearing Pressure

For the case of the penetrating Surveyor footpads, the force expression is modified to account for both normal and tangential penetration of the surface. Also accounted for is the consideration that the bottom of the footpad is a truncated cone.

Figure 5.11-5 shows a variation of footpad and crushable block penetration versus surface static bearing strength for the specified touchdown conditions. The longitudinal velocity of 11.6 fps was arrived at from interpretation of flight control data. Interpretation of TV data by JPL personnel has resulted in the conclusion that footpads 2 and 3 penetrated at least 1-1/2 inches into the lunar surface, while crushable block 3 penetrated at least 3/4 inch. From Figure 5.11-5, surface static bearing pressures, less the 6.2 psi, correspond to these measured penetrations. Shock absorber force time histories resulting from the landing conditions specified in Figure 5.11-5 are shown in Figure 5.11-6 for three surface hardness conditions. The time histories are seen to compare well with the flight data plotted in Figure 5.11-1.

In summary, reasonable correlation between measured and predicted penetrations and force time histories have been achieved for a specific soft soil model at various hardnesses. It will require extensive investigation to establish limiting relationships between penetration and surface mechanical properties. Investigations have already shown that fairly large changes can be made in friction values or in the dynamic force terms while producing relatively small changes in penetrations and force time histories. Good correlation has also been demonstrated between flight data and analyses assuming a hard surface. From landing dynamics data, therefore, it is not possible to differentiate between a soft, vertically homogeneous surface and a hard surface covered by a layer of very weak material.

5.11.3   SC-1 STRUCTURAL LOAD LEVELS DURING LUNAR TOUCHDOWN

At this time it is not known whether the SC-1 vehicle landed on a homogeneous surface, which may allow the body blocks to penetrate without crushing, or on a layered surface composed of an inch or two of very soft material resting on a rigid underlayer. The first condition may result in an equivalent loading of about 5 psi on the body blocks; the second condition, in which the blocks would crush, could exert a loading up to 40 psi on the blocks.

Using the above two pressure levels, the structural response of components on the SC-1 vehicle has been calculated based on the additional considerations of a touchdown longitudinal velocity of 10 fps with lateral velocity, pitch rate, attitude, and site slope, all zero. It is considered that these conditions approximate with sufficient accuracy the true touchdown conditions of SC-1, and that the resulting load levels are the lower and upper bounds of the actual maximum load levels experienced during SC-1 touchdown.

Figures 5.11-7, -8, and -9 define the moments and shears tabulated in Table 5.11-2 for the upper spacecraft structure. Table 5.11-3 contains compartment g load levels.
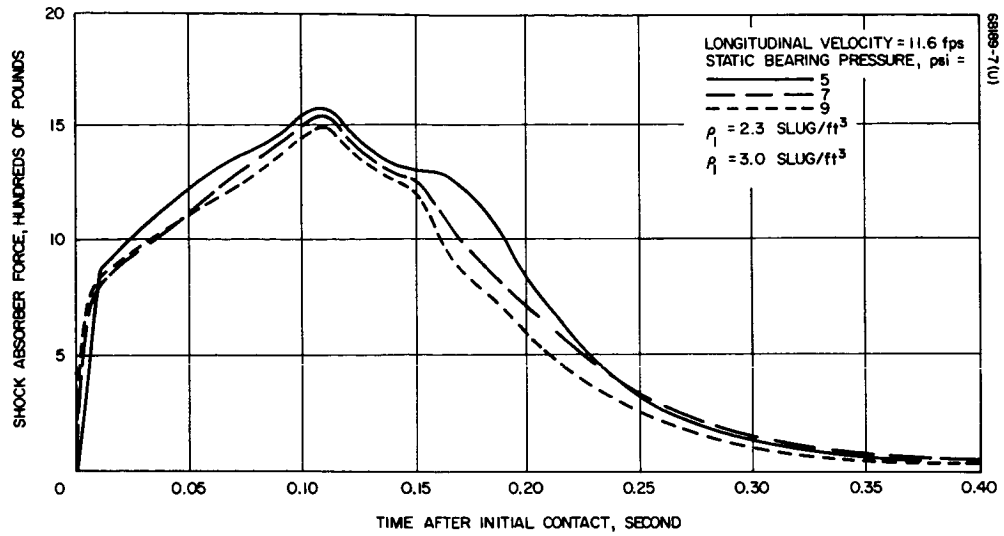
Figure 5.11-6. Shock Absorber Force-Time History
From Mathematical Model Soft Surface
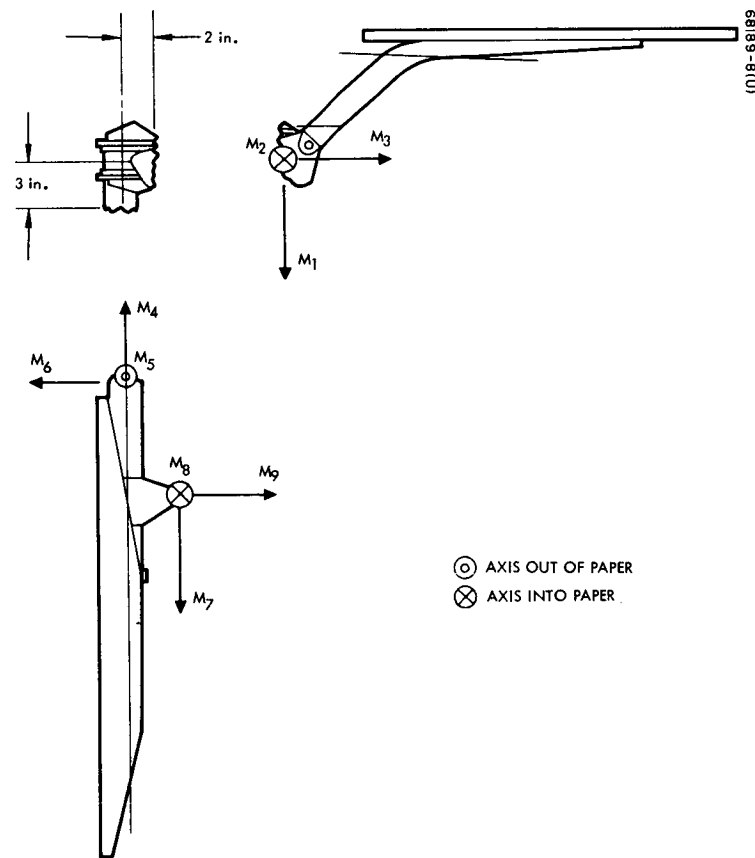
Figure 5.11-7. Solar Panel and Planar Array

1.9 in.

M_{10}

M_{12}

M_{11}

M_{14}

M_{15}

M_{13}

M_{13}

M_{15}

M_{14}

M_{17}

M_{16}

M_{18}

Z

⊙ AXIS OUT OF PAPER
⊗ AXIS INTO PAPER

(U) 6-68189
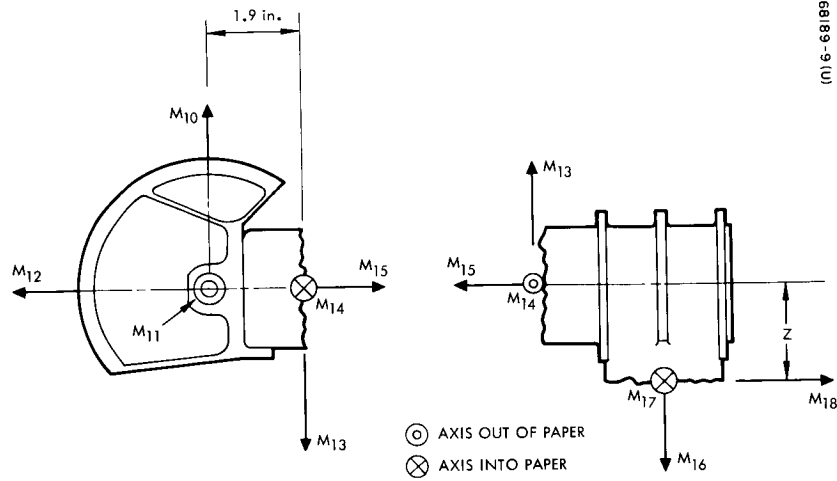
Figure 5.11-8. Elevation Motor Housing

⊄ ELEVATION
MOTOR HOUSING

19 in.

32 in.

M_{19}

M_{20}

M_{22}

M_{22}

M_{23}

(U) 6-68189-10
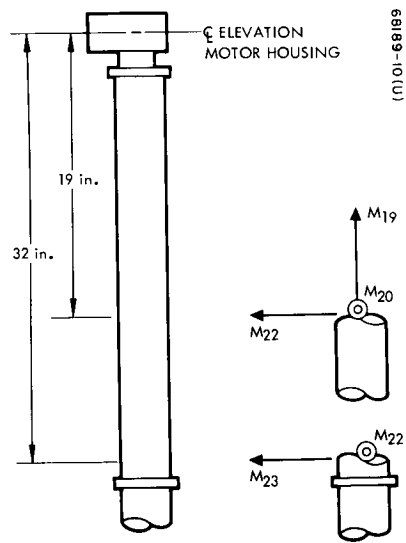
Figure 5.11-9. Structural
Moments on Mast

TABLE 5.11-2. UPPER AND LOWER BOUNDS ON MAXIMUM LOAD LEVELS IN UPPER SPACECRAFT STRUCTURE WHICH OCCURRED AT SC-1 TOUCHDOWN

Upper Spacecraft					
M_i, S_i*	Lower Bound	Upper Bound	M_i, S_i*	Lower Bound	Upper Bound
M_1	-364	-1199	M_{11}	-325	- 991
M_2	-566	-1665	M_{12}	373	-1312
M_3	140	- 407	S_{10}	- 87	- 270
S_1	- 26	- 78	S_{11}	23	- 76
S_2	- 10	29	S_{12}	- 15	92
S_3	- 5	26	M_{13}	-306	1077
M_4	-377	-1220	M_{14}	-210	- 571
M_5	-673	-2024	M_{15}	373	-1312
M_6	168	- 453	M_{16}	-302	1134
S_4	- 41	- 127	M_{17}	157	442
S_5	11	- 29	M_{18}	404	-1362
S_6	- 7	37	S_{16}	- 87	- 270
M_7	-312	1034	S_{17}	25	93
M_8	-325	- 991	S_{18}	- 15	95
M_9	373	-1312	M_{19}	-302	1134
S_7	- 87	- 270	M_{20}	-318	1760
S_8	23	93	M_{21}	770	-2487
S_9	- 15	92	M_{22}	-515	3025
M_{10}	-313	1034	M_{23}	-1104	-3688

*M_i = moment along axis 1, in pounds; S_i = shear along axis 1, in pounds.

TABLE 5.11-3. BOUNDS ON MAXIMUM G LEVELS
OCCURRING DURING SC-1 TOUCHDOWN

Lower Spacecraft		
Vertical Load, g	Lower Bound	Upper Bound
Compartment A	2.4	8.9
Compartment B	2.5	8.9
TV 3	2.7	9.9

5.11.4 EVALUATION OF VIBRATION DATA FOR AC-10/SC-1 FLIGHT ENVIRONMENT

5.11.4.1 Introduction and Summary

Five accelerometers were selected to measure vibration on SC-1 spacecraft during launch of the Atlas/Centaur-10 vehicle and for 580 seconds of powered flight. During the period of data acquisition, all accelerometers operated satisfactorily, as was evidenced in the quality of the recorded data. An oscillograph produced from taped telemetry data was evaluated to obtain preliminary information regarding the spacecraft response. These data showed the significant column base responses on the spacecraft to be low-level, high-frequency random vibration during launch, a low-level full-sine pulse transient at booster engine cutoff, and sharp spikes with high frequencies which were immediately damped out at insulation panel jettison and at Atlas/Centaur separation. The entire sequence of spacecraft responses showed close agreement with similar AC-6 instrumentations.

5.11.4.2 Instrumentation

The location and designation of the five flight vibration transducers are given in Figure 5.11-10. Four of the transducer's signals are commutated on an equal time basis and transmitted on IRIG Telemetry Channel 14. The leg 1 accelerometer signal is transmitted continuously on Channel 17. The time share arrangement restricts the recording of transient phenomenon to two accelerometers per event. This can be observed in the limited data presented in Table 5.11-4.

5.11.4.3 Data

An oscillograph record was made of both accelerometer data channels. The oscillograph had a real-time reference and was run at a paper speed of 2 ips. All tabulated AC-10 data presented in Tables 5.11-4 and -5, including rms values and frequencies, were estimated from this low-speed oscillogram.
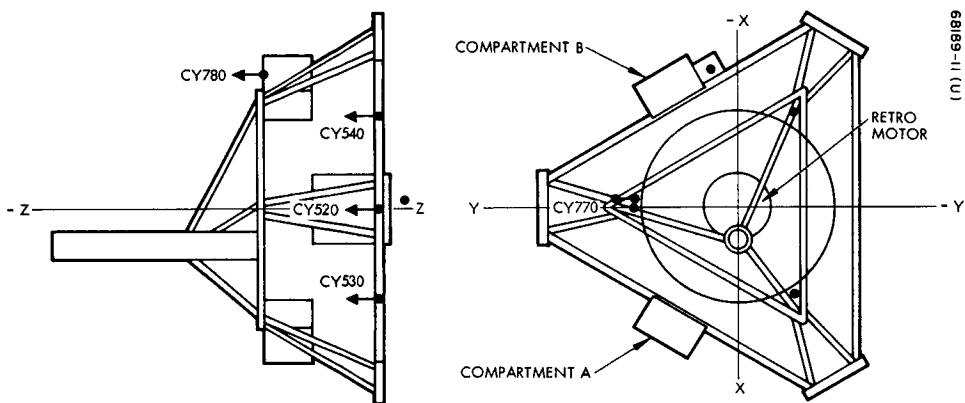
CHANNEL	LOCATION	TRANSDUCER GDA/ HUGHES NOMENCLATURE	RANGE, g	COMMENT	FREQUENCY RANGE*, cps
14	COLUMN BASE, LEG 2	CY530/V-9	± 10		
14	LEG 3	CY540/V-10	± 10	COMMUTATED	2 TO 1050
14	CENTAUR ADAPTOR	CY770	± 10	DATA	
14	FLIGHT CONTROL PACKAGE	CY780/V-11	± 10		
17	LEG 1	CY520/V-8	± 10	CONTINUOUS	2 TO 2100

*USING DISCRIMINATOR LOW PASS FILTERS SET AT APPROXIMATELY THREE TIMES STANDARD IRIG.

Figure 5. 11-10.   Transducer Location

TABLE 5.11-4. SURVEYOR I (A/C-10) POWERED FLIGHT VIBRATION ENVIRONMENT

Accelerometer	Launch $t_O - 1$ to $t_O + 35$ Random Vibration Maximum Steady State g rms (Note 2)	Atlas BECO $t_O + 142$ Transient 0 to Peak g Full-Sine Pulse	Booster Engine Jettison $t_O + 145.1$ Transients 0 to Peak g (Note 3)	Insulation Panel Jettison $t_O + 175.8$ Transients 0 to Peak g (Note 4)	Nose Fairing Jettison $t_O+202.8$ Sinusoids 0 to Peak g (Note 5)	Atlas SECO $t_O + 239.4$ Transients 0 to Peak g (Note 6)	Atlas/Centaur Separation $t_O + 241.3$ Transients 0 to Peak g (Note 4)
CY520 (Hughes-V8)	0.7	1.5 g	>10 g	>10 g	0.5 g	0.5 g	>10 g
CY530 (Hughes-V9)	0.5	1.5 g	NA	NA	NA	NA	9 g
CY540 (Hughes-V10)	0.5	NA	8 g	NA	NA	0.5 g	NA
CY770 (GD/C)	1.9	NA	NA	10 g	NA	NA	NA
CY780 (Hughes-V11)	0.7	NA	NA	NA	1 g	NA	NA

Notes:

1. NA (not available) commutated transducers not recorded.

2. At launch, random vibration on all channels is superimposed on a fundamental of 6 cps.

3. A 10 g shock less than 5 milliseconds duration.

4. Spike followed by quickly damped high-frequency vibration.

5. Four cycles at sinusoidal vibration 40 cps on CY520 and 18 cps on CY780.

6. Half-sine pulse approximately 0.1 second duration on CY520 and CY540.

Further analysis and processing of taped data would be required to determine spectral content, probability distribution and signal phase relationships. However, since the accelerometers were installed to detect unusual dynamic environment, whereas the actual flight levels were characteristically low, no further analysis of the AC-10 data is planned.

5.11.4.4 Discussion and Conclusions

The SC-10 vibration data again demonstrates the vast difference between the actual vibration inputs to the spacecraft during powered flight and the flight acceptance test (FAT) levels imposed on the spacecraft. A broadband, low-level nonstationary random vibration is experienced by the spacecraft at liftoff — 5 seconds of this vibration environment ranges from 0.7 to 0.5 g rms with less than 30 seconds in excess of 0.1 g rms. During FAT the spacecraft is exposed to 700 seconds of random vibration at 4.5 g rms.

TABLE 5.11-5. SURVEYOR I (A/C-10) DYNAMIC FLIGHT ENVIRONMENT COMPARED TO STRUCTURAL DYNAMIC MODEL 2 (A/C-6)

Z Axis Response at Attach Points (CY520, CY530, CY540)

Event	Flight Vehicle	Nature of Motion	Maximum Level	Predominate Frequency
Ignition – liftoff phase	A/C-6	Nonstationary random sinusoidal	0.7 g (rms) 7.7 cps 0.30 g 5 cycles	Broad band
	A/C-10	Nonstationary random sinusoidal	0.5 to 0.7 g (rms) 6 cps 0.6 g 40 cycles	Broad band
BECO	A/C-6	Half-sine pulse 1/2 second duration	1.3 g (peak)	
	A/C-10	Full-sine pulse 3/4 second duration	1.5 g (peak)	
Booster jettison	A/C-6	Transient duration, 230 milliseconds	5 g (peak)	High frequency
	A/C-10	Short duration	8 g (peak)	High frequency
Insulation panel jettison	A/C-6	Transient duration, 100 milliseconds	>10 g (peak)	High frequency
	A/C-10	Transient duration, 125 milliseconds	>10 g (peak)	High frequency
Nose fairing jettison	A/C-6	Sine wave for 5 cycles	0.8 g (peak)	27 cps
	A/C-10	Sine wave for 4 cycles	0.5 g (peak)	40 cps
Atlas/ Centaur separation	A/C-6	Transient duration, 100 milliseconds	>10 g (peak)	High frequency
	A/C-10	Transient duration, 250 milliseconds	>10 g (peak)	High frequency
MECO	A/C-6	Pulse, 30 milliseconds fusetime 400 milliseconds. Decay 27 cps sine modulation	0.5 g (peak) (sine)	27 cps
	A/C-10	Preliminary data not available		

The in-flight sinusoidal responses detected at the spacecraft column bases were a 6 cps 0.30 g zero to peak vibration of approximately 40 cycles duration during liftoff and 4 cycles of 40 cps vibration of 0.5 g zero to peak during nose fairing jettison. FAT vibration exposes the spacecraft to 2000 cycles of sinusoidal vibration at 1.5 g, 6500 cycles at 1.33 g, and 3000 cycles at 0.7 g.

High-frequency shocks were measured at insulation panel jettison and Atlas/Centaur separation. These transients were in excess of 10 g zero to peak at 360 to 600 cps, and completely decayed within 200 milliseconds.

Because of limitations imposed by commutation flight control sensor group, vibration data was obtained only at liftoff and during nose fairing jettison. Acceleration levels recorded during these events were similar in level to those experienced at the column bases.

The similarity in magnitude and duration of the vibration data recorded aboard the AC-6 and AC-10 vehicles (Table 5.11-5) indicates criteria can be established for defining a "typical" Atlas/Centaur vibration environment for a Surveyor payload. The GD/C preliminary flight analysis (Reference 3) states that the vibration levels experienced on AC-10 were within the ranges expected and that these values were similar to flight data obtained from AC-6.

5.11.5 REFERENCES

1. R. J. Harter, "Surveyor Spacecraft SC-1 Launch 'Quick-Look' Vibration Data," Hughes Aircraft Company, IDC 2222.5/265, 7 June 1966.

2. W. Phelps, "Quick-Look Summary, AC-10 Flight Dynamic Environment," JPL Interoffice Memo 2943-275 2941-302, 2 June 1966.

3. "Preliminary Test Results," GD/C-BN266-036, 30 May 1966.

4. W. T. Fisher, "Evaluation of Oscillograph Records of Acoustical and Vibration Data Measured During the AC-6/SC-2 Flight," Hughes Aircraft Company, IDC 2222.5/103, 19 October 1965.

5.11.6 ACKNOWLEDGEMENTS

5.12 MECHANISMS

5.12.1 INTRODUCTION

This section deals with performance of the following spacecraft equipment/functions:

a) Landing gear deployment

b) Omnidirectional antenna deployment

c) Antenna solar panel positioner (A/SPP) automatic solar panel deployment

d) A/SPP lunar operations

Performance of these equipment/functions during the SC-1 mission was excellent in all respects with the exception of the failure of omnidirectional antenna A to automatically deploy when commanded during injection. This failure is discussed in detail in Paragraph 5.12.5. The three legs and omnidirectional antenna B deployed as required in response to Centaur programmer commands during injection. Following spacecraft separation from Centaur, the solar panel was automatically deployed from its launch to its required transit position within the expected period of time. After touchdown, initial sun-earth acquisitions and subsequent lunar operations of the A/SPP (during 298 hours of the first lunar day) were executed without a single indication of any axis failing to respond to a stepping command. The total number of steps commanding the various axes after touchdown were: solar axis — 7728 steps, polar axis — 6509 steps, elevation axis — 479 steps, and roll axis — 4641 steps.

5.12.2 TABLE OF MAJOR EVENTS AND TIMES

Major SC-1 mission events and times pertinent to the analysis of mechanisms performance were as follows:

Event	Mission Time, seconds	Time (GMT)
Launch (2-inch motion)	0.000 ± 0.005	$1441{:}00.990 \pm 0.005$
Centaur extend landing gear command	$L + 714.910 \pm 0.005$	$1452{:}55.900 \pm 0.005$
Legs extended (V-01, V-02, V-03 on)	$L + 718.35 \, {}^{\pm 0.00}_{-2.40}$	$1452{:}59.34 \, {}^{+0.00}_{-2.40}$
Centaur extend omni-directional antenna command	$L + 724.77 \, {}^{+1.00}_{-0.00}$	$1453{:}05.76 \, {}^{+1.00}_{-0.00}$
Omnidirectional antenna B extended (M-02 ON)	$L + 727.35 \, {}^{+0.00}_{-2.40}$	$1453{:}08.34 \, {}^{+0.00}_{-2.40}$
A/SPP solar panel unlocked (M-14 ON)	$L + 758 \, {}^{+0.00}_{-2.40}$	$1453{:}39 \, {}^{+0.00}_{-2.40}$
A/SPP solar panel relocked (M-11 ON)	$L + 1123 \, {}^{+0.00}_{-2.40}$	$1459{:}44 \, {}^{+0.00}_{-2.40}$
A/SPP roll axis relocked (M-13 ON)	$L + 1375 \, {}^{+0.00}_{-2.40}$	$1503{:}56 \, {}^{+0.00}_{-2.40}$

5.12.3 SUMMARY OF RESULTS

Table 5.12-1 shows a comparison between expected and actual values for mechanism related performance parameters.

5.12.4 ANOMALY DISCUSSION

5.12.4.1 Omnidirectional Antenna A Deployment (TFR 18233)

As noted in Paragraph 5.12.3, telemetry data indicated that omni-directional antenna B fully extended at $1453{:}08.34 \, {}^{+0.00}_{-2.40}$ (GMT), approximately 12 minutes after launch. Since the squibs in both omnidirectional antenna pin pullers are activated by the same Centaur programmer command, omni-directional antenna A should also have deployed at this time. However, there was no indication of the telemetry switch closure (M-01 on) which should have taken place if the antenna had fully extended and locked.

Receiver A AGC data taken shortly after first acquisition showed a deep null which was totally unexpected. Subsequent measurements during the midcourse and terminal descent maneuvers continued to show abnormalities in receiver A AGC characteristics which further supported the conclusion that the omnidirectional antenna A was still either in the stowed or partially extended position. (See Paragraph 4.4 for further details regarding the RF data link abnormalities.)

TABLE 5. 12-1. PERFORMANCE PARAMETERS

Parameter	Expected Value, nominal	Measured Value
Time from Centaur extended landing gear command to legs extended indications (V-01, V-02, and V-03 ON)	2. 3 seconds	1. 04 to 3. 44 seconds
Time from Centaur extended omni-directional antenna command to omnidirectional B extended indication (M-02 ON)	2. 0 seconds	0. 18 to 3. 58 seconds
Solar axis deployment time (A/SPP solar panel auto deployment)	6 minutes 7 seconds	6 minutes 5 seconds
Roll axis deployment time (A/SPP solar panel auto deployment)	4 minutes 17 seconds	4 minutes 12 seconds
Total A/SPP solar panel auto deployment time	10 minutes 24 seconds	10 minutes 17 seconds
Solar axis launch position	+355 degrees	+355. 4 degrees
Polar axis launch position	0 degree	+0. 94 degree
Elevation axis launch position	0 degree	-0. 71 degree
Roll axis launch position	-59. 9 degrees	-60. 19 degrees
Solar axis transit position	+270 degrees	+271. 4 degrees
Roll axis transit position	0 degree	-0. 68 degree
Solar axis stepping efficiency (lunar)	>97 percent	Calculations indicate a probable 100 percent response for all axes (see Table 5. 12-4)
Polar axis stepping efficiency (lunar)	>97 percent	
Elevation axis stepping efficiency (lunar)	>97 percent	
Roll axis stepping efficiency (lunar)	>97 percent	

At approximately 1 hour 40 minutes after launch the backup omni-directional antenna extend command 0601 was sent six times from ground control. M-01 continued to indicate the not extended condition. Again, at approximately 39 hours 50 minutes after launch another unsuccessful attempt was made to extend omnidirectional antenna A by sending command 0601.

At approximately 1 hour prior to touchdown when the last transit assessment was made in a telemetry mode in which M-01 occurs, M-01 was still indicating the not extended condition. At approximately 6 minutes after touchdown, telemetry mode C was commanded on and M-01 indicated the fully extended and locked condition for omnidirectional antenna A. It is concluded, therefore, that the antenna fully extended sometime during terminal descent or at touchdown.

TFR 18233 was issued because of the failure of omnidirectional antenna A to deploy automatically. Subsequent investigation indicates that the failure was most probably caused by an excessive lateral spring force, caused by deflection of the antenna boom, at the pin puller/antenna mechanism interface. This force is believed to have resulted from antenna alignment operations (alignment for optimum antenna RF characteristics rather than mechanical alignment) after which the antenna was repositioned in the stowed position without a recheck of the adequacy of the antenna deployment spring to overcome any side loading which may have resulted from the alignment operations.

Corrective actions taken as a result of the SC-1 failure (effective for SC-2 and subsequent spacecraft) include the following:

1) Design improvements including improved surface finishes, addition of lubrication and, most important, the addition of a "kick out" spring to augment the normal deployment spring force.

2) Addition of antenna deployment tests subsequent to alignment operations (Test Requirements MS 205 and MS 206, Specification 302396A).

5.12.4.2 Omnidirectional Antenna B Deployment Time (TFR 27627)

During the analysis effort associated with this report, a second apparent anomaly was indicated. A comparison of GDC data for the Centaur extend omnidirectional antenna command, and reduced S-band Surveyor data for the omnidirectional antenna B extended command (M-02 on), indicated that the latter occurred 4.62 to 8.02 seconds before the former command was generated. TFR 27627 was, therefore, initiated.

During subsequent intensive investigations, a comparison was made of the original S-band data and corresponding Centaur VHF spacecraft telemetry data. The VHF data showed the omnidirectional antenna B extended indication to have occurred 0.18 to 3.58 seconds after generation of the Centaur extended omnidirectional antenna command as expected. Further investigation into the processing of the S-band data uncovered the fact that three complete frames of data covering 7.2 seconds of time were missing and that the subsequent data frame had been given the time indication of the first of the three missing frames. It was, therefore, established that no spacecraft anomaly was involved. Steps are presently under way to revise the data processing program to eliminate the problem.

5.12.5 CONCLUSIONS AND RECOMMENDATIONS

It is concluded that performance of the equipment/function listed in Paragraph 5.12.1 was excellent in all respects for the SC-1 transit and lunar mission with the exception of the failure of omnidirectional antenna A to

automatically deploy during injection. Telemetry data indicates that omni-directional antenna A fully extended and locked sometime during terminal descent or at touchdown.

Recommendations resulting from this analysis have already been implemented or are presently in the process of being implemented. These are as follows:

1) To demonstrate the ability of the omnidirectional antenna deployment springs to force the antenna booms clear of the pin puller yokes after completion of all alignment/assembly operations prior to flight.

2) To correct the S-band data processing program to preclude tagging data frames with incorrect times when bad frames are rejected.

5.12.6 DETAILED PERFORMANCE ANALYSIS

5.12.6.1 Landing Gear and Omnidirectional Antenna Deployments

Table 5.12-2 shows expected and actual times for Centaur programmer landing gear and omnidirectional antenna extend commands and indicates completion of deployments. Uncertainty in times derives from telemetry data sampling rates.

TABLE 5.12-2. LANDING GEAR AND OMNIDIRECTIONAL
ANTENNA B DEPLOYMENT TIMES

Event	Expected	Actual
Extended landing gear command	1452:57.09	1452:55.900 ±0.05
Legs extended indications (V-01, V-02, and V-03 on)	1452:58.20*	1452:59.34 $^{+0.00}_{-2.40}$
Extended omnidirectional antenna command	1453:07.59	1453:05.76 $^{+1.00}_{-0.00}$
Omnidirectional antenna B extended indication (M-02 on)	1453:07.76*	1453:08.34 $^{+0.00}_{-2.40}$

*Expected times are based on Centaur actual times, nominal landing gear TAT deployment times, and nominal SC-1 omnidirectional antenna FAT deployment times.

Reference to Paragraph 5.12.4 shows that the three landing gear and the omnidirectional antenna B deployment times were as expected. Expected values in Paragraph 5.12.3 for these parameters correspond to postvibration TAT deployment time data for the landing gear (two deployments: 2.31 seconds and 2.34 seconds) and SC-1 unit FAT deployment time data at -20°F for the omnidirectional antenna: omnidirectional antenna A (P/N 287300, S/N 2): 2.15 seconds; and omnidirectional antenna B (P/N 273880, S/N 2): 1.85 seconds.

5.12.6.2 Automatic Solar Panel Deployment

Automatic solar panel deployment was normal in all measurable respects. Solar axis stepping commenced immediately following the telemetry indication that the solar panel had unlocked after spacecraft/Centaur separation (14:53:39 GMT). Relock of the solar panel was indicated at 14:59:44 GMT. Roll axis stepping then commenced and continued until 15:03:56 GMT at which time roll axis relock was indicated. Concurrent with this indication, the roll axis transit lock pin puller logic switch turned off the stepping pulses to the roll motor as evidenced by cessation of characteristic stepping motor current indications on telemetry signal EP-17.

Because there is no means of counting the number of stepping pulses applied to the solar and roll stepping motors during the automatic deploy sequence, it is not possible to determine precisely the percentage response of the solar and roll axes motors to applied stepping pulses. Two indicators, however, provide substantial evidence that the response of each axis was essentially 100 percent.

The first of these indicators is the plot of roll and solar axes positions versus time shown in Figure 5.12-1. Assuming the multivibrator pulse rate to be essentially constant, missed steps (i.e., slippage of the stepping motor clutch owing to a decrease in motor torque, an increase in load, etc.) would be evidenced by a nonlinearity in the plot of axis position versus time. No such nonlinearities are indicated.

The second indicator of essentially 100 percent response derives from a comparison of the SC-1 mission and earlier solar thermal vacuum (STV) test times required to complete the automatic deploy sequence. During the STV 6A test, the automatic deploy sequence was completed in 10 minutes 24 seconds $^{+0.0}_{-2.4}$ seconds. During this test, the number of stepping pulses required was monitored and recorded (via hard lining of EP-17), and the response of each axis was subsequently calculated to be 100 percent (± certain instrumentation and data processing uncertainties). During the STV 6C test (no hard line instrumentation and, therefore, no response calculations), the total elapsed time for the automatic deploy sequence was also 10 minutes 24 seconds $^{+0.0}_{-2.4}$ seconds. During the SC-1 mission, the corresponding time interval for the automatic deploy sequence was 10 minutes 17 seconds $^{+0.0}_{-2.4}$ seconds. This represents a decrease of 1.1 percent in the nominal automatic deploy time over the STV 6A and STV 6C times.

Table 5.12-3 shows a comparison of the STV 6A test and SC-1 mission automatic deploy switch operating times and intervening periods of solar and roll axes stepping.
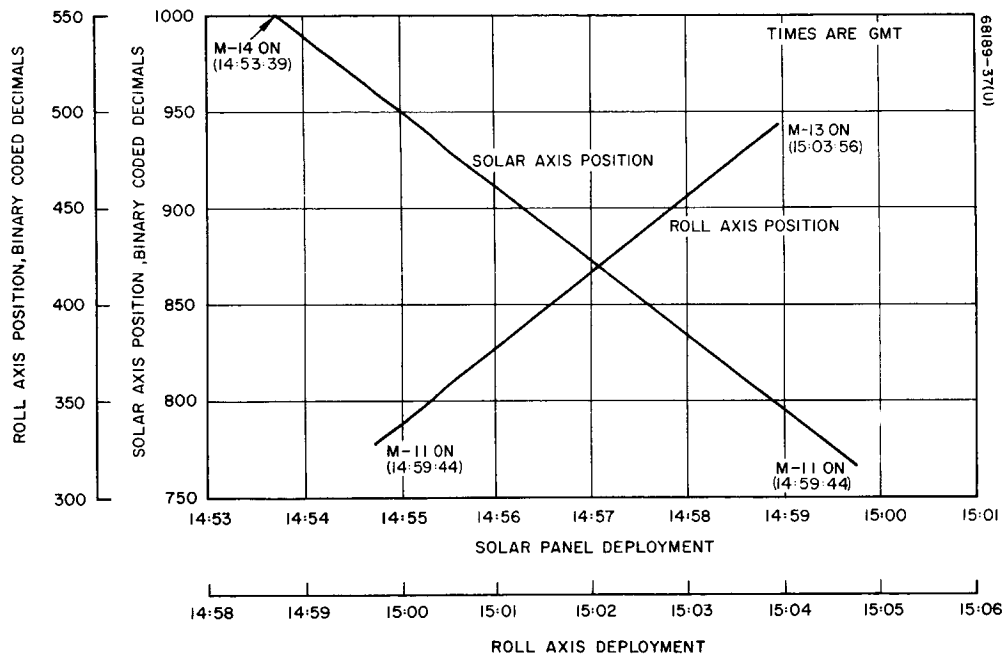
Figure 5. 12 -1.   A/SPP Automatic Deployment
Telemetry Mode C Data, 30 May 1966

GMT time

TABLE 5.12-3. SC-1 MISSION AND STV 6A SWITCH CLOSURE TIMES

	SC-1 Mission	STV 6A
M-14 on (solar panel unlock)	14:53:39, GMT	02:30:34, PDT
M-11 on (solar panel relock)	14:59:44, GMT	02:36:41, PDT
M-13 on (roll axis relock)	15:03:56, GMT	02:40:58, PDT
Solar axis stepping time (M-14 — M-11)	6 minutes 5 seconds	6 minutes 7 seconds
Roll axis stepping time (M-11 — M-13)	4 minutes 12 seconds	4 minutes 17 seconds
Total deployment time (M-14 — M-13)	10 minutes 17 seconds	10 minutes 24 seconds

On the basis of the foregoing discussion, it is concluded that the stepping response was essentially 100 percent for both the solar and roll axes during the SC-1 mission automatic solar panel deployment sequence.

Table 5.12-4 shows prelaunch and post auto deploy antenna/solar panel positioner (A/SPP) and related data for telemetry mode 4. Included also are the known launch and transit locked axes positions and the corresponding calculated positions based on corrected raw telemetry data and calibration coefficients from the SC-1 spacecraft telemetry handbook.

Based on the above data, position values calculated from corrected raw count telemetry data and telemetry handbook coefficients varied up to a maximum of 1.4 degrees from true known pinned positions. This result correlates reasonably well with known SC-1 system uncertainties, i.e., an allowable potentiometer nonlinearity of ±1.0 degree and uncorrectable random data system (root sum square) RSS errors equivalent to ±0.55 degree, plus calibration data/conversion coefficient uncertainties, etc.

For reference purposes, it should be noted that an additional position error is present in the auxiliary engineering signal processor (AESP) telemetry modes (C and T). In these modes, all telemetry raw count values are high by a factor of approximately 0.008 times the raw count position telemetry value in BCD. This offset was a signature of the SC-1 spacecraft resulting from a higher reference voltage in the AESP than in the engineering signal processor (ESP).

TABLE 5.12-4. A/SPP PRELAUNCH/POSTAUTOMATIC DEPLOY POSITION DATA (TELEMETRY MODE 4)

Raw Count Data	Raw Data		Corrected Data*	
	Prelaunch,‡ bcd	Postautomatic Deploy,‡‡ bcd	Prelaunch, bcd	Postautomatic Deploy, bcd
M-03 solar axis	993	760	986	753
M-04 polar axis	352	353	349	349
M-06 elevation axis	513	514	509	509
M-07 roll axis	324	491	321	486
S-01 reference volts	1000	1002	—	—
S-02 reference, volts return	0	0	—	—
S-05 commutator unbalance current	134	135	—	—

Position Indications Based on Calibration Coefficients and Corrected BCD Data				
	Prelaunch		Postautomatic Deploy	
Raw Count Data	Known Angle, degrees	Indicated Angle, degrees	Known Angle, degrees	Indicated Angle, degrees
M-03 solar axis	355	355.4	270	271.4
M-04 polar axis	0**	0.94	0**	0.94
M-06 elevation axis	0	-0.71	0	-0.71
M-07 roll axis	-59.9	-60.19	0	-0.68

*Corrected per Test Requirement MS 112 through MS 117, in System Test Specification 3023926 A. (Corrections for line drop and A/D conversion were not applied as these corrections were already included in the system calibration coefficients. See Table 5.12-9.)

**Polar axis not locked-based on 5/4/66 alignment data.

‡From prelaunch countdown data.

‡‡From time 150:1833:47 (telemetry mode 4).

5.12.6.3 Initial Post Landing Sun-Earth Acquisition and Repositioning

Table 5.12-8 includes the command record for the initial sun-earth acquisition for the first lunar day of Mission A. The stepping procedure followed was to cycle the stepping between the roll, solar, and polar axes when initially acquiring the sun. By this technique, the duty cycle for stepping each axis was limited to 33 percent with no dead time required for the major portion of required stepping. By the time the sun had been acquired, the planar array electrical axis was almost positioned toward earth. When sufficient db gain was obtained for TV operation, planar array fine positioning was bypassed and the spacecraft was transferred to SSAC at JPL. Simultaneous positioning of the solar panel toward the sun and the planar array electrical axis toward the earth was performed several hours later during the first postlanding Canberra pass. A breakdown of important times for the first earth day of postlanding operations is as follows:

153:08:07:42 GMT, first command of initial sun acquisition

08:55:29 GMT, final command of initial sun acquisition

09:05:25 GMT, first command of initial earth acquisition

09:19:11 GMT, final command of initial earth acquisition

12:11:03 GMT, first command of initial repositioning acquisition

13:17:49 GMT, final command of initial repositioning acquisition

During these positionings, no difficulties were experienced with regard to mechanical interferences or A/SPP malfunctions. The stepping efficiencies for this period are presented in Table 5.12-5. The angles before and after stepping have been corrected for reference voltage shift. The percentage limits shown represent only that error which could result from the lack of accurate drive potentiometer calibration data. All drive potentiometers were assumed to be linear during the mission whereas they are allowed by specification to have a nonlinearity of up to ±1 degree. This error was sufficient to put all efficiencies in brackets which allow a possible 100 percent response.

The total number of steps in each axis for initial sun-earth acquisitions and initial repositioning are presented in Table 5.12-6.

Telemetry data was analyzed to determine whether anything could be concluded regarding solar axis motor case temperature increase as a result of solar panel stepping. The conclusion was negative. Although M-10, the solar panel case temperature, rises rapidly in this period (initial acquisition), no increase can be detected as resulting from anything other than the normal temperature rise to a lunar steady state condition. Figure 5.12-2 shows a plot of A/SPP temperatures during the first lunar day.

TABLE 5.12-5. STEPPING EFFICIENCIES, FIRST LUNAR DAY

Day	Stepping Efficiency, Mechanism Axes, percent			
	Solar M-3	Polar M-4	Elevation M-6	Roll M-7
153	98.9 ± 2	100.2 ± 4	103 ± 16	98.7 ± 2
158	98.6 ± 4	100.2 ± 4	—	97.4 ± 3
165	98.7 ± 2	101.2 ± 4	103.3 ± 33	99.1 ± 1

TABLE 5.12-6. SUMMARY OF STEPPING COMMANDS

Operation	Number of Steps Commanded Each Axis				All Axes
	Solar	Polar	Elevation	Roll	
Acquisitions	922	1025	0	906	2853
Repositioning	209	122	17	171	519
Total	1131	1147	17	1077	3372

5.12.6.4   Total Number of A/SPP Steps Commanded and Effective in First Lunar Day

Table 5.12-8 contains the command record for the entire first lunar day. Table 5.12-9 presents the running step count for each of the four axes and corresponding gimbal positions calculated from the cumulative stepping count. At the end of Table 5.12-9, the final gimbal positions are recorded based upon command step counts. They agree with corrected telemetry position data (after final stepping on day 165) to less than three degrees in any axis as indicated in Table 5.12-7.

Figure 5.12-3 is a plot of the four gimbal positions as a function of time for the first lunar day based on the data tabulated in Table 5.12-9.

Specific stepping efficiencies for periods during the first lunar day which contain large blocks of stepping are given in Table 5.12-5. One hundred percent stepping efficiency was possible in all cases analyzed when a ±1 degree potentiometer nonlinearity was allowed.
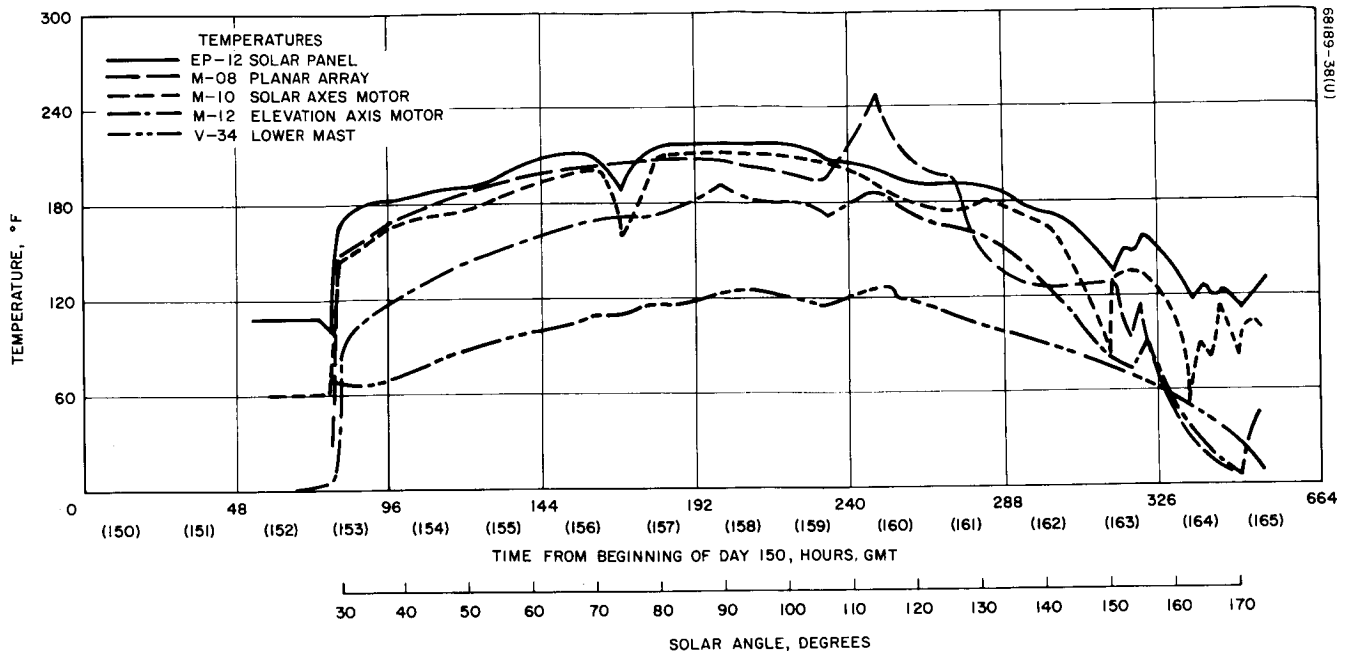
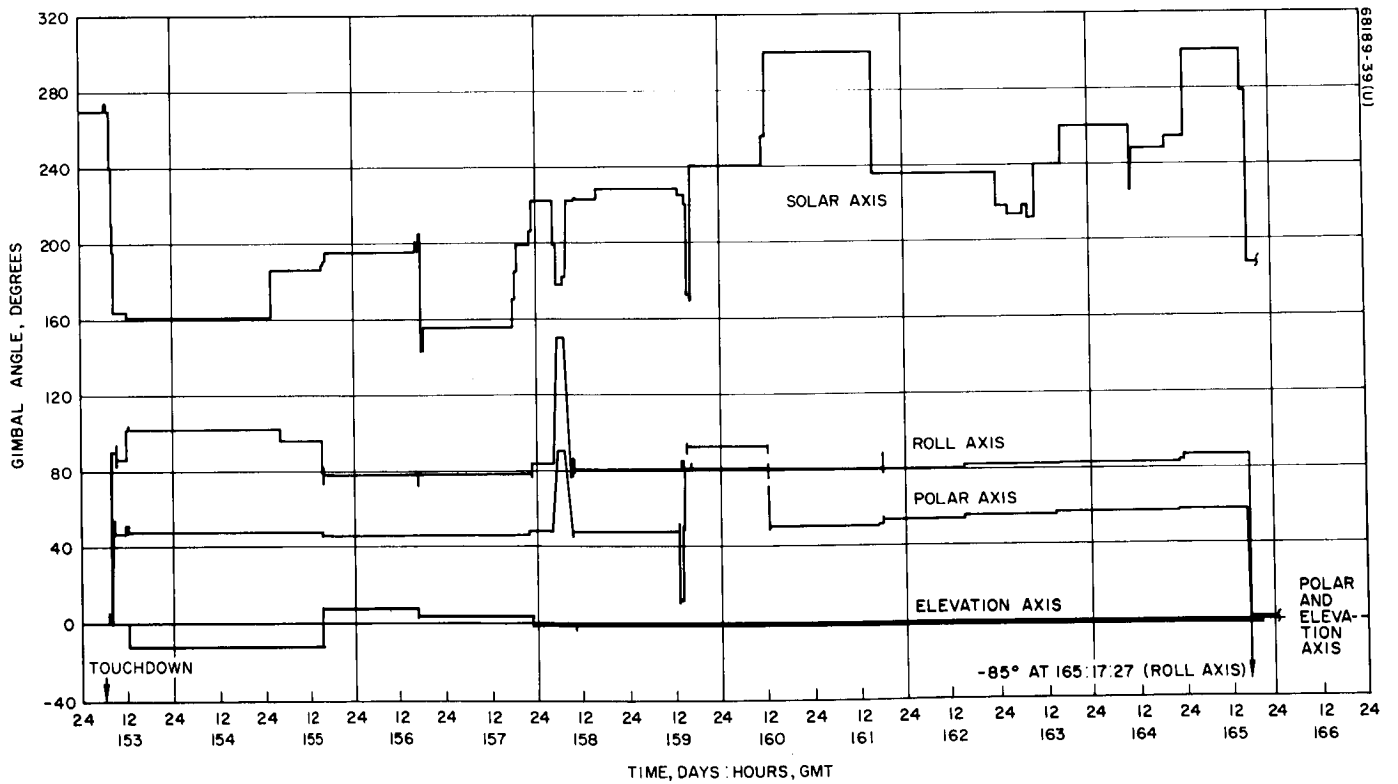Figure 5.12-2.   A/SPP Temperatures During First Lunar Day

Figure 5.12-3.   A/SPP Gimbal Positions Versus Time
First lunar day

5.12-12

TABLE 5.12-7. FINAL DAY 165 POSITION INDICATIONS

| Raw Count Data | Based on Stepping History, degrees | Telemetered Data | | Total Number Post-Touchdown Steps |
		BCD (Ref)	Degrees	
M-03 solar axis	188.5	535	191.3	7728
M-04 polar axis	1.1	352	1.1	6509
M-06 elevation axis	1.8	513	1.4	479
M-07 roll axis	-85.6	249	-85.8	4641
S-01 reference voltage	—	993	—	
S-02 reference voltage return	—	0	—	

5.12.6.5 Effect of Temperature on Stepping Efficiency

The three periods analyzed in Table 5.12-5 represent the following temperature ranges:

Day	Solar Axis Motor Case — M-10, degrees	Elevation Axis Motor Case — M-12, degrees
153	115 to 155	80 to 120
158	210 to 220	185 to 195
165	-20 to -35	-60 to -80

As shown in Table 5.12-5, there was no measurable change in stepping efficiency owing to temperature variations.

5.12.6.6 Post-Touchdown A/SPP Operations Summary

No A/SPP anomalies were detected during SC-1 first lunar day operations. Stepping efficiencies were on the order of 100 percent at all times, and at no time during the mission was it determined from the telemetry that a drive had failed to respond to a stepping command. This included the stepping of the polar axis under a maximum load condition shortly after lunar noon.

The total number of steps commanded for each axis during the first lunar day (after touchdown) were as follows:

Solar axis:	7,728
Polar axis:	6,509
Elevation axis:	479
Roll axis:	4,641
Total:	19,357

TABLE 5.12-8. A/SPP STEPPING COMMAND LOG

Start Time, day:hr:min:sec	Stop Time, hr:min:sec	Command	Quantity
153 07 13 48	07 14 07	0405	40
14 18	14 38	0401	40
14 48	15 07	0403	40
20 15	20 34	0407	40
20 44	21 04	0406	40
21 14	21 33	0402	40
21 43	22 03	0404	40
22 13	22 32	0410	40
08 07 42	08 09 42	0405	240
10 12	12 11	0402	240
12 42	14 43	0403	240
15 15	17 17	0405	240
17 57	19 58	0402	240
20 28	22 28	0403	240
23 01	25 02	0405	240
25 31	26 33	0402	120
27 02	29 03	0403	240
29 XX	30 XX	0402	120
30 22	31 43	0402	160
41 18	42 18	0402	120
45 20	45 36	0401	32
47 17	47 22	0406	4
48 26	49 53	0405	16
51 34	51 41	0406	6
52 50	53 45	0401	8
55 27	55 29	0402	2
09 05 25	09 06 46	0403	160
09 23	10 28	0404	129
12 36	12 55	0405	32
13 25	15 51	0406	96
17 12	17 30	0405	32
19 02	19 11	0403	16
12 11 03	12 11 49	405	91
13 09	14 43	403	54
15 07	15 56	410	97
16 46	16 58	402	23
24 05	25 07	405	16
25 58	26 02	406	8
27 21	27 25	401	8
28 43	28 51	402	16
29 49	29 50	401	2
37 45	42 35	405	40
43 35	43 43	406	16

Table 5.12-8 (continued)

Start Time, day:hr:min:sec	Stop Time, hr:min:sec	Command	Quantity
153 12 45 37	50 37	404	56
52 28	52 34	403	12
13 15 19	13 15 39	401	40
16 00	16 21	402	40
16 52	17 12	401	40
17 29	17 49	402	40
155 02 56	02 58	0401	200
04 50	04 50	0406	32
15 58 55	15 58 56	0404	2
16 00 30	16 00 43	0401	24
01 52	03 07	0406	150
04 55	06 17	0407	162
12 44	16 19	0406	48
17 12	21 56	0405	16
23 12	23 20	0402	16
24 15	24 27	0401	24
25 47	25 51	0402	4
36 45	38 39	0405	52
40 25	42 59	0406	30
44 17	44 21	0403	8
45 20	46 15	0404	20
47 43	47 47	0403	8
51 37	52 02	0401	49
156 17 12 30	17 12 45	0410	29
13 27	13 29	0403	2
13 56	14 01	0405	10
14 33	14 57	0401	49
18 30	19 44	0406	20
20 58	21 14	0402	32
23 18	23 50	0401	64
25 09	25 25	0402	32
27 43	27 46	0406	8
29 21	29 33	0405	24
53 47	18 19 40	0402	470
18 28 30	18 29 17	0401	101
157 06 41		0401	120
53		0401	120
07 04		0401	108
22 54		0401	60
58		0403	14

Table 5.12-8 (continued)

Start Time, day:hr:min:sec	Stop Time, hr:min:sec	Command	Quantity
157 23 00		0405	39
02		0410	47
03		0401	60
05		0401	13
10		0401	49
158 04 40 12	04 40 27	0405	30
40 57	41 11	0403	30
41 35	41 52	0402	30
43 49	44 05	0405	30
44 25	44 41	0403	30
44 56	45 13	0402	30
46 54	47 11	0405	30
47 27	47 42	0403	30
47 59	48 15	0402	30
49 58	50 15	0405	30
50 33	50 49	0403	30
51 05	51 21	0402	30
53 00	53 11	0405	30
53 33	53 49	0403	30
54 05	54 21	0402	30
56 02	56 20	0405	30
56 35	56 51	0403	30
57 46	58 02	0402	30
59 43	59 59	0405	30
05 00 15	05 00 31	0403	30
00 45	01 00	0402	30
02 47	03 04	0405	30
03 21	03 38	0403	30
04 02	04 18	0402	30
06 00	06 06	0405	30
06 36	06 53	0403	30
07 19	07 36	0402	30
09 28	09 44	0405	30
10 01	10 17	0403	30
10 32	10 48	0402	30
12 26	12 43	0405	30
13 01	13 17	0403	30
13 36	15 38	0402	47
16 16	16 33	0405	30
16 51	17 07	0403	30
19 04	19 21	0405	30
19 38	19 44	0403	30
21 47	22 04	0405	30

Table 5.12-8 (continued)

Start Time, day:hr:min:sec	Stop Time, hr:min:sec	Command	Quantity
158 05 22 22	05 22 39	0403	30
24 46	25 03	0405	30
25 21	48 59	.0403	240
49 25	54 39	0405	90
07 46 00	07 46 16	0404	30
48 36	48 53	0404	30
51 12	51 28	0404	30
53 50	54 04	0404	27
56 26	56 42	0406	30
57 05	57 20	0404	30
57 34	57 52	0401	30
59 00	— —	0117	—
08 00 57	08 01 13	0406	30
01 50	02 06	0404	30
02 29	02 45	0401	30
05 23	05 39	0406	30
06 21	06 37	0404	30
07 36	07 52	0401	30
09 34	09 51	0406	30
10 26	10 43	0404	30
11 10	11 26	0401	30
13 18	13 34	0406	30
14 01	14 18	0404	30
15 01	15 17	0401	30
17 03	17 19	0406	30
17 49	18 06	0404	30
18 34	18 50	0401	30
20 29	20 45	0406	30
21 19	21 36	0404	30
22 02	22 19	0401	30
23 59	24 15	0406	30
24 52	25 09	0404	30
25 53	26 09	0401	30
27 53	28 09	0406	30
28 59	29 15	0404	30
30 06	30 22	0401	30
31 59	32 14	0406	30
32 40	32 56	0404	30
33 27	33 43	0401	30
35 22	35 39	0406	30
36 22	36 39	0404	30

Table 5.12-8 (continued)

Start Time, day:hr:min:sec	Stop Time, hr:min:sec	Command	Quantity
158 08 37 07	08 37 23	0401	30
38 14	38 24	0401	17
41 53	42 09	0406	30
42 29	42 45	0404	30
44 43	45 00	0406	30
45 15	45 32	0404	30
47 41	47 57	0406	30
49 03	49 20	0404	30
51 28	51 43	0406	30
52 11	52 29	0404	30
55 14	55 30	0406	30
56 32	56 48	0404	30
59 20	59 36	0406	30
09 00 55	09 01 11	0404	30
03 16	03 32	0406	30
03 57	04 13	0404	30
20 03	20 16	0406	24
23 00	23 12	0406	24
26 09	26 24	0405	26
27 12	27 27	0404	30
29 49	30 00	0404	24
08 32 51	33 09	0405	34
35 07	35 25	0406	34
35 37	35 55	0403	34
10 38 56	10 39 19	0401	16
41 25	41 35	0402	8
42 17	44 29	0410	20
45 52	45 54	0407	2
51 40	52 04	0407	18
16 10	16 11	0401	49
159 13 07 19	13 07 37	0402	30
27 37	27 54	0403	32
32 17	14 06 56	0404	608
14 18 14	18 31	0405	32
19 50	52 50	0403	576
57 24	54 41	0406	32
55 44	56 01	0403	32
15 01 25	15 01 30	0406	4
03 25	03 35	0403	8
28 24	28 42	0402	32
29 05	29 12	0403	32
31 04	31 21	0402	32
31 31	31 48	0403	32
33 25	33 41	0402	32

Table 5. 12-8 (continued)

Start Time, day:hr:min:sec	Stop Time, hr:min:sec	Command	Quantity
159 15 33 55	15 34 07	0403	32
35 46	36 03	0402	32
36 10	36 27	0403	32
38 06	38 22	0402	32
38 40	38 57	0403	32
40 37	40 53	0402	32
41 01	41 08	0403	32
42 56	43 06	0402	32
43 22	43 38	0403	32
45 15	45 31	0402	32
45 39	45 55	0403	32
47 33	47 47	0402	32
48 14	48 19	0403	32
49 54	50 11	0402	32
50 17	50 33	0403	32
52 07	52 24	0402	32
52 29	52 46	0403	32
54 20	54 36	0402	32
54 41	54 58	0403	32
56 32	56 48	0402	32
56 52	16 11 54	0403	288
16 13 09	13 25	0405	32
15 01	15 19	0406	32
15 43	16 00	0402	32
20 20	39 57	0401	576
160 11 45 43	11 48 22	401	120
12 19 40	12 20 11	404	60
20 29	20 45	401	30
22 26	22 56	404	60
23 10	23 26	401	30
25 05	25 37	404	60
25 45	26 01	401	30
27 38	28 09	404	60
28 17	28 33	401	30
30 12	30 44	404	60
30 52	31 08	401	30
32 46	33 16	404	60
33 24	33 39	401	30
35 19	35 49	404	60
36 02	36 17	401	30
37 55	38 26	404	60
38 36	38 52	401	30
40 31	41 02	404	60
41 10	41 25	401	30
43 04	43 35	404	63
43 50	44 06	401	30

Table 5.12-8 (continued)

Start Time, day:hr:min:sec				Stop Time, hr:min:sec			Command	Quantity
160	12	45	45	12	46	21	405	57
		46	30		46	47	401	30
		49	41		50	03	404	40
		50	26		50	37	401	20
		53	21		54	36	403	30
		56	14		56	22	406	16
		57	27		57	45	405	32
		58	55		59	04	406	16
161	16	59	33	17	00	06	0402	64
	17	01	46		02	03	0403	32
		03	56		18	05	0402	448
		20	59		21	35	0405	64
		25	19		29	11	0406	80
		31	38		33	14	0405	32
		36	42		36	59	0403	32
		39	01		39	26	0404	48
		41	42		42	55	0403	32
162	15	09	35	15	12	30	0403	40
		13	57		15	30	0405	32
		17	12		18	56	0406	16
		20	05		21	37	0404	16
163	00	35	—	—	—		0402	53
	03	49	—	—	—		0402	43
	07	21	—	—	—		0401	45
	—	—					0402	60
	10	10	—	—	—		0401	144
	16	58	30	16	58	35	0405	8
	17	00	52	17	01	04	0403	24
		02	56		09	45	0401	168
	—	—		—	—		0402	200
164	11	13	17	11	16	13	0401	96
	18	30	26	18	30	32	0401	48
	22	12					0405	14
		13					0403	21
		14					0405	24
165	01	55					0401	368
	16	56					0402	174
		58					0406	240
	17	01					0404	240
		03					0402	240
		05					0406	240
		08					0404	240
		10					0402	240
		13					0406	240
		15					0404	240
		18					0402	240
		21					0407	24
		22					0406	240
		25					0404	202
		27					0406	427

TABLE 5.12-9. CUMULATIVE STEPS AND CORRESPONDING GIMBAL ANGLES

Time, day: hr: min: sec				Gimbal Angles, degrees				Cumulative Number of Steps Each Axis			
day	hr	min	sec	M3	M4	M6	M7	N3	N4	N6	N7
153	07	13	48	270	0	0	0				
				275	5	5	5	40	40	40	40
		22	32	270	0	0	0	80	80	80	80
	08	08					30				320
		11		240				320			
		13			15				320		
		17					60				560
		19		210				560			
		21			30				560		
		24					90				800
		33		195				680			
		26		180	45			800	800		
		28		160				960			
		31									
		42									
		45		164				992			
		47					89.5				804
		49					91.5				820
		52					90.75				826
		53		165				1000			
		55		164.75				1002			
	09	06			55				960		
		10			46.94				1089		
		13					94.75				858
		14					82.75				954
		17					86.75				986
		19			47.94				1105		
	12	12					98.125				1077
		13			51.315				1159		
		15				-12.125				177	
		17		161.875				1025			
		24					100.125				1093
		26					99.125				1101
		27		162.875				1033			
		29		160.875				1049			
		30		161.125				1051			
		40					104.125				1141
		44					102.125				1157
		47			47.815				1215		
		52			48.565				1227		
	13	15		161.125				1091			
		16		161.125				1131			
		17		166.125				1171			
		18		161.125				1211			
155	02	57		186.125				1411			
	04	50					98.125				1189
	15	59			48.44				1229		
	16	01		189.125				1435			
		02					79.375				1339
		05				8.125				339	
		13					73.375				1387
		20					75.375				1403
		23		187.125				1451			
		24		190.125				1475			
		26		189.625				1479			
		37					81.875				1455
		41					78.125				1485
		44			48.94				1237		
		46			47.69				1257		
		48			48.19				1265		
		52		195.75				1528			
156	17	12				4.5				368	
		13			48.315				1267		
		14					79.375				1495
		15		201.875				1577			
		19					76.875				1515
		21		197.875				1609			
		24		205.875				1673			

Table 5.12-9 (continued)

Time, day: hr: min: sec			Gimbal Angles, degrees				Cumulative Number of Steps Each Axis			
			M3	M4	M6	M7	N3	N4	N6	N7
156	17	25	201.875				1705			
		28				75.875				1523
		29				78.875				1547
	18	10	143.125				2175			
		29	155.75				2276			
157	06	41	170.75				2396			
		53	185.75				2516			
	07	04	199.25				2624			
	22	54	206.75				2684			
		58		49.29				1281		
	23	00				83.75				1586
		02			-1.125				415	
		05	222				2806			
158	04	40	218.25	51.765	-1.125	87.5	2836	1311	415	1616
		44	214.5	53.64		91.25	2866	1341		1646
		48	210.75	55.515		94	2896	1371		1676
		51	207	57.39		97.75	2926	1401		1706
		54	203.25	59.265		101.5	2956	1431		1736
		56	199.5	61.14		105.25	2986	1461		1766
	05	00	195.75	63.015		109	3016	1491		1796
		03	192	64.89		112.75	3046	1521		1826
		07	188.25	66.765		116.5	3076	1551		1856
		10	184.5	68.64		120.25	3106	1581		1886
		13	178.625	70.515		124	3153	1611		1916
		17		72.39		127.75		1641		1946
		19		74.265		131.5		1671		1976
		22		76.14		135.25		1701		2006
		25				139				2036
		40		91.14				1941		
		52				150.25				2126
	07	50		83.83				2058		
		57	182.375	81.955		146.5	3183	2088		2156
	08	02	186.125	80.08		142.75	3213	2118		2186
		06	189.875	78.205		139	3243	2148		2216
		10	193.625	76.33		135.25	3273	2178		2246
		14	197.375	74.455		131.5	3303	2208		2276
		18	201.125	72.58		127.75	3333	2238		2306
		21	204.875	70.705		124	3363	2268		2336
		25	208.625	68.83		120.25	3393	2298		2366
		29	212.375	66.955		116.5	3423	2328		2396
		33	216.125	65.08		112.75	3453	2358		2426
		36	219.875	63.205		109	3483	2388		2456
		42	222	61.33		105.25	3500	2418		2486
		45		59.455		101.5		2448		2516
		48		57.58		97.75		2478		2546
		52		55.705		94		2508		2576
		56		53.83		91.25		2538		2606
	09	00		51.955		87.5		2568		2636
		04		50.08		83.75		2598		2666
		22				77.75				2714
		26				81				2740
		29		46.705				2652		
		33				85.25				2774
		35				81				2808
		36		48.83				2686		
	10	39	224				3516			
		41	223				3524			
		43			-3.625				435	
		50			-1.125				455	
	16	10	229.125				3573			
159	13		225.375				3603			
		27		50.83				2718		
		32		12.83				3324		
	14	18				85				2840
		19		48.83				3900		
		54				81				2872
		55		50.83				3932		
	15	01				80.5				2876
		03	221.375	51.33			3635	3940		

Table 5.12-9 (continued)

Time, day: hr: min: sec	M3	M4	M6	M7	N3	N4	N6	N7
159 15 28	217.375	53.33			3667	3972		
	213.375	55.33			3699	4004		
	209.375	57.33			3731	4036		
	205.375	59.33			3763	4068		
	201.375	61.33			3795	4100		
	197.375	63.33			3827	4132		
	193.375	65.33			3859	4164		
	189.375	67.33			3891	4196		
	185.375	69.33			3923	4228		
	181.375	71.33			3955	4260		
	177.375	73.33			3987	4292		
56	173.375	75.33			4019	4324		
16 11		93.33				4612		
13				84.5				2908
15				80.5				2940
16	169.375				4051			
39	241.375				4627			
160 11 46	256.375				4747	4534		
12 20	260.125	89.58			4777	4672		
23	263.875	85.83			4807	4732		
26	267.625	82.08			4837	4792		
28	271.375	78.33			4867	4852		
31	275.125	74.58			4897	4912		
33	278.875	70.83			4927	4972		
36	282.625	67.08			4957	5032		
38	286.375	63.33			4987	5092		
41	290.125	59.58			5017	5152		
44	293.875	55.83			5047	5212		
46	297.625	52.08			5077	5272		
50		49.58				5312		
51	300.125				5097			
54		51.455				5342		
56				78.5				2956
58				82.5				2988
59				80.5				3004
161 17 00	292.125				5161			
02		53.455				5374		
04	236.125				5609			
21				88.5				3068
27				78.5				3148
32				80.0				3160
37		55.455				5406		
39		52.455				5454		
42		54.455				5486		
162 15 11		56.955				5526		
14				84.0				3192
18				82.0				3208
21		55.955				5542		
163 00 39	229.5				5662			
03 49	224.125				5705			
07 21	229.75				5750			
08 -	222.25				5810			
10 10	240.25				5954			
16 58				83.0				3216
17 00		57.455				5566		
17 03	261.25				6122			
					6322			
164 11 12	236.25	57.455	-1.125	83.0				
11 13	248.25				6418			
18 30	254.25				6466			
22 12				84.75				3230
13		58.767				5587		
14				87.75				3254
165 01 55	300.25				6834			
16 56	278.50				7008			
17 01	248.5	43.767		57.75	7248	5827		3494
08	218.5	28.767		27.75	7488	6067		3734
15	188.5	13.767		-2.25	7728	6307		3974
21			1.875				479	
22				-32.25				4214
25		1.142				6509		
27				-85.625				4641

5.12.7 DATA SOURCES

Sources of data for the analysis contained in this section of the report were as follows:

1) General Dynamics/Convair report GD/C-BNZ66-037, 15 July 1966 (liftoff and Centaur programmer command times used in Paragraph 5.12.2 and Table 5.12-2).

2) Centaur VHF telemetry data (times for the legs extended and omnidirectional antenna B extended indication used in Paragraph 5.12.3 and Table 5.12-2).

3) JPL Magnetic Tape 2927 (SFOF via ETR) for data relating to signals M-03, M-07, and M-11 used in Figure 5.12-1.

4) Hughes Aircraft Company CDS line printer data for SC-1 STV 6A(12/28/65) and STV 6C (1/21/66) A/SPP auto deployment switch closure times used in Paragraph 5.12.7.1 and Table 5.12-3.

5) JPL magnetic tape 117X (Joberg data) for frame time 150:1833:47 telemetry mode 4 for post auto deployment BCD data used in Table 5.12-4.

6) ETR CDS line printer data (launch pad countdown, 5/30/66) for prelaunch BCD data used in Table 5.12-4.

7) SPAC TTY 4 and 6, SPAC hand recorded command records, and JPL command magnetic tapes for compiling the A/SPP stepping command log of Table 5.12-8.

8) SFOF bulk printer data (Format 38) for obtaining the final A/SPP position (BCD) readings used in Table 5.12-7.

5.12.8 ACKNOWLEDGEMENTS

The following people contributed to this section of the report:

W. A. Moynier, coordinator

L. L. Gamer

R. L. Lackman

5.13 TELEVISION

5.13.1 INTRODUCTION

The spacecraft television system consists of a survey television camera, television auxiliary, spacecraft calibration charts, and spacecraft transmission system. Included also is a descent television camera (not used in the SC-1 mission) employed to take pictures during lunar approach.

The purpose of the survey camera is to take pictures of the spacecraft and of the local lunar landscape during the postlanded phase. The survey camera is characterized by a 600 line roster with 600 picture elements per line. In addition, the camera has a zoom lens capability providing either a 25 millimeter or a 100 millimeter focal length. Color filters can be inserted in the lens optical path by adjusting the position of a four-sector filter wheel. The direction of camera viewing is altered by commanding a camera panning mirror in azimuth and elevation. In the period immediately after touchdown, prior to earth acquisition by the high gain antenna, or in the event of failure of the high gain antenna or of the high power transmitter, the television system can provide a reduced scan rate (200 lines) and lower picture quality compatible with transmission bandwidth under these conditions.

5.13.2 MAJOR TELEVISION SUBSYSTEM EVENTS

Table 3-5 in Section 3.3 summarizes the lunar events taking place throughout the first lunar day and indicates the general picture taking sequences employed. The total number of pictures taken during each earth day is shown in Table 5.13-1.

5.13.3 SUMMARY OF RESULTS

At this writing, the majority of the lunar TV pictures have not been made available to postmission analysis personnel for study and analysis. Thus, this report is very superficial and qualitative in nature as it is based only on the press-released photographs.

The survey television camera took approximately 10,316 pictures during the first lunar day of which the first 11 pictures were in the 200 line mode (prior to positioning the planar array). The camera system responded

TABLE 5. 13-1. NUMBER OF TV PICTURES TAKEN
DURING FIRST LUNAR DAY

Earth Day Number	Number of TV Pictures
153	145 (11 in 200 line mode)
154	863
155	395
156	662
157	867
158	1048
159	0 } lunar
160	0 } noon
161	1759
162	1373
163	1363
164	1321
165	520

to every command up to day 163 when elevation stepup commands inter-
mittently failed to be effective (see subsection 5. 13. 5. 3).

Observation of the limited number of available photographs indicates
that the TV system produced high quality pictures as evidenced by their
resolution, gray scale rendition, and apparent signal-to-noise ratio (see
Figure 1-1, Section 1). Some of the pictures exhibit noise traces of a
coherent nature whose origin at this time is unknown.

The color pictures released indicate that the spacecraft TV calibration
charts can be used as a color processing standard for the four colors (red,
green, blue, and white) on the chart and thus provide reasonable confidence
that lunar surface colors, having a smooth spectrum, can be reproduced
fairly accurately.

5. 13. 4 ANOMALY DESCRIPTION

The following four anomalies were reported during the SC-1 lunar
operations phase:

1) TFR 27503 reported on the glare problem encountered during
days 153 and 154.

2) TFR 27504 reported the failure of the camera mirror elevation
potentiometer on day 166.

3) TFR 27505 reported on the lack of stepping response for each elevation command subsequent to the potentiometer failure in item 2 above.

4) TFR 27509 reported on the loss of camera frame identification data due to false sync words being generated by the identification data.

Each of the above anomalies will be described in further detail below, and the analysis performed on said anomaly will be outlined.

5. 13. 4. 1   Glare

A glare problem in the survey television system was known to exist since testing in 1964 by United States Geodetic Survey at the Bonito Lava Flow test site in Flagstaff, Arizona. Subsequent to the above tests, a new camera mirror hood was designed to minimize the sun glare problem and is scheduled to be used on spacecrafts 5, 6, and 7. However, the above tests were not extensive enough to provide a profile of mirror azimuth and elevation position with respect to sun direction that could be used during lunar operations to avoid the regions where the glare problem existed. During the first 2 days (153 and 154) of lunar operations, the glare problem presented the most difficulty. On subsequent days, this problem was virtually eliminated by avoiding glare regions.

No analysis of this problem has yet been accomplished due to the lack of SC-1 pictures exhibiting glare.

5. 13. 4. 2   Elevation Potentiometer Failure

On day 163 the elevation potentiometer winding opened at a point corresponding to approximately 15 degrees above the horizontal. The potentiometer specification, 988680-1, indicates the potentiometer has a design life in high vacuum of 6000 cycles, where a cycle constitutes a complete traverse of the mechanical-electrical range of the potentiometer. Thus, any given step position should withstand some 6000 operations through that position. There were some 25,000 elevation step commands sent to the spacecraft at the time of failure. With approximately 20 step positions over the useful elevation range, each step position, on the average, would have received approximately 1250 operations, which is well below the above stated design life. In addition, the failure occurred at an upper elevation position which most likely received even less than that average amount.

It was recognized sometime ago at Hughes that several potential failure modes existed for these potentiometers. An extensive program to find suitable remedies was undertaken. As a consequence of this program, SC-5 and subsequent spacecraft will have potentiometers lubricated with niobium diselinide for the mirror and lens assemblies.

5. 13. 4. 3   Failure Of Elevation Stepping

On day 165, shortly before sunset, the camera mirror failed to respond to several elevation stepup commands. However, the elevation stepdown commands brought about normal response. The mirror was able to be stepped up in elevation by sending repeated stepup commands with an efficiency of approximately 25 percent in response. The television task effort for that day, 165, consisted of the following:

1) Wide angle panorama

2) Narrow angle, sector 17

3) Narrow angle, sector 18

4) Narrow angle, sector 19

5) Narrow angle, sector 1

6) Narrow angle, sector 2

During the course of item 6 above, the apparent binding of the camera mirror in stepup commands occurred. At that point, elevation scans were terminated and azimuth scanning was initiated under a reduced work schedule. Fifteen more pictures were then taken. The sun corona experiment was then initiated and continued until sunset.

The TV Mirror Unit Detail Specification 236120 requires that the TV mirror be capable of being stepped in elevation for 2600 steps. A cursory analysis at Hughes indicated that the elevation drive was stepped some 27,000 steps at the time the binding occurred. This is approximately 10 times beyond its design life specification. At the same time, the azimuth drive, which has a design life of 102,000 steps, had received only some 3500 steps.

In addition, the failure of the elevation potentiometer is believed to have increased the torque required to step the mirror in elevation. It is recommended that on subsequent missions scanning techniques be used that make better use of the azimuth drive life while conserving elevation drive life. Additionally, the azimuth and elevation drive mechanisms have been redesigned for SC-5 and subsequent spacecraft to provide greater torque margins.

5. 13. 4. 4   Loss Of Frame Identification Data

The loss of frame identification data due to false sync words contained in the identification data itself was known prior to SC-1 launch. This problem was correctly diagnosed during SC-2 mission sequence testing. Subsequent analysis led to a correction of this problem by using a double sync word which will be implemented on spacecrafts 3 through 7.

5. 13. 5 CONCLUSIONS AND RECOMMENDATIONS

The SC-1 spacecraft television system met and exceeded all its design goals based upon the limited information available to make such a judgment.

It would seem prudent even yet to analyze, from an engineering standpoint, the great bulk of TV data obtained during the SC-1 lunar phase. Of interest in future missions is the azimuth and elevation limits of regions of glare as a function of solar azimuth and elevation in spacecraft coordinates. To be determined is the origin of coherent noise traces apparent in many of the TV pictures. The TV system point spread function can be determined from microdensitometer traces of star images. The number of cycles of each camera function during the mission should be determined so that comparisons can be made of these values against design life values to establish the adequacy of the present camera design. It is therefore recommended that the TV data required for a thorough analysis of Mission A be furnished to Hughes.

5. 13. 6 ACKNOWLEDGEMENTS

L. E. Blanchard coordinated this section.

5.14 SC-1 TRANSIT TRAJECTORY

5.14.1 TRAJECTORY ANALYSIS

The SC-1 spacecraft was launched from ETR launch site 36A at
Cape Kennedy, Florida, on Monday, 30 May 1966, using a General Dynamics/
Convair (GD/C) Atlas/Centaur (AC-10) boost vehicle. Liftoff occurred at
14:41:00.990 GMT. Two seconds after liftoff, the launch vehicle began a
13-second programmed roll that oriented the vehicle from a pad aligned
azimuth of 105 degrees to a launch azimuth of 102.285 degrees. At 15 seconds,
a programmed pitch maneuver was initiated. The nominal and actual times
for the Atlas/Centaur boost phase events are summarized in Table 5.14-1.
All mark times were nominal except Mark 8 Centaur main engine cutoff,
which occurred 6 seconds late. It was subsequently determined that this
value is within the three σ tolerance. The launch phase ascent trajectory
profile is illustrated in Figure 5.14-1.

Separation of Surveyor from Centaur occurred at 14:53:37.2 GMT on
30 May 1966 at a geocentric latitude and longitude of 17.6 and 312.1 degrees,
respectively. The spacecraft was in sunlight at separation and never entered
either the earth's or the moon's shadow during the transit trajectory. The
direction cosines of the spacecraft-sun direction at injection in spacecraft
coordinates are $X = -0.18897$, $Y = 0.63563$, and $Z = -0.00419$.

The predicted view periods for the three committed tracking stations
are shown in Table 5.14-2. This summary is a compilation of the pre- and
postmidcourse trajectories. The rise and set criteria are included under
the column marked Event. This table shows that Tidbinbilla (Canberra),
Australia, did not see the spacecraft until late in the flight. Some trajectories
yield a small view period for this station during the first Johannesburg pass.

Since the midcourse maneuver was performed on 31 May at 0645,
Goldstone had viewed Surveyor for about 4-1/2 hours premidcourse and for
about 3-3/4 hours postmidcourse. Pre- and postlanding Goldstone visibility
was approximately 4 and 5 hours, respectively. Predicted touchdown time
was 2 June 1966 at 06:17:36.8.

Figure 5.14-2 shows the trajectory path on the stereographic projec-
tion of each of the committed DSIF stations. Of special interest is the first
pass at Tidbinbilla (Canberra), Australia, which shows a maximum elevation
of about 4.5 degrees, just below the horizon mask.

TABLE 5.14-1. MARK EVENTS

Mark Number	Event	Nominal Time Seconds	Actual Time Seconds
	2-inch motion (liftoff) (14:41:00.99 GMT)	0.0	0.0
1	Booster engine cutoff (guidance discrete, staging acceleration 5.7g)	142.5	142.2
2	Jettison booster package	145.6	145.6
3	Jettison insulation panels	176.5	176.2
4	Jettison nose fairing	203.5	203.0
5	Sustainer engine cutoff (by propellant depletion)	239.7	239.3
6	Atlas/Centaur separation	241.7	241.8
7	Start Centaur main engines (SECO + 11.5 seconds)	251.2	251.9
8	Centaur main engine cutoff (guidance discrete)	683.3	689.3
9	Surveyor landing gear extend command	715.2	715.5
10	Surveyor omnidirectional antenna extend command	725.7	725.7
11	Surveyor high-power transmitter on	746.2	745.4
12	Centaur/Surveyor electrical disconnect	751.7	752.3
13	Separate spacecraft	757.2	757.1
14	Admit guidance	762.2	759.5
15	Start H_2O_2 engines (V), 180-degree turnaround mode	802.2	N.A.
16	Stop H_2O_2 engines, 180-degree turnaround mode	822.2	N.A.
17	Start retrothrust (Centaur tank blowdown)	997.2	996.0
18	Stop retrothrust	1247.2	1247.7
19	Energize power changeover switch	1247.2	1258.5
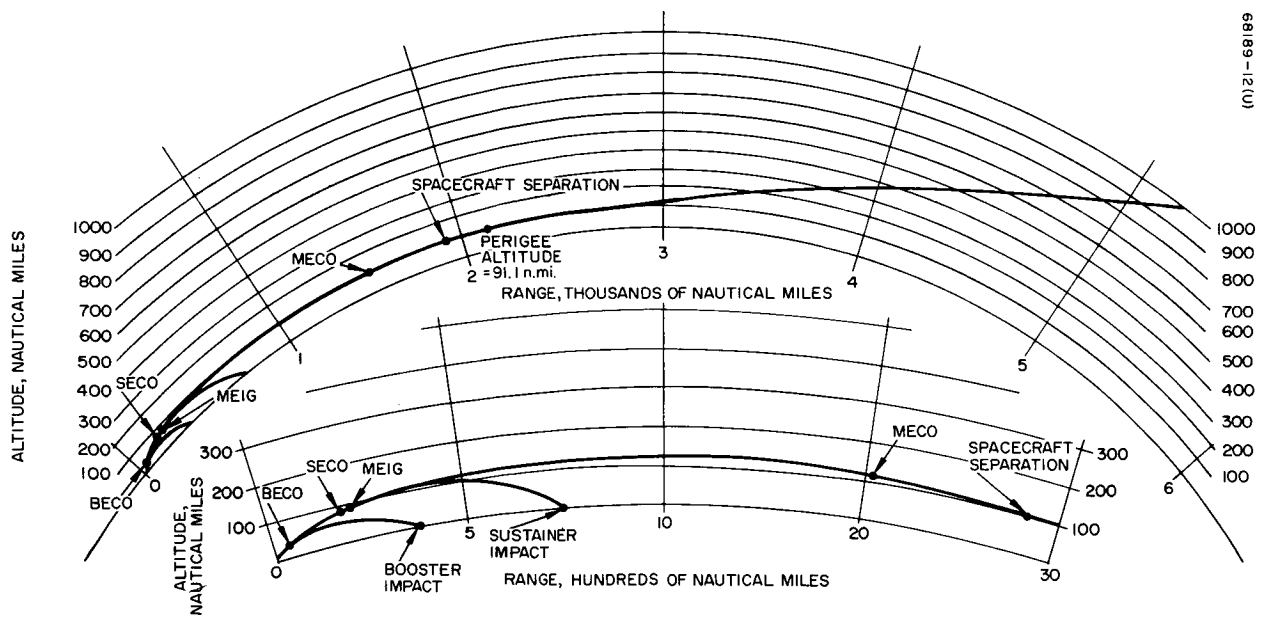
Figure 5.14-1.   Launch Phase Trajectory Profile

TABLE 5.14-2.   PREDICTED VIEW PERIOD SUMMARY

Station	Event	GMT Time			
		May - June 1966	Hr	Min	Sec
DDS 51 Johannesburg	5° Elevation rise	30	15	04	30
DDS 11 Goldstone	5° Elevation rise	31	02	08	40
DDS 51 Johannesburg	90° Hour angle set	31	02	16	36
DDS 42 Tidbinbilla	5° Elevation rise	31	05	59	23
DDS 11 Goldstone	5° Elevation set	31	10	33	47
DDS 51 Johannesburg	270° Hour angle rise	31	15	00	04
DDS 42 Tidbinbilla	5° Elevation set	31	19	25	16
DDS 11 Goldstone	5° Elevation rise	1	02	23	28
DDS 51 Johannesburg	90° Hour angle set	1	02	58	45
DDS 42 Tidbinbilla	5° Elevation rise	1	06	29	44
DDS 11 Goldstone	5° Elevation set	1	11	08	04
DDS 51 Johannesburg	270° Hour angle rise	1	15	14	32
DDS 42 Tidbinbilla	5° Elevation set	1	19	36	12
DDS 11 Goldstone	5° Elevation rise	2	02	25	13
DDS 51 Johannesburg	90° Hour angle set	2	03	09	12
DDS 42 Tidbinbilla	5° Elevation rise*	2	06	38	55
DDS 11 Goldstone	5° Elevation set*	2	11	25	08

*View periods of moon's center.
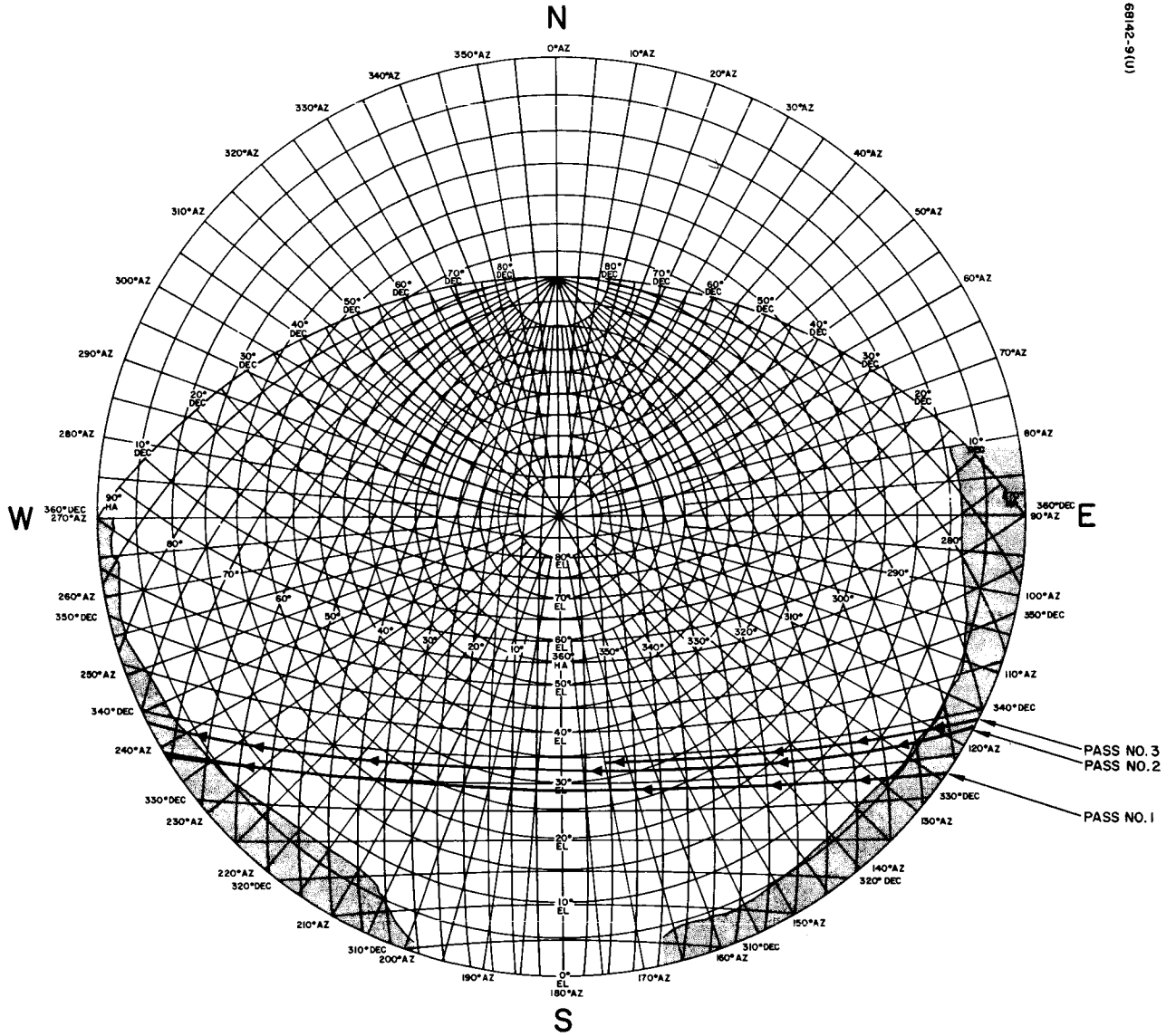
a) DSIF 11, Pioneer Station

Figure 5.14-2. AZ-EL and HA-DEC
Coordinates, Stereographic
Projection

5.14-5
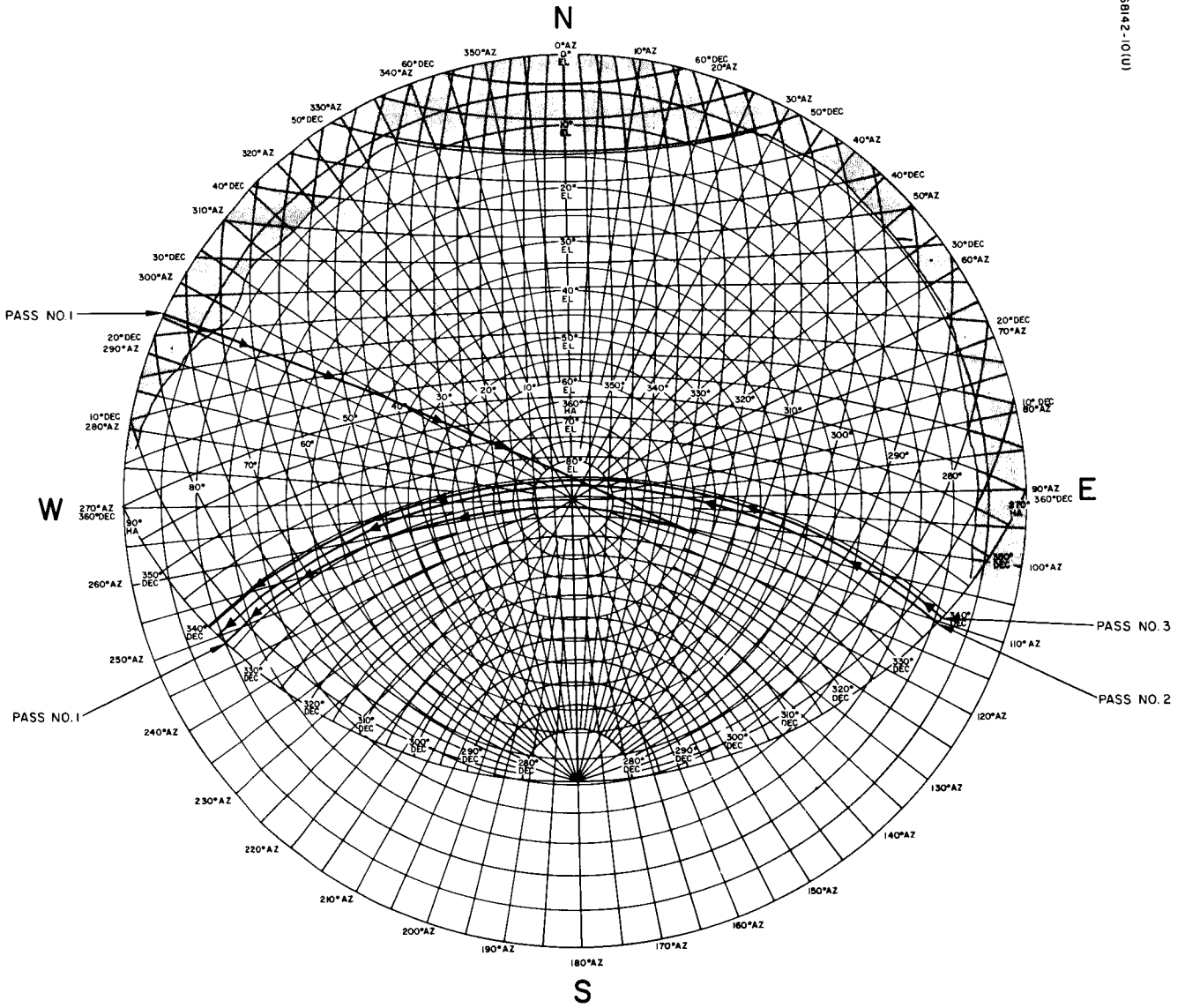
b) DSIF 51, Johannesburg Station

Figure 5.14-2 (continued). AZ-EL and HA-DEC
Coordinates, Stereographic Projection
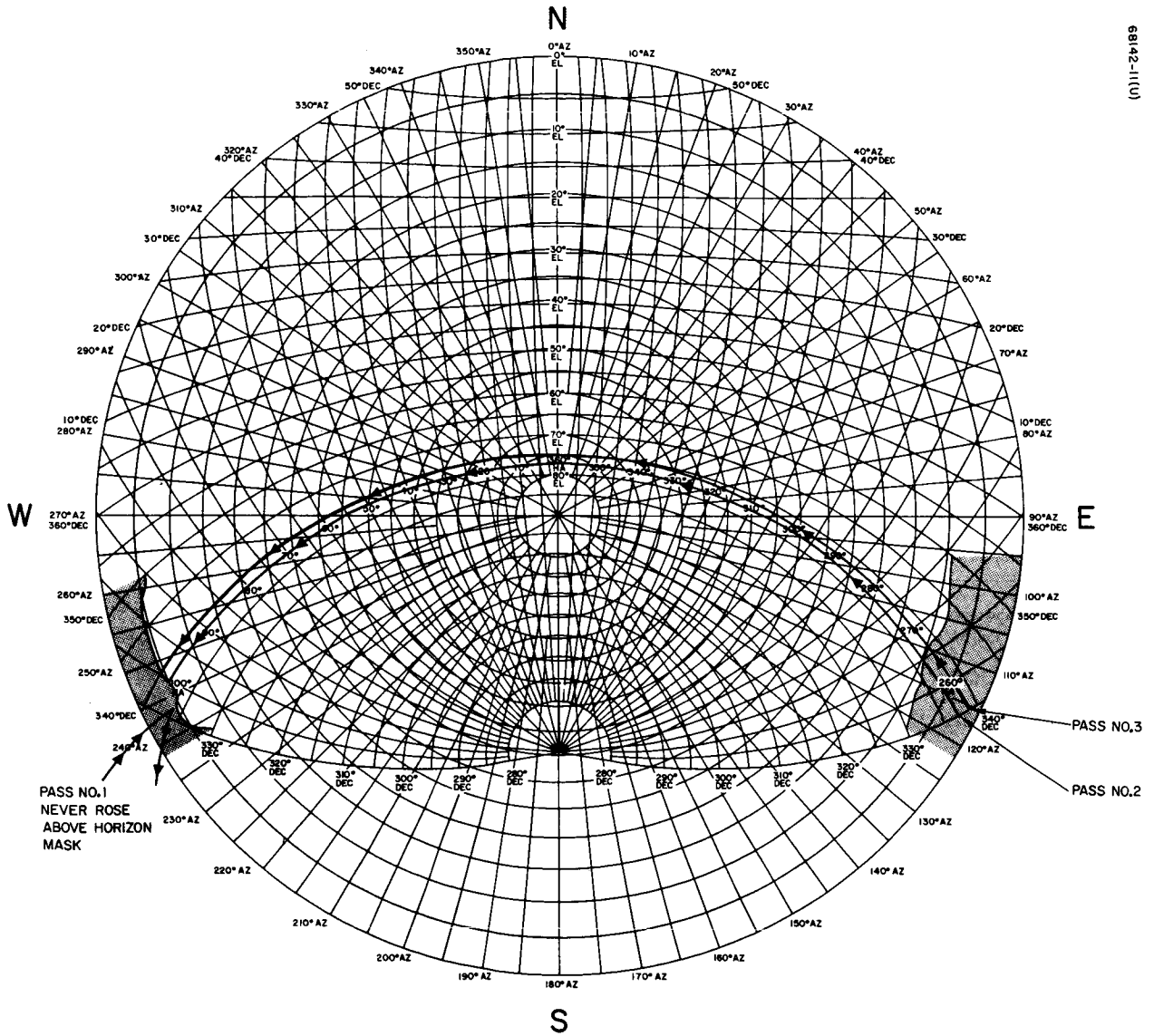
c) DSIF 42, Canberra Station

Figure 5.14-2 (continued). AZ-EL and HA-DEC
Coordinates, Stereographic Projection
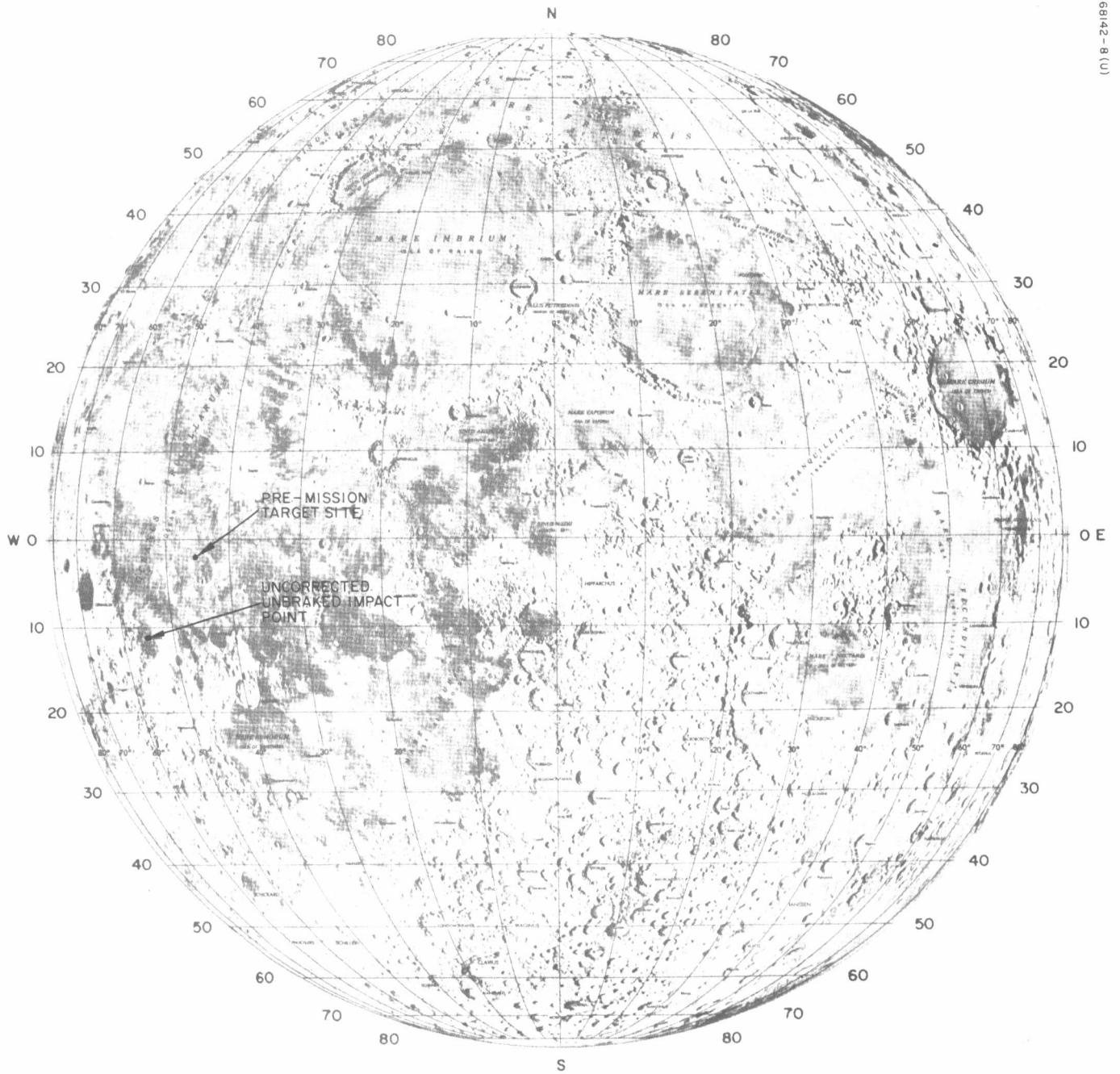
Figure 5.14-3. Surveyor I Premission Target and Uncorrected Impact Points
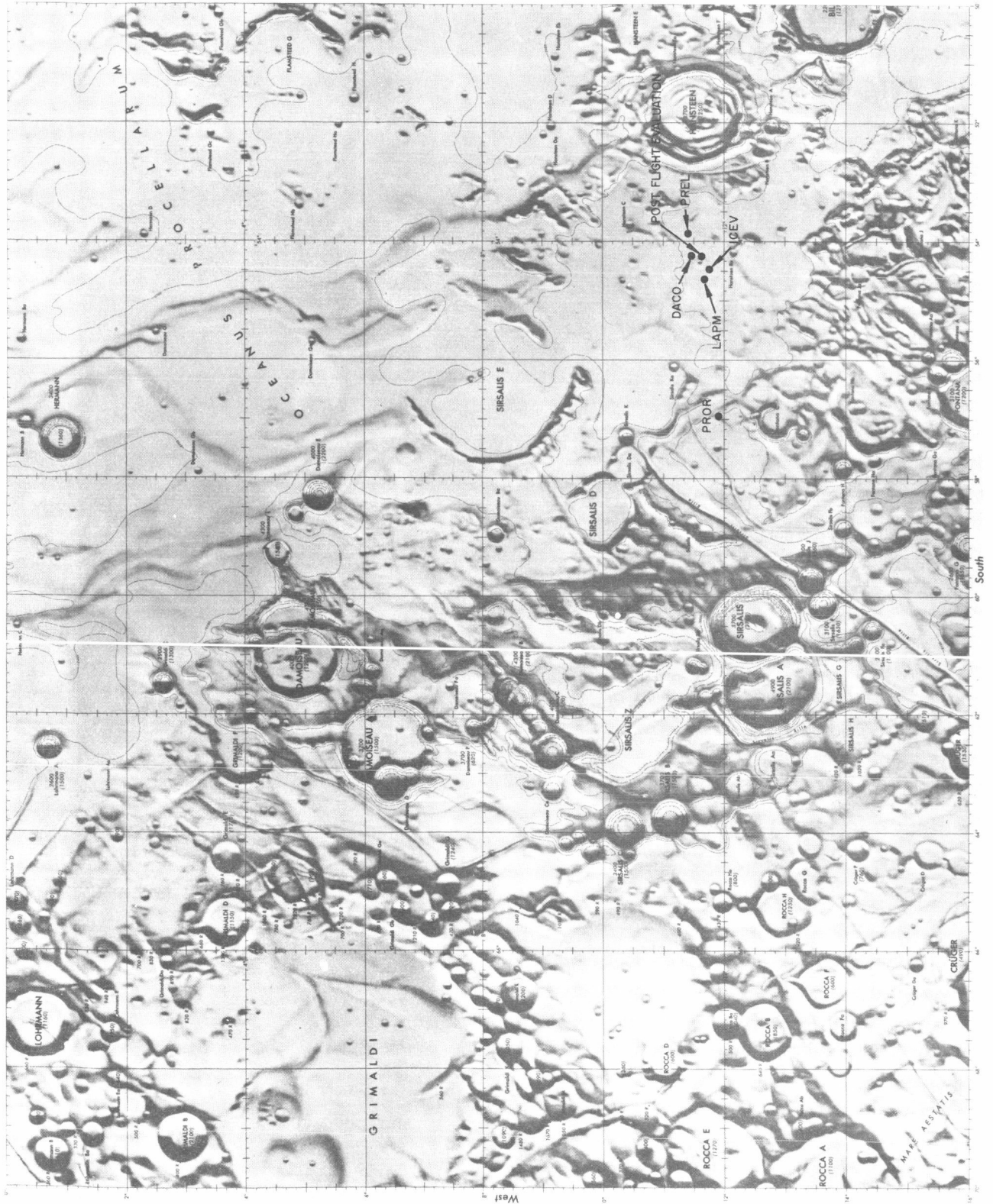
Figure 5.14-4. Surveyor I Premidcourse Orbit Determination Results

In Table 5. 14-3 pre- and postmidcourse injection and terminal conditions have been tabulated. These results were obtained several days after the mission and are considered final.

The proximity of the uncorrected and the original aim point is shown in Figure 5. 14-3. The uncorrected, unbraked impact point is located on the western edge of Oceanus Procellarum west of the crater Hansteen. The coordinates are approximately -11. 425 degrees latitude and 305. 853 degrees longitude. The original aim point is approximately 400 km to the northeast just north of the crater Flamsteed (i. e. ,-3. 25 degrees latitude and 316. 17 degrees longitude).

Figure 5. 14-4 is an enlarged region in the area of the uncorrected impact site. A few selected orbit computations are shown.* As more and more tracking data was acquired, the predicted site moved eastward, converging on the coordinates noted above.

Figure 5. 14-5 gives the earth track traced by Surveyor I. Specific events such as sun and Canopus acquisition, midcourse maneuver, touchdown, and rise and set times for the DSIF stations are also shown. Figures 5. 14-6 and 5. 14-7 are plots of probe geocentric radius and velocity as a function of time from injection (separation). Figure 5. 14-8 shows the earth-probe-moon, sun-probe-moon, and earth-probe-sun angles versus time from injection (separation). Figure 5. 14-9 shows the cone and clock angles as a function of time. The coordinate system is defined on the figure. In the cruise mode, the spacecraft -Z axis is aligned to the sun and the -X axis to the projection of Canopus. Figures 5. 14-10 and 5. 14-11 give the selenocentric radius and velocity as a function of time from injection.

Figure 5. 14-12 illustrates the Centaur and Surveyor trajectories. The projection of each trajectory is plotted on the earth's equatorial plane. The best estimate of the Centaur injection conditions was obtained from ETR. These conditions were computed inflight based upon postretro data. A mission design constraint states that the Centaur/Surveyor separation distance must be 336 km by at least 5 hours after injection to eliminate possible Centaur interference during Canopus acquisition. The required separation distance was reached 2 hours and 17. 5 minutes after launch. The Centaur passed above and behind the moon about 6 hours and 20 minutes after Surveyor I touchdown.

---

*DACO — Data consistency orbit
 PREL — Preliminary midcourse orbit
 ICEV — Initial condition evaluation orbit   See Reference 1.
 LAPM — Last premidcourse orbit
 PROR — Predict orbit

TABLE 5.14-3. PRE- AND POSTMIDCOURSE INJECTION AND TERMINAL CONDITIONS

Coordinate System	Premidcourse Injection Conditions, 30 May 1966, 14:53:37.385 GMT					
Inertial Cartesian	X = 2813.6136 km	Y = 5574.0461 km	Z = 1979.7524 km	DX = -8.3688738 km/sec	DY = 5.5320036 km/sec	DZ = -4.4497759 km/sec
Inertial spherical	RAD = 6550.2540 km	DEC = 17.592224 deg	RA = 63.216706 deg	VI = 10.974589 km/sec	PTI = -1.2120495 deg	AZI = 114.75517 deg
Earth-fixed spherical	RAD = 6550.2540 km	LAT = 17.592224 deg	LON = 312.14293 deg	VE = 10.562934 km/sec	PTE = -1.2592931 deg	AZE = 115.78965 deg
Orbital elements	C3 = -1.2639824 km²/sec²	ECC = 0.97923824	INC = 30.044723 deg	TA = -2.4498112 deg	LAN - 276.45973 deg	APF - 145.31695 deg

Coordinate System	Premidcourse Encounter Conditions, 2 June 1966, 05:28:59.985 GMT					
Selenocentric	RAD = 1738.09 km	LAT = -11.419473 deg	LON = 305.85900 deg	VP = 2.6649810 km/sec	PTP = -79.992989 deg	AZP = 266.77994 deg
Miss parameter earth equator	BTQ = -585.25804 km	BRQ = 305.93221 km	B = 660.39495 km			
Miss parameter moon equator	BTT = -656.92308 km	BRT = 67.634913 km	B = 660.39565 km			

Coordinate System	Postmidcourse Injection Conditions, 31 May 1966, 06:45:53.800 GMT					
Inertial Cartesian	X = -103401.67 km	Y = -107006.61 km	Z = -66323.279 km	DX = -0.88951855 km/sec	DY = -1.5378124 km/sec	DZ = -0.62099156 km/sec
Inertial spherical	RAD = 1629.1439 km	DEC = -24.023111 deg	RA = 225.98155 deg	VI = 1.8819512 km/sec	PTI = 76.179004 deg	AZI = 72.573537 deg
Earth-fixed spherical	RAD = 1629.1439 km	LAT = -24.023111 deg	LON = 236.18758 deg	VE = 10.581803 km/sec	PTE = 9.9447604 deg	AZE = 270.74016 deg
Orbital elements	C3 = -1.3516429 km²/sec²	ECC = 0.97691524	INC = 29.371361 deg	TA = 159.89571 deg	LAN = 278.34842 deg	APF - 144.00209 deg

Coordinate System	Postmidcourse Encounter Conditions, 2 June 1966, 06:15:14.632 GMT					
Selenocentric	RAD = 1735.6000 km	LAT = -2.3555486 deg	LON = 316.64097 deg	VP = 2.6553638 km/sec	PTP = -83.868529 deg	AZP = 343.30690 deg
Miss parameter earth equator	BTQ = -253.86534 km	BRQ = -327.05272 km	B = 414.01824 km			
Miss parameter moon equator	BTT = -114.52272 km	BRT = -397.86410 km	B = 414.01824 km			

68142-2 (U)
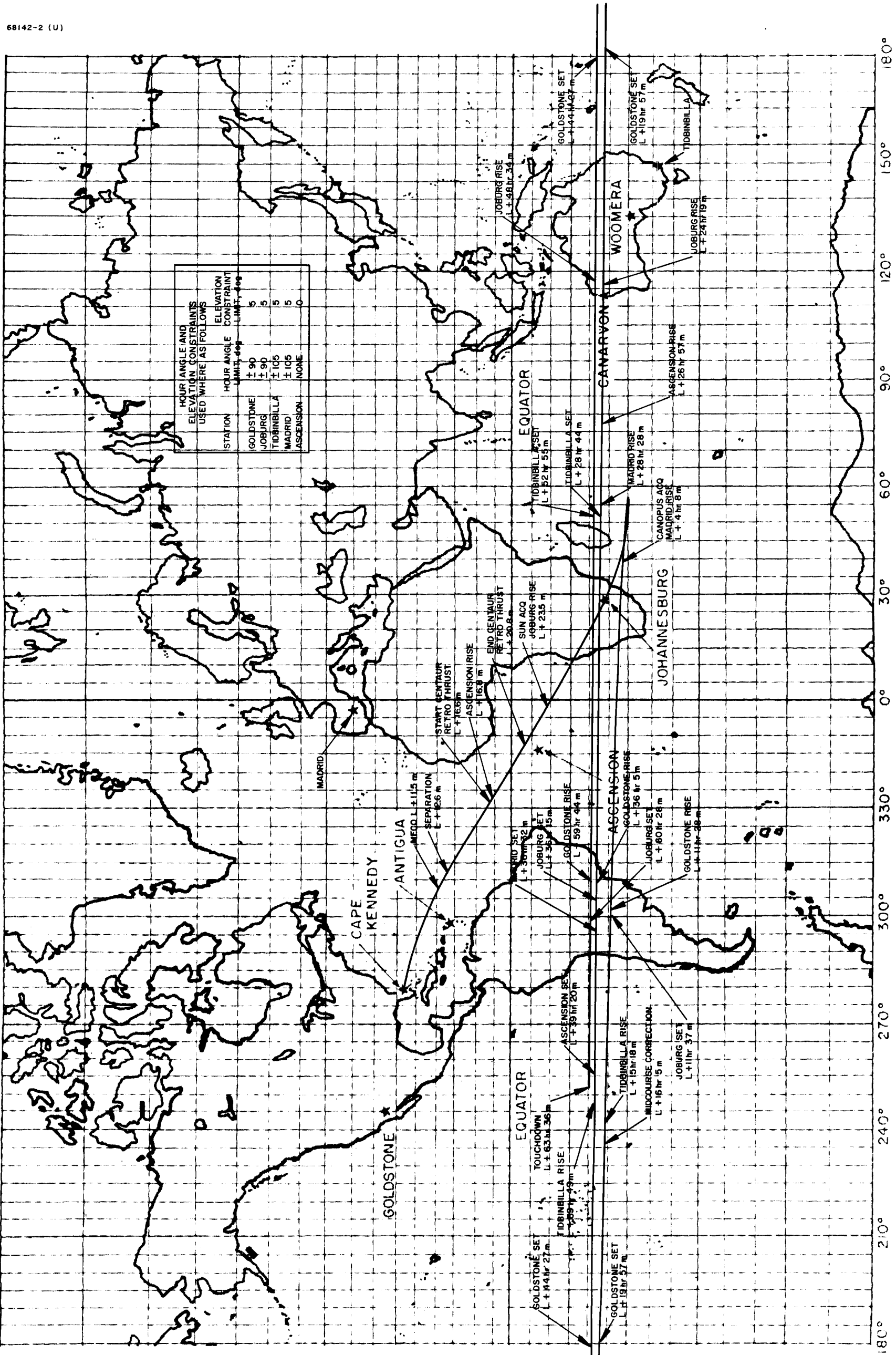
Figure 5.14-5. Surveyor I Earth Track

5.14-13

FOLDOUT FRAME

FOLDOUT FRAME

5-144
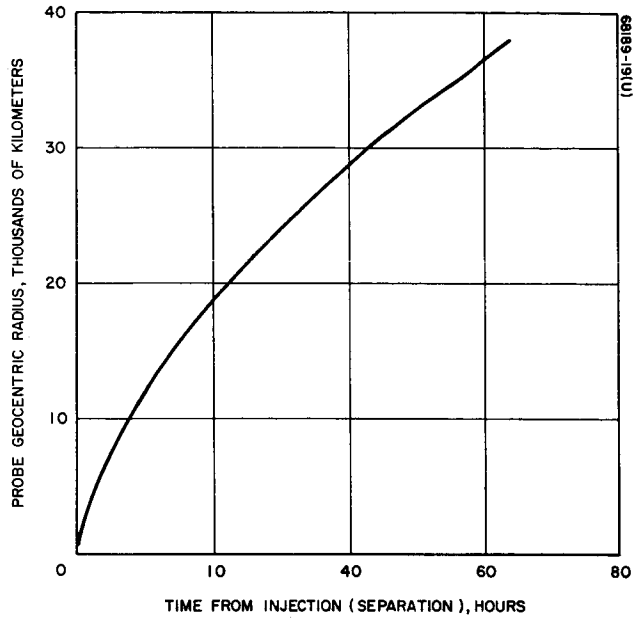
Figure 5.14-6. Probe Geocentric
Radius Versus Time
From Injection
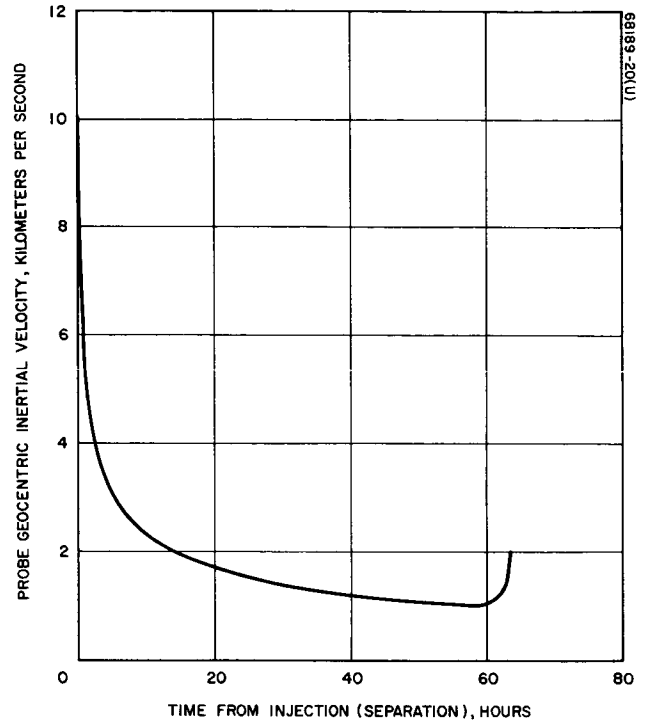
Figure 5.14-7. Probe Geocentric
Inertial Velocity Versus
Time From Injection
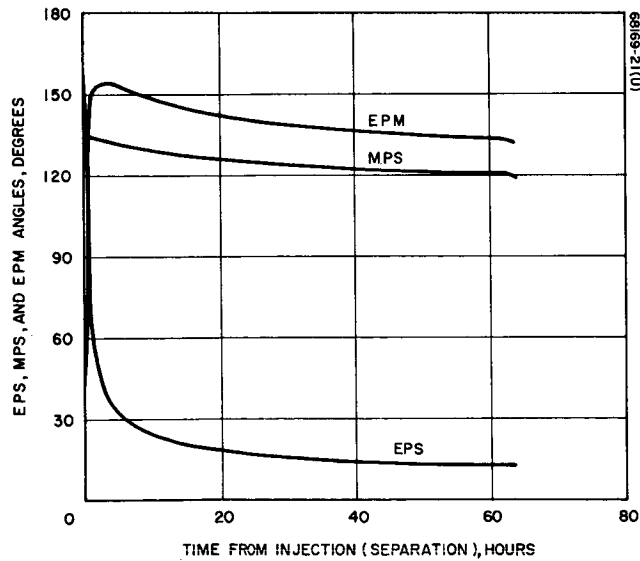
Figure 5.14-8. Earth-Probe-Sun,
EPS, Sun-Probe-Moon, MPS,
and Earth-Probe-Moon,
EPM, Angles Versus
Time From Injection
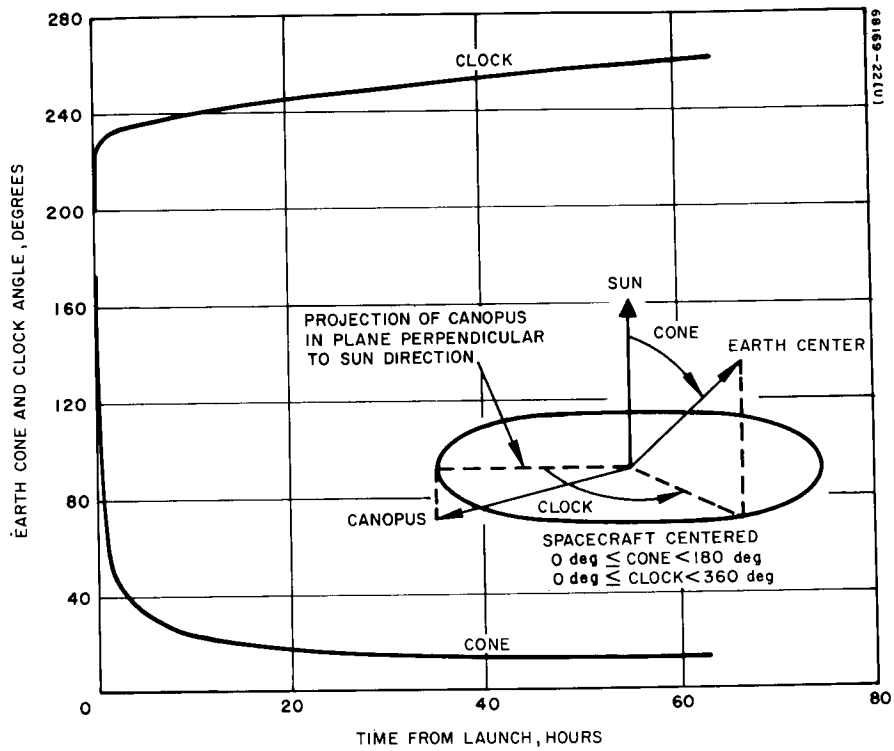
Figure 5.14-9. Earth Cone and Clock Angle
Versus Time From Launch
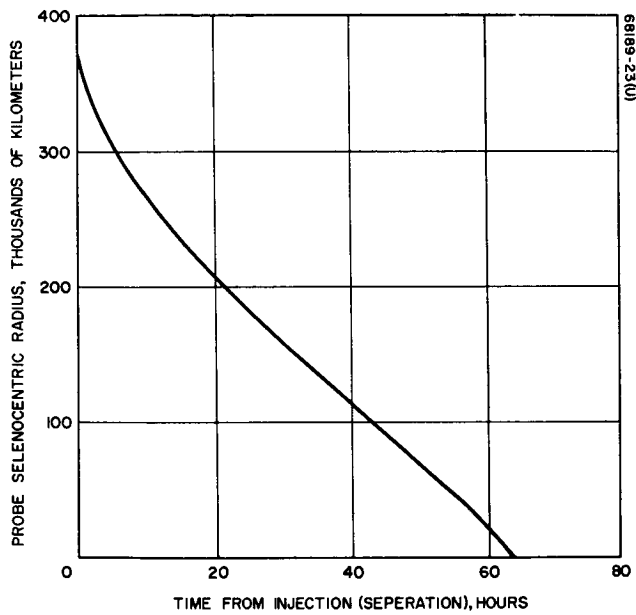
Figure 5. 14-10. Probe Selenocentric
Radius Versus Time
From Injection
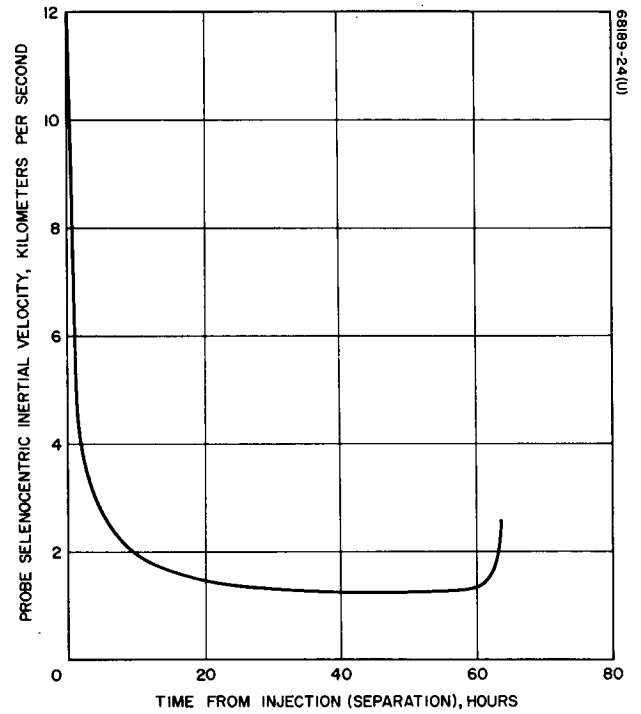
Figure 5. 14-11. Probe Selenographic
Inertial Velocity Versus
Time From Injection
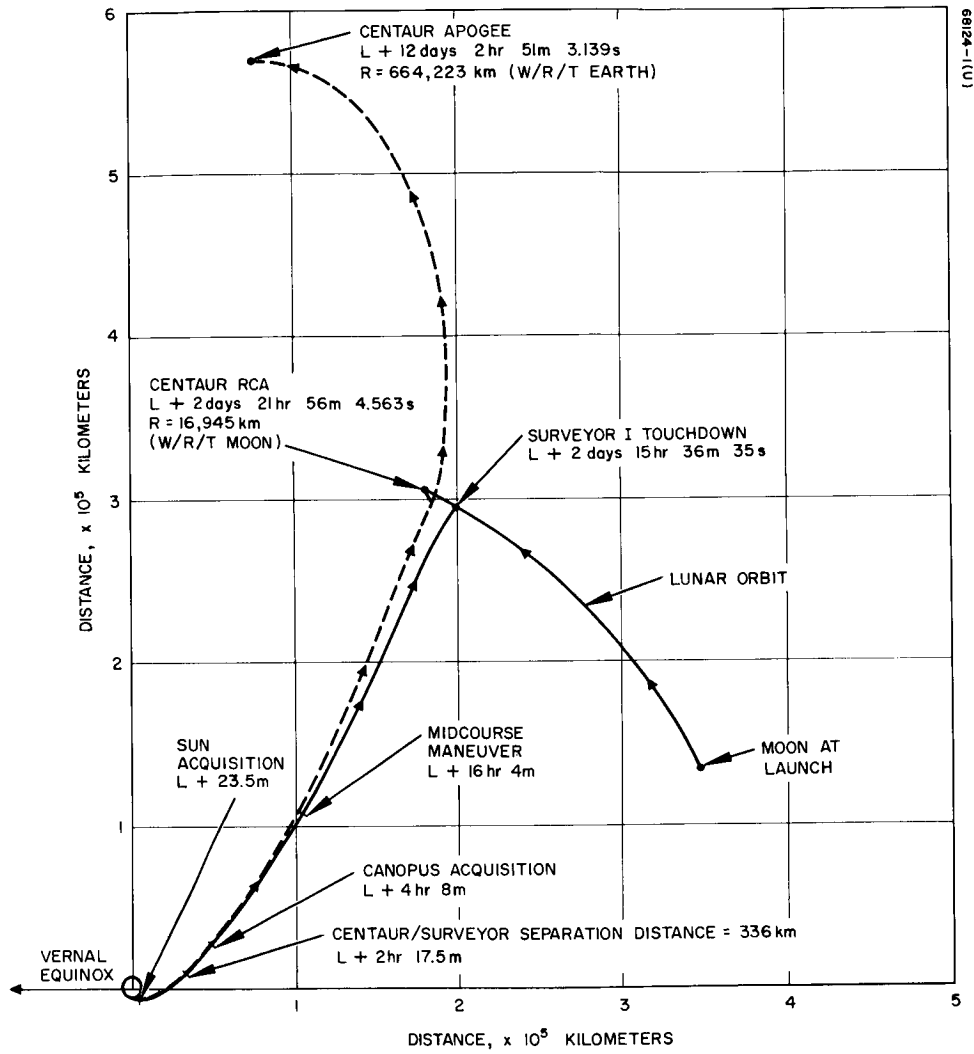
Figure 5.14-12. Surveyor and
Centaur Trajectory in Earth's
Equatorial Plane

During lunar encounter, the Centaur experienced a 5-degree orbit plane change and an increase in vis viva energy of about 0.5 km^2/sec^2. First apogee occurred 11 June 1966 at 17:32:04.139 at 644,223 km. Perigee occurred 23 June 1966 at 21:15:30.923 with a radius of closest approach to the earth of 32,722 km.

5.14.2 MANEUVER ANALYSIS

5.14.2.1 Midcourse Phase

The Surveyor I midcourse correction, computed to enable the space-craft to soft land at the desired landing site of -2.33 degrees latitude and 316.17 degrees longitude, was 20.35 m/sec. This correction was executed upon ground command at approximately 06 hours and 45 minutes GMT on 31 May 1966. The resulting soft landing site is estimated to be at -2.411 degrees latitude and 316.655 degrees longitude, well within the 3 σ dispersions predicted prior to the correction. Figure 5.14-13 shows the prelaunch targeted site, the in-flight aim point, the actual soft landing site, and the associated dispersions.

The 99 percent dispersions are shown as an ellipse on the surface with a semimajor axis of 38.7 km and a semiminor axis of 28.7 km. In order to take advantage of the small uncertainties that resulted from the small required correction, the aim point was biased to the north approximately 0.92 degree by changing the aim point from the original targeted value of -3.25 and 316.17 degrees, thereby minimizing the probability of landing in the craters Flamsteed or Flamsteed E. Dispersions on the actual landing site are presently estimated to be 5 km in latitude and 2 km in longitude. This is based on orbit determination data only. Reference 2 gives preliminary results based on TV data concerning lunar landmarks.

The maximum midcourse correction capability, as a function of the unbraked impact speed, is shown in Figure 5.14-14. The expected 3 σ Centaur injection guidance dispersions and the effective lunar radius are also shown. The midcourse capability contours are in the conventional R-S-T coordinate system defined in Reference 3.

The maneuver execution time of 15.85 hours after injection was chosen. This time allowed 4 hours and 36 minutes of premidcourse and 3 hours and 49 minutes of postmidcourse visibility from the Goldstone tracking facility.

The predicted results of the selected midcourse correction and other alternatives considered are given in Table 5.14-4. The required velocity component in the critical plane, to correct miss only, was 3.74 m/sec. The noncritical direction component that resulted from a weighted selection of flight time, main retro burnout velocity, and vernier propulsion system fuel margin was 20 m/sec. Figure 5.14-15 shows the possible flight times, burn-out velocities, and fuel margins for the range of available noncritical component velocity corrections. The fuel margin and arrival times were

FINAL AIM POINT

ESTIMATED LANDING SITE

INITIAL AIM POINT

PRE-MIDCOURSE EXECUTION
AND TRACKING ERRORS

SUNLINE MANEUVER

3.05 m/sec

LETRONNE

West
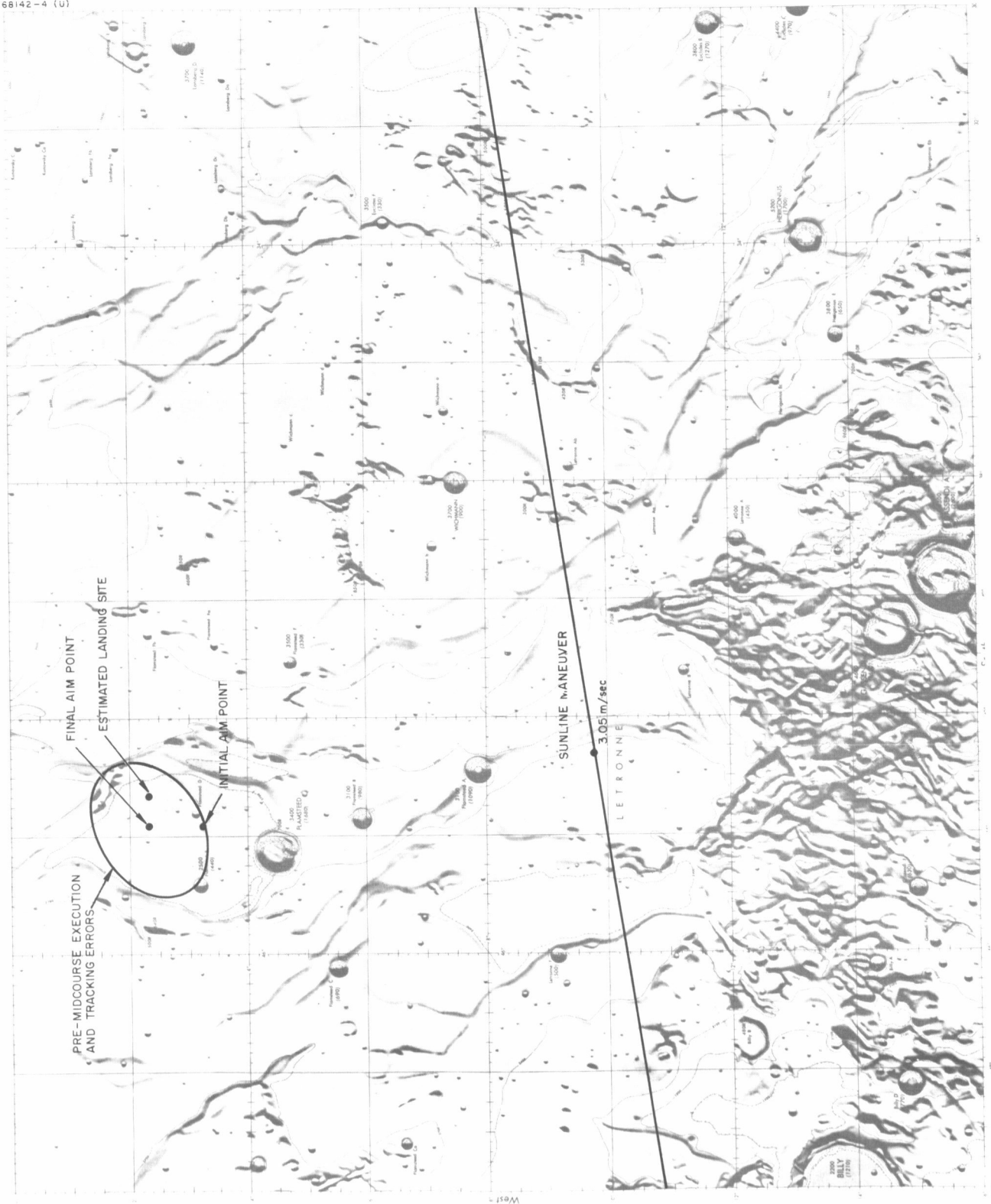
Figure 5.14-13. Surveyor I Landing Location

MAXIMUM AUTOMATICALLY TIMED MANEUVER

V_{IMP} = 2.672 2.663 2.653 km/sec

-12 -10 -8 -6 -4 -2

UNCORRECTED MISS

TARGETED SITE

DISPERSION ELLIPSE

-12 -10 -8 -6 -4 -2 0 2 4 6 8 10 12 TQ

T, THOUSANDS OF KILOMETERS

R, THOUSANDS OF KILOMETERS

EFFECTIVE LUNAR RADIUS

3σ IMPACT VELOCITY ERROR = 5.48m/sec
3σ FLIGHT TIME ERROR = 25.3 min

TARGETED SITE = LAT = -3.25° LONG = 316.17°
UNCORRECTED MISS = LAT = -11.53° LONG = 305.33°
AIMING POINT = LAT = -2.33° LONG = 316.17°

RQ

Figure 5.14-14.   Midcourse Capability Contours for 30 May Launch

σ_L = 115 degrees, midcourse at 15.5 hours

TABLE 5.14-4. MIDCOURSE MANEUVER ALTERNATIVES

	Final M/C	Alternate Considerations			
		No M/C	40 Hour	One Rotation	Sun
Midcourse Data					
Velocity magnitude, m/sec	20.35		21.18	3.51	2.91
Critical plane, m/sec	3.74		6.96	3.36	
Noncritical direction, m/sec	20.00		20.00	1.00	
Propellant weight, pounds	16.81		17.49	2.90	2.40
First rotation, roll, degrees	-86.50		-77.57	0	0
Second rotation, yaw, degrees	-57.99		-44.43	-35.56	0
Omnidirectional antenna	B-B		B-B	B-B	B
Engine burn time, seconds	20.80		21.65	3.58	2.97
Spacecraft mechanization errors, 3σ, km, (on the surface)					
SMAA	31.0	0	32.2	5.35	4.44
SMIA	30.6	0	31.8	5.12	4.25
Terminal Data					
Latitude (aim point), degrees	-2.33	-11.53	-2.33	-3.25	-9.86
Longitude, degrees	316.17	305.53	316.17	316.17	317.29
Incidence angle, degrees	6.02	10.14	6.02	5.75	1.62
Impact speed, km/sec	2.655	2.666	2.656	2.665	2.665
Burnout velocity, fps	392.	514.	400.	500.8	506.9
Burnout altitude, feet	28,571		28,353	38,137	38,673
Fuel margin, pounds	33.9	33.3	33.8	33.4	33.1
Descent propellant, pounds	120.7		120.7	135.3	136.02
Descent time, seconds	170.5		170.4	184.2	184.9
First rotation, roll, degrees	89.33	89.33	89.33	89.33	89.33
Second rotation, yaw, degrees	59.92	59.92	59.92	59.92	59.92
Third rotation, roll, degrees	94.09	94.09	94.09	94.09	94.09
Ignition delay, seconds	7.825		7.96	6.37	6.37
Landing site errors, 3σ, km, (orbit determination plus spacecraft mechanization)					
SMAA	38.7	23.2	34.2	23.8	23.6
SMIA	28.7	17.2	32.8	17.9	17.7

5.14-22

Figure 5.14-15. Possible Flight Times, Burnout
Velocities, and Fuel Margins for Range of
Available Noncritical Component
Velocity Corrections

acceptable over a wide spectrum. Flight control stability considerations, however, made a nominal main retro burnout below 450 ft/sec highly desirable. Plus 20 m/sec was chosen as a good compromise reducing the burnout velocity to 392 ft/sec. If the maneuver strategy were to correct miss plus flight time, the required noncritical component would have been 4.3 m/sec, giving a total of approximately 6.1 m/sec.

Since the aim point was changed during the flight, the above required correction does not properly evaluate the performance of the Centaur guidance system. Using the results of the last premidcourse orbit and correcting to the original aim point gives a miss only requirement of 3.55 m/sec. Miss plus flight time was 5.89 m/sec.

A preliminary analysis of the actual execution error can be obtained from the data presented in Table 5.14-5 (Reference 1). This table gives the midcourse velocity error in inertial Cartesian coordinates. A velocity magnitude error of 0.081 m/sec and a maximum pointing error of 0.221 degree is obtained by rotating two spacecraft coordinates. The direction cosines of the pointing error in spacecraft coordinates are $x = -0.00230$, $y = -0.00258$, $z = -1.0$. Table 5.14-6 presents the landing site and flight time errors attributable to the maneuver and orbit determination errors separately and totally (Reference 1).

15.14.2.2 Alternate Considerations

During the premidcourse phase, the following alternate possibilities were analyzed and eliminated:

1) No midcourse correction. This choice would have resulted in a soft landing attempt at the uncorrected impact site. This possibility was eliminated, primarily because the landing site was outside the Apollo landing region. Apollo landing sites are constrained to be within ±45 degrees longitude and ±5 degrees latitude. Of secondary importance was the high nominal main retro burnout velocity of 525 ft/sec.

2) A midcourse correction during the second Goldstone period approximately 40 hours after injection. This choice would have yielded approximately the same magnitude velocity correction and terminal conditions, with a significant improvement in landing site uncertainty, as the maneuver selected. It was felt that the improvement in landing site uncertainty did not outweigh the possibility of not being able to make a correction at the second Goldstone pass because of a hardware failure.

3) One rotation maneuver. By selecting a noncritical velocity component of approximately 1 m/sec, it would have been possible to align the spacecraft in the proper direction with only one attitude rotation, yaw ± -35 degrees. Since the resultant burnout velocity would have been 500 ft/sec, this choice was eliminated.

TABLE 5.14-5.   ESTIMATED MIDCOURSE VELOCITY ERRORS AT
END OF MIDCOURSE MOTOR BURN

Midcourse Velocity Differences

	ΔDX, m/sec	ΔDY, m/sec	ΔDZ, m/sec	Δ V, m/sec
OD estimate[*]	19.7963	4.3296	0.2873	20.266
Commanded maneuver[**]	19.8918	4.2710	0.28911	20.347
Maneuver error[***]	0.0955	-0.0586	0.002	0.081

[*]OD estimate = Current best postmaneuver estimate (20 post) minus
current best premaneuver estimate (17 post) mapped
to maneuver epoch.

[**]Commanded maneuver = Midcourse velocity increment computed by
Maneuver Analysis Group based on LAPM XB
orbit.

[***]Maneuver error = Commanded maneuver minus OD estimate.

TABLE 5.14-6.   ESTIMATED MIDCOURSE ERRORS MAPPED TO
UNBRAKED IMPACT POINT

Source	ΔB· TT, km	ΔB· RT, km	Δt_impact, sec	Δ Latitude (lunar)		Δ Longitude (lunar)	
				deg	≈km	deg	≈km
OD errors[*]	13.887	-5.692	-11.187	0.102	3.060	0.301	9.030
Maneuver Errors[**]	9.955	7.159	12.443	-0.128	-3.84	0.171	5.13
Overall Errors[***]	23.842	1.467	1.256	-0.026	-0.780	0.472	14.160

[*]OD errors = Current best premaneuver estimate (17 post) minus orbit
used for maneuver computations (LAPM XB).

[**]Maneuver errors = Overall errors minus OD errors.

[***]Overall errors = Current best postmaneuver estimate (20 post) minus
aiming point.

4) Sunline correction. The possibility of performing a velocity correction along the spacecraft sun direction was investigated and eliminated because the desired site could not be reached and the resultant burnout velocity for any reasonable site would have been too high. The sunline maneuver trace is shown in Figure 5.14-13.

5.14.2.3 Attitude Maneuver Considerations

Following computation of the magnitude and direction of the midcourse vector ($\overline{\Delta V_{m/c}}$), four pairs of spacecraft rotations and corresponding DSIF motions were calculated and the results compared with respect to prestored omnidirectional antenna patterns in the midcourse command program. Figure 5.14-16 shows the trace of the DSIF vector, in spacecraft coordinates, for each rotation pair. The figure shows that the cruise mode DSIF vector immediately prior to midcourse is located at $\theta = 160$ degrees and $\phi = -57$ degrees in spacecraft coordinates.

A positive roll of 3.5 degrees will decrease ϕ to -60.5 degrees with θ remaining constant. A subsequent pitch of -57.99 will change the DSIF position to $\theta = 139$ degrees and $\phi = 74.3$ degrees. However, a negative roll maneuver of -86.5 degrees will decrease ϕ to 29.4 degrees, and a following yaw will move the DSIF position to $\theta = 139$ degrees and $\phi = 164$ degrees. Pitch-yaw and yaw-pitch sequences each end at $\theta = 139$ degrees and $\phi = 74.3$ degrees.

As any one maneuver pair will correctly position the spacecraft prior to midcourse, the pair that maximizes probability of mission success through continuous, high antenna gain and maximum sun lock time is chosen. In as much as omnidirectional antenna A was believed to still be in its prelaunch stowed position, all analysis of spacecraft rotations were directed toward constraining the DSIF to high-gain regions of omnidirectional antenna B. As shown in Figure 5.14-16, the DSIF trace terminates in a low-gain region for three of the four maneuver sequences (roll-pitch, pitch-yaw, and yaw-pitch). The obvious selection of roll-yaw was made because the antenna gain during and following the rotations remains high. Minor considerations contributing to this choice were: 1) Sun lock is retained during the initial roll, and 2) the spacecraft had previously performed a yaw maneuver during sun acquisition.

The magnitudes of the selected maneuver were a roll of -86.50 degrees and a yaw of -57.99 degrees. The required engine burn time was 20.8 seconds.

The maneuver timing plan, as shown in Figure 5.14-17, illustrates the computation of various maneuver and ignition times. The earliest and latest allowable midcourse execution times bound the nominal execution time and are shown to be 10 minutes before and after the nominal time. The 10-minute values represent a tradeoff between operational times and required landing
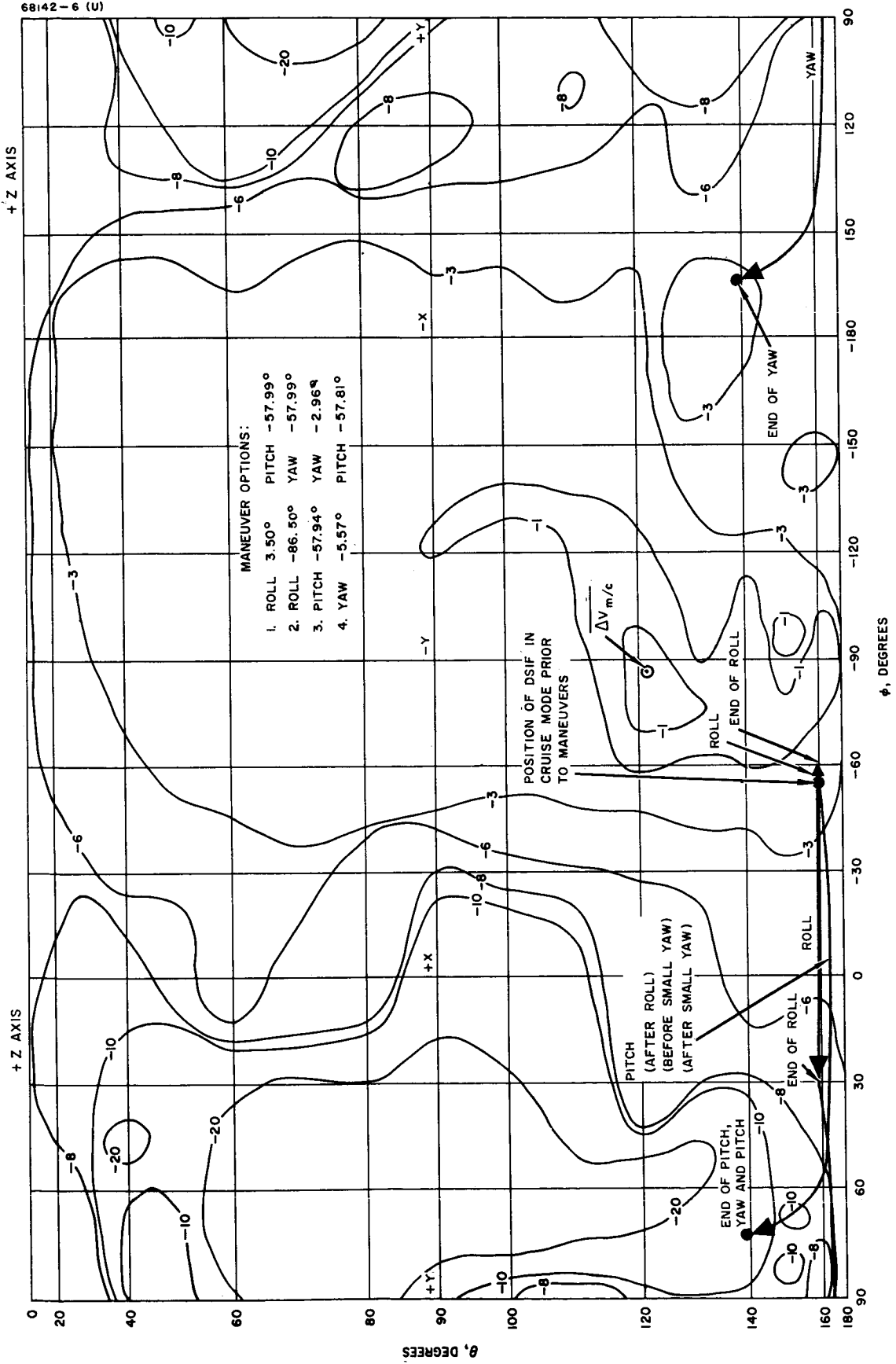
Figure 5.14-16. Omnidirectional Antenna B Downlink
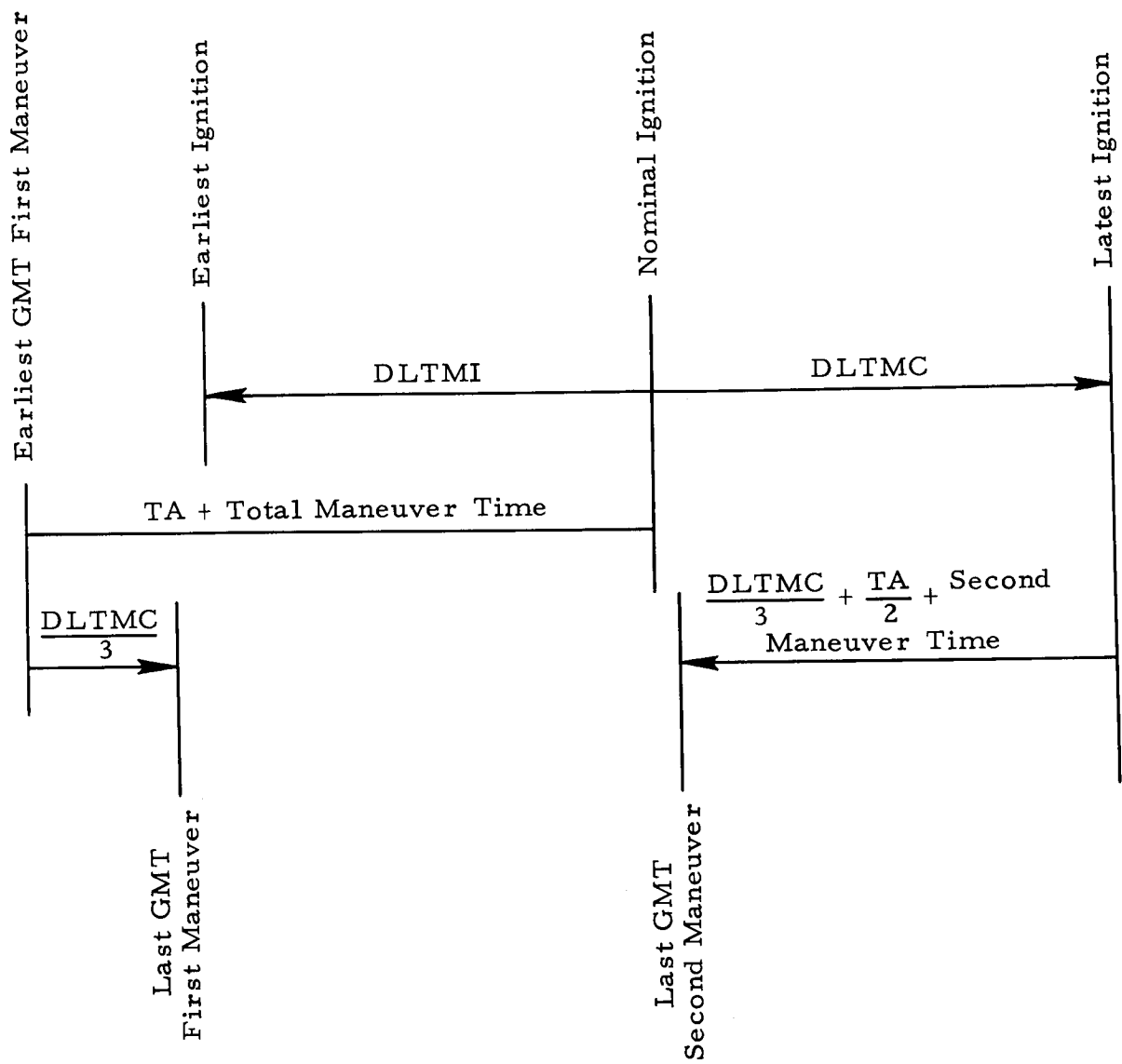
For Surveyor 1:

$$TA = 10 \text{ minutes}$$
$$DLTMI = 10 \text{ minutes}$$
$$DLTMC = 10 \text{ minutes}$$
$$\text{First maneuver} = 173 \text{ seconds}$$
$$\text{Second maneuver} = 116 \text{ seconds}$$

Figure 5.14-17.   Maneuver Timing Plan

accuracy. Execution of the engine burn time outside of this 20-minute window would result in a considerable bias in terminal parameters.

It is notable that the engine burn was commenced within 1 second of the nominal ignition time. The earliest GMT of first maneuver or earliest allowable break of sun lock is shown to be nominal ignition less the total maneuver time, less TA (the operational time necessary to transmit and verify spacecraft commands). By previous agreement with SPAC, a value of 10 minutes was used. The last GMTs of first and second maneuvers are computed based upon DLTMI, DLTMC, TA, and the maneuver times. These two GMTs serve as guides to proper execution of spacecraft rotations.

The resulting midcourse message, as shown in Figure 5.14-18, contains the operational data necessary for the proper execution of the mid-course maneuver.

5.14.2.4   Terminal Phase

Following the midcourse maneuver, only one significant problem remained to be solved prior to the terminal phase: to obtain a decision on the terminal attitude maneuvers. All other problems, such as burnout velocity, propellant margin, time of flight, etc., were essentially determined at midcourse. Subsequent postmidcourse orbits would only affect these parameters in a minor way. Section 5.15 contains a detailed evaluation of the key events following the terminal attitude maneuvers. Ninety-nine percent propellant dispersions versus burnout velocity data in given in Figure 5.14-19.

5.14.2.5   Terminal Attitude Maneuvers

Because of the apparent failure of antenna A to deploy, attitude maneuvers in the terminal phase were selected to optimize signal strength from antenna B. Study of this problem showed that there were two possible maneuver sequences that would maintain relatively high signal strength during and following the maneuvers. The first maneuver sequence was a roll-yaw-roll combination that gave a final spacecraft roll orientation such that the DSIF station was in the most favorable location (Figure 5.14-20). The second maneuver sequence was a roll-pitch combination with the roll maneuver being nonstandard (<90 degrees). This maneuver sequence also resulted in an equally favorable final roll orientation (Figure 5.14-20).

SURVEYOR GUIDANCE PROGRAMS

MICOM

MIDCOURSE COMMAND FORMAT

13

NOMINAL GMT OF IGNITION			JULIAN DATE	2439276.78125000	MAY 31, 1966	6 45	.000
FIRST GMT OF IGNITION			JULIAN DATE	2439276.77430555	MAY 31, 1966	6 35	.000
LAST GMT OF IGNITION			JULIAN DATE	2439276.78819444	MAY 31, 1966	6 55	.000
EARLIEST GMT OF FIRST MANEUVER			JULIAN DATE	2439276.77096090	MAY 31, 1966	6 30	11.023
MAGNITUDE OF FIRST MANEUVER	ROLL TURN	-86.5033 DEG.	ROLL TURN		COMMAND TIME	-173.0066 SEC.	
MAGNITUDE OF SECOND MANEUVER	YAW TURN	-57.9855 DEG.	YAW TURN		COMMAND TIME	-115.9710 SEC.	
MAGNITUDE OF DELTA-V	+.20347260E-01 K/S. ENGINE BURN TIME	20.8001 SEC.					
OMNIDIRECTIONAL ANTENNA, FIRST MANEUVER . . . B							
OMNIDIRECTIONAL ANTENNA, SECOND MANEUVER . B							
LAST GMT OF FIRST MANEUVER			JULIAN DATE	2439276.77291666	MAY 31, 1966	6 33	.000
LAST GMT OF SECOND MANEUVER			JULIAN DATE	2439276.78125000	MAY 31, 1966	6 45	.000

MCCOM   TRANSMISSION TO SPAC SUCCESSFUL

READ   MCCOM   INTERFACE

WRITE   MCCOM   INTERFACE

Figure 5.14-18. Midcourse Maneuver Message
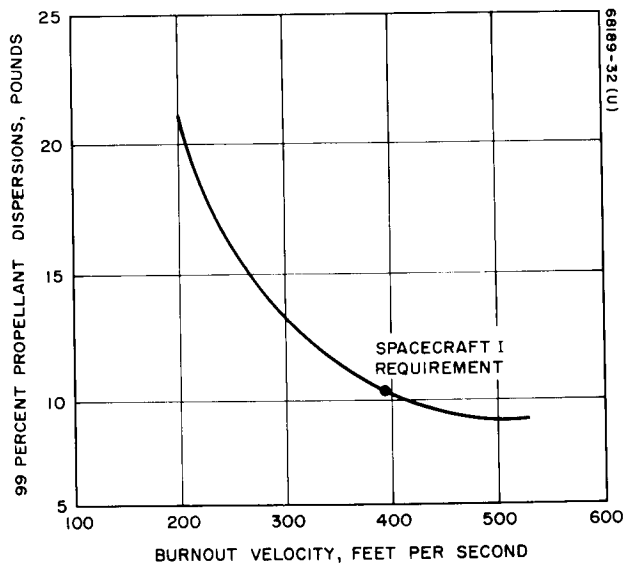
Figure 5.14-19. 99 Percent Propel-
lant Dispersions Versus
Burnout Velocity
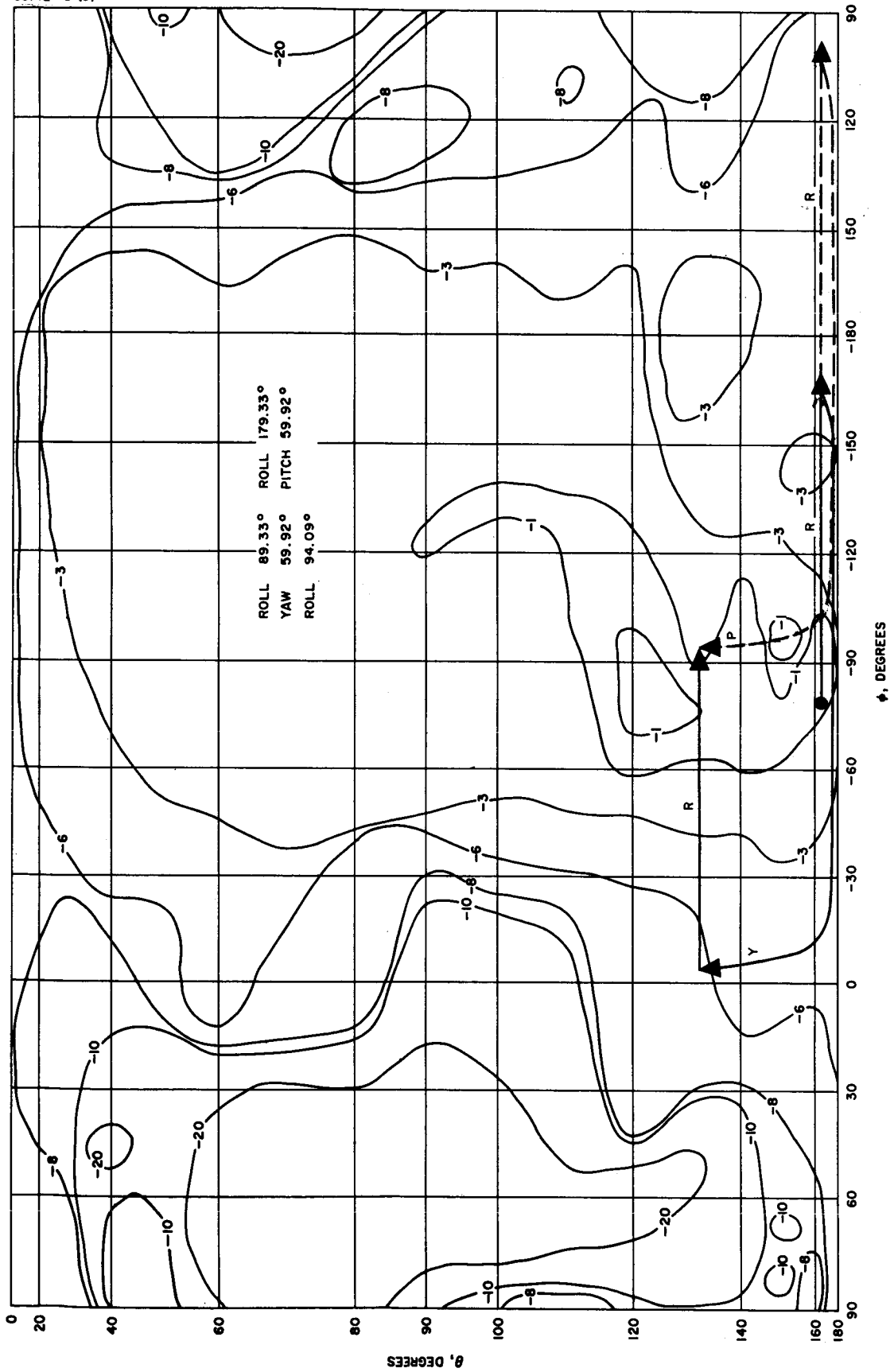
Figure 5.14-20. Terminal Maneuver Data
Antenna B contour patterns – down-link

However, the latter maneuver sequence had several disadvantages that the first sequence did not have. First, the pitch maneuver channel had not been exercised at midcourse as had the yaw channel and, while there was no reason to suspect that the pitch channel would not work, there was intuitive reason for "sticking with a winner." Second, the roll-pitch combination could not be computed directly with the MTGS programs, and thus there could be no compensation for a sensor group deflection of 0.34 degree and a known Y gyro drift of approximately 0.75 deg/hr. The net result of these two uncompensated error sources was an estimated 0.4 degree offset in the retro thrust vector as shown in Figure 5.14-21. With this expected thrust offset, the 3σ maximum flight path angle at the start of the vernier phase burnout was 28 degrees as compared to 20 degrees when these errors are compensated.

Because of these two disadvantages, the roll-yaw-roll sequence was finally chosen. To offset the increased operational time disadvantage inherent in a three-maneuver sequence, the first maneuver was executed 38 minutes prior to retro ignition rather than the standard 33 minutes generally used to minimize gyro drift error. This execution allowed 3 minutes to complete the first maneuver and 2 minutes to set up for the second maneuver so that it could be executed at 33 minutes. The additional 5 minutes operational time was allowable because, during the first roll maneuver, sun lock was maintained. Thus pitch and yaw attitude errors owing to gyro drifts were held to zero until the second maneuver was executed. In addition, of course, the gyro drift rates were being compensated for to the extent that they were constant and accurate.

Final attitude maneuver magnitudes were based on SPAC supplied gyro drift rates of zero in the pitch axis, 0.75 deg/hr on the yaw axis, and 0.2 deg/hr in the roll axis.

5.14.2.6 Actual Landing Location

The best estimate of the actual landing site is a latitude of -2.411 degrees and a longitude of 316.655 degrees. This estimate is based upon an unbraked impact point of -2.356 degrees and 316.642 degrees.

The terminal guidance program predicted that the difference between unbraked impact and landing would be 1.13 km along the surface in the trajectory plane (i.e., at an azimuth of 343.4 degrees). Since landing, a study of telemetry data shows that there was an additional 42 ft/sec lateral velocity not considered in the terminal guidance solution. This lateral component would add another 0.59 km to the difference, bringing the total to 1.72 km.

5.14.2.7 Backup Command Options

A number of backup command execution times were computed for the Surveyor I mission. These included the following:
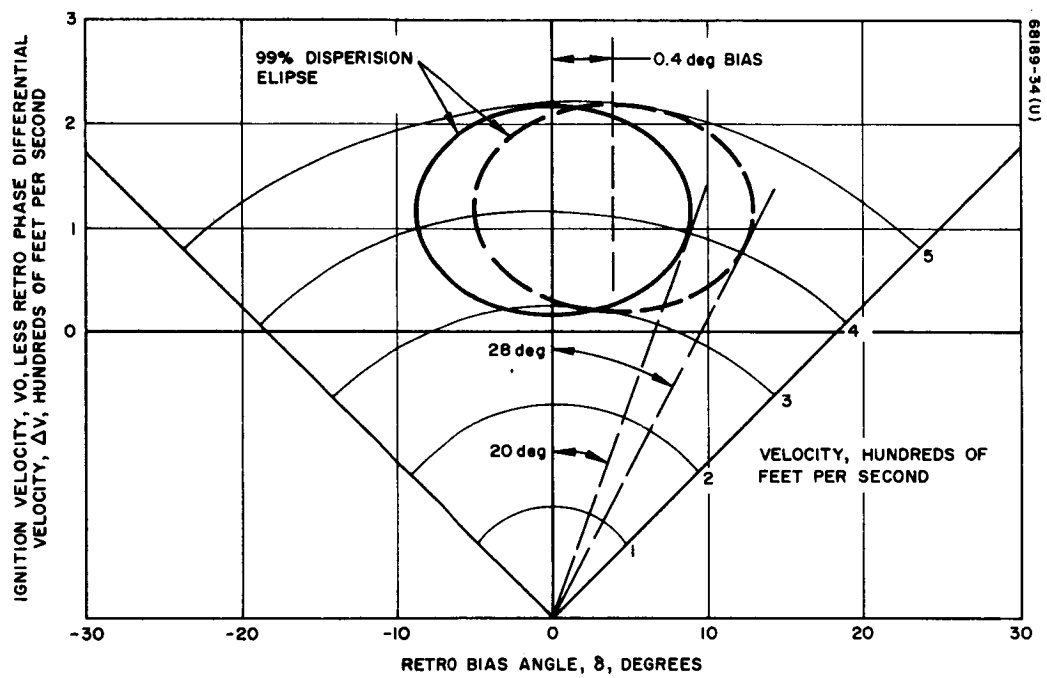
Figure 5.14-21. Retro Burnout Velocity Diagram

1) The optimum time to send the emergency altitude marking radar command. The strategy employed to generate this command is specified in Reference 4 and is based upon a predicted probability that the marking radar will work (i.e., 0.999 for Surveyor I).

2) The time to send the altitude marking radar command given that the marking radar will not work. The command could have been sent at this time if confirmation of AMR power on and AMR enable were not received.

3) The time to start the emergency terminal descent command tape. This tape would have been used if the counter was inoperative and would originate with the vernier ignition command.

The final value for the first command was computed after the final estimate of the unbraked impact time and the uncertainty associated with it became available. The numbers used are a result of the final YB orbit, generated at mark -40 minutes. At this time, mark was predicted to occur at 06:14:37.97. (It actually occurred at 06:14:38.47 ± 0.05.) The uncertainties associated with executing the command (orbit determination and manual implementation) were estimated to be $[0.44^2 + 0.25^2]^{1/2} = 0.51$ (1 σ). Using this value and the amount of vernier engine propellant available, a red line delay time of 1 second is specified (Reference 4). Known fixed delays such as the propagation delay, operator delay, command generator, and command decoder delays totaled 2.125 seconds. Fixed delays were anticipated by executing the command early. The final command value, rounded to the nearest second, was 06:14:37. The backup command should have arrived at the spacecraft approximately 1.2 seconds after mark. It actually arrived 1.04 ± 0.15 seconds after the mark.

For the latter two options, the approach taken was to determine a new burnout altitude centered with respect to the total burnout capability defined by the midcourse maneuver, descent contour, and predicted nominal burnout velocity. In general, the new burnout altitude is greater than the nominal value, and this higher burnout altitude gives rise to earlier desired backup ignition and mark command times. These backup command times for the SC-1 mission are as follows:

GMT (radar mark)	6:14:34
GMT (vernier ignition)	6:14:41

These commands were not sent as they were not required. Figure 5.14-22 is a reproduction of the final terminal maneuver command message.

5.14.2.8 Gyro Drift Measurements

An anomaly was seen in the DSS-42 two-way doppler residuals during its second view period. A check with the SPAC area revealed that this anomaly coincided with a gyro drift check started at 07:34:15 GMT on 1 June.

SURVEYOR GUIDANCE PROGRAMS
TERCOM

30

68189-35(U)

TAU (FFM)	FIRST GMT OF FIRST MANEUVER		JULIAN DATE	2439278.73384278	JUNE 2,.1966	5 36 44.017	
TAU (K)	GMT OF 1000		JULIAN DATE	2439278.75246727	JUNE 2, 1966	6 3 33.173	
TAU (TR)	GMT OF MARK		JULIAN DATE	2439278.76014110	JUNE 2, 1966	6 14 36.191	
OMNI1/AMC1	FIRST MANEUVER	OMNIDIRECTIONAL ANTENNA = B	AXIS = ROLL	POLARITY AND MAGNITUDE = +.17866349E+03SEC			
OMNI2/AMC2	SECOND MANEUVER	OMNIDIRECTIONAL ANTENNA = B	AXIS = YAW	POLARITY AND MAGNITUDE = +.11984636E+03SEC			
OMNI3/AMC3	THIRD MANEUVER	OMNIDIRECTIONAL ANTENNA = B	AXIS = ROLL	POLARITY AND MAGNITUDE = +.18817331E+03SEC			
OMNI4/AMC4	FOURTH MANEUVER	OMNIDIRECTIONAL ANTENNA = B	AXIS =	POLARITY AND MAGNITUDE = +.00000000E+00SEC			
OMNI5/AMC5	FIFTH MANEUVER	OMNIDIRECTIONAL ANTENNA = B	AXIS =	POLARITY AND MAGNITUDE = +.00000000E+00SEC			
ANROT	PLANAR ARRAY POLAR ANGLE		+.42318224E+02DEG				
TSTART	VERNIER ENGINE THRUST		MI				
DTIG	MAIN RETRO TIME DELAY		+.78258039E+01SEC				
SRN33	UNCERTAINTY IN UNBRAKED IMPACT TIME						
TERCON	TRANSMISSION TO SPAC SUCCESSFUL		00.5SEC				
READ TERCON	INTERFACE						
WRITE TERCON	INTERFACE						

Figure 5.14-22. Terminal Maneuver Message

At this time, the spacecraft was allowed to drift in all three axes. The drift was allowed to continue until 09:52:16 GMT at which time the spacecraft was returned to Canopus lock. Figure 5.14-23 shows an abrupt shift in the residuals at this latter time.

5.14.3 REFERENCES

1. "Surveyor I Flight Path Analysis and Command Operations Report," Hughes Aircraft Company, SSD 68142R, 24 June 1966.

2. "Surveyor I Preliminary Results," National Aeronautical And Space Administration Five-Day Science Report, PD-97, 30 June 1966, JPL.

3. L. Davids, C. Meredith, and J. Ribarich, "Midcourse and Terminal Guidance Operations Programs," Hughes Aircraft Company, SSD 4051R, April 1964.

4. G. A. Young, "Minutes of Meetings and Recommendation for AMR Mark and Retro Sequence Backup Procedures for Mission A," Hughes Aircraft Company, Letter 2253.3/345, 20 July 1965.

5. "Surveyor I Flight Path And Its Determination From Tracking Data," JPL Report (To be published).

5.14.4 ACKNOWLEDGEMENTS
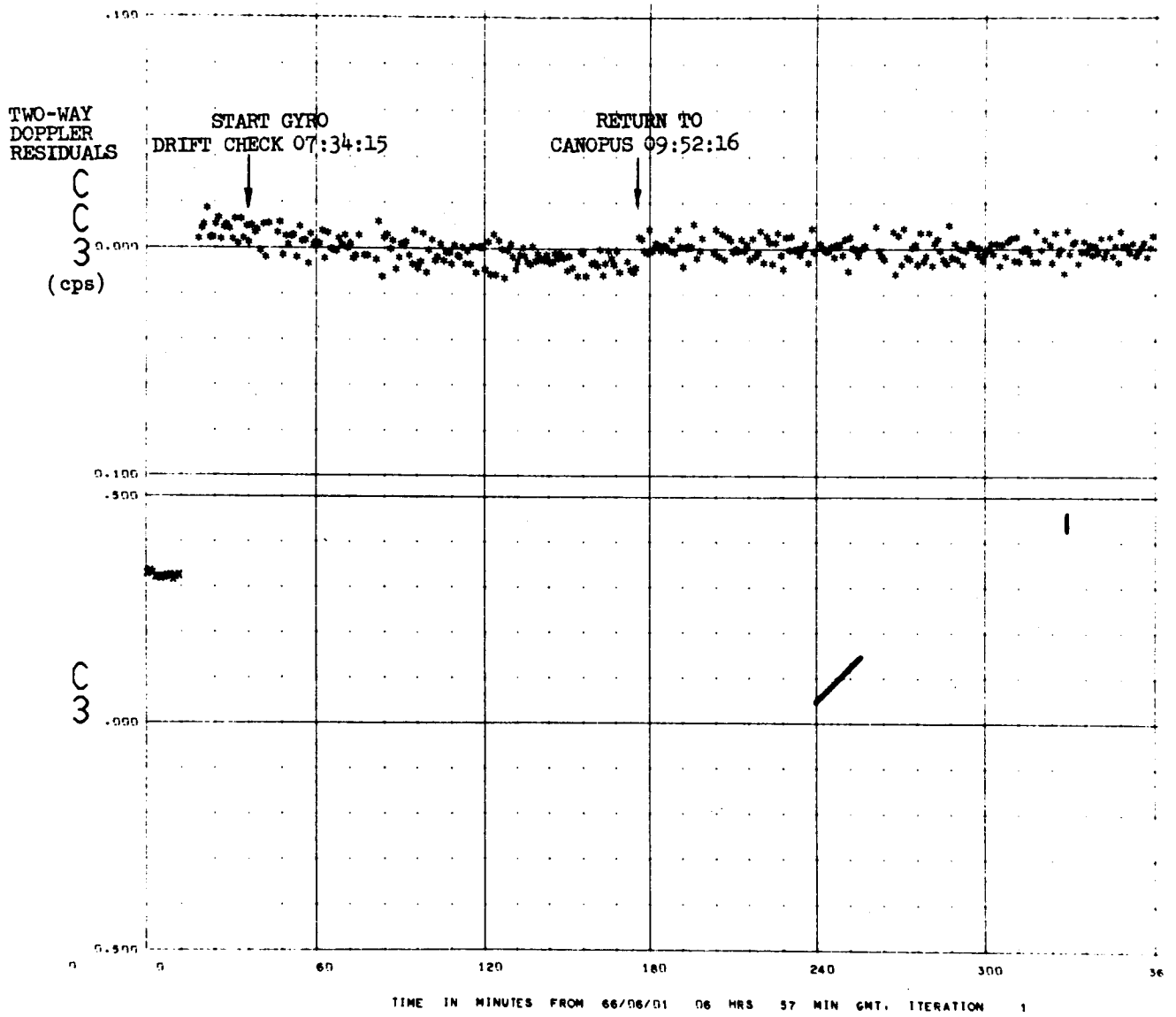
Figure 5.14-23. Two-Way Doppler
Residuals Observed During
Gyro Drift Check

5.15 TERMINAL DESCENT TRAJECTORY PERFORMANCE

5.15.1 INTRODUCTION

The terminal descent and landing phase is designed to take place as described below.

The transition from coast mode II to the terminal descent phase occurs with the start of the preretro attitude maneuvers. These maneuvers are used to reposition the attitude of the spacecraft from the sun-star reference such that the expected direction of the retro thrust vector will be aligned with respect to the velocity vector so as to achieve the desired retro burnout conditions. Following completion of the attitude maneuvers, the altitude marking radar (AMR) is activated. The AMR is preset to generate a mark signal when the range to the lunar surface is 60 miles. A backup mark signal, delayed a short interval after the AMR mark should occur, is transmitted to the spacecraft to initiate the automatic sequence in the event the AMR mark is not generated. The desired delay between the altitude mark and retro ignition is stored in the flight control programmer by ground command. Vernier engine ignition is automatically initiated 1.1 seconds prior to retro ignition.

During the retro phase, spacecraft attitude is maintained in the inertial direction established at the end of the preretro maneuvers by the vernier attitude control system, and the total vernier thrust is maintained at mid-thrust. As the mass of the vehicle decreases due to the expenditure of retro and vernier propellant, the spacecraft thrust to mass ratio (T/M) increases from approximately 4 g_e (g_e = 32.2 ft/sec^2) at ignition to 10 g preceding burnout. Prior to burnout, the inhibit is removed from the acceleration switch output and the doppler radar and altimeter (RADVS) is activated.

As the thrust decays during retro burnout, the acceleration switch signals when the T/M level has dropped to 3.5 g_e. At this time, the vernier engine thrust command is automatically changed to high thrust, and a counter in the flight control programmer is initiated. After 12.0 seconds following the receipt of the burnout signal, the explosive bolts attaching the retro to the spacecraft are activated, allowing the retro case to separate from the spacecraft. Following a programmed delay of 2.15 seconds after the initiation of separation, the vernier thrust command is reduced to low thrust to control the vehicle T/M level at 0.9 g_m (g_m = 5.32 ft/sec^2).

When reliable radar operation occurs, attitude control of the vehicle is switched from inertial control to radar control, and the spacecraft maneuvers to align the vernier thrust axis to the velocity vector. When the combined range and velocity, as measured by the radar, indicate that the spacecraft has descended to the programmed range/velocity descent profile, the total vernier engine thrust is controlled to achieve a trajectory along this profile. When a velocity of 10 ft/sec is reached, attitude control of the spacecraft is switched to inertial reference, and thrust control is servoed to maintain descent velocity at 5 ft/sec. At an altitude of 14 feet above the surface, the radar generates a signal that commands vernier engine cutoff, and the vehicle free falls to the lunar surface. The touchdown impact is absorbed by the spacecraft landing system, thus completing the terminal descent phase of the mission.

Spacecraft performance was close to nominal for the entire terminal descent period. All events occurred as per the spacecraft design. The only observed condition that might be considered an anomaly was the loss of radar lock during the retro separation phase; however, since relock was obtained with substantial time margin prior to the start of the vernier descent phase, this condition did not affect terminal descent performance. (See Section 5.10 for further detail.) A listing of telemetered terminal descent conditions versus predicted for major event times during terminal descent is given in Table 5.15-1. A discussion of spacecraft performance in each of the major periods of the terminal descent phase is presented in the following section.

5.15.2   TABLE OF MAJOR EVENTS AND TIMES

Table 5.15-1 lists the significant terminal descent events and the most accurate determination of each event's time of occurrence. The first time column is the time at which the event was observed at the DSIF. The second time column is the time at which the event would have occurred at the spacecraft. This time is the DSIF time either plus or minus the one-way transit time delay depending on whether the event is a command or a telemetered spacecraft action. The tolerance is the uncertainty in these times due to the telemetry sampling rate limitation. The third column indicates the source of the information.

The entries in the source column have the following meanings:

DSIF magnetic tape — taking data directly from processed DSIF 11 telemetry magnetic tapes and interpolating between "before and after" frames

ETR magnetic tape — same as above but for tapes originating at ETR

CDC command tape — command paper tape from the DSIF CDC

TABLE 5.15-1. BEST ESTIMATE TIMES FOR SC-1 TERMINAL DESCENT

Event	Time, GMT		Source
	At DSIF 11	At Spacecraft	
High power transmitter on command	05:20:18.393	05:20:19.63	DSIF magnetic tape
Start roll maneuver	05:36:46.295	05:36:47.54	DSIF magnetic tape
Start yaw maneuver	05:41:47.766	05:41:49.01	DSIF magnetic tape
Start second roll	05:45:17.745	05:45:18.99	DSIF magnetic tape
AMR on command	06:09:57.5 ± 0.5	06:09:58.74 ± 0.5	CDC command tape
AMR on telemetry			
AMR enable command	06:12:57.778	06:12:59.02	ETR magnetic tape
AMR enable telemetry			
AMR mark	06:14:39.703 ± 0.05	06:14:38.47 ± 0.05	Extrapolation of magnetic register count
AMR backup command	06:14:38.269	06:14:39.51	ETR magnetic tape
Vernier engine ignition	06:14:47.558 ± 0.05	06:14:46.32 ± 0.05	Extrapolation of magnetic register count
Retro engine ignition	06:14:48.658 ± 0.05	06:14:47.42 ± 0.05	Extrapolation of magnetic register count
3.5 g point	06:15:27.665 ± 0.1	06:15:26.43 ± 0.1	Reference 1
3.5 g switch actuation	06:15:27.943 ± 0.015	06:15:26.70 ± 0.015	Reference 1
Retro separate signal	06:15:39.943 ± 0.015	06:15:38.70 ± 0.015	Reference 1
Retro ejected signal	06:15:40.066 ± 0.5	06:15:38.83 ± 0.5	DSIF magnetic tape
Start RADVS	06:15:42.093 ± 0.015	06:15:40.85 ± 0.015	Reference 1
Loss of mode 2 data	06:16:00.146		DSIF magnetic tape
Start of mode 3 data	06:16:01.321		DSIF magnetic tape
First segment acquisition	06:16:05.893 ± 0.01	06:16:04.65 ± 0.01	Reference 1
End segment 1	06:16:17.225 ± 0.02	06:16:15.99 ± 0.02	Reference 1
End segment 2	06:17:10.494 ± 0.05	06:17:09.25 ± 0.05	Reference 1
1000-foot mark	06:17:10.502 ± 0.05	06:17:09.26 ± 0.05	DSIF magnetic tape
End segment 3	06:17:19.281 ± 0.04	06:17:18.04 ± 0.04	Reference 1
10-ft/sec mark	06:17:28.729 ± 0.025	06:17:27.49 ± 0.025	DSIF magnetic tape
13-foot mark	06:17:34.178 ± 0.025	06:17:32.94 ± 0.025	DSIF magnetic tape
Touchdown	06:17:35.678 ± 0.065	06:17:34.43 ± 0.065	DSIF magnetic tape

Extrapolation of   — data taken from DSIF 11 telemetry tapes by
magnitude register   extrapolating back the slope of the magnitude
counting   register countdown to where (and thus when)
                            it started

Reference 1   — data taken from DSIF 11 telemetry tapes but
                            uncertainty reduced by assuming magnitude
                            register timing is correct and then correlating
                            events controlled by the magnitude register.

5.15.3 SUMMARY OF RESULTS

The significant terminal descent performance parameters are summarized in Table 5.15-2 along with the required and/or predicted value.

5.15.4 ANOMALY DESCRIPTION

No anomalies were evident during this phase of the mission.

5.15.5 CONCLUSIONS AND RECOMMENDATIONS

1) The SEMBET scheme for determining the telemetry error source values seemed to perform extremely well. Because an error was noted in V_Z that had not been modeled in the SEMBET program, it is recommended that the error model therein be expanded to include spacecraft system errors as well as telemetry errors.

2) It was noted that the SEMBET program actually made very little correction to the telemetered trajectory, which is to say that the telemetry system was very nearly error free. Therefore, it is recommended that no time should be expended in using SEMBET on future flights if inspection of the telemetry data in real time reveals that the trajectory was extremely nominal as it was for SC-1.

3) It is recommended that the automatic zero-setting feature of the PREPRO program be removed in order to preclude the possibility of a time discrepancy appearing between the tabulated and plotted data sets.

4) The PREPRO and TELTAB programs presently process and print out only the telemetry data appropriate to the trajectory reconstruction scheme. However, since all telemetry data passes through these programs, it is recommended that they be coded to be able to optionally process and print out all telemetry signals in the modes applicable to the terminal descent.

TABLE 5.15-2. SUMMARY OF TERMINAL DESCENT
PERFORMANCE PARAMETERS

Parameter	Required Value	Predicted Value	Best Estimate	Comments
Retro phase initial conditions				
Time (DSIF 11)	03:56 to 08:16	153:06:14:47.04	153:06:14:47.558	
Attitude	< 25 degrees	5.87 degrees	6.13 degrees	
Slant range	< 316,800 feet	248,000 feet		Errors in initial conditions (R, V) are masked by other error sources.
Velocity	8000 → 8850 ft/sec	8566 ft/sec		
Retro burnout conditions				
Slant range		28,570 feet	27,820 feet	
Longitudinal velocity	< 650 ft/sec	392 ft/sec	425 ft/sec	
Lateral velocity		30 ft/sec	71.3 ft/sec	
Attitude	< 45 degrees	1.8 degrees	-4.09 degrees	
Misalignment angle during retro				
In-plane	≤ 1 degree	0	0.26 degree	
Out-of-plane	≤ 1 degree	0	0.08 degree	
1000-foot mark conditions				
Slant range	1000 ± 80 feet	1000 feet	1028 feet	
Velocity	104 ± 2.2 ft/sec	104 ft/sec	103.1 ft/sec	
Attitude		0.2 degree	1.11 degrees	
10-ft/sec mark conditions				
Slant range	43 ± 15 feet	43 feet	43 feet	
Velocity		8.6 ft/sec	8.4 ft/sec	
Attitude		0.1 degree	0.7 degree	
Engine cutoff conditions				
Slant range	14 ± 4.5 feet	14 feet	13 feet	Radar range data based on range and velocity data.
Velocity	5 ± 1.5 ft/sec	5.0 ft/sec	5 ft/sec	
Attitude	0 ± 4.8 degrees	0.1 degree	0.3 degree	
Touchdown conditions				
Free fall time		1.5 seconds	1.50 seconds	
Longitudinal velocity — RADVS				
Longitudinal velocity — trajectory	≤ 20 ft/sec	12.8 ft/sec	12.2 ft/sec	Based on initial velocity and free fall time
Longitudinal velocity — impact			10 ft/sec	
Latitudinal velocity — RADVS				
Latitudinal velocity — trajectory	≤ 7 ft/sec	0	0.6 ft/sec	
Latitudinal velocity — impact			1 ft/sec	
Attitude — RADVS	≤ 8 degrees	0		
Attitude — trajectory			0 degree	
Attitude — impact			1 degree	
Vernier propellant used	≤ 177.1 pounds	136.9 pounds	139.0 pounds	

5.15.6 PERFORMANCE ANALYSIS

5.15.6.1 Velocity Change due to Thrusting During Retro Phase

Determination of Ignition Conditions

The ignition velocity V_0, flight path angle γ, and roll angle φ serve as initialization parameters and are determined from tracking data. The 3 σ uncertainty in free flight velocities is < 0.5 ft/sec, and since ignition altitude has a calculated 3σ inaccuracy of 1000 feet due to marking range errors (with a V = 8500 ft/sec), the equivalent velocity uncertainty is

$$gt = 5 \times \frac{1000}{8500} = \frac{50}{85} = 0.6 \text{ ft/sec}$$

Hence, the total uncertainty in ignition velocity is 0.8 ft/sec when these two independent error sources are combined. The direction of $\underline{V}_0$ at ignition has an uncertainty of 0.07 degree. Therefore, the best error ignition conditions are

$$V_o = 8565.2 \pm 0.8 \text{ ft/sec}$$

$$\gamma_o = -84.09 \pm 0.07 \text{ degree}$$

Gravity Induced Component of Velocity

During the retro phase (from vernier ignition to start of RADVS controlled descent) gravity contributes to the spacecraft velocity by an amount $\int \underline{g}\, dt$. Lunar gravity varies in magnitude from 4.9 ft/sec^2 (at vernier ignition) to 5.28 ft/sec^2 (at start of RADVS). In addition, $\underline{g}$ varies in direction since the spacecraft has horizontal motion. The change in direction of $\underline{g}$ over the retro phase is about

$$\sin^{-1} \left[\frac{V \sin \Psi\, dt}{R_{\ell}} \right] = 0.22 \text{ degree.}$$

Since the vehicle spends more time at lower altitudes than at higher ones, the average value of g for the retro phase will be closer to 5.28 ft/sec^2. The average value of g over the retro phase was 5.16 ft/sec^2. The time duration of the retro phase is 54.535 seconds. (See Table 5.15-1.) Actual numerical integration of $\int g\, dt$ gives gt = 281.7 $\pm$ 1 ft/sec.

Thrust Induced Velocity Change

The two methods used to calculate velocity change during the retro phase due to the thrusting of the engines are as follows:

1) $\underline{\Delta V}$ from vector addition — The vector equation (Figure 5.15-1a) $\underline{V}_{B/O} = \underline{V}_o + \underline{g}t + \underline{\Delta V}$ can be solved to find $\underline{\Delta V}$. $\underline{V}_o$ and $\underline{g}t$ are available as discussed above; the spacecraft axis components of $\underline{V}_{B/O}$ (the burnout velocity, i.e., the velocity at start of RADVS) are available from telemetry. The axial velocity V_z is known to

an estimated accuracy of better than 1 percent at a given time based on correlation of simulated versus actual discrete time events such as segment intercept and vernier engine cutoff. V_x and V_y at burnout have calculated uncertainties of 4 and 1.5 ft/sec, respectively, based on 3σ telemetry and sensor errors.

$$V_{B/O_x} = 70.2 \pm 4 \text{ ft/sec}$$

$$V_{B/O_y} = -4.0 \pm 1.5 \text{ ft/sec}$$

$$V_{B/O_z} = 425 \pm 4.3 \text{ ft/sec}$$

This method will yield ΔV to an accuracy of 4.5 ft/sec. δ_I, the in-plane angle (Figure 5.15-1b) between $\underline{V}_O$ and z, defined > zero when z is "above $\underline{V}_O$," as shown, is known to be ± 0.027 degree based on the uncertainties in V_{B/O_x} which is primarily in-plane; δ_O, the out-of-plane angle between these two directions, is known to be ± 0.01 degree based on V_{B/O_y} uncertainties, δ_O is positive when z has a component out of the paper.

This method yields

$$\Delta V = 8420.2 \pm 4.5 \text{ ft/sec}$$

$$\delta_I = 0.261 \pm 0.027 \text{ degree}$$

$$\delta_O = 0.08 \pm 0.01 \text{ degree}$$

2) $\underline{\Delta V}$ from doppler data – Figure 5.15-2 shows the radial velocity change during retro phase versus time. The lower curve is from raw doppler data; the upper curve is corrected for temperature dependent frequency drift of the transmitter aboard the spacecraft. Both curves include the gt velocity due to lunar gravity.

ΔV is found by dividing the radial velocity change over the retro phase, 5501 ft/sec, by the cosine of the angle ζ between the tracking station — spacecraft line and the thrust axis, and then adding the gravity induced velocity component in the thrust direction, gt cos ξ as shown in Figure 5.15-1c. ζ and ξ are not coplanar since the Z axis does not lie in the plane of the spacecraft station and moon center. A correction must be made for the earth's rotation, which accounts for part of the doppler velocity seen by the tracking station as follows:

$$V_{ROT} = 4.7 \text{ ft/sec} \pm 0.1$$
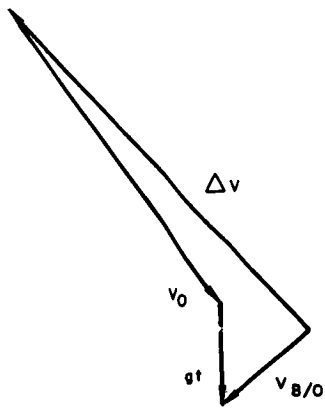
a) Vector Diagram

Figure 5. 15-1. Spacecraft
Velocity During
Retro Phase
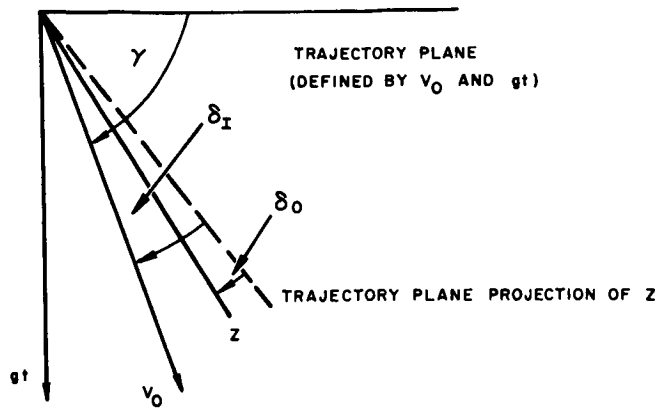
b) Trajectory Plane

Figure 5. 15-1 (continued). Spacecraft
Velocity During Retro Phase
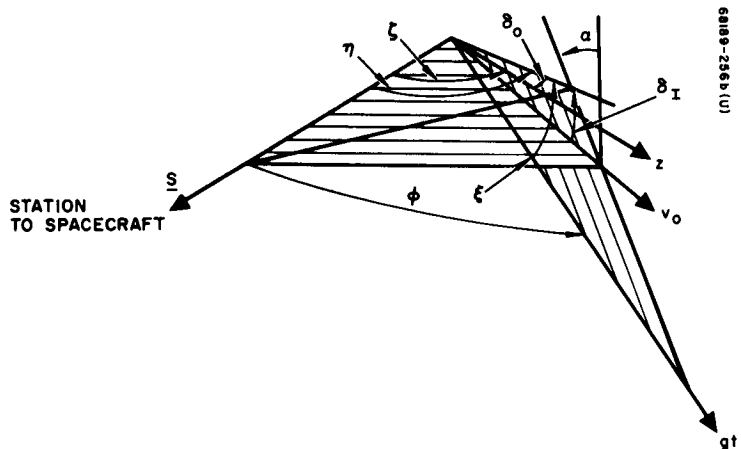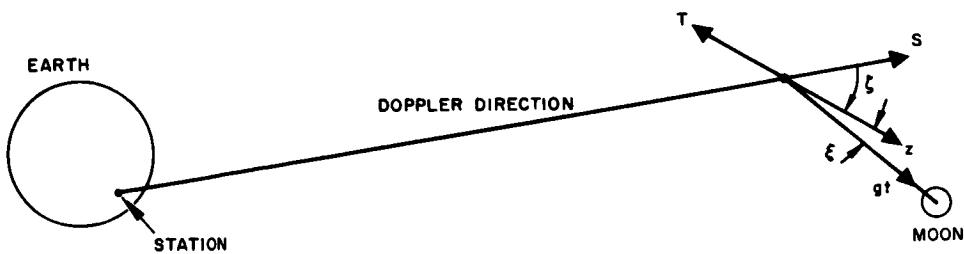
c) Doppler Geometry

Figure 5. 15-1 (continued). Spacecraft Velocity During Retro Phase
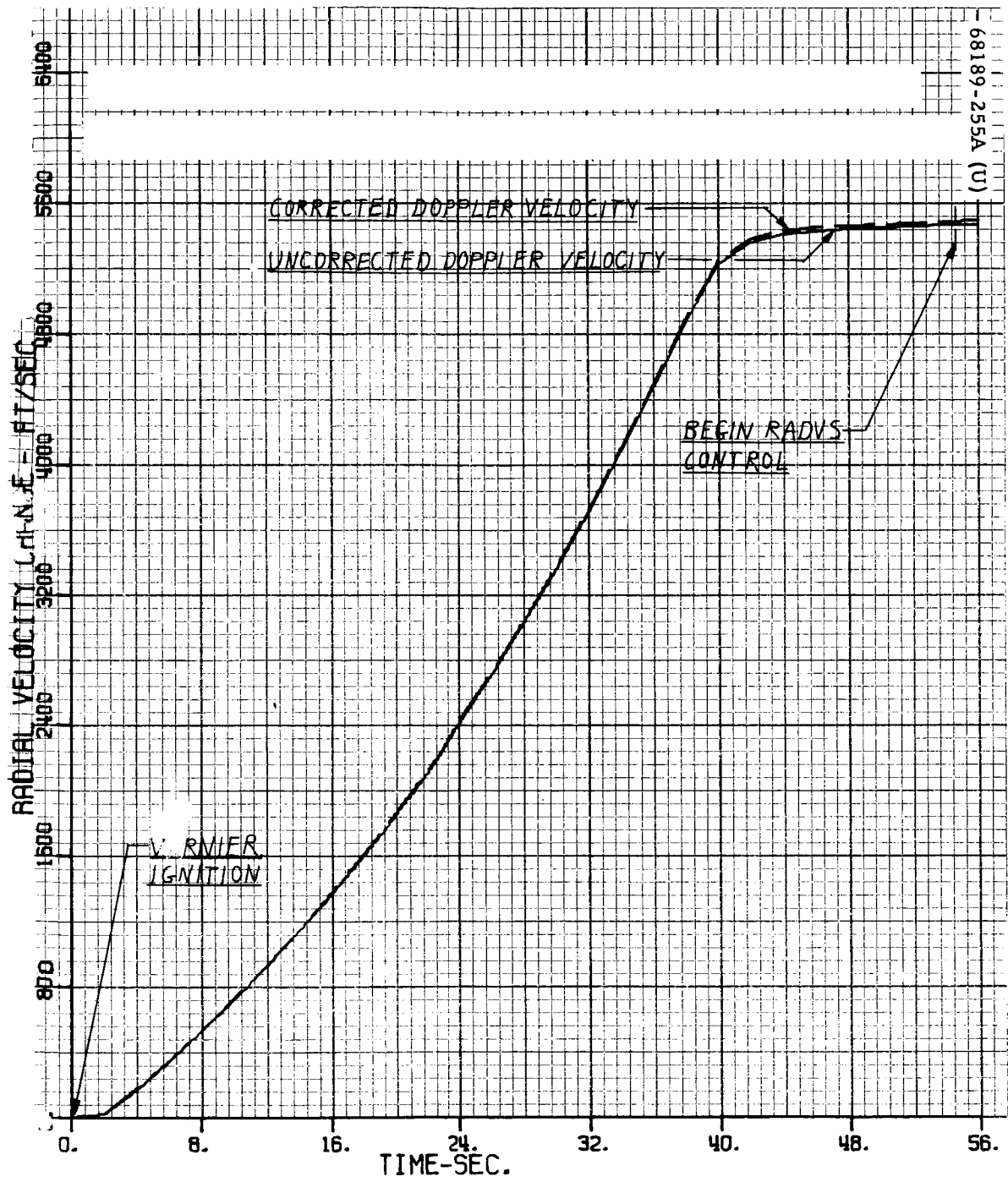
Figure 5.15-2.   Spacecraft Radial Velocity Change Relative to Earth
Retro phase — vernier ignition to RADVS control

Earth
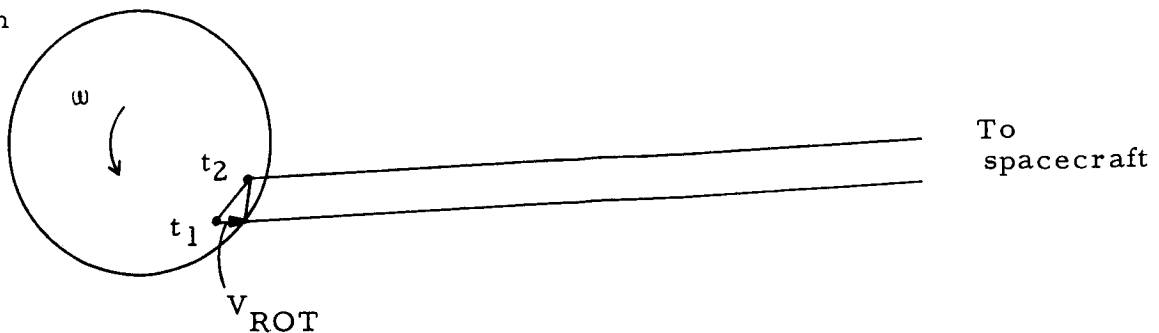
If ΔV_{DOPP} is the velocity change seen by the tracking station

$$\Delta V_{DOPP} = \Delta V \cos \zeta - gt \cos \varphi - V_{ROT}$$

or

$$\Delta V = \frac{\Delta V_{DOPP}}{\cos \zeta} + gt \frac{\cos \varphi}{\cos \zeta} + \frac{V_{ROT}}{\cos \zeta}$$

Values of the various angles in degrees shown in Figure 5.15-1c are as follows:

$$\delta_I = 0.261$$

$$\delta_o = 0.08$$

$$\alpha = 6.501$$

$$\xi = 6.17$$

$$\zeta = 47.450$$

$$\eta = 47.559$$

$$\varphi = 48.490$$

Hence

$$\Delta V = \frac{5501}{\cos 47.45} + 281.75 \frac{\cos 48.49}{\cos 47.45} + \frac{4.7}{\cos 47.45} = 8417.9$$

So, from doppler data, $\Delta V = 8417.9 \pm 8.8$ ft/sec.

The inaccuracy is due primarily to errors in the angles ζ and φ; the former is known to be ± 0.08 degree from tracking data combined with in-and out-of-plane attitude error calculations, and the latter to be ± 0.12 degree from known lateral translation of the spacecraft during descent.

Comparison of ΔVs and Retro Performance Implications

It is interesting to note that not only do the absolute magnitudes of ΔV check surprisingly well, but, out of necessity, so does the inertial thrusting direction as computed from burnout conditions. The doppler data is inherently one-dimensional and, to be useful in computing the retro thrust ΔV, the angular information supplied by the vector addition method of computing ΔV must be accurate. Thus, due to the geometric relation of the earth vector and trajectory plane, an uncertainty of 0.1 degree in the out-of-plane angle (δ_0) would cause a 7.0 ft/sec variation in the total ΔV as computed by doppler. Since the two ΔVs check to better than 3 ft/sec, this would give added confidence in the thrusting direction computed from the telemetered and corrected burnout conditions.

Assuming a nominally performing main retro and vernier system, the main retro phase ΔV should have been 8453 ft/sec as compared to 8420 ft/sec actual. Of the nominal 8453 ft/sec total ΔV, the vernier system contributed approximately 187 ft/sec. If the vernier system is considered to have performed nominally as the telemetry indicates, then the percentage ⌐ ₐₛ in retro total impulse (δ Timp/Timp) is

$$\frac{\delta\ \text{Timp}}{\text{Timp}} = \frac{\delta\Delta V}{\Delta V\ \text{retro}} \times 100\ \text{percent}$$

$$= \frac{8420 - 8453}{8453 - 187} \times 100\ \text{percent}$$

$$= 0.40\ \text{percent}$$

The uncertainty based on the more accurate method of computing ΔV (vector addition) is ±0.054 percent assuming a nominal inerts weight loss.

5.15.6.2 Main Retro Thrust Versus Time Curve

Two independent methods used to calculate the retro's thrust versus time curve are as follows:

1) Thrust/time from retro accelerometer data — Before being used to calculate a thrust curve, the raw accelerometer data is given the following three corrections:

   a) Biases are removed by comparing telemetered values with known values of acceleration which occur at times such as those prior to vernier ignition (zero g), after retro separation (0.9 g), etc.

   b) A scale factor error is removed. This is done by integrating the unbiased accelerometer data over time and comparing the resulting integral with the retro phase ΔVs found by the other two methods of computing ΔV described above. The

scale factor is then the integral divided by the mean of the other two ΔVs. The unbiased acceleration divided by this scale factor is then assumed free of bias and scale factor errors.

c) A hysteresis error is removed by actually determining two biases: one for the rising part of the acceleration curve, and the other for the falling part.

The bias on each part of the curve can be removed to an accuracy of 0.1 g_{earth}, and the accuracy of the scale factor is 0.1 percent.

The corrected acceleration is then used in the equation

$$T(t) = \frac{a(t)}{g_o} \left[W_o - \int_o^t \frac{T(t)}{I_{sp}} dt \right]$$

which is integrated numerically to obtain total thrust (W_o is weight at retro ignition). Vernier thrust is then subtracted out to obtain the retro thrust.

I_{sp} for this calculation is found from the relation below where W_L is the weight lost from retro ignition to burnout.

$$I_{sp} = \frac{\Delta V}{g_o \, \ell n \frac{W_o}{W_o - W_L}}$$

Figures 5.15-3a and b show S/C-1 thrust-time curves as determined from accelerometer data with the nominal predicted plot, raw accelerometer, and corrected accelerometer curves also shown. The difference between Figures 5.15-3a and b lies solely in the fact that the plots in Figure 5.15-3b have been corrected for accelerometer stiction by putting the curve through peak values. Since stiction could not be completely removed, the thrust-time curves cannot be assumed to be very accurate, but general trends can be obtained from both curves. Both accelerometer thrust curves start higher than the nominal, then drop below the nominal about 16 seconds after retro ignition, and begin to tail off sooner.

2) Thrust/time from doppler data — Figure 5.15-4 shows the main retro thrust curve as constructed from doppler counts received at Goldstone; the nominal predicted curve is also plotted. To construct the curve, a retro phase simulation trajectory program using a nominal thrust curve calculates nominal radial velocities relative to the tracking station and converts these to doppler counts that the station would receive from a stable spacecraft transmitter on a nominal trajectory.
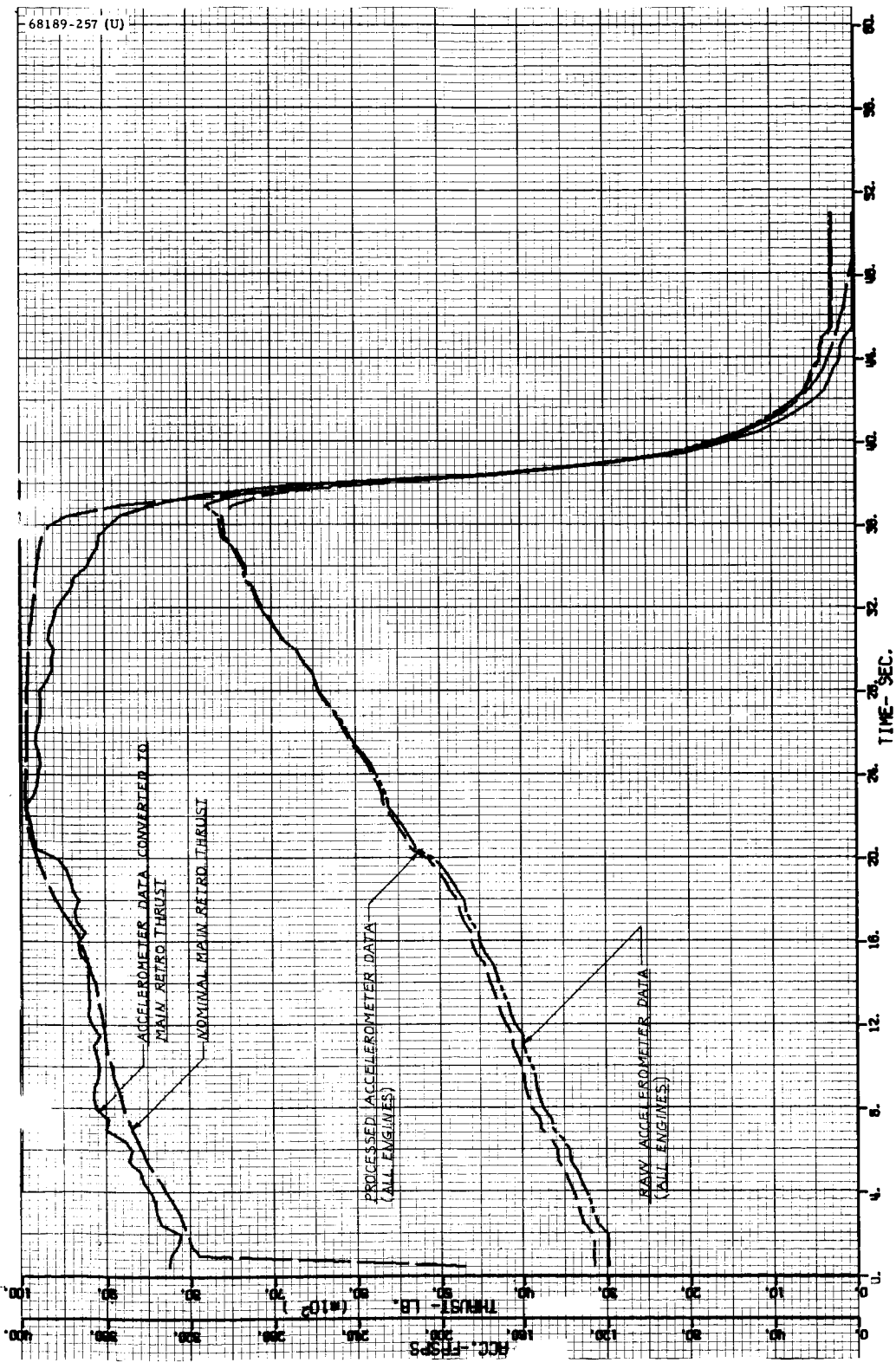
a) Normal

Figure 5.15-3. Unsmoothed Retro Phase Thrust and Acceleration Versus Time
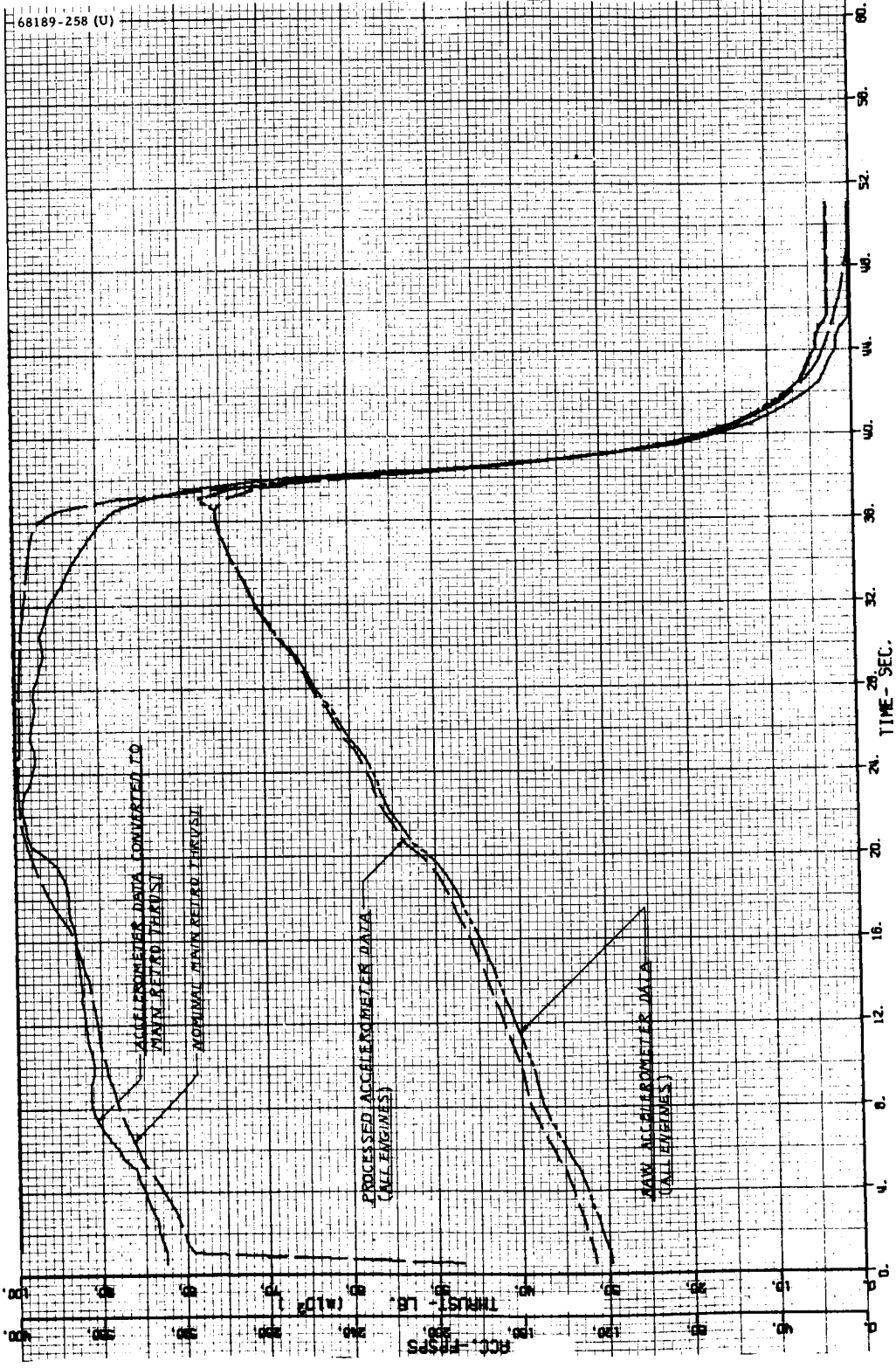
b) Also Corrected for Stiction

Figure 5.15-3 (continued). Unsmoothed Retro Phase Thrust and
Acceleration Versus Time

68189-259 (U)

DOPPLER DATA CONVERTED TO MAIN RETRO THRUST

NOMINAL MAIN RETRO THRUST

THRUST - LB. (x10⁵)

TIME - SEC.
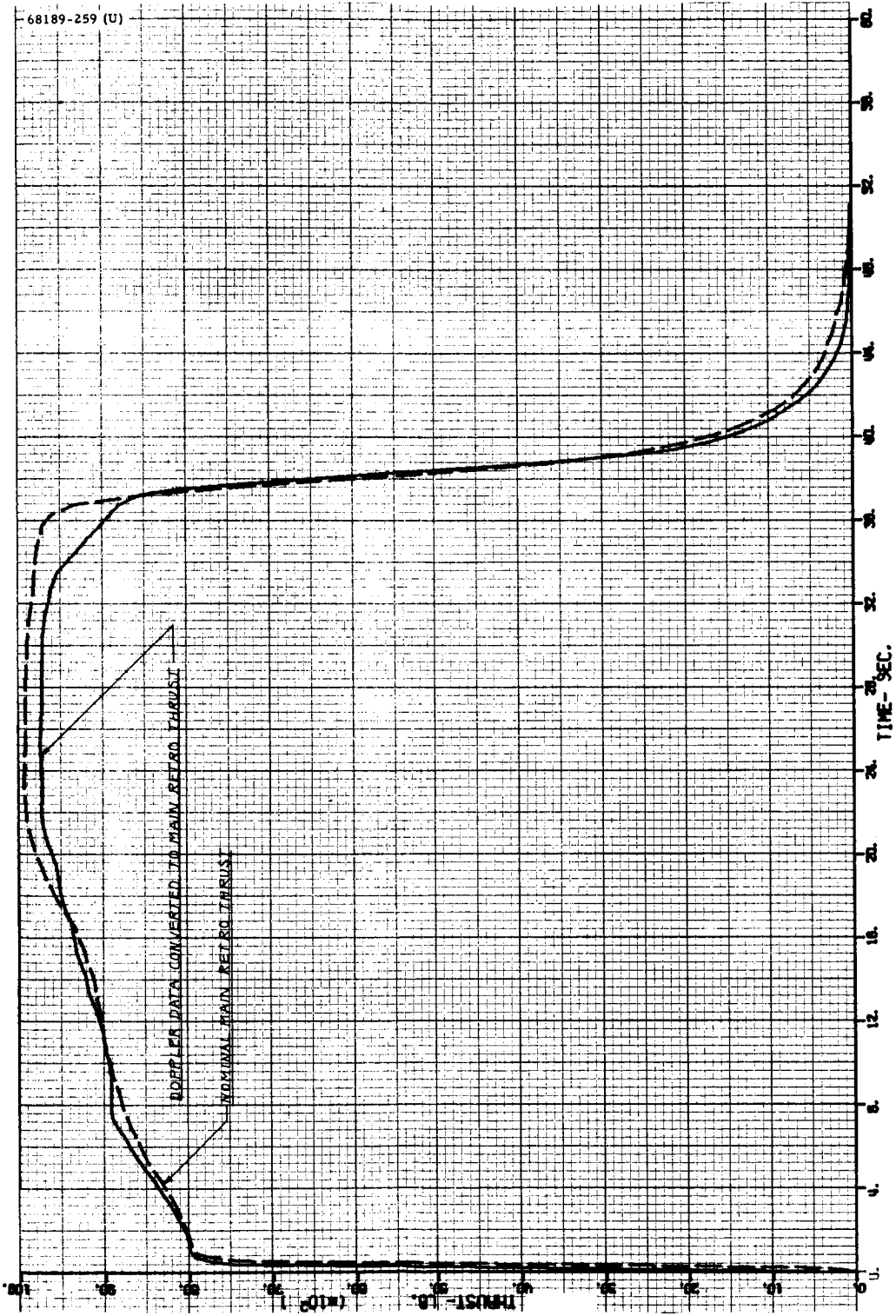
Figure 5.15-4. Main Retro Thrust and Acceleration
Versus Time (Doppler)

The nominal thrust curve is then perturbed until the doppler data from the perturbed curve is arbitrarily close to the doppler data actually received. For each point considered on the thrust curve, a difference between actual and perturbed counts over a 2-second interval of four counts (i.e., about 0.4 ft/sec) is considered close enough. In addition, the sum of such differences is constrained to be within 40 counts (4.3 ft/sec).

Radial velocity divided by the cosine of the angle between the tracking station and the thrust direction (47.45 ± 0.08 degrees) gives total velocity. When gt cos ξ is added,* the remaining velocity differences are entirely due to thrusting and give the thrust acceleration. Multiplication by the mass then gives the thrust level.

Misalignment between V_o and z is accounted for, as is the loss of inert mass (14.20 lb_m). Since the data used was taken at 2-second intervals, the accuracy of the thrust curve during the transient phases at ignition and tailoff is somewhat questionable.

Comparison of Two Methods for Retro Thrust/Time Curves
_____

Comparing the doppler curve against the accelerometer curve corrected for stiction, it is obvious that the former is much smoother. Both start off somewhat higher than the nominal, cross over the nominal near 16 seconds, show a much more gradual transition into tailoff than does the nominal, and both go to zero more quickly after the 3.5 g point than does the nominal. Peak thrust for the accelerometer curve is 9910 pounds, whereas for the doppler curve it is 9750. (Peak nominal thrust is 9930.) Both curves seem to show the same general trends, i.e., "bumps" in the same places, but these bumps appear larger on the accelerometer curve. This tendency to exaggerate by the accelerometer may be due to stiction, the effects of which can be removed imperfectly at best; peak thrust on the accelerometer curve occurs atop one of these "bumps," and so may also be somewhat exaggerated.

5.15.6.3   Determination of Touchdown Conditions
_____

Figures 5.15-5 and 5.15-6 show Z velocity (V_z) and slant range (SR) obtained from telemetry data as corrected by SEMBET** for telemetry bias and scale factor errors.

The discrete event times determined from all appropos telemetry data in the neighborhood of touchdown, referenced to the time base (153:06:14:00) on the attached plots, are as follows:

"10-ft/sec mark"   —   208.6 seconds (06:17:28.6)

_____

*The gravity term is added rather than subtracted because it is actually -ΔV, rather than ΔV, which is determined from doppler data.
**See subsection 5.15.6.7 for description of the SEMBET program.
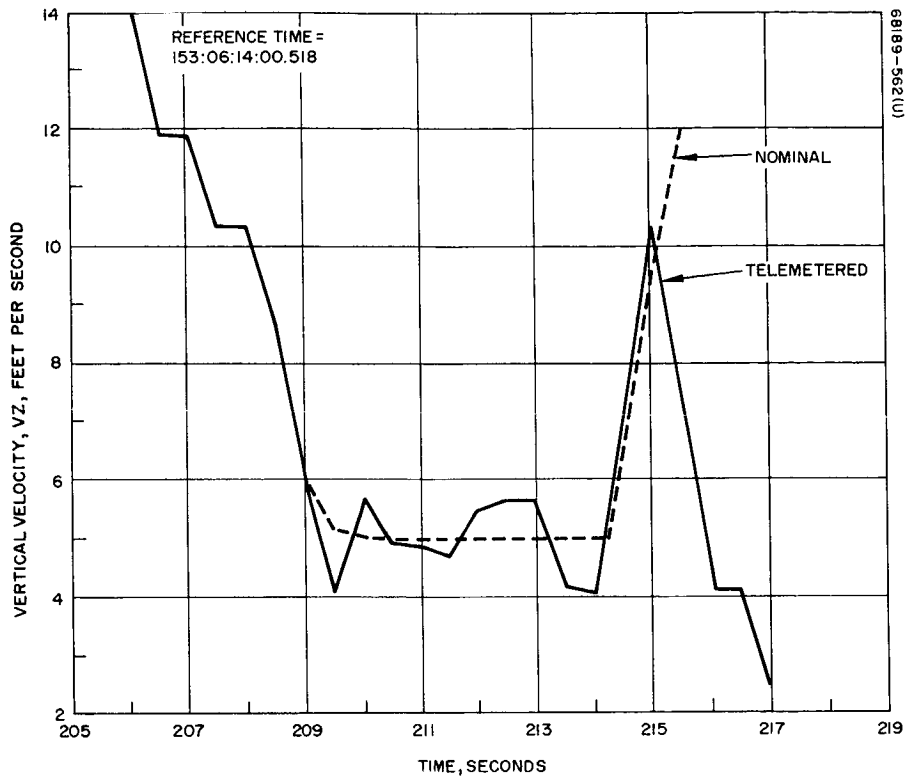
Figure 5.15-5.   Nominal and Telemetered Z
Velocity Versus Time
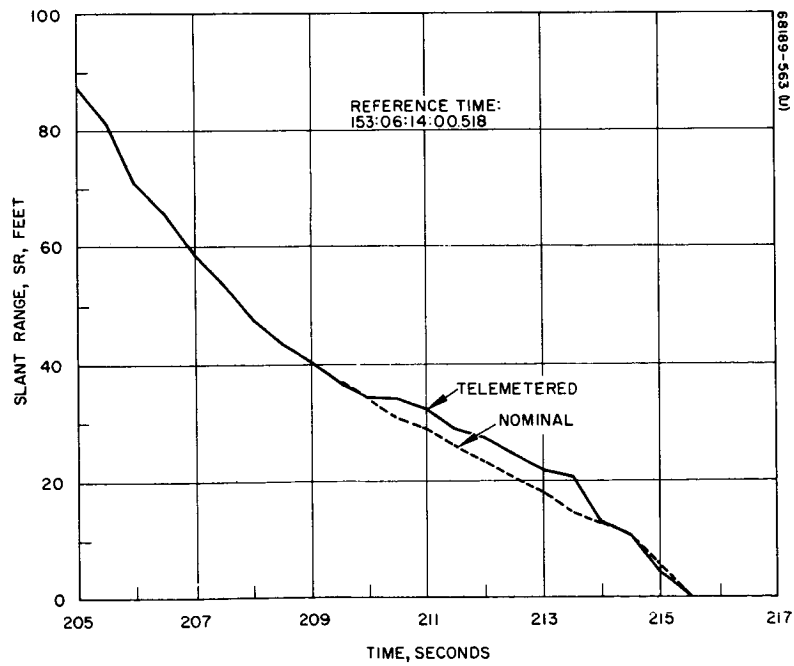
Figure 5.15-6.   Nominal and Telemetered Slant
Range Versus Time

Vernier engine cutoff — 214. 1 seconds (06:17:34. 1)

Touchdown   — 215. 6 seconds (06:17:35. 6)

From Figure 5. 15-6 SR is observed to be 43 feet at the "10-ft/sec mark" point, while from Figure 5. 15-6 V_Z is observed to be 8. 4 ft/sec with some uncertainty due to the noise content of the data. Premission data indicates that the mark should have occurred at a nominal velocity of 8. 6 ft/sec.

At cutoff, SR is observed to be 13 feet. The V_Z data during the constant velocity phase is somewhat noisy, so rather than using the V_Z value at 214. 1 seconds as an observed cutoff velocity, V_Z was assumed to be constant over the interval (210. 0 $\leq t \leq$ 214. 0), and the mean V_Z value therein was assumed to be the representative cutoff velocity. The cutoff velocity thus determined is 4. 9 ft/sec with a standard deviation of 0. 4 ft/sec.

In order to check the validity of the SR and V_Z values at the "10-ft/sec mark" and cutoff points the spacecraft simulation program (TD 1) was initialized at the start of the final maximum acceleration phase and allowed to proceed to touchdown. The data from the TD 1 run was then compared with the telemetered data beginning at the "10-ft/sec mark" point.

On Figures 5. 15-5 and 5. 15-6, plots of the TD 1 results (dashed lines) are superimposed on the telemetry plots (solid lines). The TD 1 program from which the dashed lines were plotted was set for a nominal run, i. e. , it was set to begin commanding a constant 5 ft/sec velocity at a measured V_Z of 8.6 ft/sec until SR reached 13 feet, whereupon the engines were shut down.

Figure 5. 15-5 shows an excellent agreement between the telemetered and nominal V_Z data, and Figure 5. 15-6 also shows excellent SR agreement with the exception of the portion spanning the constant velocity phase. In this phase, the telemetered SR values appear to be biased above the nominal values by approximately 3. 5 feet. If it is assumed that the telemetered SR value is indeed correct, then it can be reasoned that the spacecraft either experienced a significant rotation at the initiation of inertial hold (from which it somehow recovered when the engines were cut off), or that it came abruptly to a near dead halt when 5 ft/sec was commanded, accelerated quickly back up to 5 ft/sec over the phase, and then made up for its deficit by falling rapidly just prior to cutoff.

Neither of the two preceding spacecraft performance explanations is supported in any way by other telemetry data, nor are they in fact even possible. Neither the thrust command, gyro float angle, nor RADVS velocity data indicate that any drastic rotation was either commanded or experienced at the beginning of the constant velocity phase. Furthermore, the rotation implied by the telemetered SR value would have to be in the neighborhood of 25 degrees and would have to reach its full excursion in about 1 second, which is far beyond the spacecraft's rotational capability. Similarly, the thrust commands, acceleration error, and velocity data do not indicate any such unusual occurrences.

Furthermore, examination of the SR telemetered data reveals that the spacecraft acceleration (or deceleration) at the beginning of the constant velocity phase would be nearly 19 ft/sec for a full second in order to flatten the SR value at that point to the degree that it appears. Similarly the telemetered SR value indicates that the spacecraft would have "fallen" with a downward acceleration of over 7 ft/sec^2 for a full second prior to cutoff. It is neither possible for the spacecraft to produce the thrust necessary to occasion an upward acceleration of 19 ft/sec^2, nor is it possible for the spacecraft to fall with a downward acceleration of 7 ft/sec ^{2} even if the engines were shut off.

Therefore, it is assumed that the discrepancy between the telemetered and TD 1 SR values during the constant velocity phase is due to the introduction of a telemetry error in the SR channel over that interial. While it is not the purpose of this section to investigate the cause of any such telemetry error, let it be pointed out that the constant velocity phase is initiated by removing the output of the function generator (V_Z commanded) from the control loop and substituting a constant voltage value proportional to 5 ft/sec. Unloading the function generator in this manner presents a greater input impedance to the incoming SR signal, causing a possible rise in the SR value at that time if no compensation is made. The foregoing is offered as a possible explanation for the observed rise in the SR signal over the interval.

Perhaps the most salient observation made from the comparison plots, however, is that the elapsed times from the "10 ft/sec mark" to cutoff to touchdown agree to within at least 0.1 second. They may actually agree more closely than that but the relatively coarse granularity of the telemetered data precludes a more accurate determination of the appropriate signals. Partial derivative search studies have shown that the partial derivative of cutoff altitude with respect to cutoff time (about the nominal) is 4 ft/sec, and that the partial derivative of commanded constant velocity with respect to cutoff time is 1.25 ft/sec^2. Since the cutoff times between the TD 1 simulation and the telemetry data agree to within 0.1 second, then it may be assumed that the cutoff altitude of 13 feet is correct to within 0.4 foot and that the constant velocity of 5 ft/sec is correct to within 0.125 ft/sec.

There was no reason to question the validity of the V_x and V_y telemetry signals near touchdown so the mean values of 0.6 ft/sec for V_x and 0.0 ft/sec for V_y are assumed to be the correct lateral touchdown velocities. The TD 1 simulation run gives a value of V_z at touchdown of 12.2 ft/sec.

Spacecraft conditions from the "10 ft/sec mark" to touchdown are tabulated in Table 5.15-2.

5.15.6.4   Vernier Propellant Consumption

Table 5.15-3 presents a tabulation of propellant consumption from individual tanks based on vernier engine acceptance test performance data, both specific impulse and mixture ratio. The use of in-flight propellant temperature data was considered for possible updating of the mixture ratio but was found to have a negligible effect on total consumption, i.e., less than 0.2 pound deviation in total oxidizer or fuel consumption. In arriving at this conclusion, engine 2 (S/N 541) was considered because its propellant temperatures deviated the most from acceptance test temperatures. Based on test data,

engine 2 was found to have a sensitivity of 4×10^{-4} lb/lb/°F (∂ MR/Tdif) due to oxidizer-fuel temperature differences and 2.1×10^{-4} lb/lb/°F (∂ MR/Tab) sensitivity due to absolute shift in both propellant temperatures. Since both in-flight temperature difference and temperature shift were in the direction of increasing mixture ratio the following equation can be applied:

$$\Delta MR = \frac{\partial MR}{\partial Tdif} \Delta \, Tdif + \frac{\partial MR}{\partial Tab} \Delta \, Tab$$

$$\approx \left(4 \times 10^{-4} \frac{lb/lb}{°F} \right) (40°) + \left(2.1 \times 10^{-4} \frac{lb/lb}{°F} \right) (10°)$$

$$\Delta MR = 0.012 \text{ lb/lb} .$$

Considering the propellant consumed by engine 2, the variation in oxidizer consumed as a function of mixture ratio is

$$\frac{\partial Ox}{\partial MR} = \frac{(fuel \, consumed)^2}{total \, propellant} = 6.7 \text{ pounds}$$

Therefore, the maximum error in Table 5.15-3, due to the assumption of acceptance test data, would be 0.08 pound in oxidizer and fuel for engine 2. Since the other engines experienced temperatures closer to their acceptance test values, the total error is less than 0.2 pound. It should be noted that when the accuracy of the acceptance test data is considered, this error proves minor.

TABLE 5.15-3.   VERNIER PROPELLANT USAGE, POUNDS

Engine Tanks	Engine 1 Oxidizer Tank	Engine 1 Fuel Tank	Engine 2 Oxidizer Tank	Engine 2 Fuel Tank	Engine 3 Oxidizer Tank	Engine 3 Fuel Tank	Totals Calculated Engine 1	Totals Calculated Engine 2	Totals Calculated Engine 3	Totals Calculated Oxidizer	Totals Calculated Fuel	Totals Calculated Oxidizer Plus Fuel	Preterminal Mission Predictions, Oxidizer Plus Fuel
1. Midcourse	3.34	2.14	3.34	2.17	3.34	2.18	5.48	5.51	5.52	10.02	6.49	16.51	16.81
2. Main retro	8.71	5.60	8.73	5.67	8.72	5.70	14.31	14.40	14.42	26.16	16.97	43.13	41.89
3. Vernier phases	16.07	10.37	16.02	10.49	15.97	10.42	26.44	26.51	26.39	48.06	31.28	79.34	78.16
4. Total used	28.12	18.11	28.09	18.33	28.03	18.30	46.23	46.42	46.33	84.24	54.74	138.98	136.86
5. Average mixture ratio							1.553	1.532	1.532			1.539	
6. Total loaded	36.36	24.94	36.43	24.91	36.40	24.92	61.30	61.34	61.32	109.19	74.77	183.96	
7. Trapped (lines and expulsion efficiency)	0.43	0.28	0.43	0.28	0.43	0.28	0.71	0.71	0.71	1.29	0.84	2.13	
8. Usable loaded (item 6 minus item 7)	35.93	24.66	36.00	24.63	35.97	24.64	60.59	60.63	60.61	107.90	73.93	181.83	181.9
9. Usable loaded less total used	7.81	6.55	7.91	6.30	7.94	6.34	14.36	14.21	14.28	23.66	19.19	42.85	
10. Propellant remaining after one tank runs dry assuming propellant is consumed at midcourse thrust levels	0	1.55	0.14	1.25	0.16	1.26	1.55	1.39	1.42	0.30	4.06	4.36	4.8
11. Nominal propellant margin — nominally usable propellant in excess of nominal consumption (item 9 minus item 10)	7.81	5.00	7.77	5.05	7.78	5.08	12.81	12.82	12.86	23.36	15.13	38.49	33.9*

*Includes median shift of 5.7 pounds for uneven propellant consumption.

The method for computing total propellant consumption will be described in the three basic sections of midcourse, main retro phase, and vernier phase. Common to all of these sections is a digital computer program that models the spacecraft to the extent necessary for accurate propellant computations. In the midcourse computation, as in the others, both mixture ratio and specific impulse as a function of thrust are included in the program for the three engines. This allows an accurate numerical integration of spacecraft weight as a function of time, even when there is a significant difference in individual engine performance.

Other important ground rules and parameter values used in the following analysis are listed in Table 5.15-4.

TABLE 5.15-4. GROUND RULES FOR VERNIER PROPELLANT COMPUTATIONS

Parameters	Values
Midcourse maneuver	20.35 m/sec
Retro phase duration	54.68 seconds
Vernier thrust levels — retro phase	
Retro burn	197.2 pounds
Retro tailoff and separation	273.1 pounds
Vernier phase initial conditions	
Velocity	430 ft/sec
Altitude	27,820 feet
Flight path angle	4.1 degrees
Spacecraft weight	727.6 pounds
Vernier Engine Performance Parameters	Acceptance test data

Midcourse

Based on the midcourse maneuver magnitude requirement of 20.35 m/sec, which from postflight analysis appears to be accurate to within 0.1 m/sec, and the known spacecraft weight, Table 5.15-3 presents the propellant consumption of the three vernier engines. The total propellant consumption is approximately 0.3 pound less than the operations prediction because of the simplifying assumption of constant spacecraft weight used in the operational computer programs.

Main Retro Phase

The main retro phase propellant consumption computations are inherently the most inaccurate because of the "open loop" nature of the thrust commands. While at midcourse the change in spacecraft velocity is a very accurate measure of engine impulse, during the retro phase the main retro engine overshadows any expected variation in vernier performance.

Premission computations of vernier thrust levels were based on command current outputs obtained from the flight control programmer acceptance test data and thrust versus input current characteristics obtained from vernier engine test data. The resultant thrust levels obtained were 197.2 pounds during retro burn and 273.1 pounds during retro separation. Because the telemetered thrust commands are very temperature sensitive, it would appear that the above thrust values are still the most accurate. As an example of this temperature sensitivity, consider the telemetered thrust levels during the 0.9 g minimum acceleration phase and the constant velocity phase (2.0 g) just before touchdown. It is known that the required thrust levels during these phases are nearly equal because of decreasing spacecraft mass, yet telemetered thrust values indicate differences from 3 to 6 pounds. On the other hand, premission tests of the flight control programmer indicated deviations in the nominal thrust commands of less than 0.2 pound, with specification limits of less than 0.7 pound.

Because of the apparent inaccuracy of telemetry thrust commands, premission values were used in the computer model of the main retro phase. Since telemetry data indicates an increase of the retro phase time of approximately 0.6 second, this change was made in the computer model.

While telemetered thrust commands are not too useful for their steady-state values, they are very valuable in analyzing system transients and, in particular, those caused by retro thrust misalignments. Any deviation of the retro thrust vector from the spacecraft center of gravity will cause moments that the vernier system must null out, thus causing uneven propellant consumption between engines. SC-1 data indicates relatively small misalignments resulting in a maximum thrust deviation about the nominal of about 2 pounds for engine 2. The maximum resulting impulse deviation about the nominal is approximately 14 lb-sec or 0.05 pound of propellant. Because this deviation was so small, the propellant results in Table 5.15-3 assumes all engines thrusted at the same level during the retro phase.

Vernier Phase

To compute propellant consumption during the vernier phase, the computer model was initialized with the present best estimate of burnout conditions. A simulated descent of the spacecraft to touchdown was run and discrete time events were compared with telemetry data as a measure of model accuracy. Table 5.15-5 presents time comparisons for first segment intercept, segment end points, 10 ft/sec mark, and vernier engine cutoff at the 13-foot mark. As will be noted, all time points compare within 0.1 second, indicating a very good fit. In particular, the excellent correspondence in times from initial segment intercept to end of the first segment

TABLE 5.15-5.   ACTUAL VERSUS MODEL TIME COMPARISONS

Event	Time From Start of Vernier Phase (Start RADVS Controlled Descent), seconds	
	Telemetry	Three-Dimensional Computer Model
First segment acquisition	23.8	23.8
End first segment	35.1	35.2
End second segment	88.4	88.7
End third segment	97.2	97.0
10-ft/sec mark	106.6	106.4
13-foot mark	112.1	112.2

indicates that the simulated velocity at intercept must be accurate. In addition, the combination of accurate velocity at intercept with good time correspondence in first segment intercept points out that the initial conditions of altitude and velocity are also accurate.

The almost perfect time correlation of points along the trajectory to vernier engine cutoff give added confidence in the model's accuracy and show that the spacecraft functioned in an almost perfectly nominal manner. It would take a very unlikely combination of abnormal spacecraft performance and erroneous initial conditions to give as good a fit as indicated in Table 5.15-5.

One of the obvious spacecraft functions that the computer model cannot simulate in detail is individual vernier engine thrust fluctuations caused by completely random radar noise. However, the model does simulate average thrust levels as indicated by the accurate time correspondence and, since the vernier engines specific impulse is relatively flat with thrust, a randomly varying thrust gives the same total impulse as its average thrust when integrated over time.

Another simplification in the model that could have been simulated but was not considered important enough is the center of gravity offset from the spacecraft's geometric center. Depending on the phase of the mission, the center of gravity offset reached values as large as 0.1 inch. The maximum effect of this offset would cause variations in propellant consumption between engines up to 0.1 pound but would have no effect on total propellant consumption.

The model accuracy, excluding the above two considerations, may be described in terms of the total effective velocity change, that is, the sum of burnout velocity and gravitational losses ("gt" term). With total time in the gravitational field known to 0.1 second, the uncertainty in gt is less than 1 ft/sec. Since the uncertainty in burnout velocity is probably less than 5 ft/sec, and the total differential velocity is 1018 ft/sec, the probable error in the final results is less than 0.5 percent. As a comparison, this is equivalent to an error or uncertainty in vernier specific impulse of 1.5 seconds.

Total vernier propellant consumption based on the above model and best estimate of burnout conditions is 79.3 pounds as compared to the pre-retro prediction of 78.1 pounds.

Propellant Margin

During the mission, propellant margin figures are based on computing the amount of usable propellant on board at touchdown with a probability of 50 percent. In practice, the computation is done by taking the results of running the operational terminal descent computer program (similar to the program used in the previous computations) and combining this with median shift results obtained from a Monte Carlo simulation of the terminal descent. The median shift, based on specified values of retro moment and mixture ratio dispersions, is the amount of additional propellant that must be loaded to allow for uneven consumption between vernier tanks rather than variations in total propellant consumption. During the mission, 5.7 pounds of propellant were allowed for this effect, resulting in a predicted propellant margin of 33.9 pounds. Based on postmission analysis, it is clear that there was very little moment to correct during the retro phase and, therefore, very little or none of the 5.7-pound allowance was necessary for this purpose. In addition, vernier propellant temperatures were not extreme and, therefore, the 3σ mixture ratio variation allowance of 0.1 is probably far greater than the actual. While postmission data does not allow one to be too quantitative, a postflight "engineering" guess at the necessary allowance for uneven consumption would be 1.0 pound.

Item 11 of Table 5.15-3 gives a best estimate of 38.5 pounds for the nominal propellant margin at touchdown. Therefore, the best estimate of propellant margin with a 50 percent probability would be this value less 1.0 pound or 37.5 pounds. To compute the 99 percent minimum propellant margin, a number must be placed on the vernier specific impulse variations.

5.15.6.5 Spacecraft Landing Location

Surveyor landed in a relatively flat region with the coordinates 43.306 degrees west and 2.427 degrees south. This position, known to an accuracy of about 5 miles (3σ), was found from the best orbit determination data available and by using the terminal guidance program. The telemetry data when analyzed showed an additional 42 ft/sec lateral velocity component not used in the terminal descent program. This difference, when added to the results obtained from the computer program, moved the final Surveyor landing location to the one specified above, a move of only 3616 feet.

This landing site is 1.13 kilometers short (southeast) of the unbraked impact point (where it would have crashed had the retro rocket not fired). Both locations lie in the trajectory plane which is inclined at 13.3 degrees west of north (76.7 degrees from lunar equator).

Attempts are currently being made to fit all the best Surveyor I telemetry data available to a six degree of freedom program to determine even more accurately where Surveyor I is located. The results are not expected to move the landing location any significant amount.

5.15.6.6 Retro Case Landing Location

The retro case was allowed to fall free of the spacecraft after fuel depletion. At the time of separation, the spacecraft retro case assembly was at an altitude of 28,982 feet descending at 442.47 ft/sec, and was at a 4.1-degree angle from the vertical in a trajectory plane aligned 13.3 degrees east of south (76.7 degrees inclined to the lunar equator).

The spherical case landed some 1590 feet south and east of its dis-engaged point at a velocity of 710 ft/sec. This placed it 300 feet from Surveyor I along its plus X axis, in a direction 13 degrees east of south.

The uncertainty of its location (3σ) is ±200 feet when referenced to the separation point and is approximately one-half of this when referenced to the spacecraft. The reason for this apparent reduction is that both retro case and spacecraft have some common uncertainties in the initial conditions used in computing their landing location.

5.15.6.7 Trajectory Reconstruction

This subsection reconstructs the vernier phase of the terminal descent trajectory in order to provide a best estimate of the actual trajectory parame-ters in that phase. The following paragraphs provide a description and plots of the nominal spacecraft trajectory from retro ignition to touchdown, describe the telemetry processing techniques used and give plots of the more salient telemetered quantities that apply to trajectory reconstruction. They also give plots of a nominal trajectory, initialized with telemetry data at the inception of the steering phase, and show a comparison between the applicable telemetered parameters and their nominal counterparts in the vernier phase. In addition, a brief description is given of the SEMBET technique used to determine the telemetry errors that caused the differences between the telemetry data and the nominal data. The trajectory recon-struction effort is finalized by providing a simulated vernier phase trajectory that has been fitted to the telemetry data via the error determination scheme. This trajectory then is the desired best estimate. The subsection is com-pleted by plots of telemetry data corrected for the determined errors along with plots of the final differences between the corrected telemetry data and the best estimated trajectory.

Retro and Vernier Nominal Trajectory

Figures 5.15-7a through 5.15-7L are plots made from the output of a six-degree-of-freedom (6DOF) spacecraft simulation program, initialized with DSIF tracking data at the time of retro ignition. Therefore, these plots show nominal or predicted spacecraft parameters throughout the retro-vernier phases and include the following parameters: slant range, xyz velocities, vernier engine thrust commands, gyro error signals, instantaneous spacecraft weight, and center of gravity location.

The time base on the plots of the nominal data has been adjusted (for comparative purposes) such that zero time thereon corresponds to 153:06:14:0.518 GMT.

Retro and Vernier Telemetered Trajectory

Figures 5.15-8a through 5.15-8m are plots of the following received telemetry signals: slant range, V_x, V_y, V_z, T_1, T_2, T_3 (thrust commands), φ_x, and φ_y (gyro error signals).

All applicable telemetry signals are determined continuously in the spacecraft and are available for transmission at all times but are done so by a commutator that telemeters only one signal at a time. The signals to be telemetered are represented as voltage outputs in the spacecraft and are digitized into counts before transmission. The DSIF tracking station then receives the telemetry in the form of a train of binary bits, which contains the digitized signals plus code words appropriately inserted to separate commutation cycles (called "frames").

The telemetry data supplied to Hughes is in the form of a train of frames, each one marked with a time word that denotes the reception time of that frame at the DSIF station.

The preprocessing program (PREPRO) used to reduce the telemetry data performs two major functions: 1) transforming the data from raw counts to appropriate engineering units, and 2) interpolating the data to even stepsizes.

The transformation to engineering units is accomplished via the application of sets of calibration coefficients used in fifth-order transformation equations of the form

$$\text{Meu}(i) = \sum_{j=0}^{5} [K(i,j) \, Mc(i)^j]$$

where $Mc(i)$ is the ith telemetry signal in counts, $K(i,j)$ is the calibration coefficient for the jth order term of the ith signal, and $Meu(i)$ is the ith telemetry signal in engineering units. The sets of calibration coefficients used for the signals plotted in Figures 5.15-8a through 5.15-8m are found in Table 5.15-6.
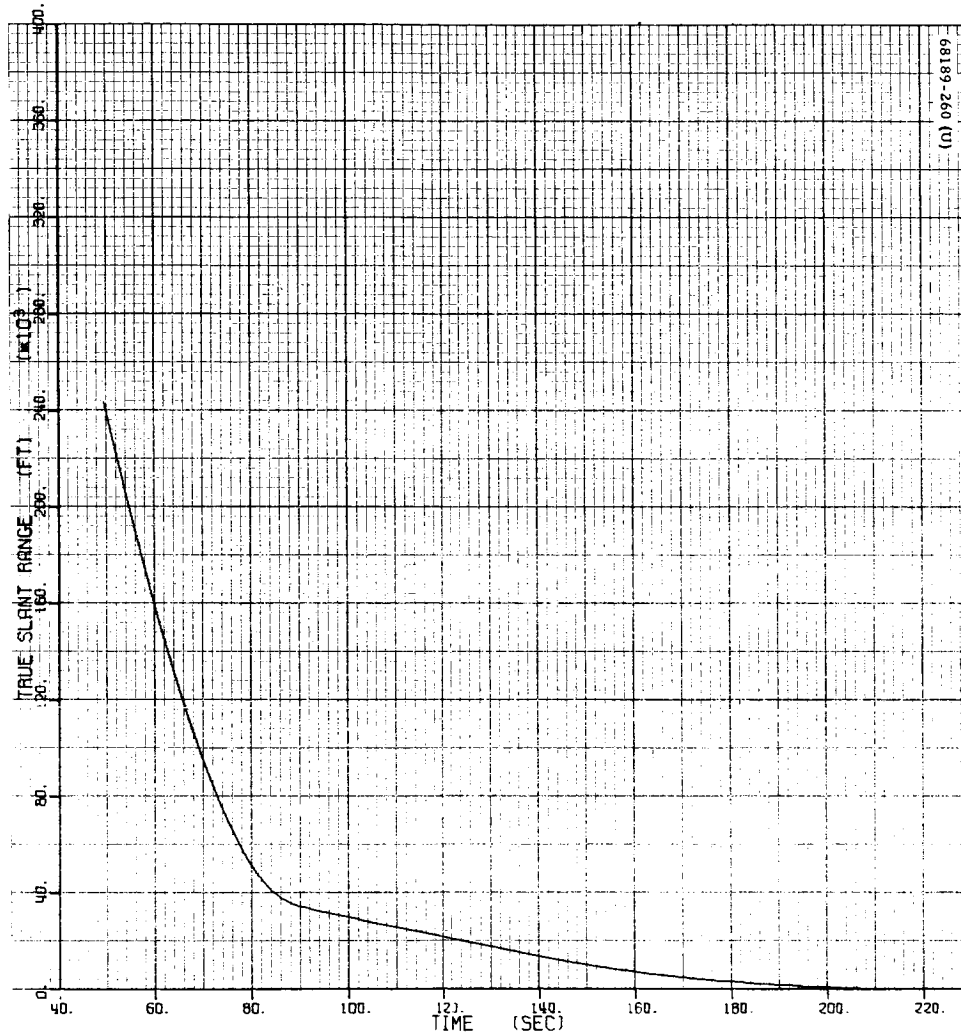
a) Nominal Slant Range, feet X 10^3

Figure 5.15-7.   Nominal Plots From Six-Degree-of-
Freedom Simulation Program
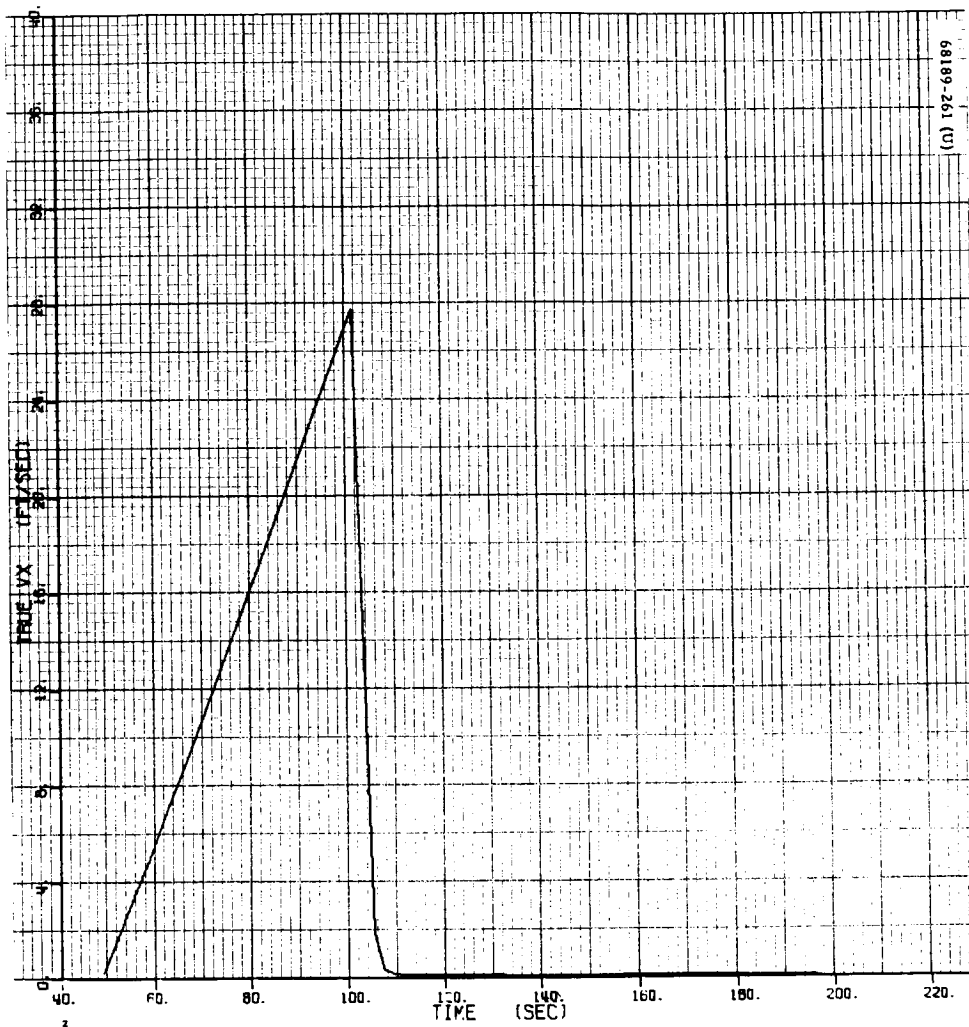
b) Nominal X Velocity, ft/sec

Figure 5.15-7 (continued). Nominal Plots From Six-
Degree-of-Freedom Simulation Program
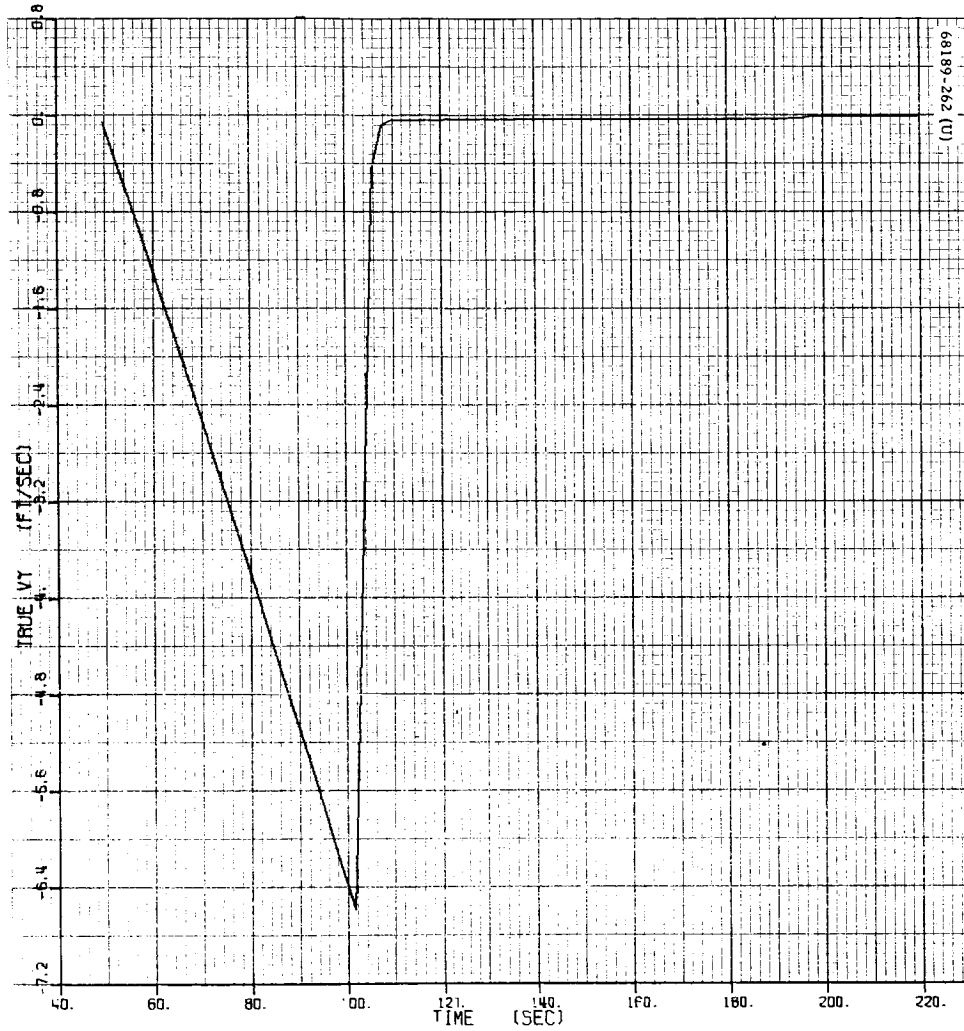
c) Nominal Y Velocity, ft/sec

Figure 5.15-7 (continued). Nominal Plots From Six-
Degree-of-Freedom Simulation Program
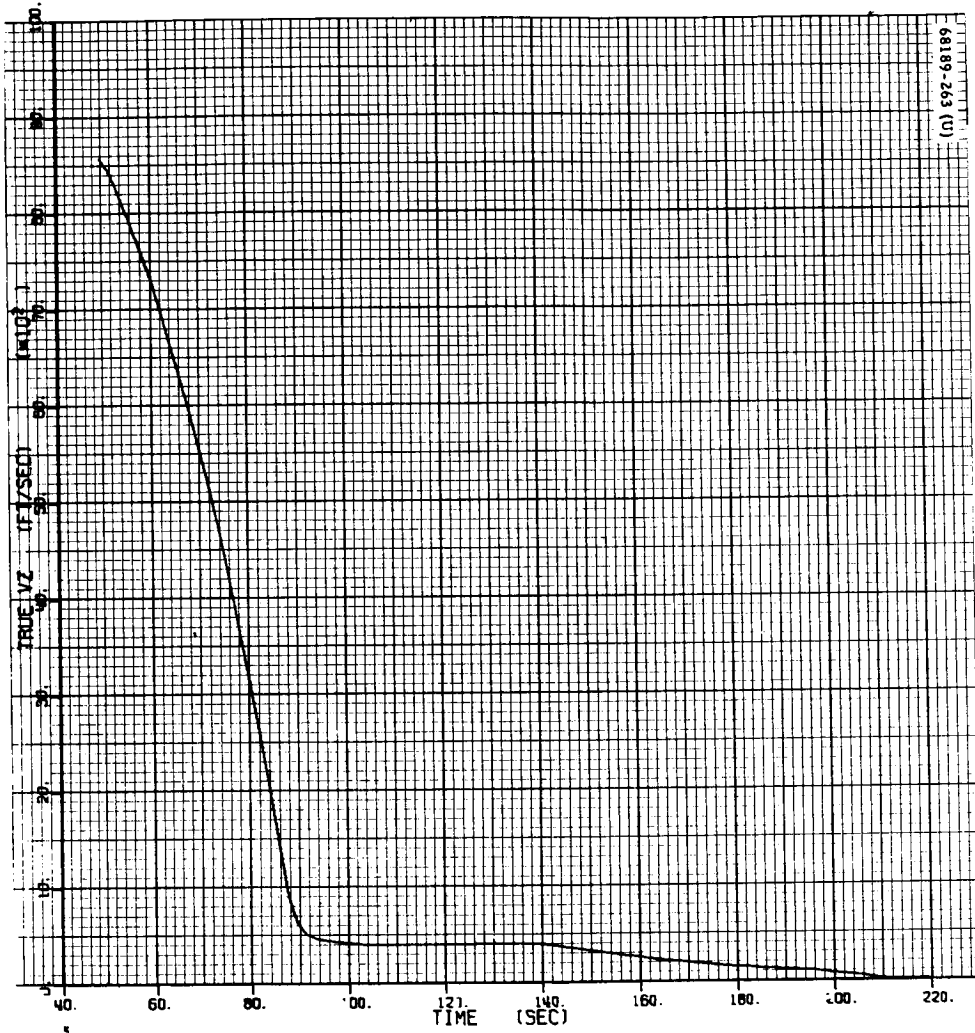
d) Nominal Z Velocity, ft/sec $\times$ 10^2

Figure 5.15-7 (continued). Nominal Plots From Six-
Degree-of-Freedom Simulation Program
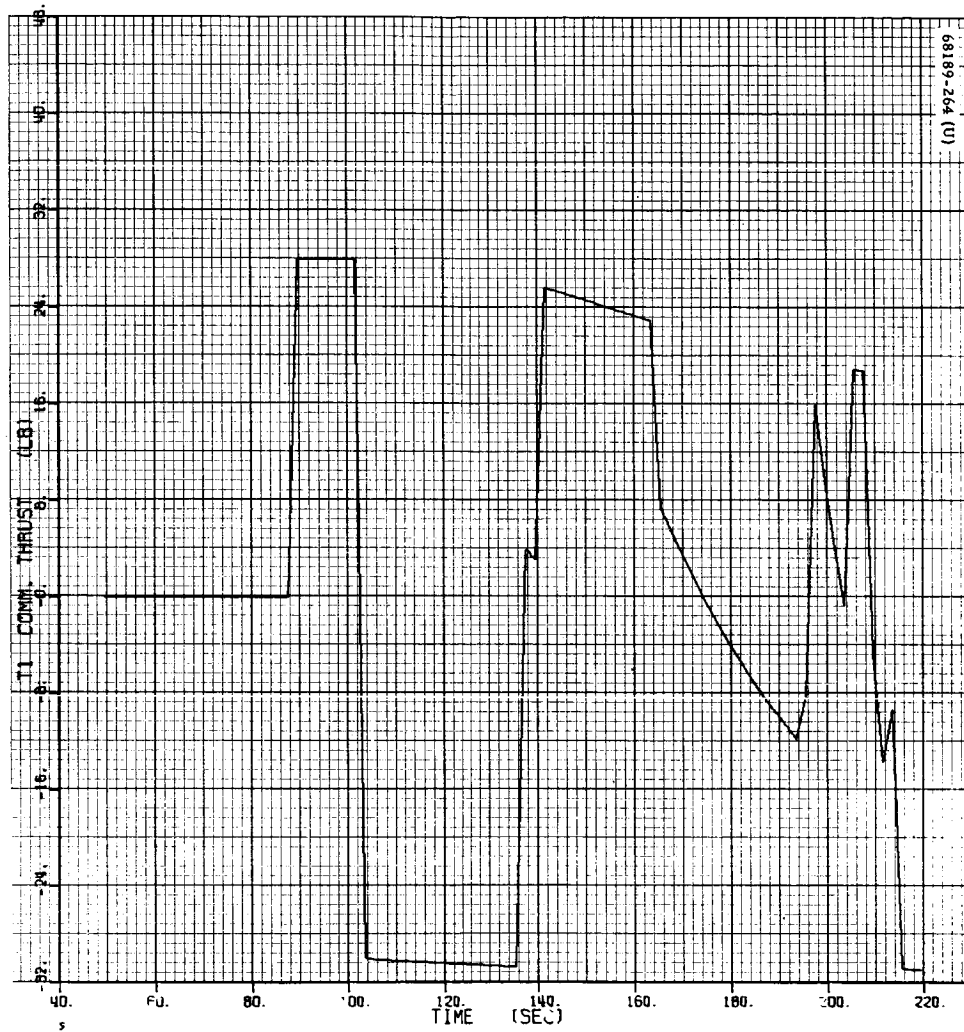
e) Nominal Vernier Engine 1 Thrust Command

Figure 5. 15-7 (continued). Nominal Plots From Six-
Degree-of-Freedom Simulation Program
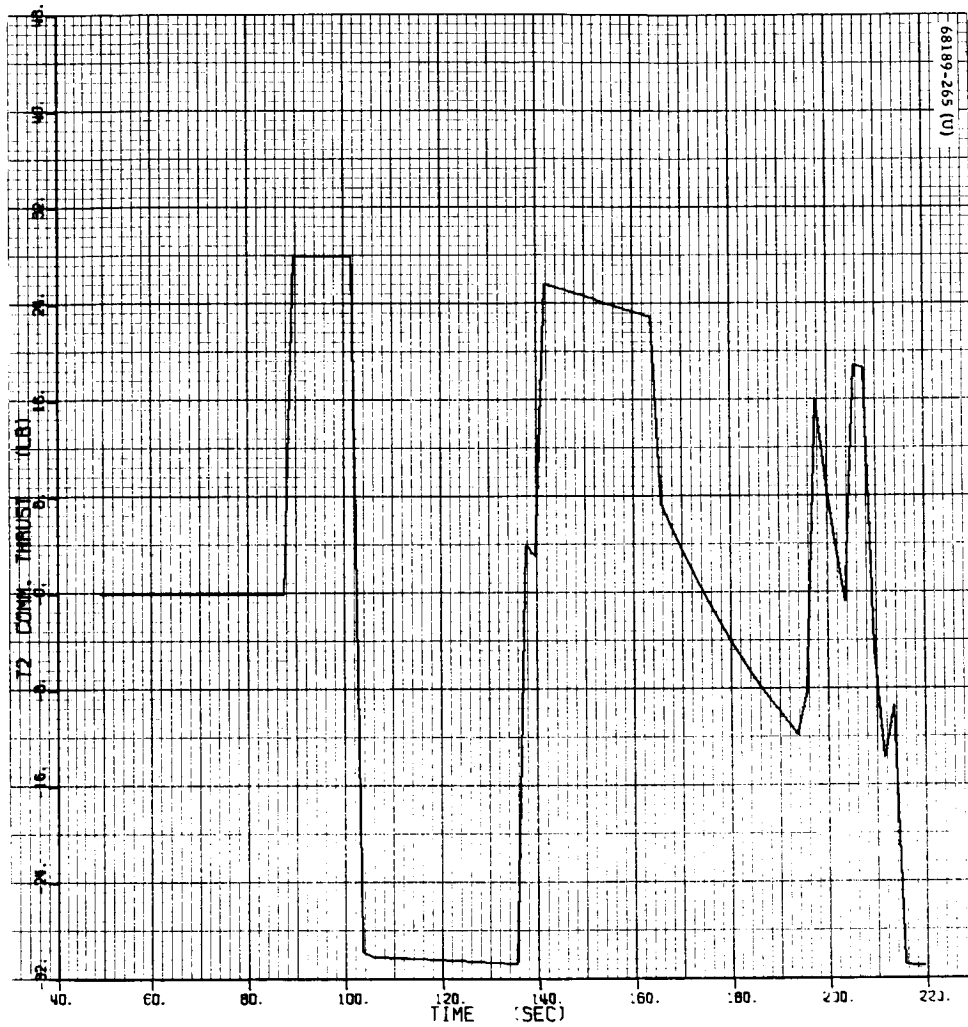
f) Nominal Vernier Engine 2 Thrust Command

Figure 5. 15-7 (continued).   Nominal Plots From Six -
Degree-of-Freedom Simulation Program

g) Nominal Vernier Engine 3 Thrust Command

Figure 5.15-7 (continued). Nominal Plots From Six-Degree-of-Freedom Simulation Program
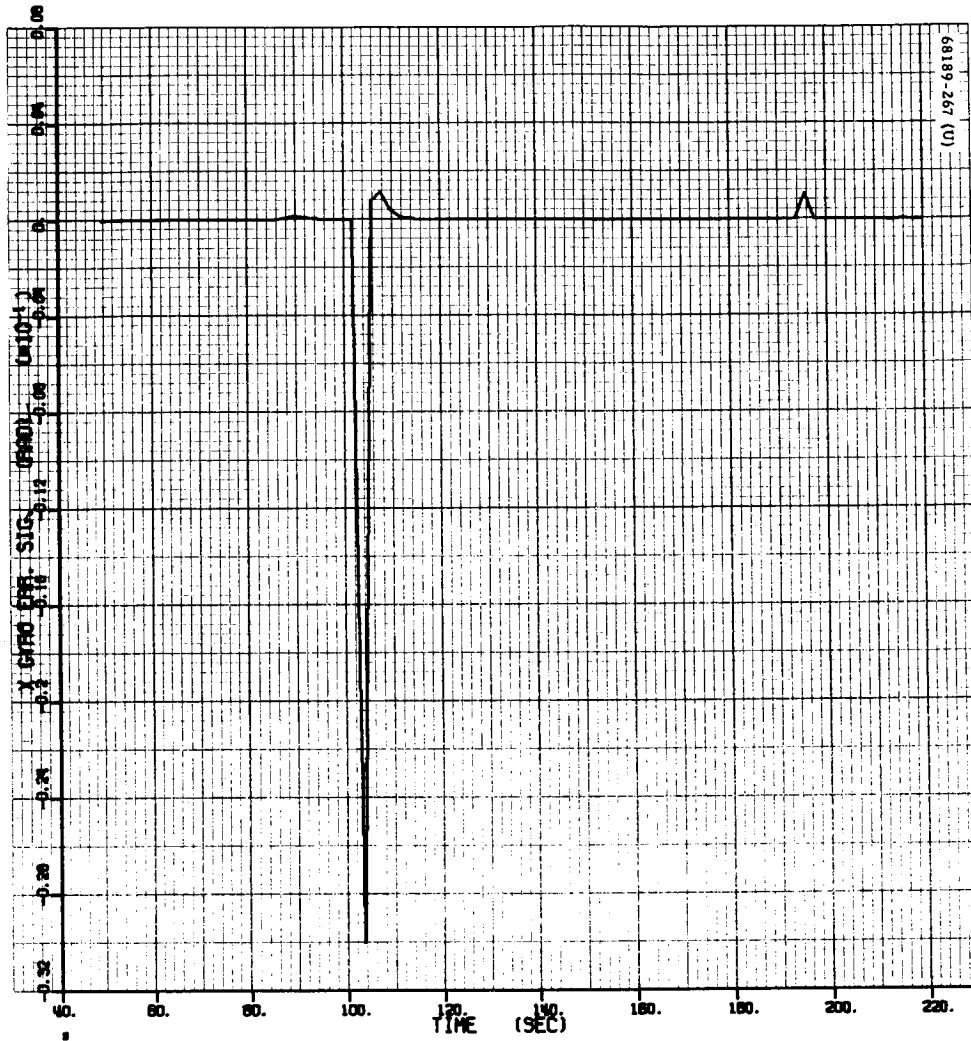
h) X Gyro Error Signal, degrees $\times 10^{-1}$

Figure 5.15-7 (continued). Nominal Plots From Six-
Degree-of-Freedom Simulation Program
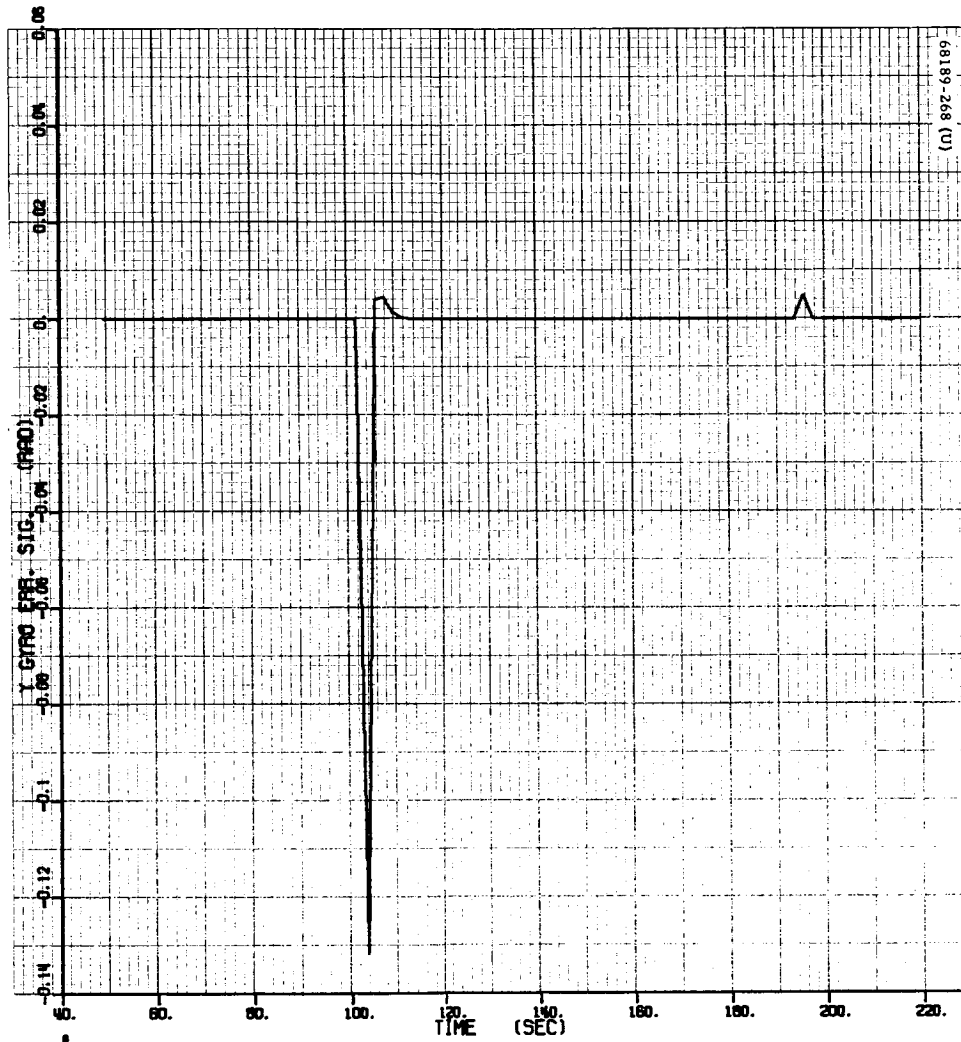
i) Y Gyro Error Signal, degrees

Figure 5. 15-7 (continued). Nominal Plots From Six-
Degree-of-Freedom Simulation Program
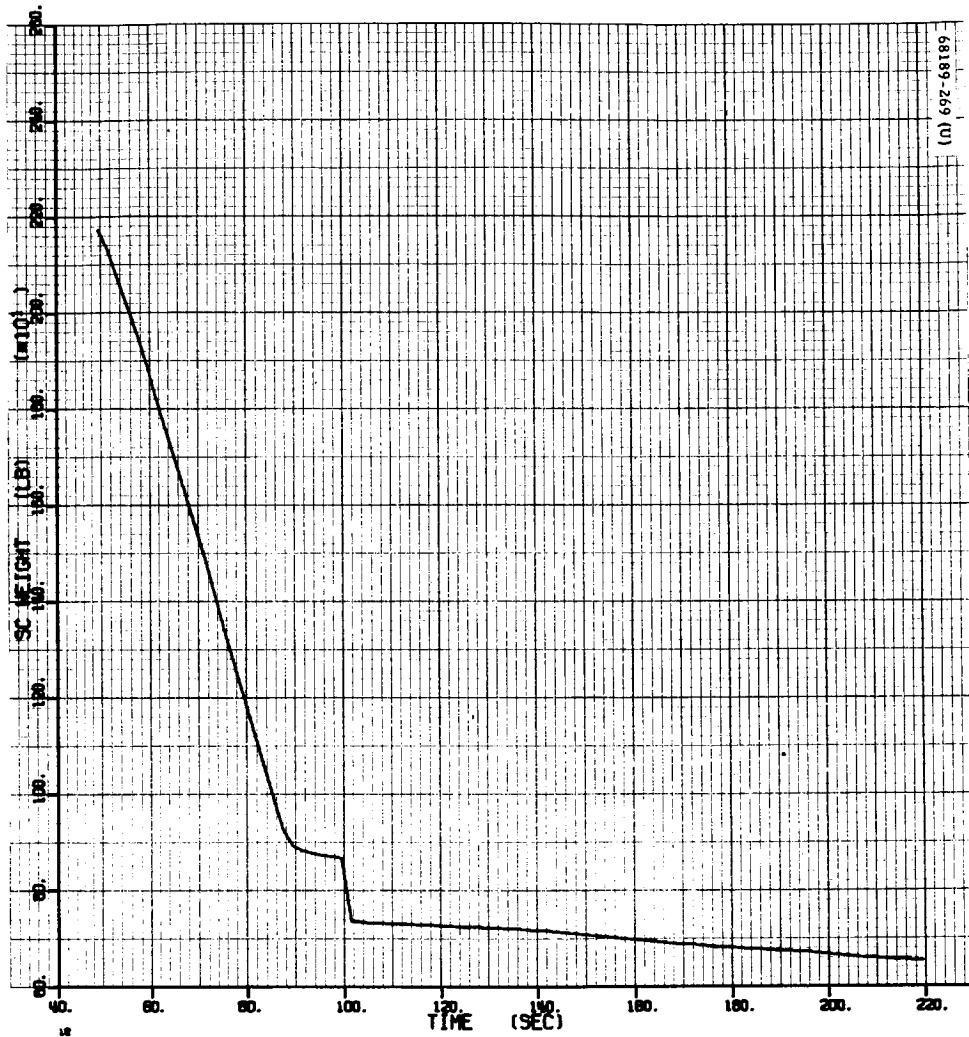
j) Spacecraft Weight, pounds

Figure 5.15-7 (continued). Nominal Plots From Six-
Degree-of-Freedom Simulation Program
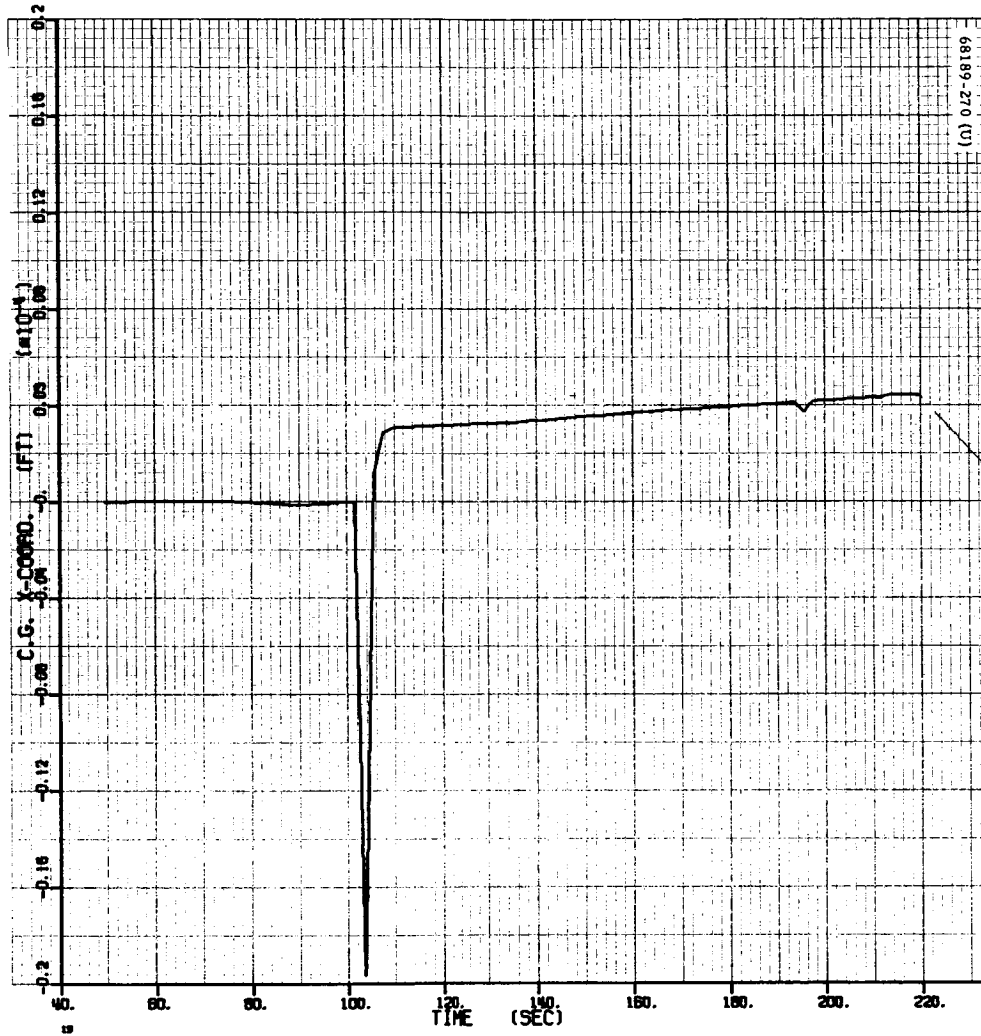
k) Center of Gravity, X Coordinate, feet X 10^{-4}

Figure 5.15-7 (continued). Nominal Plots From Six-
Degree-of-Freedom Simulation Program

1) Center of Gravity, Y Coordinate, feet × 10^{-4}

Figure 5. 15-7 (continued). Nominal Plots From Six-Degree-of-Freedom Simulation Program
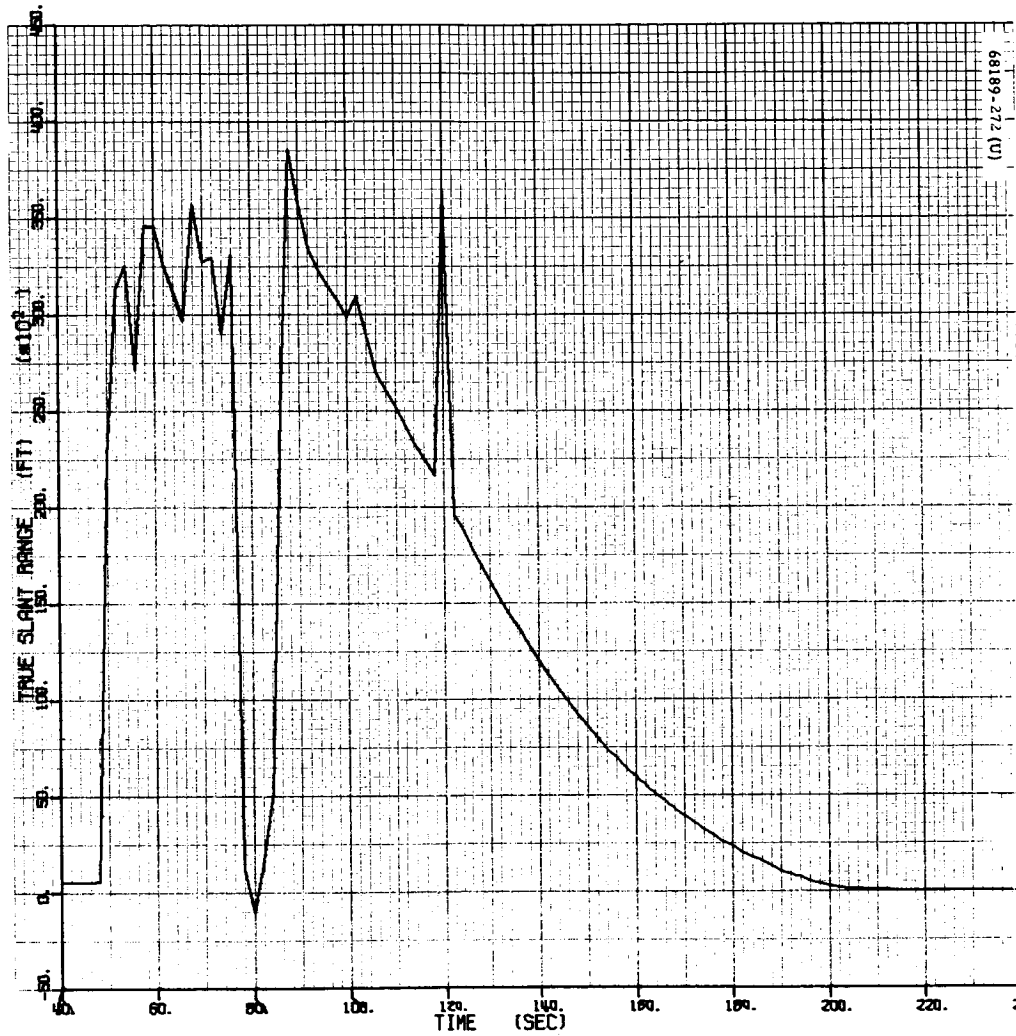
a) Telemetry Slant Range, feet x 10^2

Figure 5. 15-8. Spacecraft Telemetry Plots
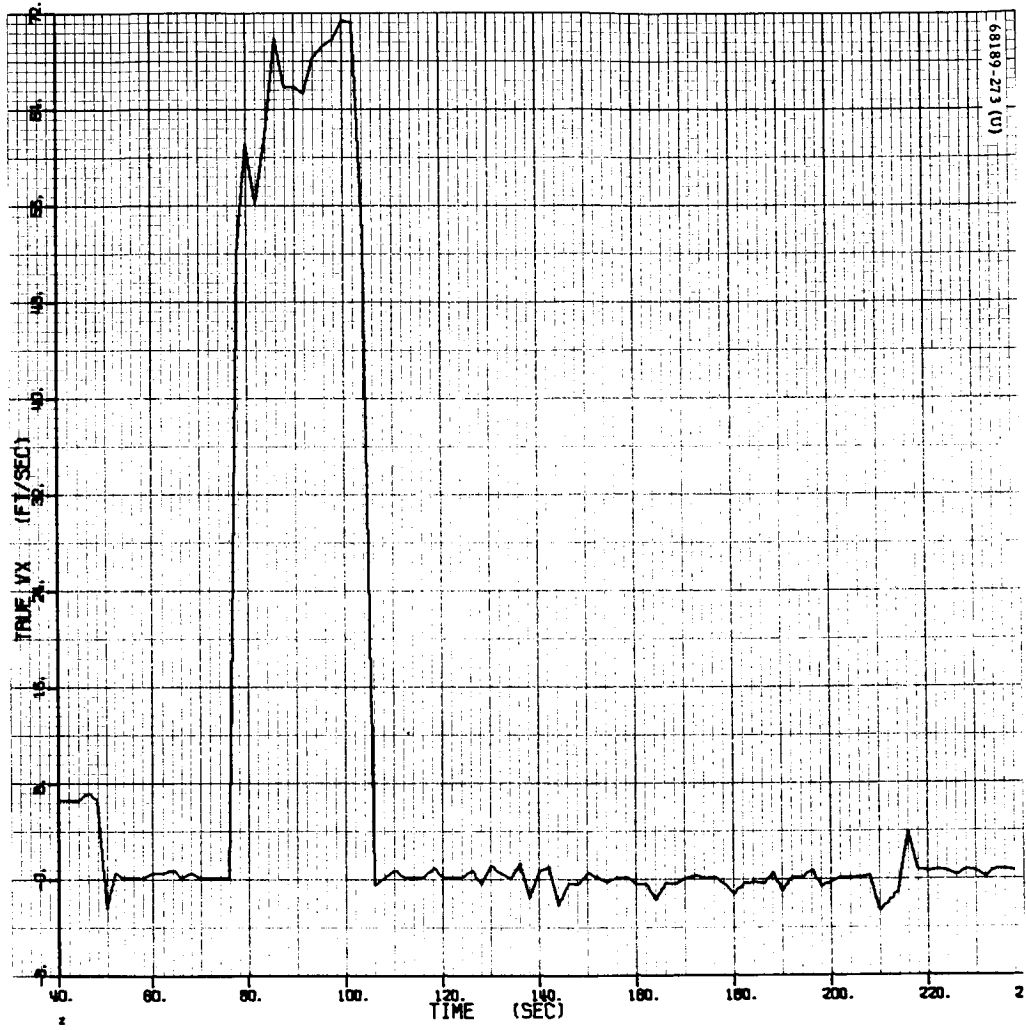
b) Telemetry X Velocity, ft/sec

Figure 5.15-8 (continued). Spacecraft Telemetry Plots
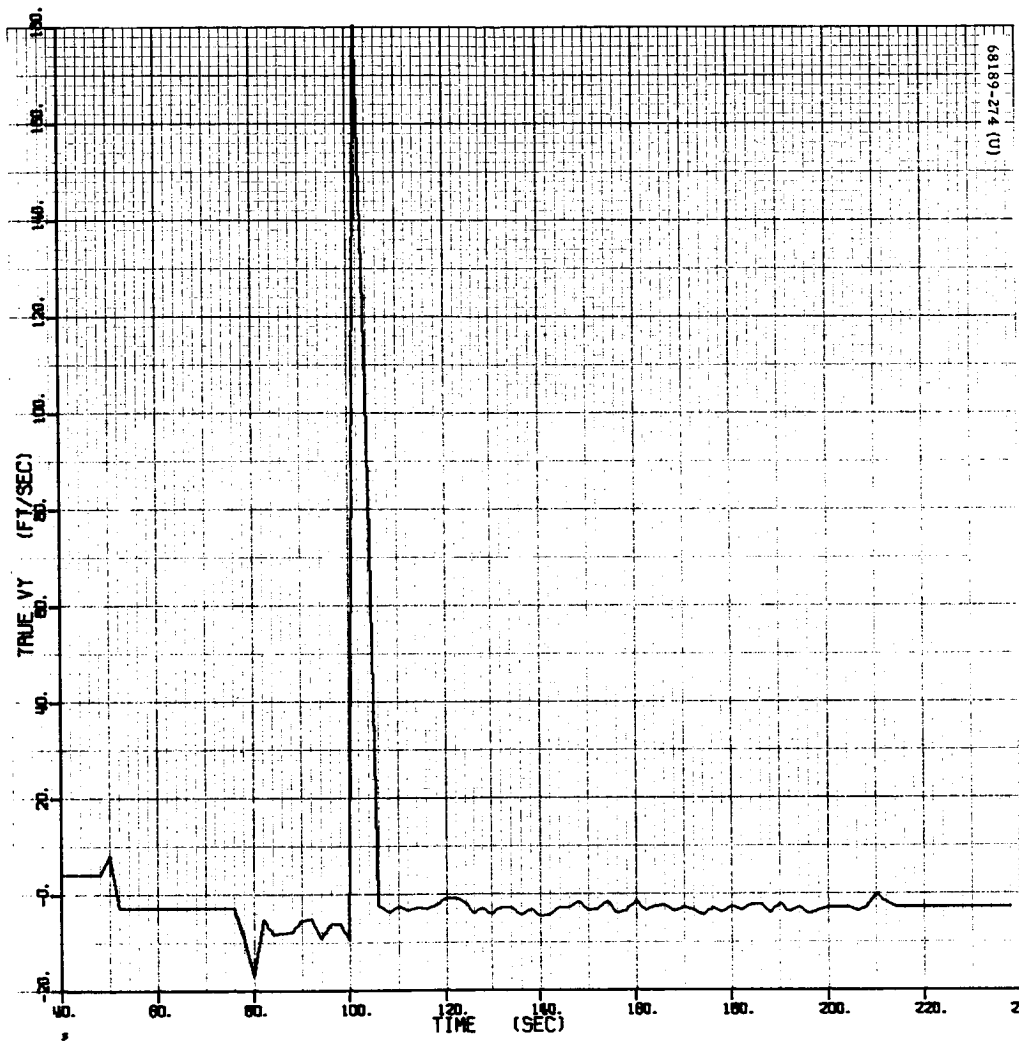
c) Telemetry Y Velocity, ft/sec

Figure 5.15-8 (continued). Spacecraft Telemetry Plots
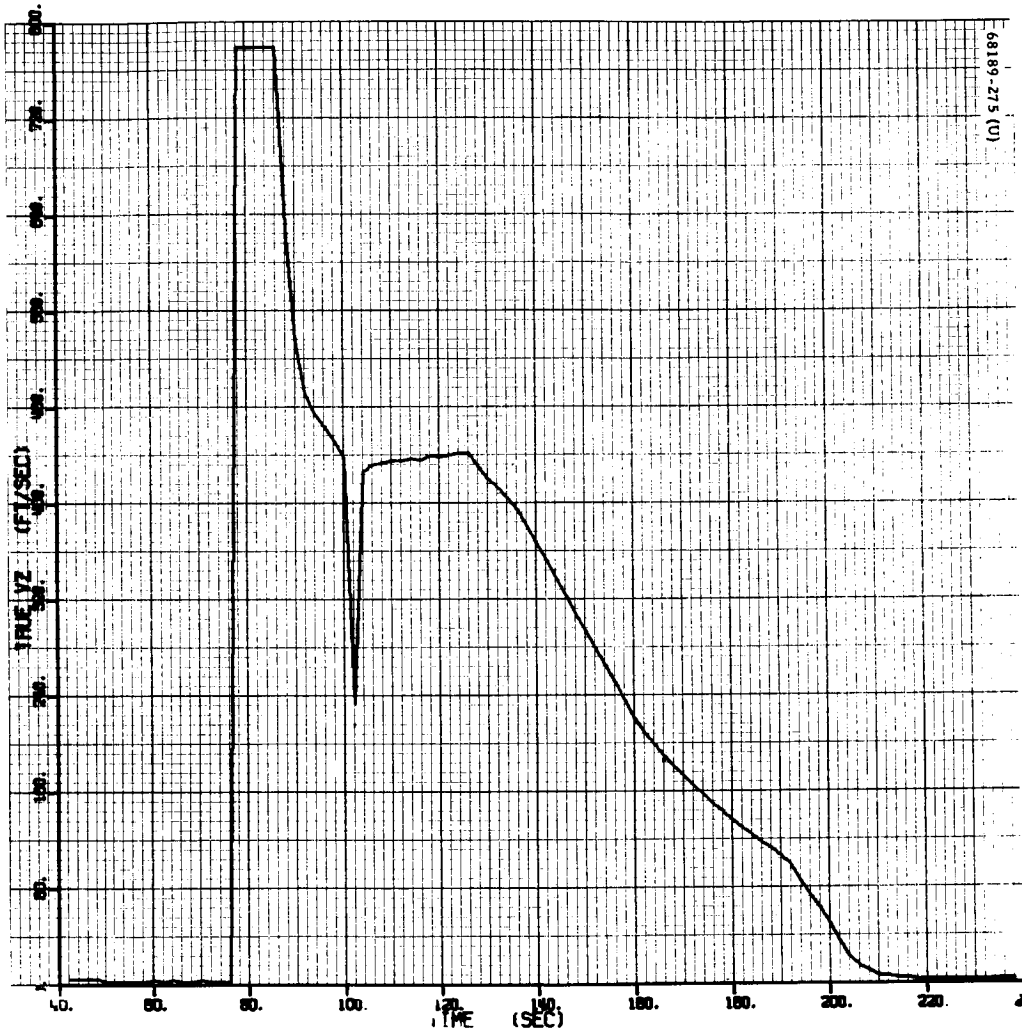
d) Telemetry Z Velocity, ft/sec

Figure 5.15-8 (continued). Spacecraft Telemetry Plots
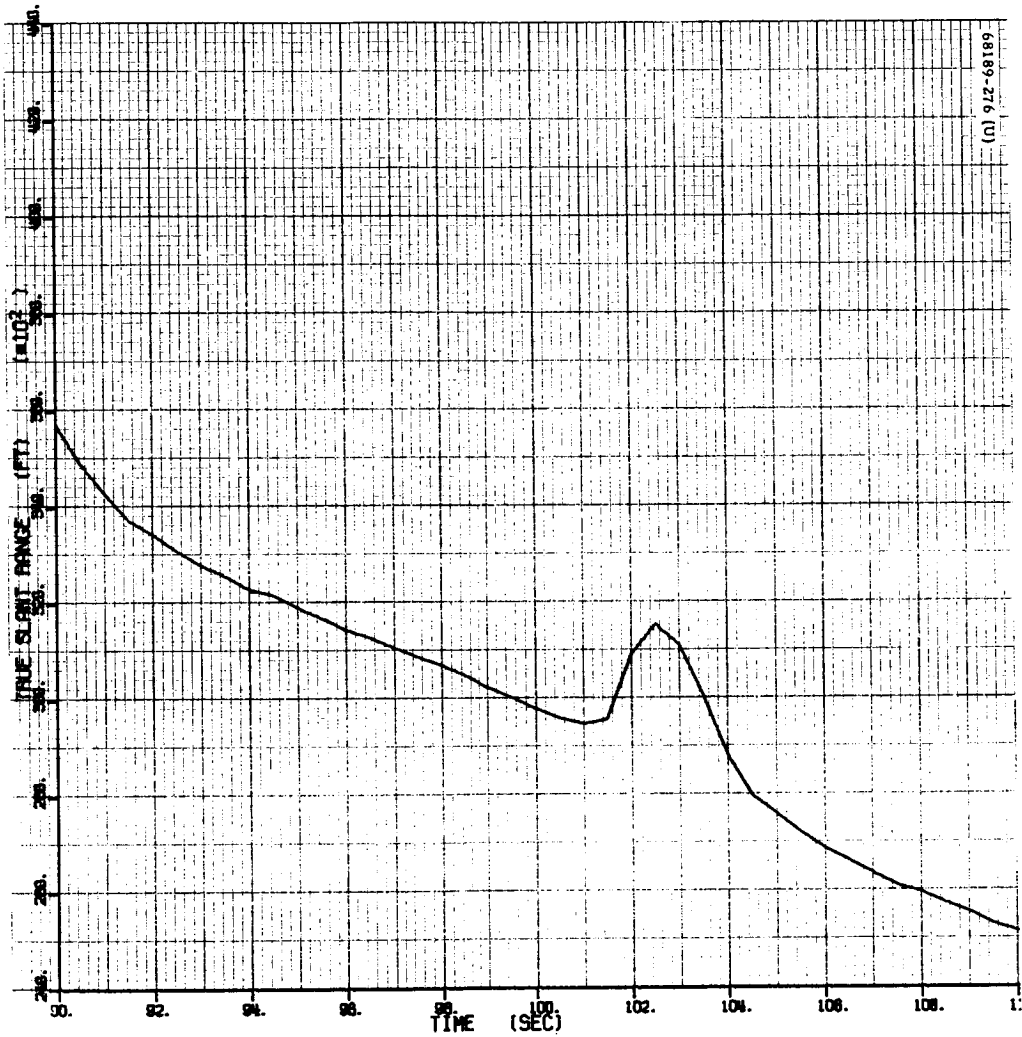
e) Telemetry Slant Range (Steering), feet $\times$ 10^{2}

Figure 5.15-8 (continued). Spacecraft Telemetry Plots
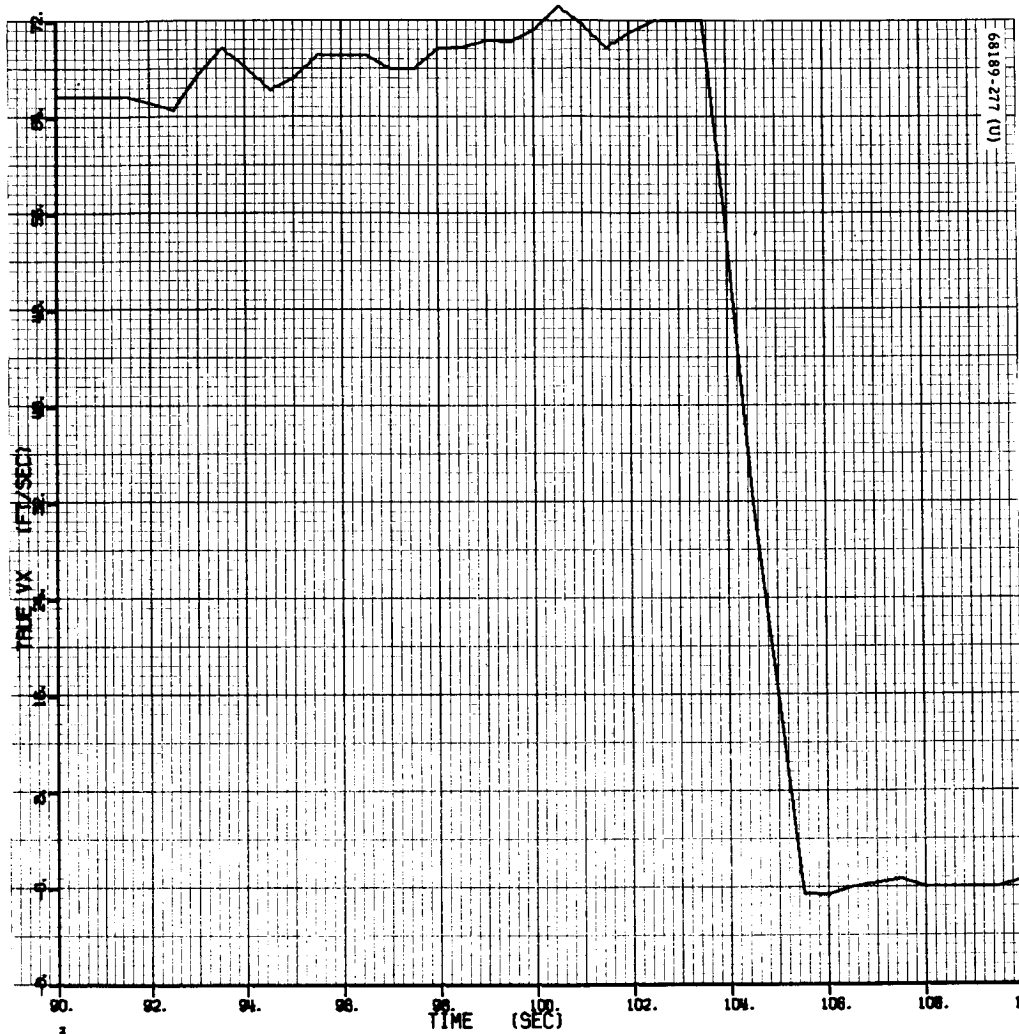
f) Telemetry X Velocity (Steering), ft/sec

Figure 5.15-8 (continued). Spacecraft Telemetry Plots
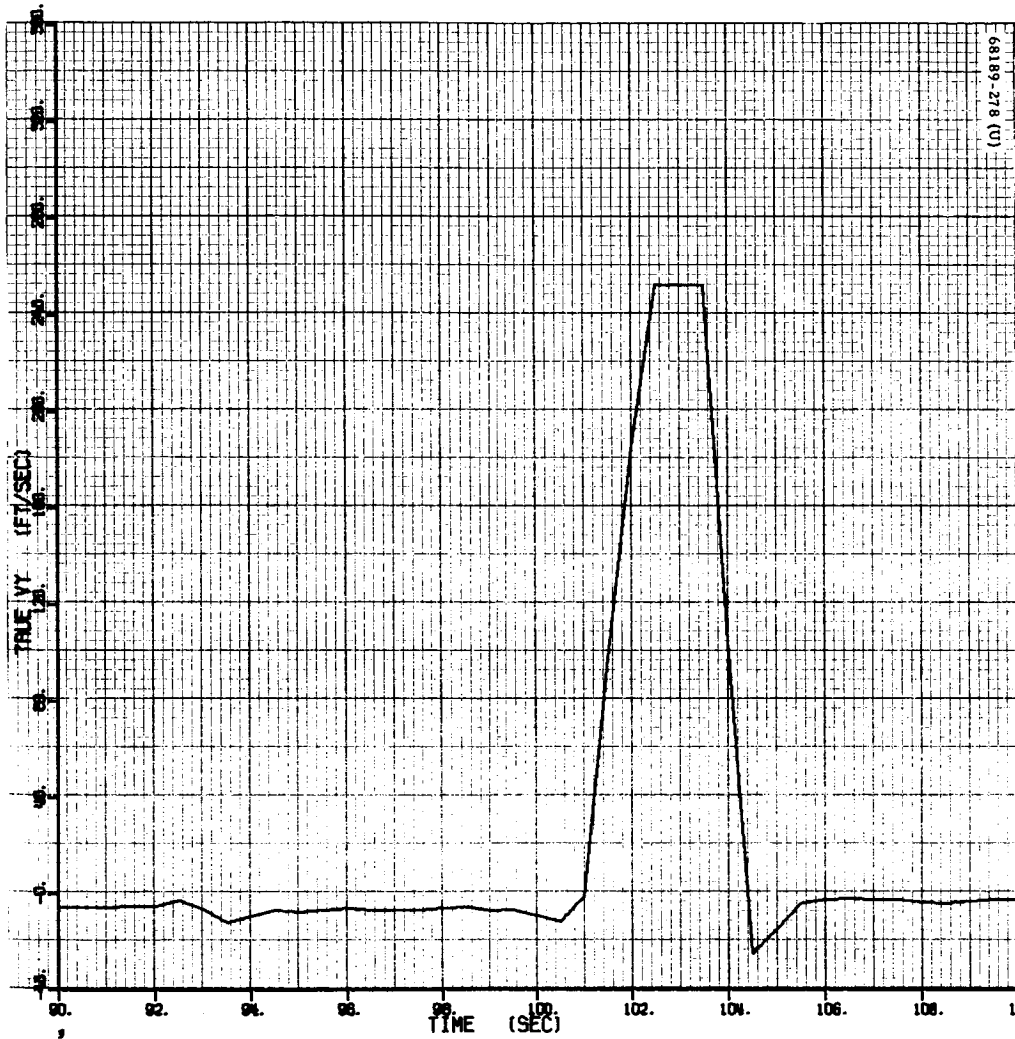
g) Telemetry Y Velocity (Steering), ft/sec

Figure 5. 15-8 (continued). Spacecraft Telemetry Plots
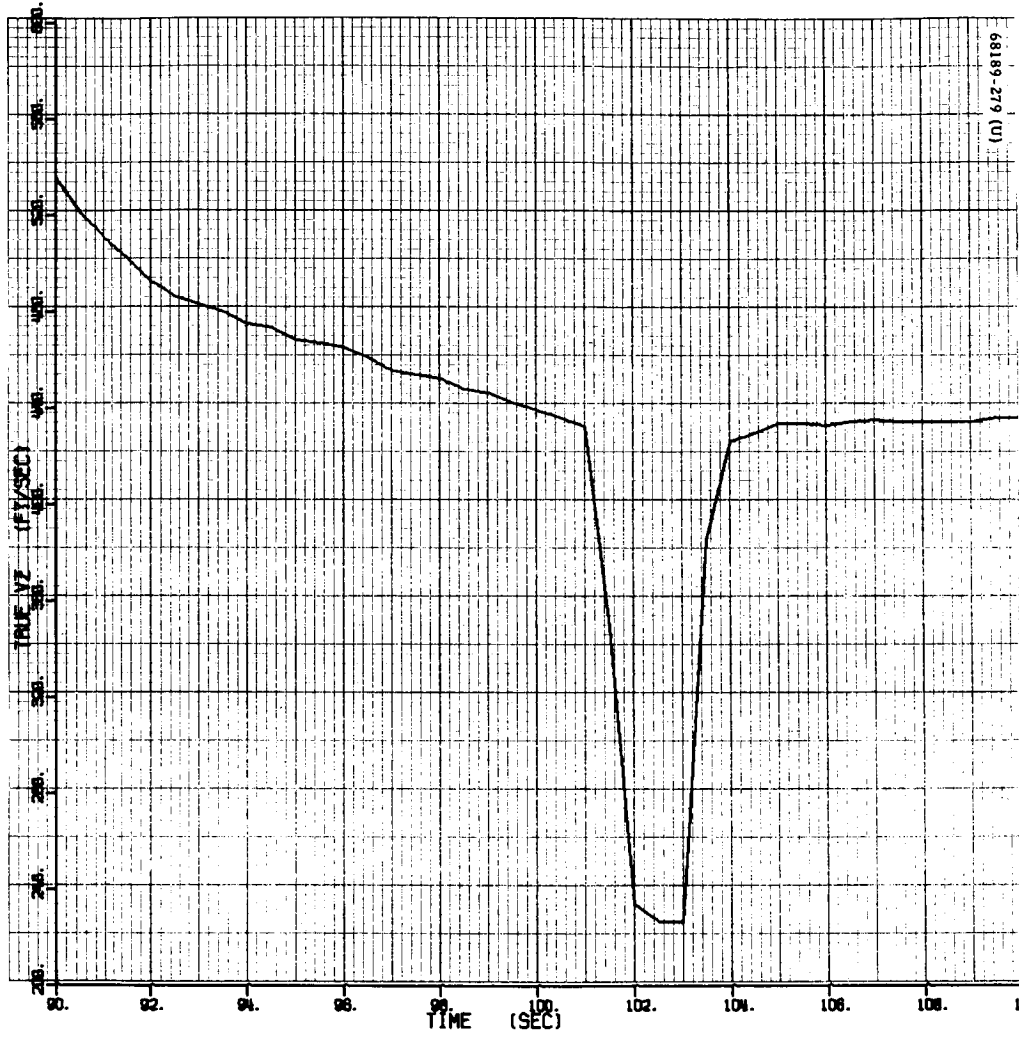
h) Telemetry Z Velocity (Steering), ft/sec

Figure 5.15-8 (continued). Spacecraft Telemetry Plots
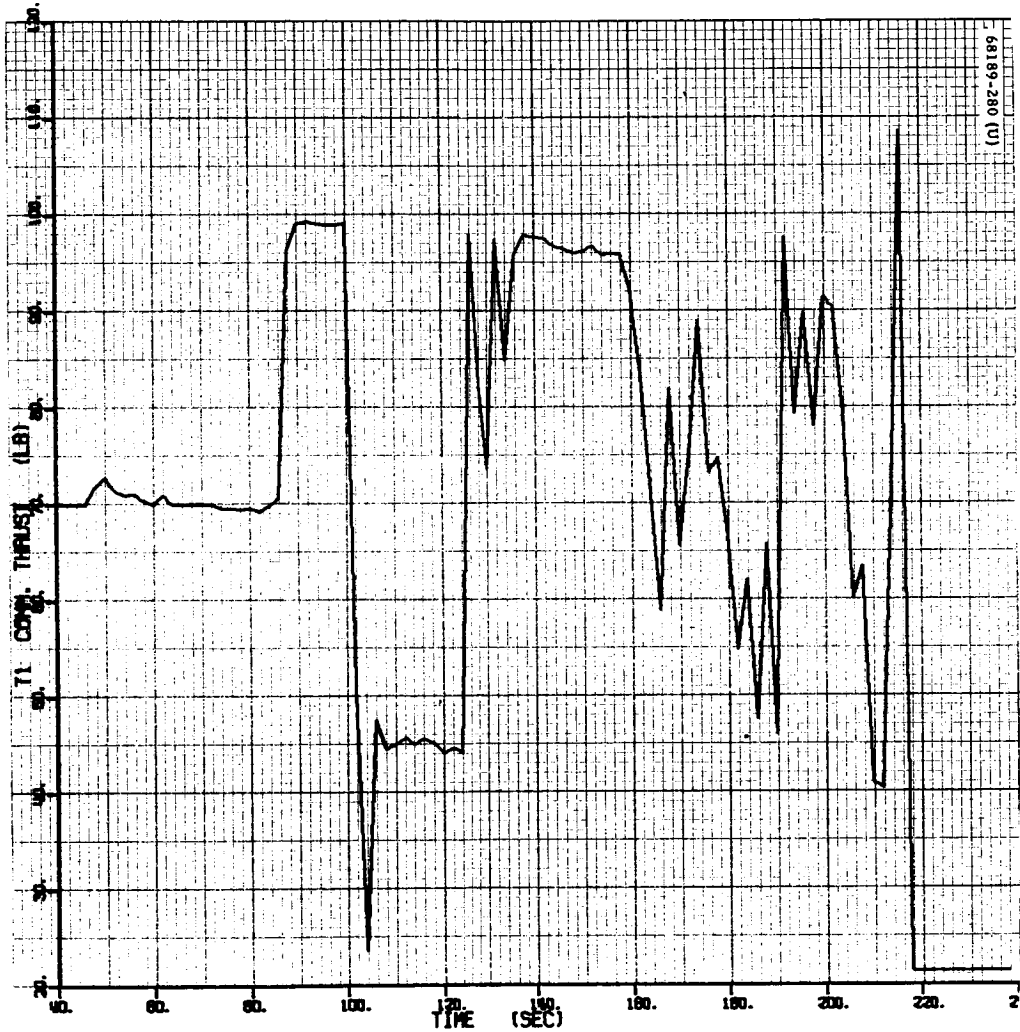
i) Telemetry Vernier Engine 1 Thrust Command, pounds

Figure 5.15-8 (continued).   Spacecraft Telemetry Plots
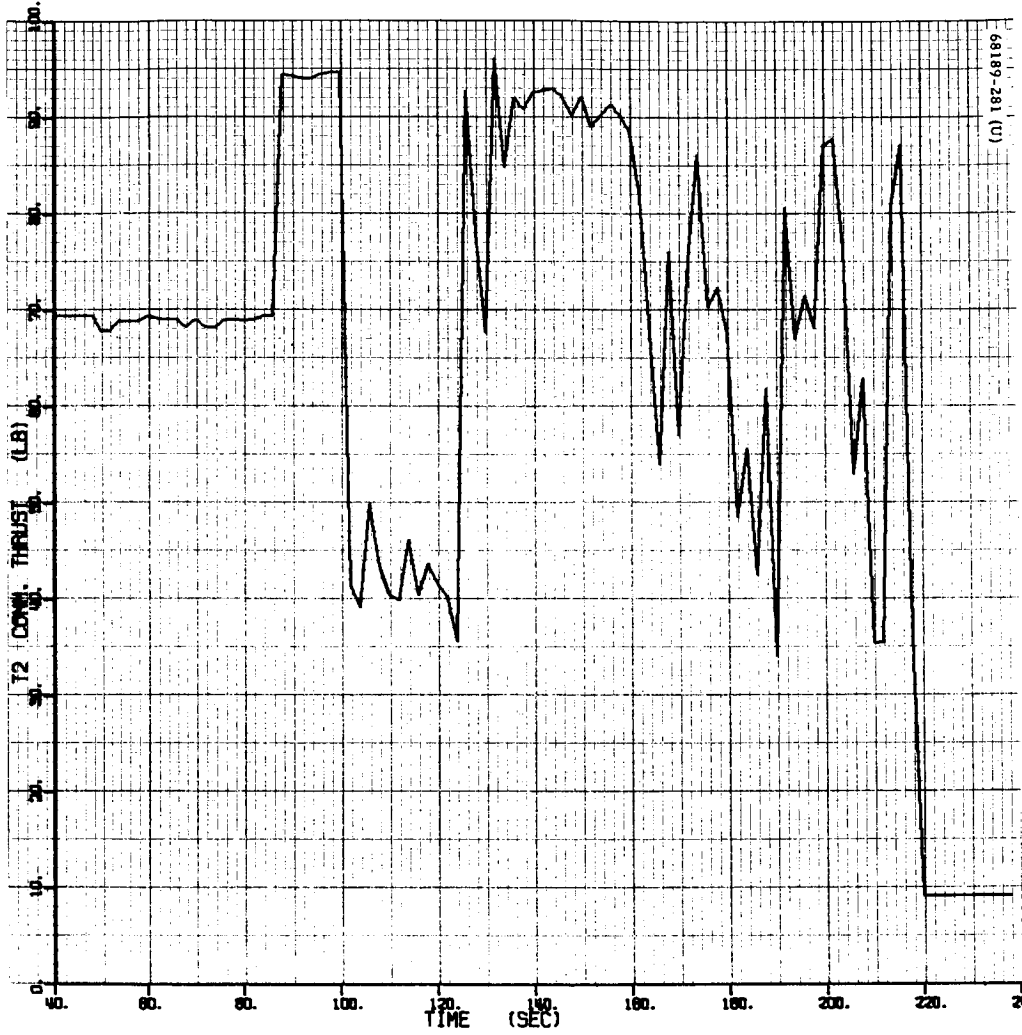
j) Telemetry Vernier Engine 2 Thrust Command, pounds

Figure 5. 15-8 (continued).   Spacecraft Telemetry Plots
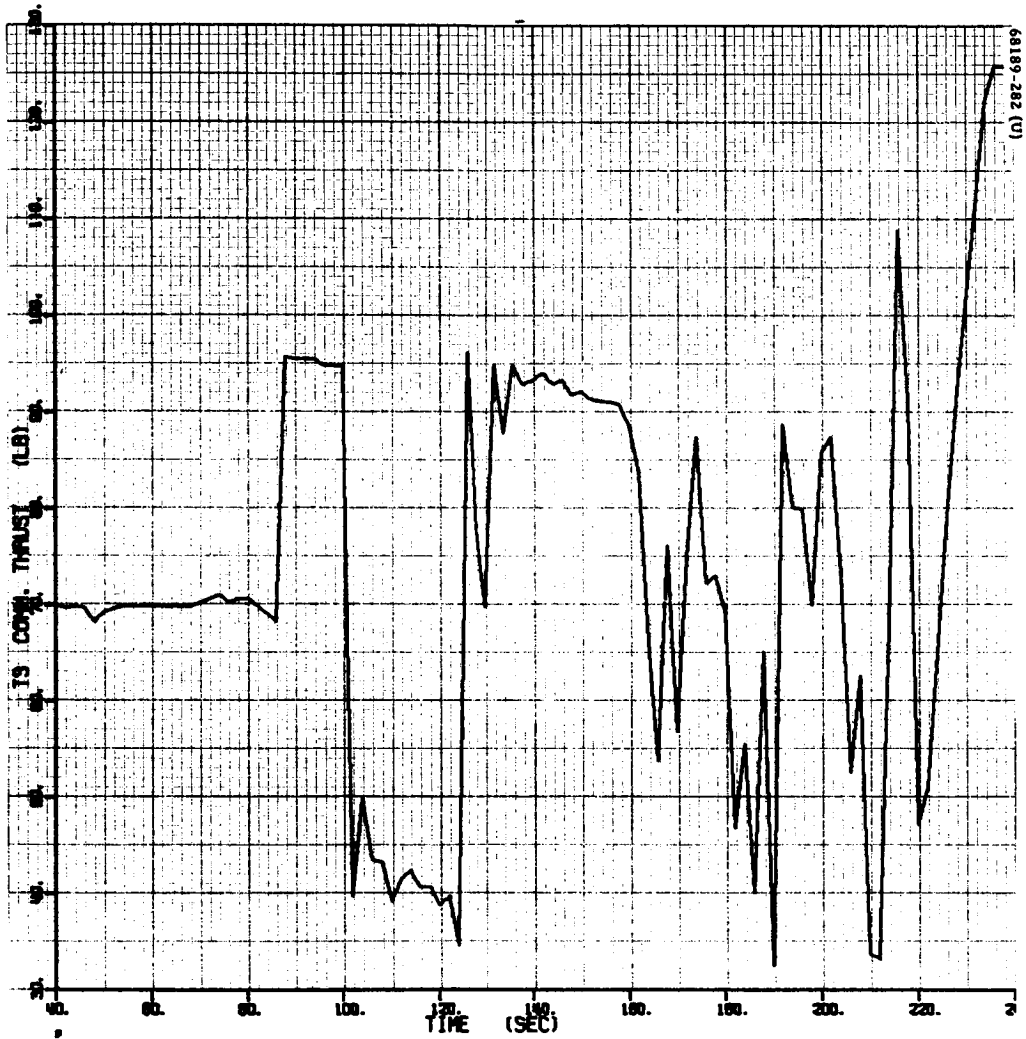
k) Telemetry Vernier Engine 3 Thrust Command, pounds

Figure 5. 15-8 (continued). Spacecraft Telemetry Plots
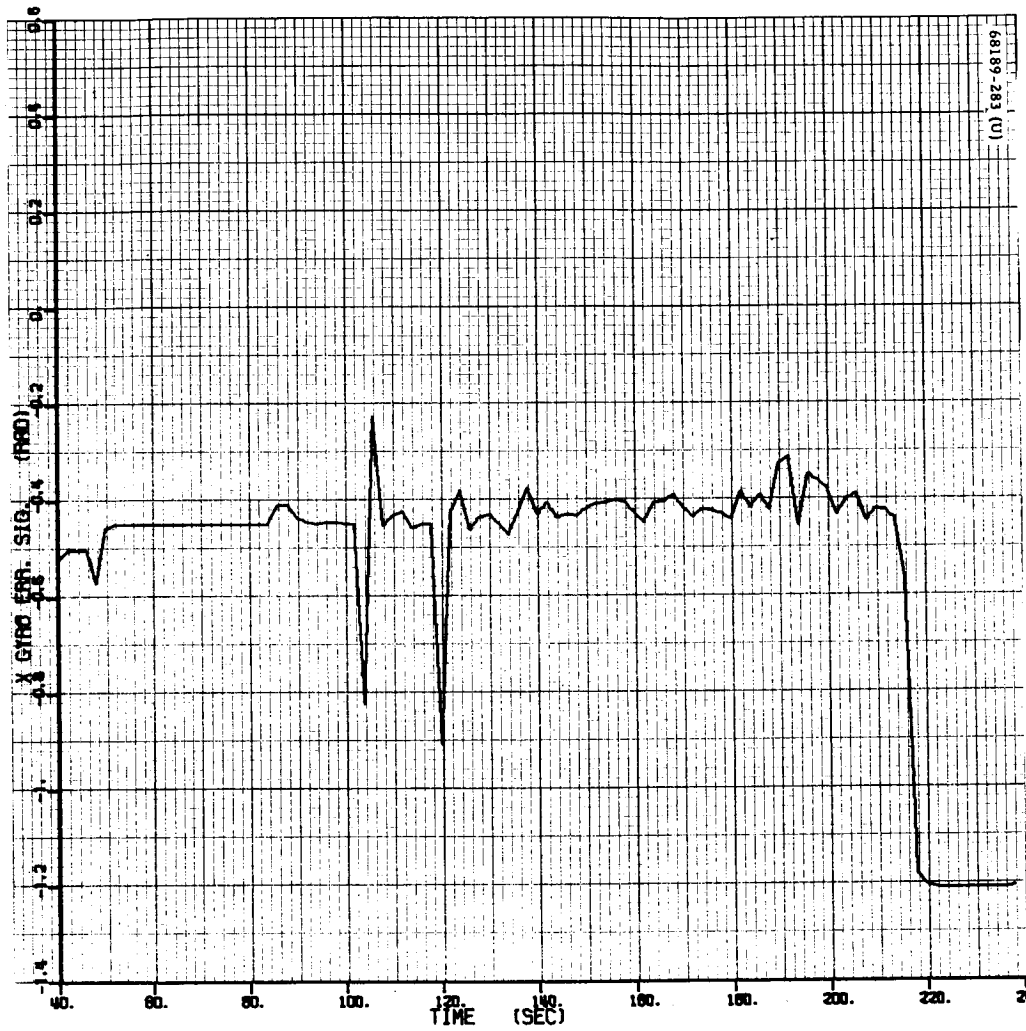
1) Telemetry X Gyro Error Signal, degrees

Figure 5.15-8 (continued). Spacecraft Telemetry Plots
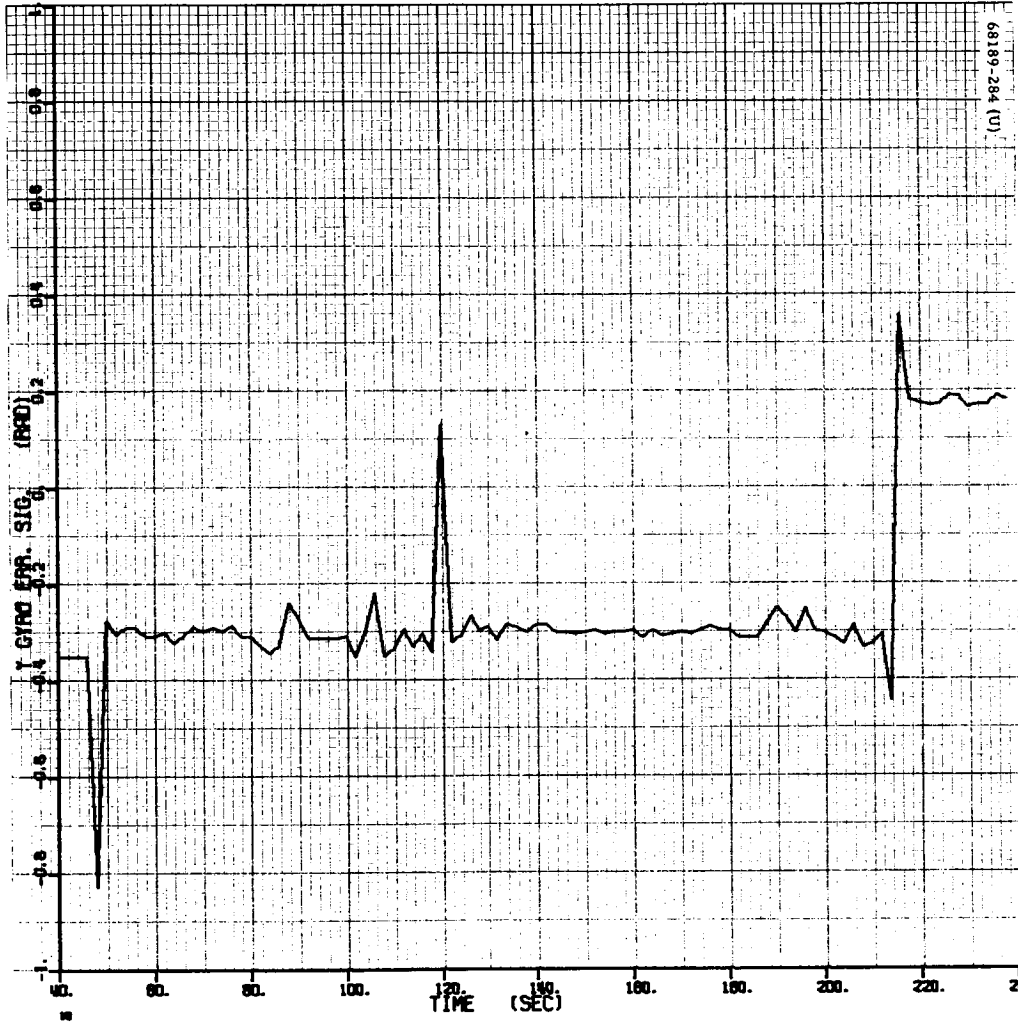
m) Telemetry Y Gyro Error Signal, degrees

Figure 5.15-8 (continued). Spacecraft Telemetry Plots

TABLE 5.15-6.   CALIBRATION COEFFICIENTS FOR TELEMETRY SIGNALS

Signal	Order					
	0	1	2	3	4	5
AZ	-0.35100000E-00	0.3000000	0	0	0	0
ΔA	-0.16676100E-02	0.20105299E-03	0.95448299E-03	-0.58296199E-03	0.14654600E-03	-0.12893300E-04
T_1	0.21426900E+02	0.32304999E+02	-0.16116500E+02	0.75384799E+01	-0.15569700E+01	0.11962000E-00
T_2	0.91796298E+01	0.56772199E+02	-0.37049299E+02	0.16104499E+02	-0.31958199E+01	0.23820700E-00
T_3	0.90646198E+01	0.60538100E+02	-0.41386700E+02	0.18123599E+02	-0.36200500E+01	0.27106800E-00
u	0.64736299E+01	0.44634999E+01	-0.21441499E+01	0.89184400E+00	-0.16891400E-00	0.11869500E-01
PPC	-0.79296099E+01	0.62915500E+01	-0.33361699E+01	0.13379700E+01	-0.25151200E-00	0.17641599E-01
RCP	0.77880399E+01	-0.73378399E+01	0.49163899E+01	-0.22618599E+01	0.49011700E-00	-0.40337099E-01
SR	-0.10292900E+01	0.82168598E+01	0	0	0	0
φ_x	0.73171299E+01	-0.39379799E+01	0.96290100E+00	-0.34514200E-00	0.5706999 E-01	-0.36692099E-02
φ_y	0.70894999E+01	-0.46255200E+01	0.19999500E+01	-0.87420800E+00	0.18076999E-00	-0.14280300E-01
V_x	-0.33828799E+03	0.11890600E+03	0	0	0	0
V_y	-0.33633800E+03	0.11798000E+03	0	0	0	0
V_z	-0.19147500E+02	0.15991700E+03	0	0	0	0

The computer program (POSTPR) that produces the machine plots of all data found in this section must accept the independent variable data in even stepsizes and, since the telemetry commutator does not sequence the transmitted signals in an even stepsized fashion, it became necessary to cause the PREPRO program to read in the commutated telemetry data two frames at a time and then interpolate between the respective signal values to even stepsized intervals. PREPRO can output the interpolated data at any density and was set to output the data for the plots herein at a density of 2 points/sec. The interpolation is done after the signals have been converted to engineering units.

PREPRO produces two separate outputs in the form of magnetic tapes, one wherein the signals have been converted to engineering units but are left in commutator sequence (for listing purposes by the TELTAB program), and one wherein the interpolation is done and the data is reformatted for use in the plotting program.

The TELTAB program lists the data in commutator sequence and keeps a running account of the changes occurring in the digital word signals. TELTAB makes note of the times at which the digital word discretes change state and prints out appropriate comments as to the meaning of each, as they occur.

With respect to the time base on the telemetry plots, it should be mentioned that a slight discrepancy exists between the plotted data and the TELTAB data. The receipt time of the first telemetry frame in mode 2 (as recorded on TELTAB) is listed as 0.509 second, which means that it was received 0.509 second after a previously determined zero-set time of

153:6:14:0.009 GMT. PREPRO, however, contains an automatic zero-setting sequence that outputs the interpolated data with a time base zero-set to the first frame time. Therefore, when referencing the plotted data to GMT, it must be noted that zero time on the plots corresponds to a GMT of 153:6:14:0.518.

Due to the time offset described above, the times on the plots at which some of the more important events occurred during the descent are as listed in Table 5.15-7. These event times were taken from digital word data.

Figures 5.15-8a through 5.15-8d show telemetry plots of SR, V_x, V_y, and V_z throughout the retro-vernier phases plus some pre-ignition and post-touchdown data, while Figures 5.15-8e through 5.15-8h show the same signals with more detail in the neighborhood of steering.

TABLE 5.15-7. EVENT TIMES IN SECONDS AFTER REFERENCE TIME

Event	Time on Plot
Vernier ignition	47.039
Retro ignition	48.439
3.5 g switch	88.028
Retro eject	99.437
Start RADVS	101.837
Segment acquisition	125.497
1000-foot mark	190.033
10-ft/sec mark	208.265
13-foot mark	213.684
Touchdown	214.997

The RADVS system is turned on 0.5 second subsequent to retro ignition, whereupon the SR beam enters a sweep mode and the V_x, V_y, V_z signals are clamped to zero after sufficient warmup time. Figures 5.15-8a through 5.15-8d show the SR beam sweeping after retro ignition, and show V_y clamped solidly to a value of -2.79 ft/sec, which can be interpreted as a telemetry system bias. V_x and V_z do not appear to clamp to any definite value, but close inspection of the data on the TELTAB listing indicates

that V_x was clamped to a value of 0.199 ft/sec for most of the applicable region. V_z, on the other hand, actually switches back and forth between 2.7 and 4.2 ft/sec with approximately equal time spent at each value, so no definite telemetry bias can be extracted from the V_z data in this region. The V_x, V_y, and V_z plots show the DVS beams locking at about 77.5 seconds, and the SR plot shows the expected drop and recovery of that signal as the V_z compensation in the SR network experiences the upswing of the V_z signal.

The next area of interest is that near the time of steering (see Figures 5.15-8e through 5.15-8h). The discrete for the beginning of RADVS controlled descent was received at a time corresponding to 101.837 seconds on the plots, and the discretes RORA and RODVS indicated that a beam 3 dropout occurred, spanning an interval from 102.027 to 104.027 seconds. Close inspection of the SR, V_x, V_y, and V_z data, however, reveals that the dropout region spanned a different interval than indicated by the discretes, which is reasonable since the digital word containing the RORA and RODVS discretes is telemetered only once per second in mode 2. A beam 3 dropout affects V_y and V_z which, in turn, affects SR. The V_y signal indicates that the dropout started somewhere between 100.5 and 101.0 seconds, while the V_z signal indicates that it started no earlier than 101.0 seconds. This difference existing between V_y and V_z is plausible since each signal is telemetered only twice per second in mode 2. V_x is not affected by the beam 3 dropout and, as such, is a good indicator of the exact time that steering commenced, which is observed to be very nearly 103.5 seconds. At 103.5 seconds, however, the V_y and V_z signals are observed to be still in the return portions of their respective dropout excursions, and, in the case of V_y, it could be reasoned that this is due to the telemetry delay time were it not for the fact that upon return of V_y from its excursion it overshoots the value to which it finally steers. Such an overshoot is indicative of the control system steering to a positive V_y for a short time before steering to a negative value. This indicated momentary false steering about the X axis is corroborated by the X gyro error signal (Figure 5.15-8ℓ) which shows a rather large double excursion at the time of steering. The vernier engine thrust command plots (Figures 5.15-8i through 5.15-8k) also show a definite downward spike in the engine 1 signal at the time of steering, which is also indicative of an attempt to momentarily steer out a positive V_y.

The rest of the telemetry plots are fairly self-explanatory except for the SR plots and the gyro error signals, which all contain a spike at about 120 seconds. These spikes were caused by the particular processing technique used to bridge the gap between telemetry modes 2 and 3 data and should not be considered as part of the actual data.

One final note with respect to V_z: after touchdown V_x and V_y returned to their previously determined bias values, and V_z settled out to a value of 2.7 ft/sec, which can be assumed to be the correct bias value for that signal.

Nominal Vernier Trajectory

A good comparison between predicted and actual terminal phase trajectories with an eye toward telemetry error determination cannot be effected simply by a straight differencing of the sets of data presented in the

preceding two sections. The SR, V_x, V_y, and V_z data is of prime importance in the trajectory determination scheme, and the telemetry plots show that this data does not even become reliable until shortly before burnout. Furthermore, due to retro dispersions, the telemetered burnout conditions were notably different than the nominal. Table 5.15-8 lists the nominal and telemetered conditions at the inception of steering. Therefore, it seems reasonable to preclude comparison of nominal and telemetered trajectory parameters until the beginning of steering, which is a good reference point.

Figures 5.15-9a through 5.15-9i show plots of SR, V_x, V_y, V_z, T_1, T_2, T_3, φ_x, and φ_y as output by the 6DOF simulation program, initialized at the beginning of steering with telemetry data.

Vernier Comparison

A digital computer differencing program (BETCOM) was used to produce the plots found in Figures 5.15-10a through 5.15-10i. The BETCOM program reads the telemetry data from one magnetic tape, reads the nominal data from another tape, aligns the data sets in time, and outputs the difference between the two (telemetered quantities minus nominal) on a third tape suitable for plotting by the POSTPR program.

Concerning the difference plots herein, the BETCOM program was set to align the telemetered and nominal data sets at touchdown rather than at the beginning of steering. The reason for such an alignment is that the telemetery error sources treated in the SEMBET program (see "SEMBET Error Determination") are much more easily modeled if the difference between the telemetered and nominal quantities tends toward a bias-only value as the telemetered quantity approaches zero. In fact, error simulations have shown that such an alignment will cause the difference plots to have the appearance characteristic of the error sources causing the differences. This is to say that a positive bias in the telemetry system will cause a positive offset in the difference plots, and a positive scale factor error will cause a positive proportional reading in the plots. It can be shown that aligning the times at any other point besides touchdown will not produce this desirable effect.

TABLE 5.15-8. NOMINAL VERSUS TELEMETERED BURNOUT
CONDITIONS

Parameter	Nominal	Telemetered*
SR	28, 415 feet	29, 503 feet
V_x	28.62 ft/sec	72.19 ft/sec
V_y	-6.77 ft/sec	-6.82 ft/sec
V_z	393.22 ft/sec	432.18 ft/sec

*No biases removed.
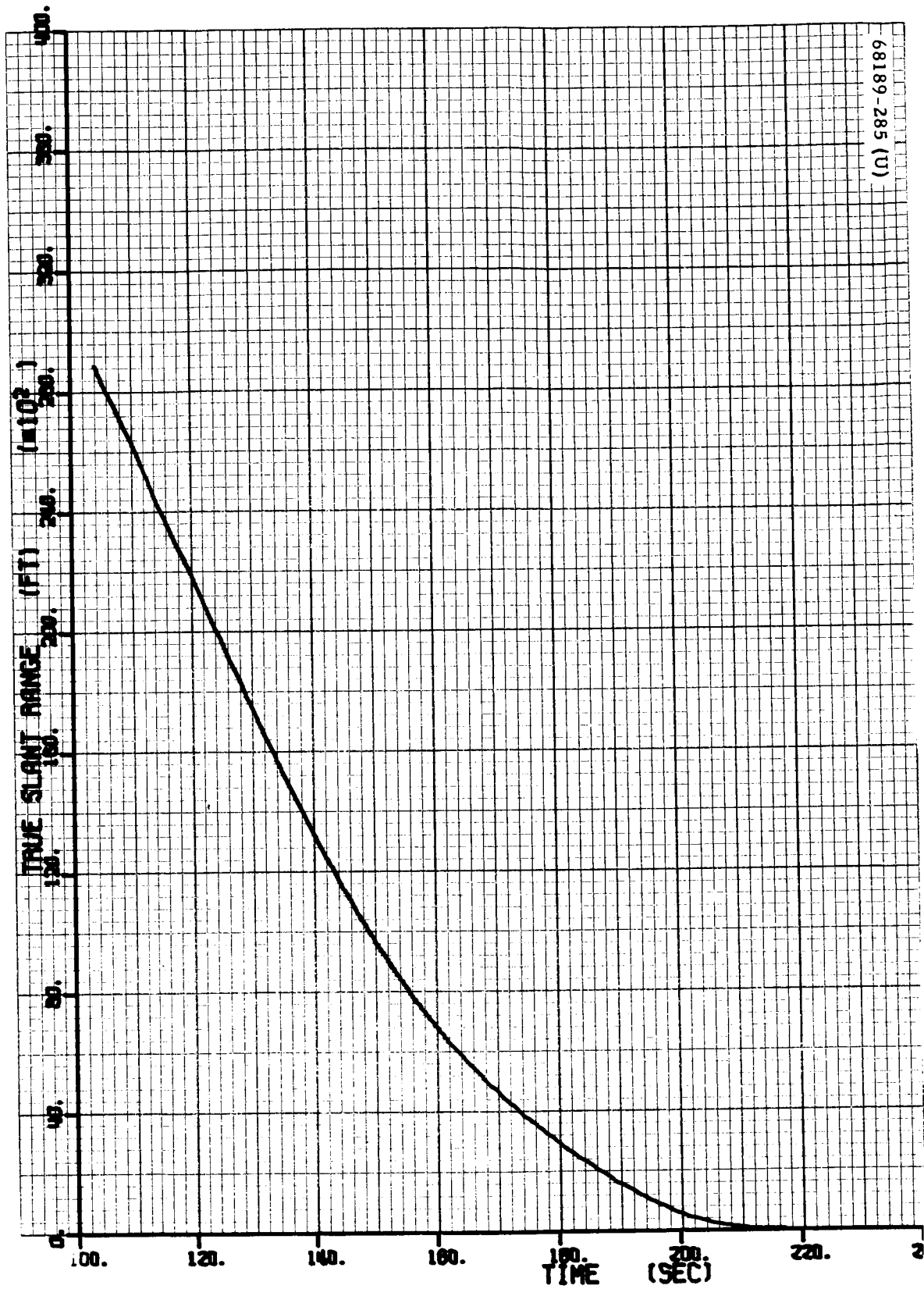
a) Nominal Vernier Phase Slant Range, feet × 10^2

Figure 5.15-9. Nominal Vernier Phase Plots, Initialized With Telemetry
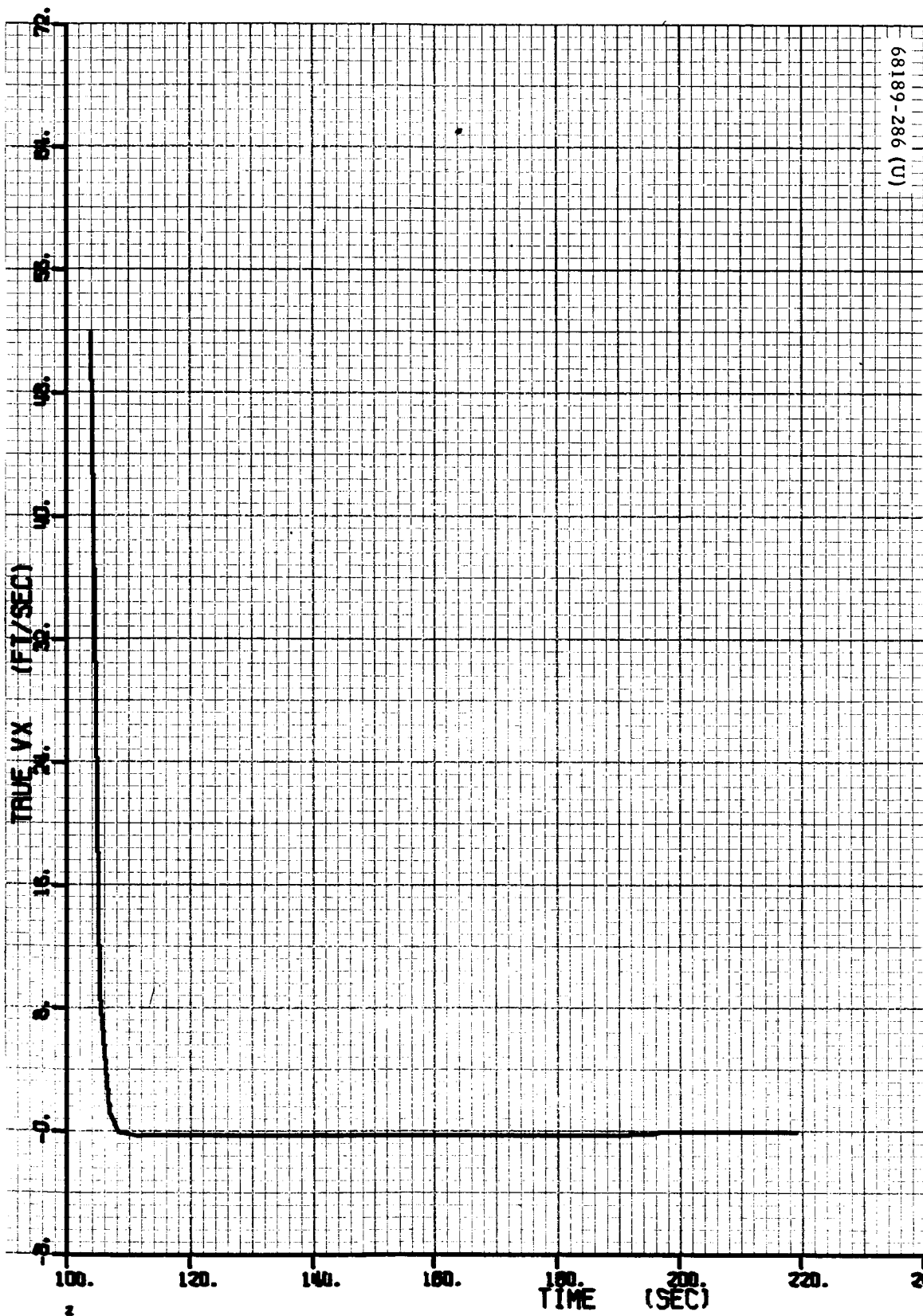
b) Nominal Vernier X Velocity, ft/sec

Figure 5.15-9 (continued).   Nominal Vernier Phase Plots,
Initialized With Telemetry
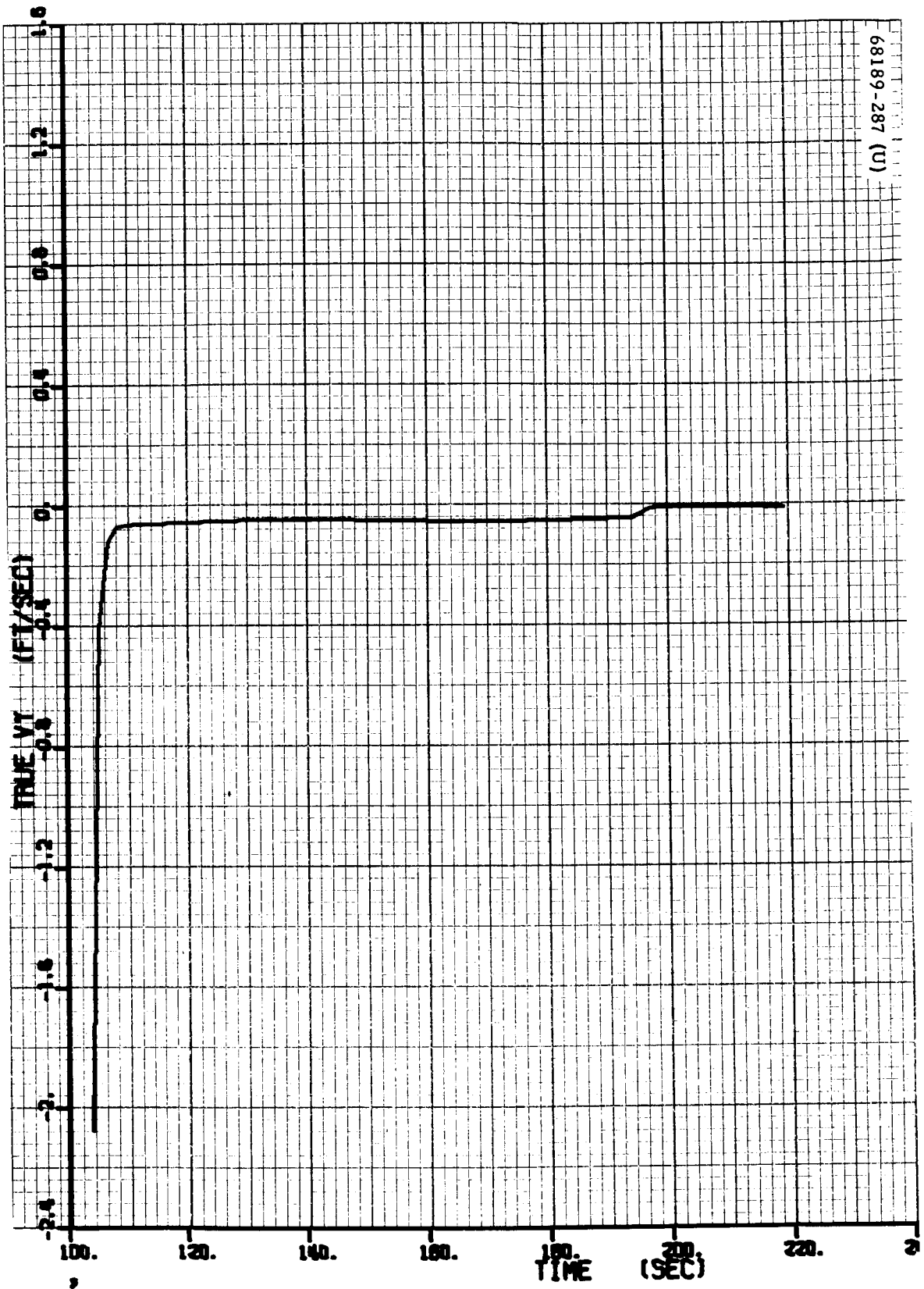
c) Nominal Vernier Y Velocity, ft/sec

Figure 5.15-9 (continued). Nominal Vernier Phase Plots,
Initialized With Telemetry
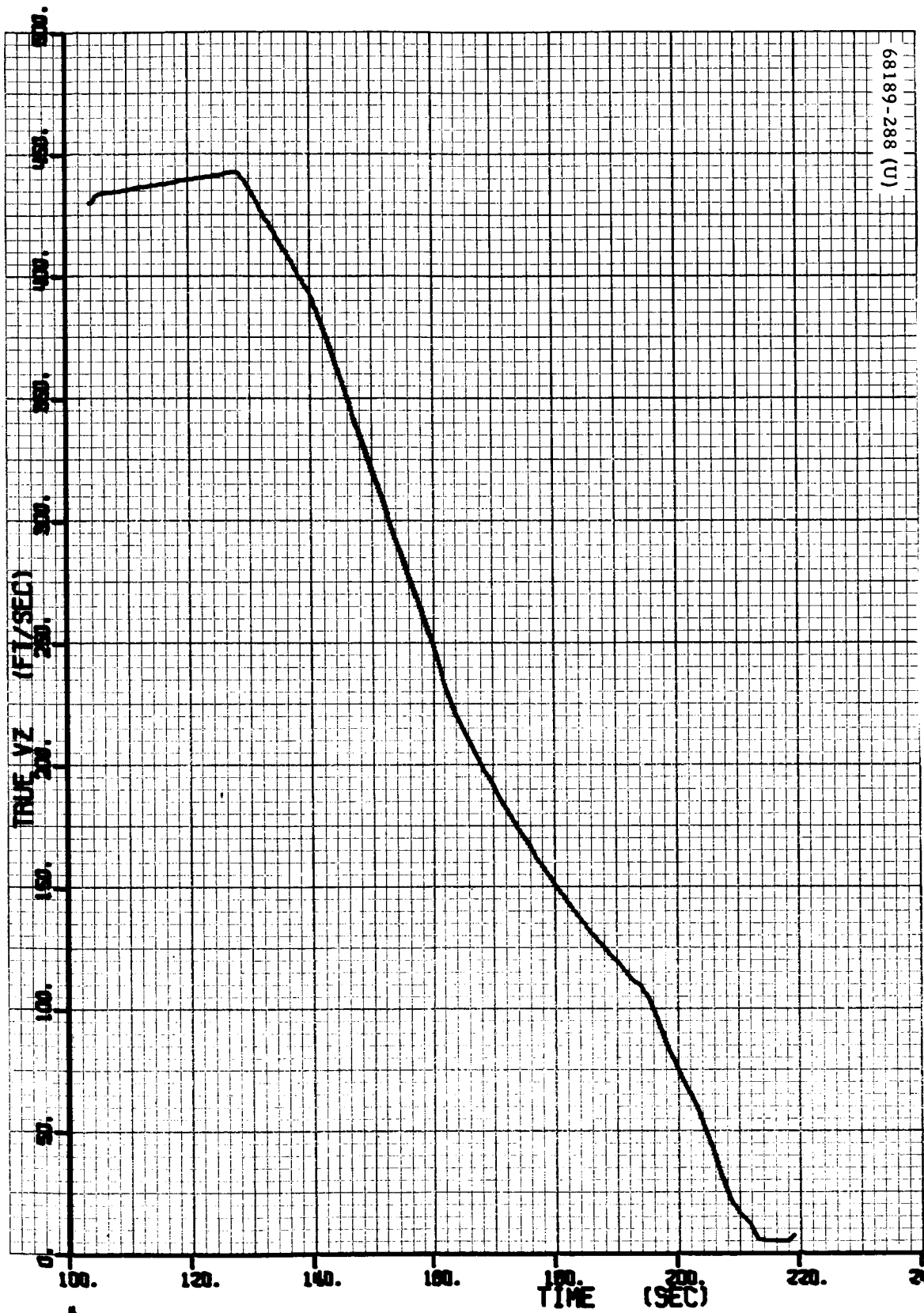
d) Nominal Vernier Z Velocity, ft/sec

Figure 5.15-9 (continued). Nominal Vernier Phase Plots,
Initialized With Telemetry
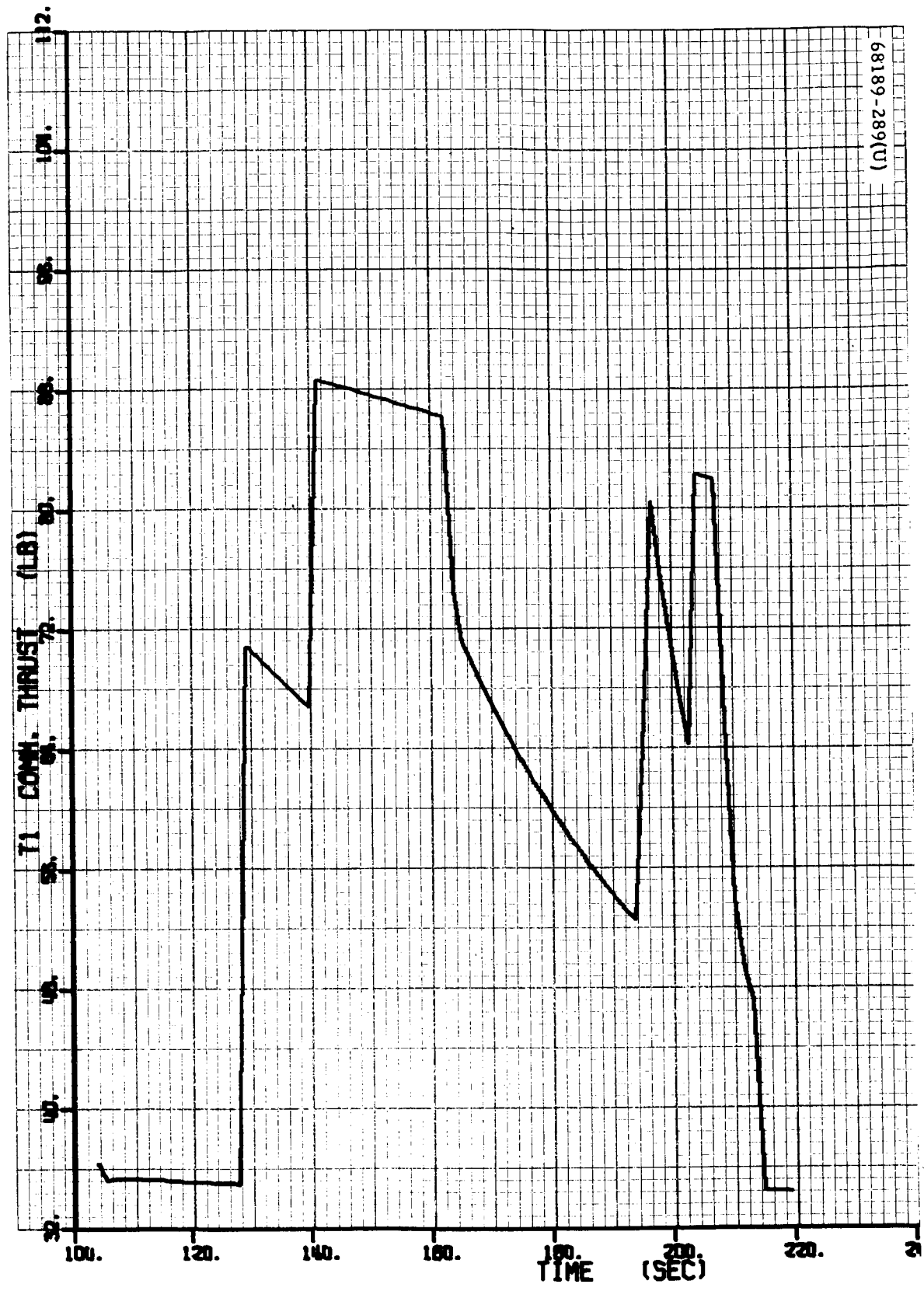
e) Nominal Vernier Engine 1 Thrust Command, pounds

Figure 5.15-9 (continued). Nominal Vernier Phase Plots,
Initialized With Telemetry
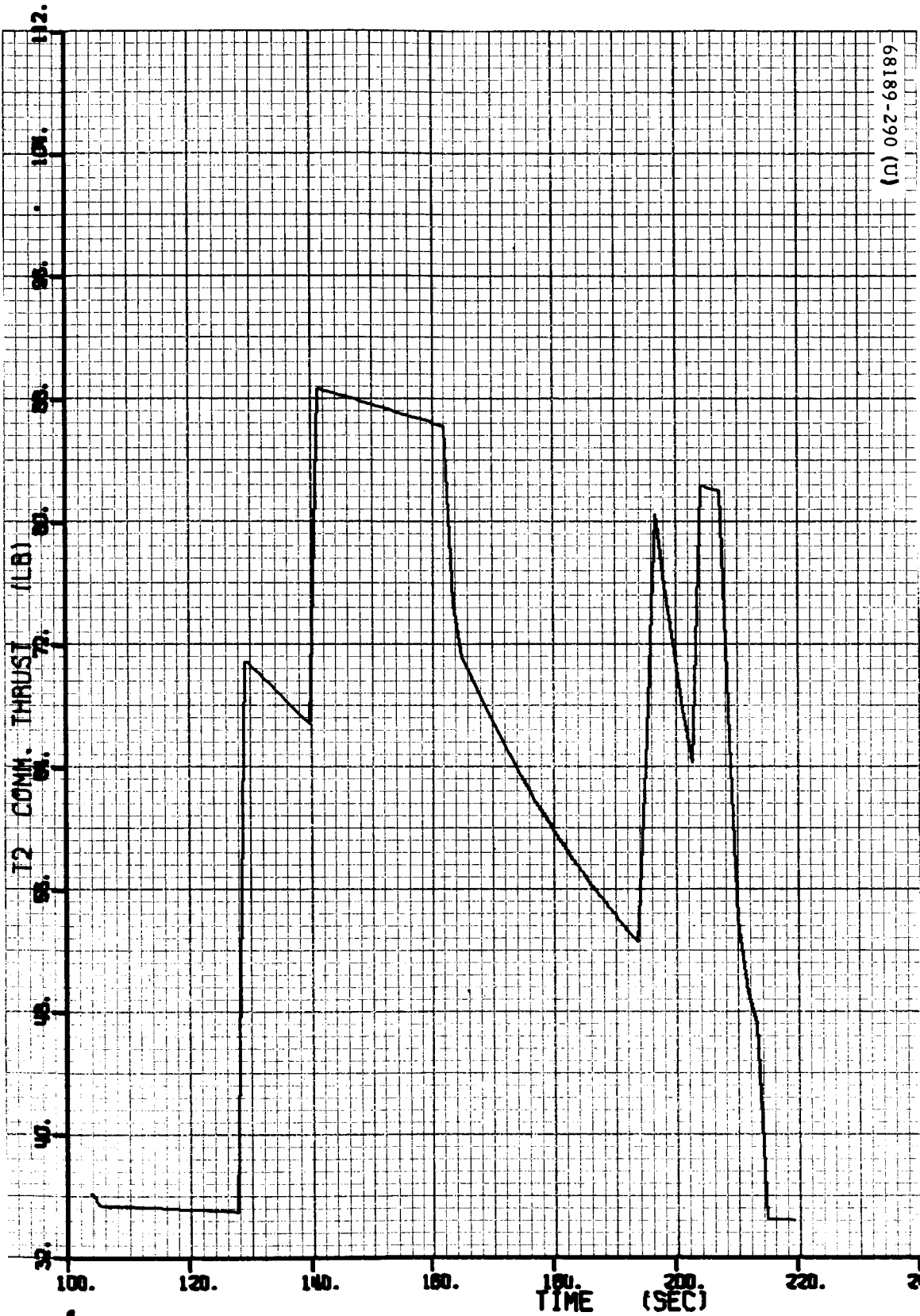
f) Nominal Vernier Engine 2 Thrust Command, pounds

Figure 5.15-9 (continued). Nominal Vernier Phase Plots,
Initialized With Telemetry
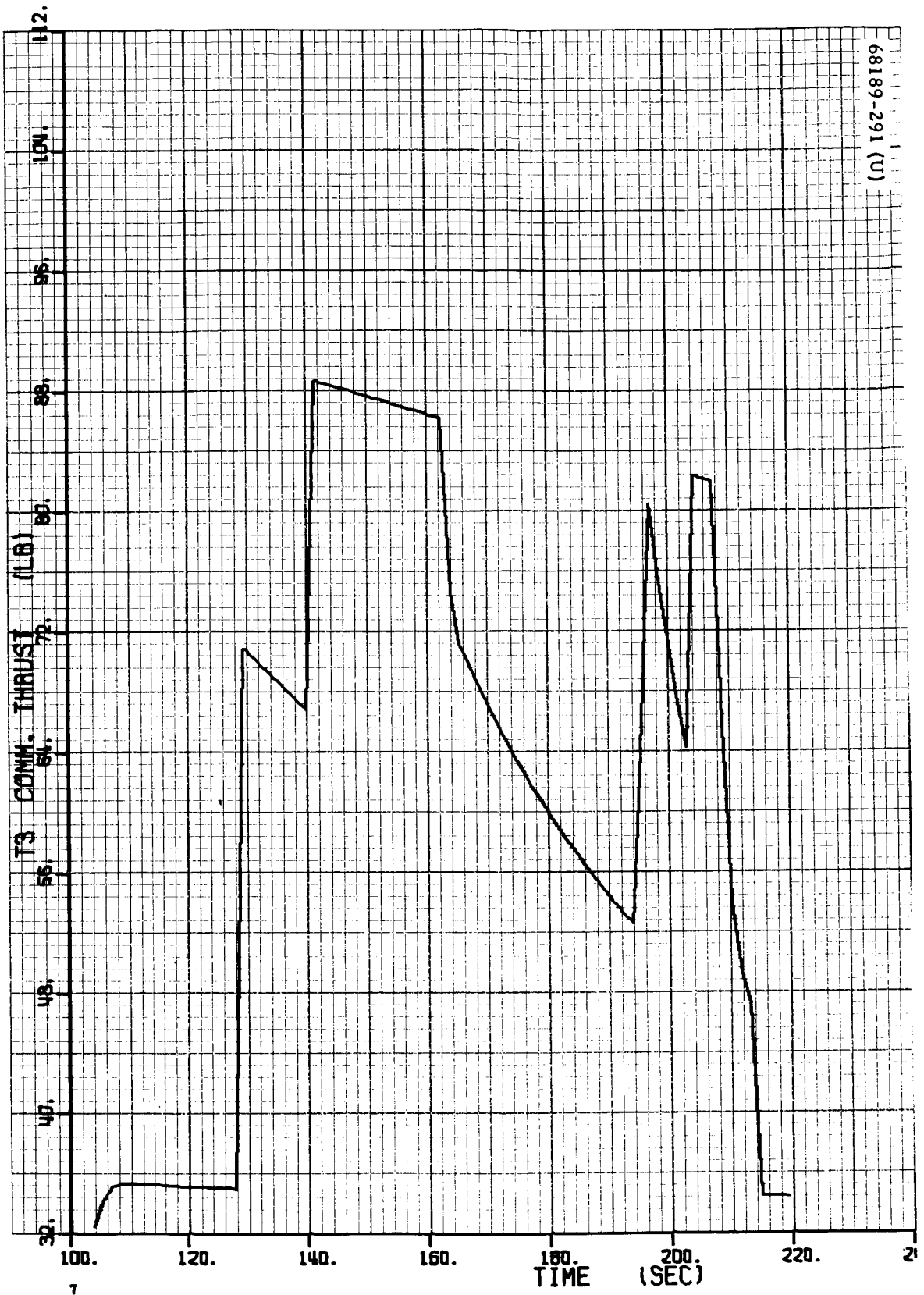
g) Nominal Vernier Engine 3 Thrust Command, pounds

Figure 5.15-9 (continued).   Nominal Vernier Phase Plots,
Initialized With Telemetry
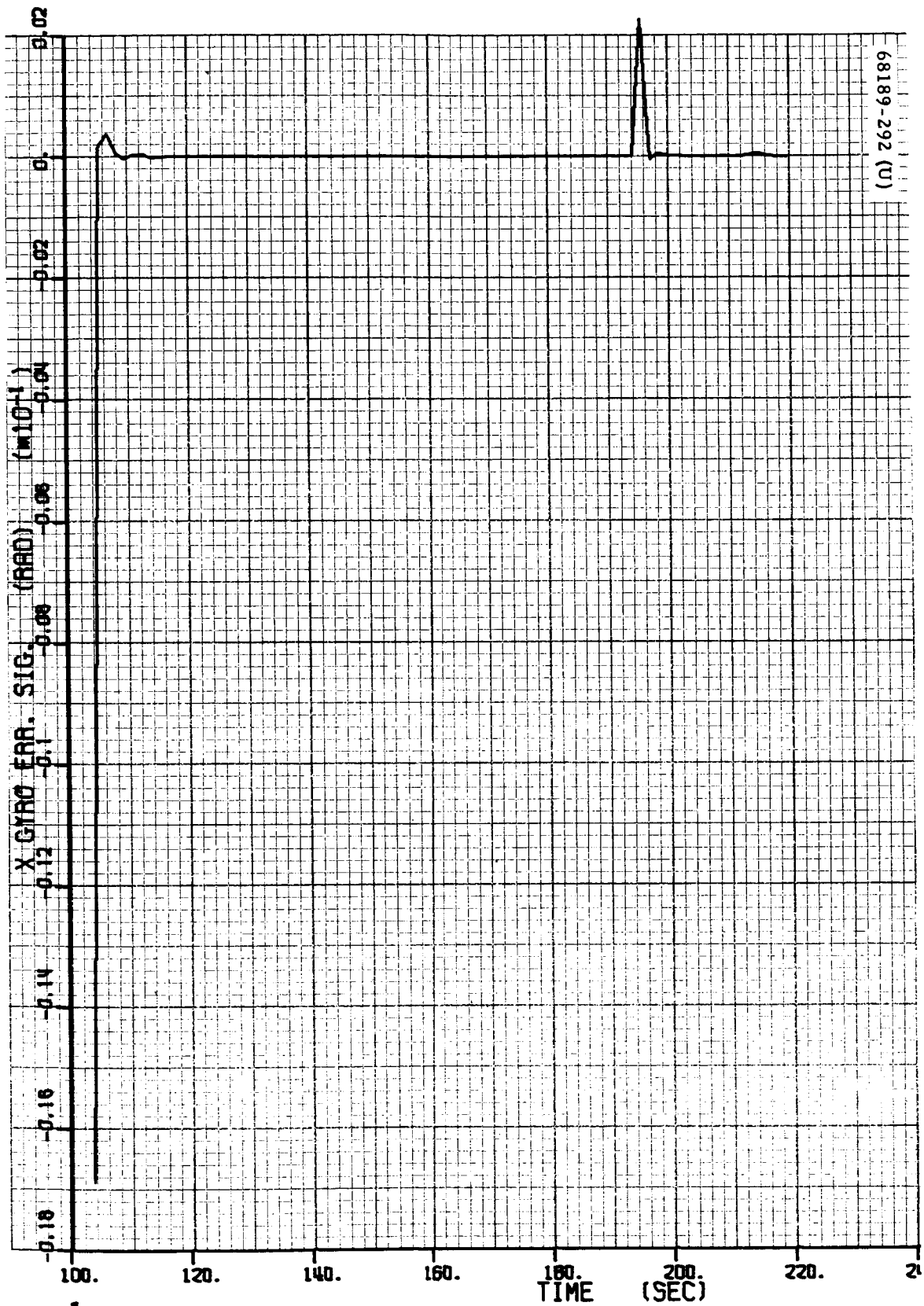
h) Nominal Vernier X Gyro Error Signal, degrees $\times 10^{-1}$

Figure 5.15-9 (continued). Nominal Vernier Phase Plots,
Initialized With Telemetry
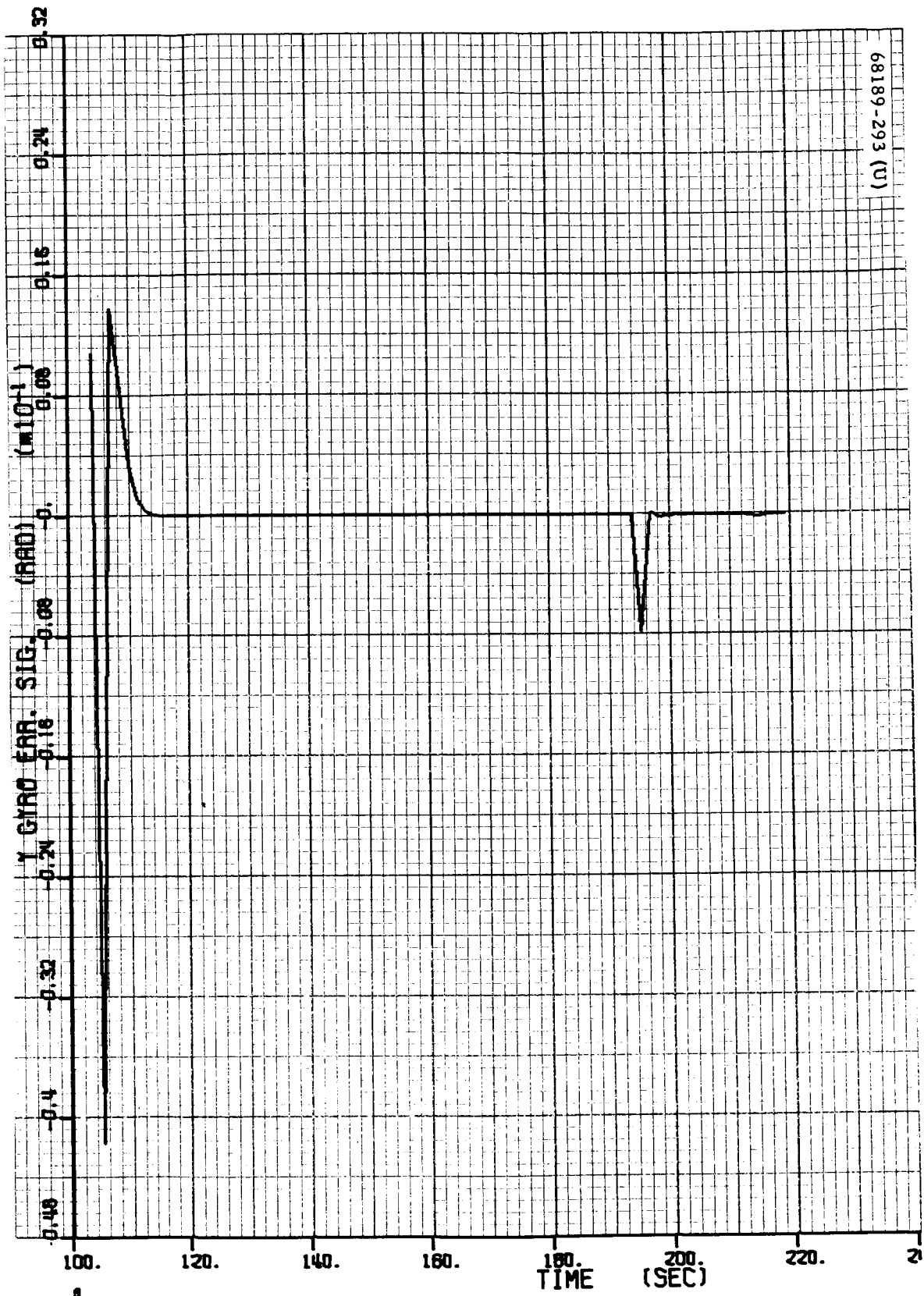
i) Nominal Vernier Y Gyro Error Signal, degrees, $\times 10^{-1}$

Figure 5. 15-9 (continued). Nominal Vernier Phase Plots,
Initialized With Telemetry

5. 15-64
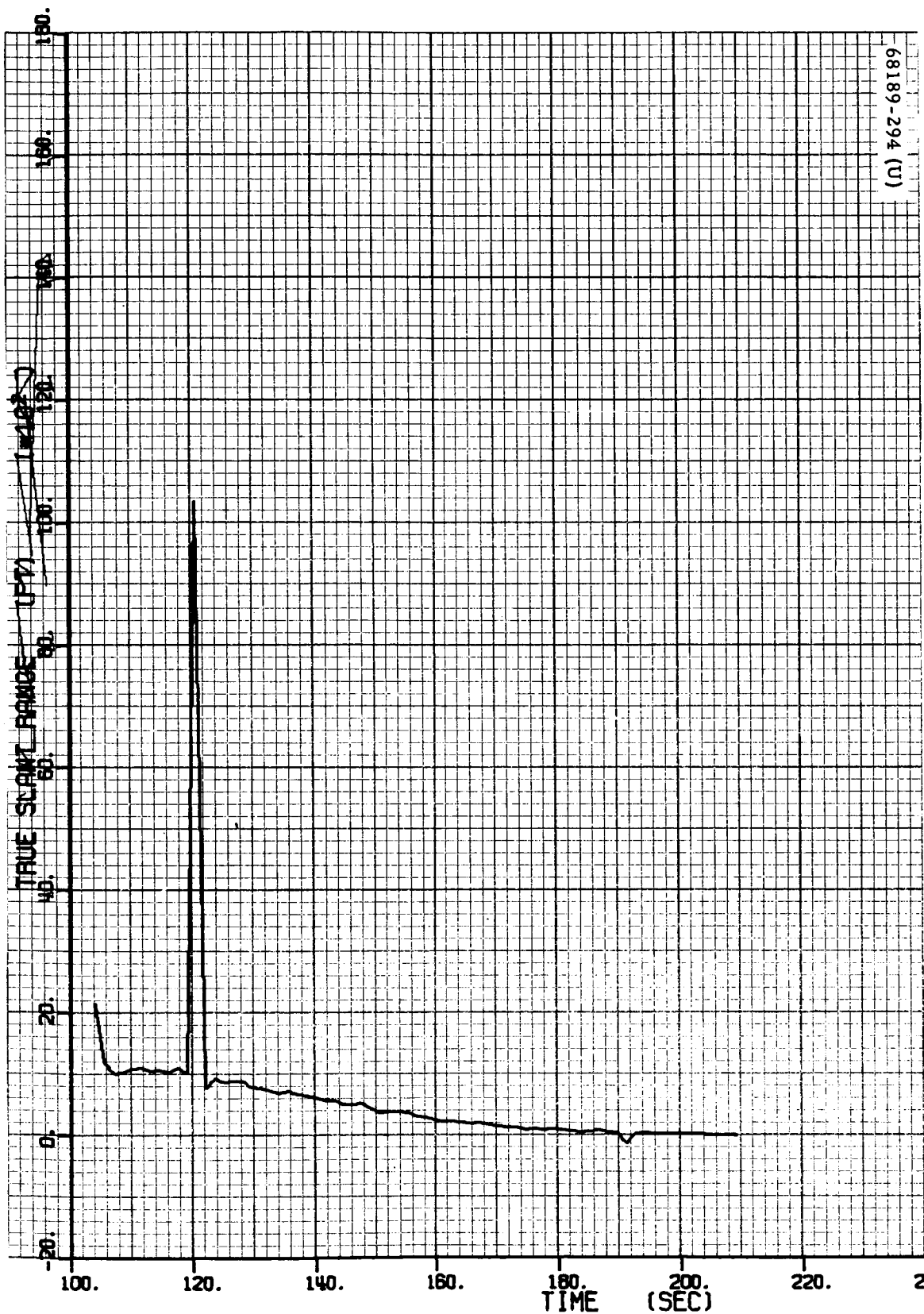
a) $\triangle$ Slant Range (Initial), feet $\times$ 10^2

Figure 5. 15-10.   Differences of Telemetry and Nominal
Data From BETCOM
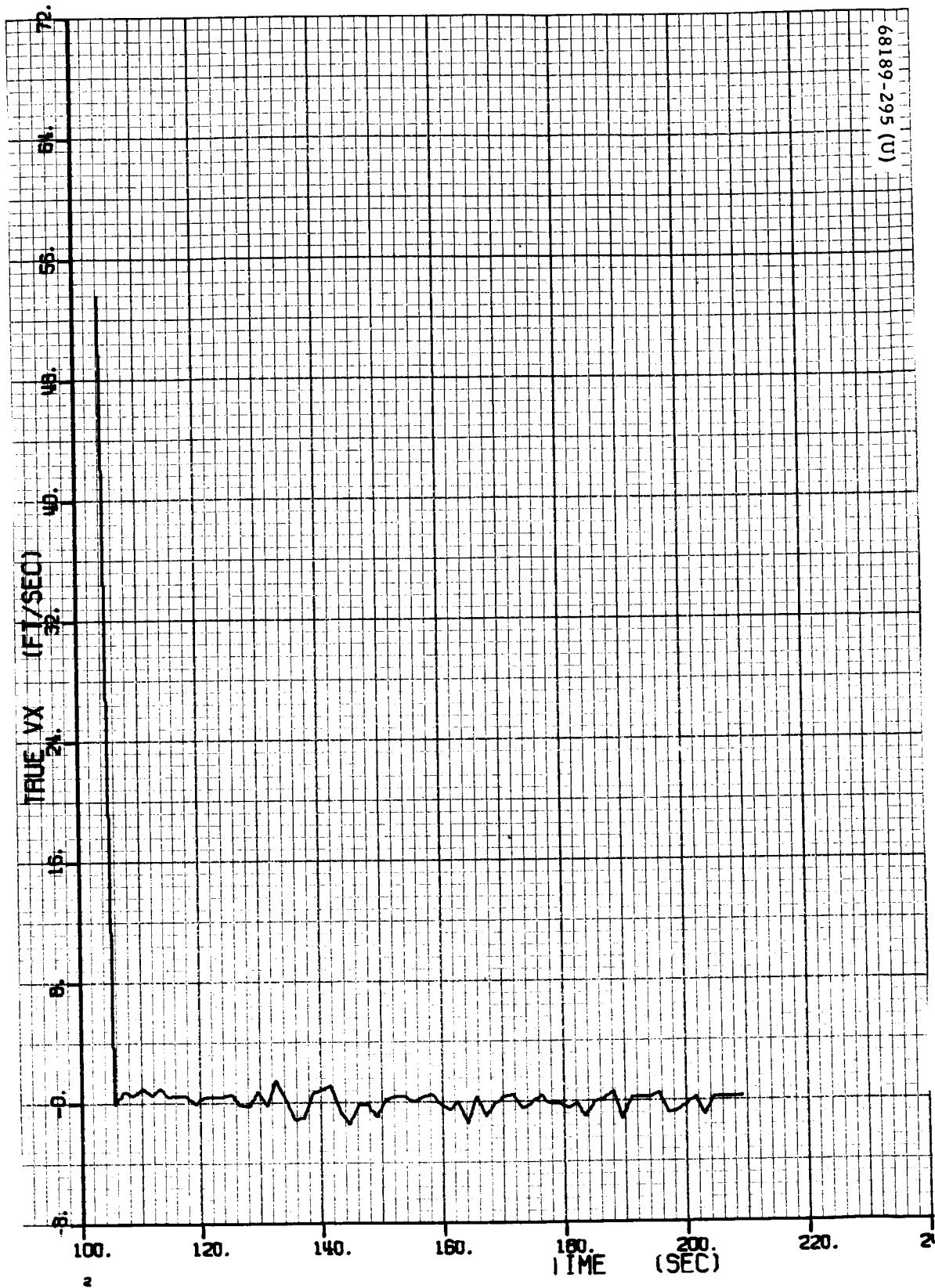
b) Δ X Velocity (Initial), ft/sec

Figure 5.15-10 (continued). Differences of Telemetry and
Nominal Data From BETCOM

5.15-66
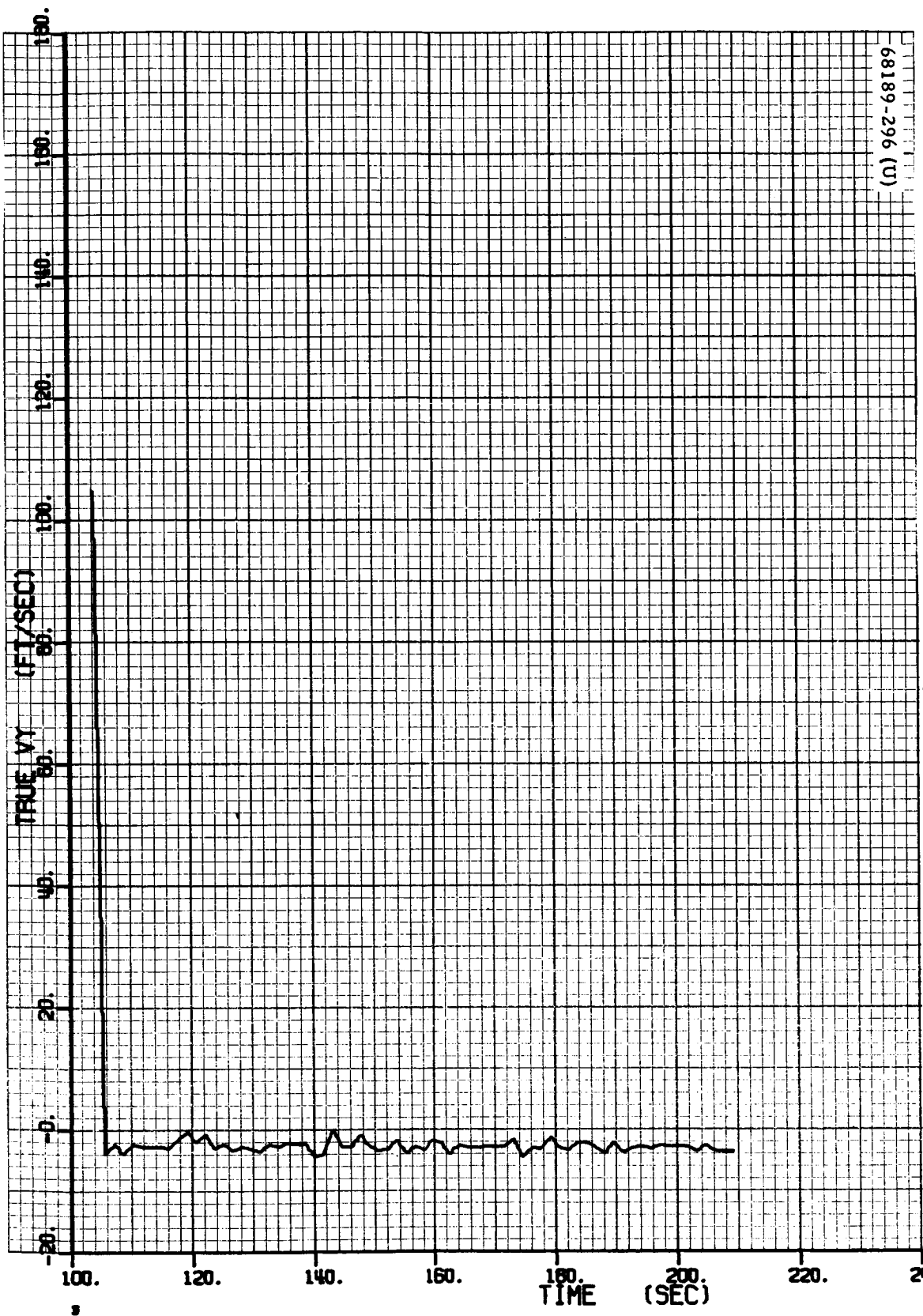
c) Δ Y Velocity (Initial), ft/sec

Figure 5. 15-10 (continued).   Differences of Telemetry and
Nominal Data From BETCOM
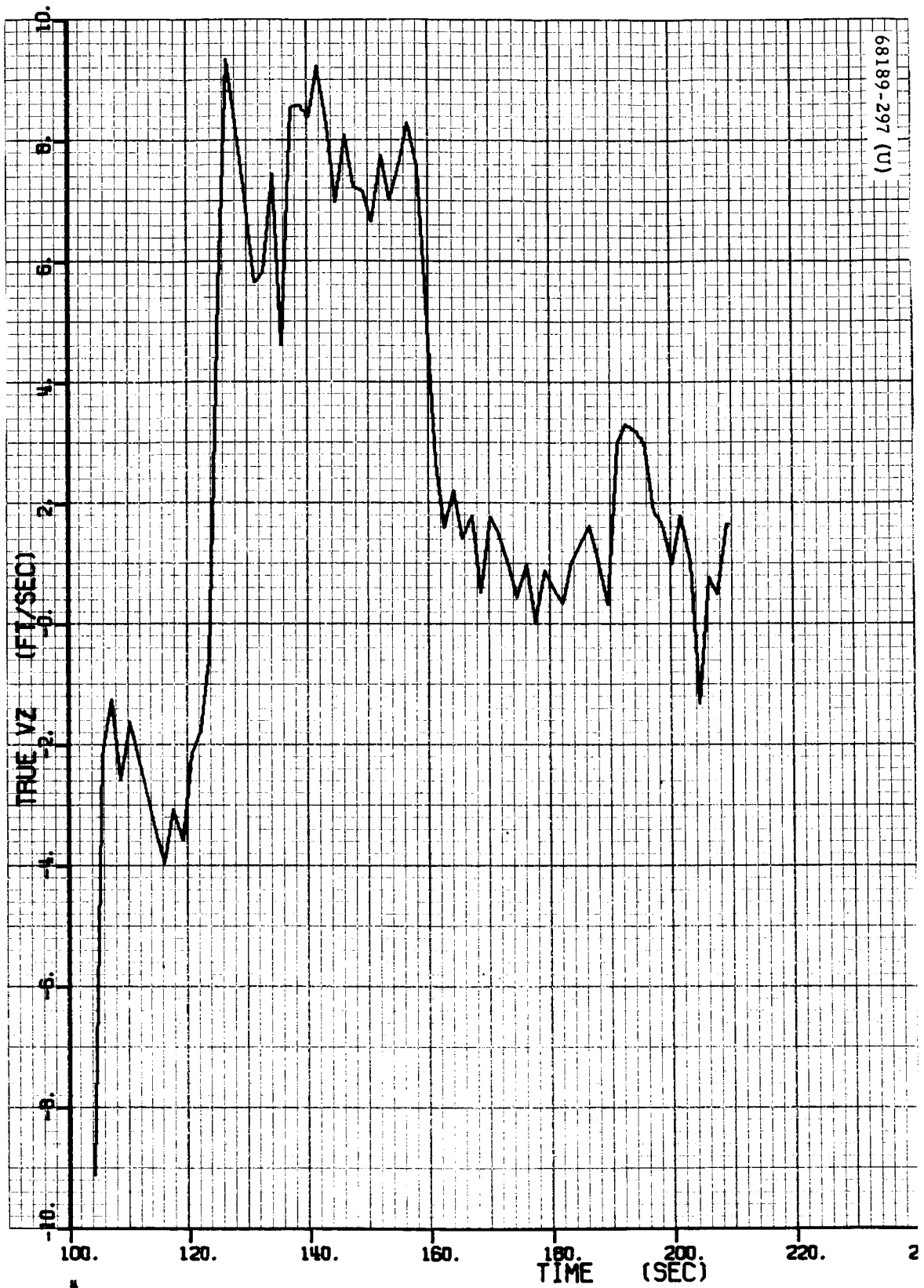
d) Δ Z Velocity (Initial), ft/sec

Figure 5.15-10 (continued). Differences of Telemetry and
Nominal Data From BETCOM

5.15-68
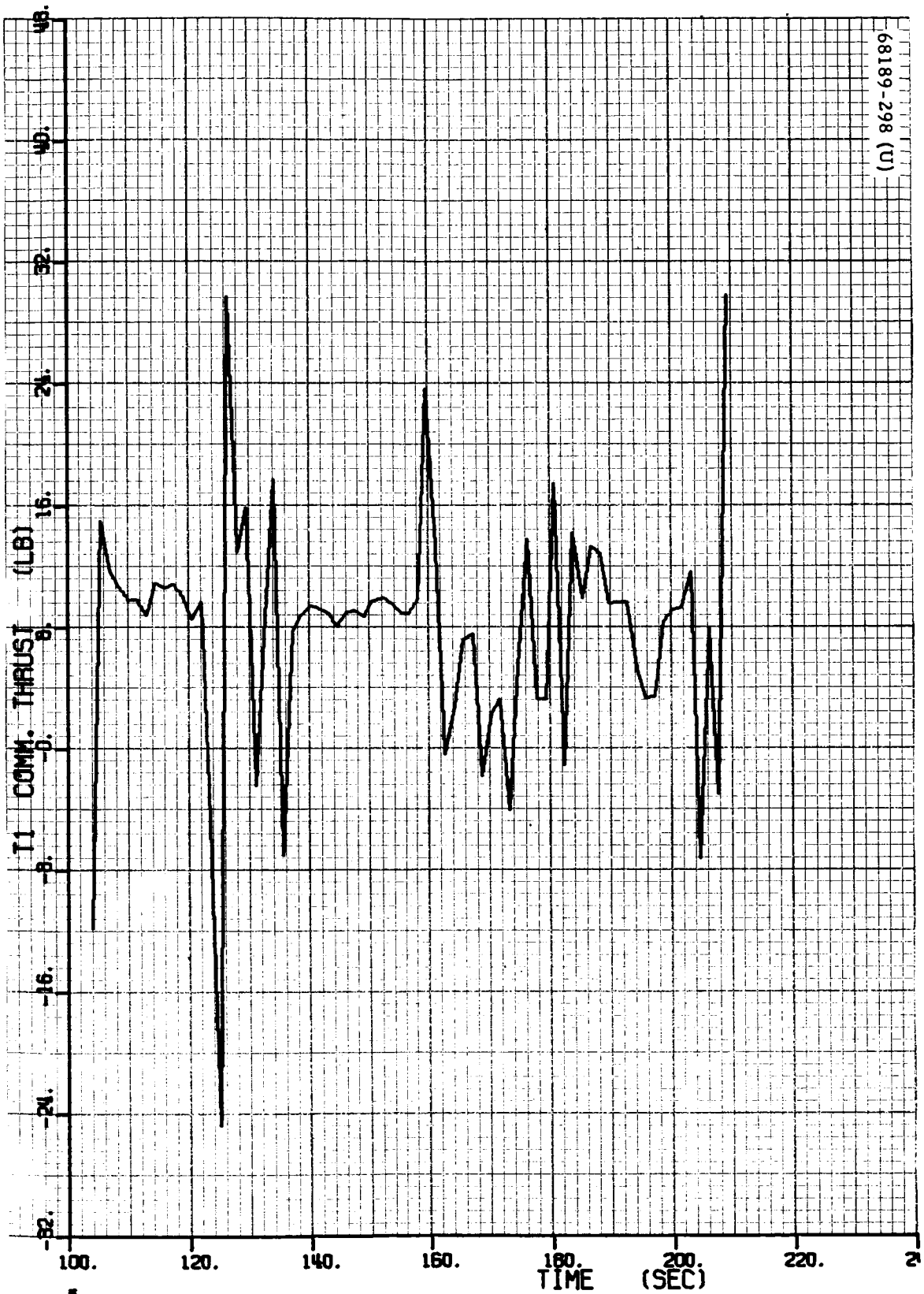
e) Δ Vernier Engine 1 Thrust Command (Initial), pounds

Figure 5.15-10 (continued). Differences of Telemetry and
Nominal Data From BETCOM
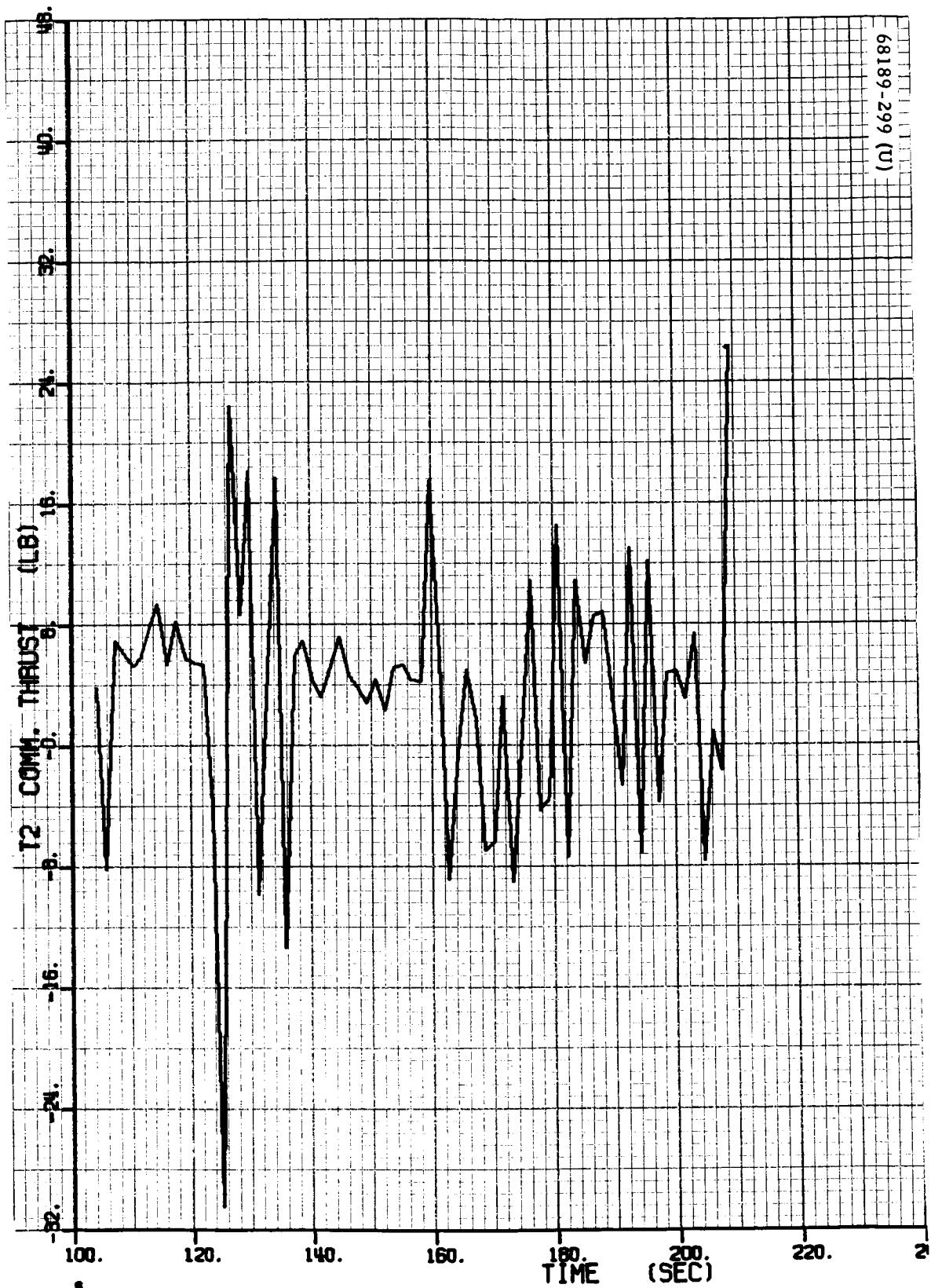
f) Δ Vernier Engine 2 Thrust Command (Initial), pounds

Figure 5. 15-10 (continued). Differences of Telemetry and
Nominal Data From BETCOM
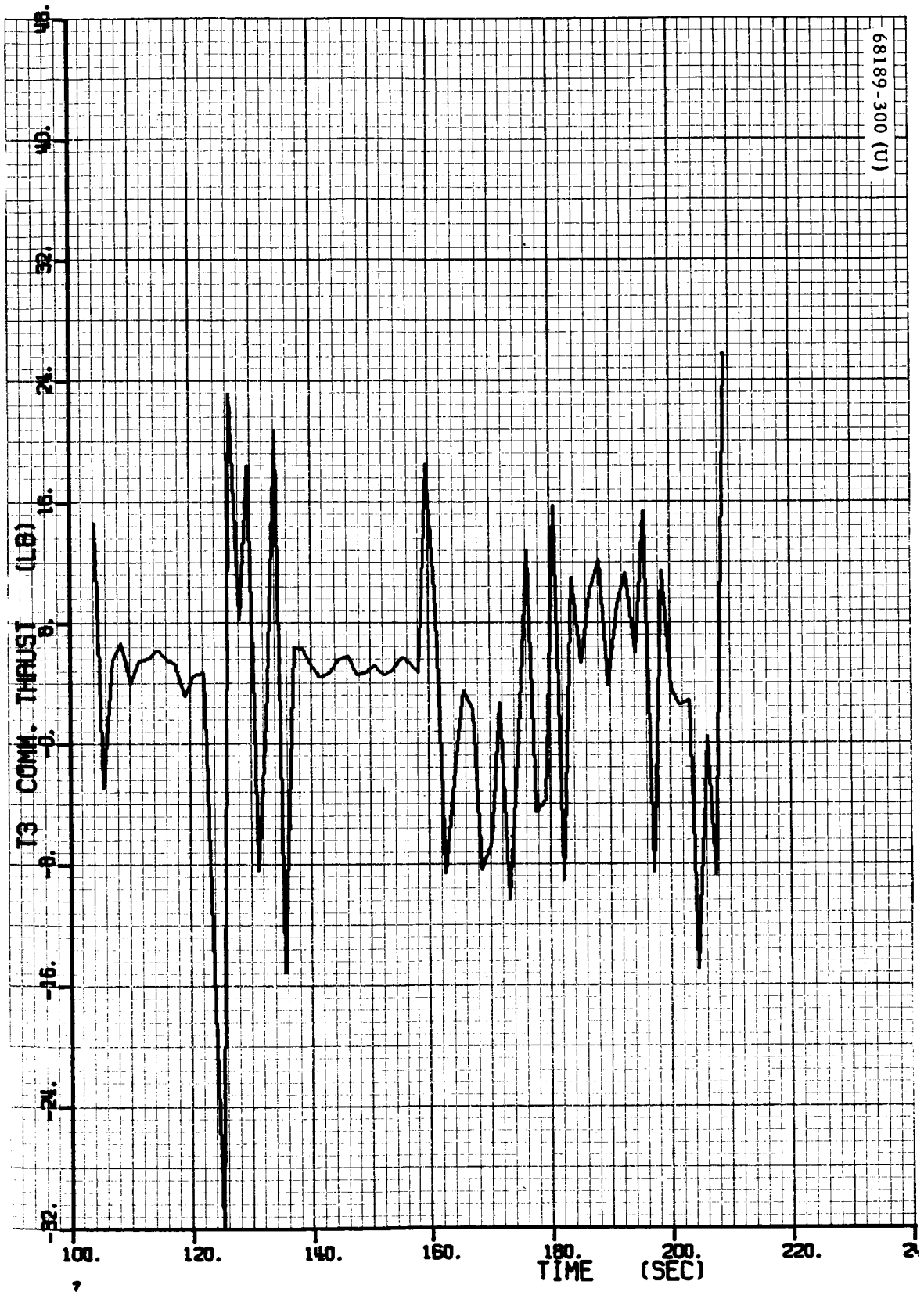
g) Δ Vernier Engine 3 Thrust Command (Initial), pounds

Figure 5. 15-10 (continued). Differences of Telemetry and
Nominal Data From BETCOM

h) Δ X Gyro Error Signal (Initial), degrees

Figure 5.15-10 (continued). Differences of Telemetry and
Nominal Data From BETCOM

5.15-72

i) Δ Y Gyro Error Signal (Initial), degrees

Figure 5. 15-10 (continued).   Differences of Telemetry and
Nominal Data From BETCOM

5. 15-73
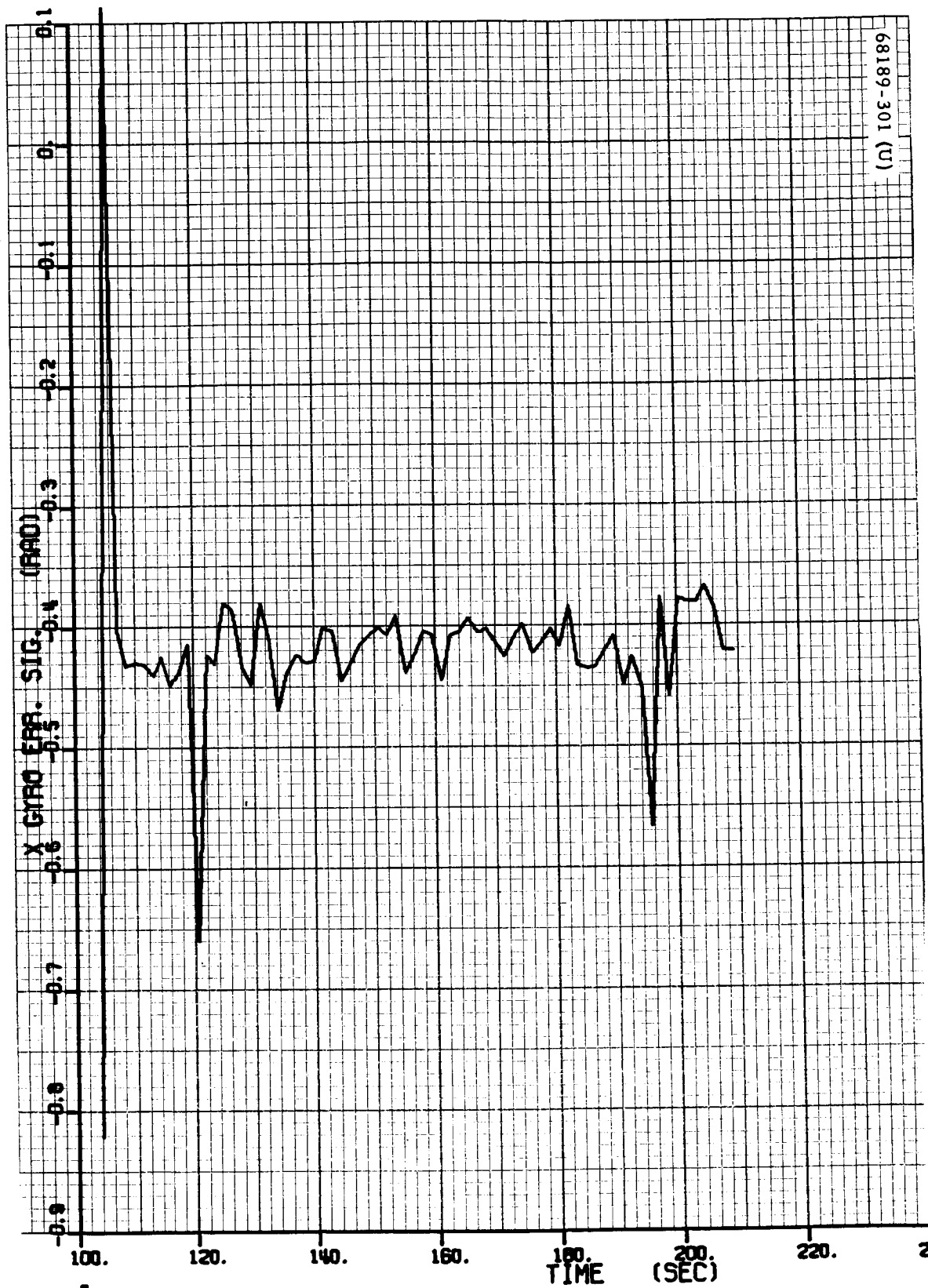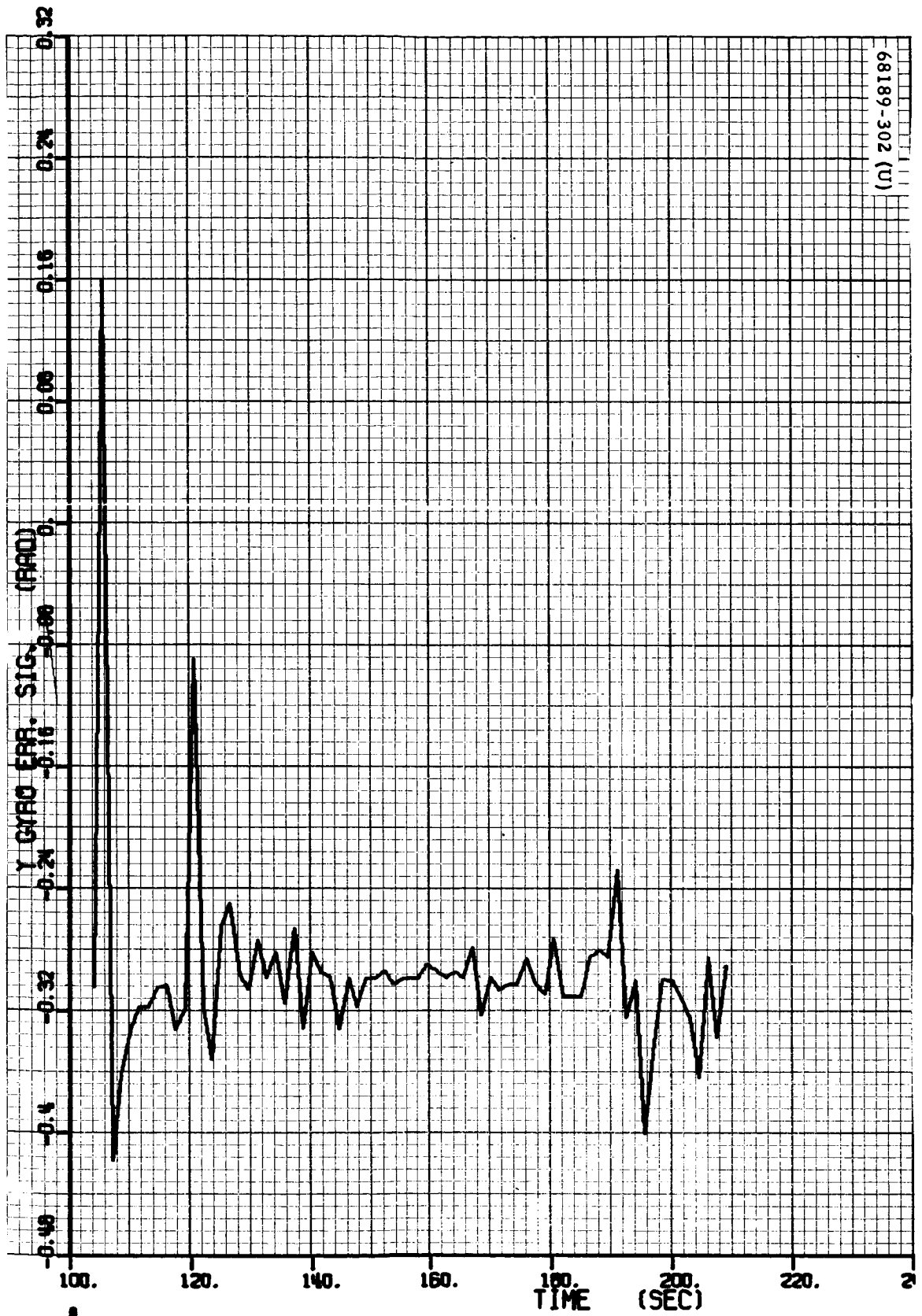
The ΔSR plot shows a definite scale factor error therein, reaching a value of slightly over 1000 feet at maximum, with a bias value that is considerably less in its effect than the scale factor error. The 2000-foot discrepancy at 103. 5 seconds occurs because the telemetered SR value had not recovered from the beam 3 dropout at that time; the spike at 120 seconds is the telemetry processing error previously mentioned; and the small cusp at 190 to 192 seconds is due to the SR telemetry gain change at 1000 feet.

After the initial spikes due to the beam 3 dropout, the ΔV_x and ΔV_y plots show almost constant differences throughout. The V_z plot, however, does not contain characteristics indicative of a significant bias or scale factor error, but does contain a significant acceleration-looking profile, which among other things could be due to a scale factor error in the accelerometer.

Due to the fact that the 6DOF program outputs smooth thrust commands whereas the spacecraft thrust commands are pulsating, the ΔT_1, ΔT_2, and ΔT_3 plots are necessarily noisy in appearance. Comparisons at the minimum -g phase (105 to 122 seconds) and at saturated conditions (138 to 158 seconds), however, show fairly good behavior except for probable biases.

The $\Delta \varphi_x$ and $\Delta \varphi_y$ plots are fairly constant after the initial spikes, but settle out to values indicative of very large negative biases. The spikes at 120 seconds are again due to the telemetry processing.

SEMBET Error Determination

The nominal trajectory data and the telemetry data were input to the SEMBET program for adjustment. The SEMBET program is modeled with time varying partial derivatives that relate the measured differences between the telemetered and nominal trajectories to bias and scale factor errors in the telemetry system. It then adjusts the error source values in such a way that the nominal trajectory best fits the telemetered trajectory in the least squares sense. When the effect of the error source values solved for in the adjustment are removed from the telemetry data, the remaining trajectory is the best estimate thereof in the statistical minimum-variance sense (for the particular error model used).

The adjustment performed by SEMBET was weighted in the sense that unequal importance was attached to the telemetry signals in certain portions of the trajectory. The weighting was a noise-only type in that a 2-second sliding arc second degree filter was used from which to extract midpoint variance data, and was normalized in the sense that the variances thus obtained were divided by the respective nominal signal values at the appropriate points in time. Such a scheme automatically precludes the implementation of a tedious editing procedure since the variances will be so large at points of near-discontinuity (spikes) that the data therein will be virtually disregarded by the adjustment.

Processing the vernier phase data by SEMBET yielded the error source values listed in Table 5.15-9. Listed next to the bias and scale factor errors are the one-standard-deviation (1σ) values for each. The 1σ values are actually the square roots of the diagonal elements of the covariance matrix associated with the least-squares adjustment and, as such, supplies information as to how well the adjustment scheme is able to pronounce on the error values. More specifically, if an error is given as A with a 1σ value of B, it can be said broadly that A is known to within $\pm$B. The 1σ values in the table are, for the most part, quite small.

Some interesting observations from Table 5.15-9 are as follows: 1) with the exception of the SR signal, all the scale factor errors are extremely small, 2) the V_x and V_y bias values solved for are virtually identical with the values observed on the telemetry signals (see "Retro and Vernier Telemetered Trajectory"), 3) the φ_x and φ_y bias values solved for could amost have been guessed at from the difference plots.

A word needs to be said about V_z. It was noted in "Vernier Comparison" that the ΔV_z plot did not conform to a shape characteristic of a bias or scale factor error. The SEMBET program is so modeled, however, that it will attempt to fit the ΔV_z curve to a bias/scale-factor combination whether it fits very well or not. Note that the bias and scale factor errors given for V_z in the table are not unreasonable in size, but note the standard deviation values. The 1σ values are much larger than the error values themselves, which, in effect, is simultaneously saying that the solution values are totally unreliable and that the values thus determined produce a very poor fit with the ΔV_z data. The 2.7 ft/sec bias was listed as an additional bias for V_z since this is the value determined from the post-touchdown data.

Best Estimate of Trajectory

The error source values listed in Table 5.15-9 were applied to the trajectory data (2.7 ft/sec bias with no scale factor error for V_z) in order to find a corrected set of conditions from which to initialize the 6DOF program. The corrected conditions at the beginning of steering are given in Table 5.15-10.

The plots given in Figures 5.15-11a through 5.15-11i show the trajectory parameters output from the 6DOF program initialized to the conditions given in Table 5.15-10. As a second check on this simulated best estimate of trajectory, the segment intercept time, segment change times, and touchdown time from the 6DOF final simulation were checked with the same times from the telemetry data, with a resulting discrepancy of 0.3 second in the worst case. Therefore, it can be assumed that this trajectory is a very accurate estimate of the actual.

Corrected Telemetry and Final Differences

As a final check on the trajectory reconstruction, the errors solved for in "SEMBET Error Determination" were removed from the telemetry

TABLE 5.15-9. TELEMETRY ERROR VALUES
FROM SEMBET

| Signal | Bias Error | | Scale Factor Error, percent | |
	Mean	Standard Deviation	Mean, percent	Standard Deviation
SR	4.713 feet	0.53	3.689**	0.69
V_x	0.1947 foot	0.06	0.2318	0.09
V_y	-2.786 ft/sec	0.04	0.1942	0.12
V_z	1.026 ft/sec*	5.29	0.2136*	3.42
	2.7 ft/sec	—	—	—
T_1	8.063 pounds	2.46	-0.4613	0.23
T_2	4.192 pounds	1.97	0.0179	0.01
T_3	3.924 pounds	1.89	-0.6429	0.31
φ_x	-0.4216 degree	0.09	-0.3617	0.10
φ_y	-0.3044 degree	0.11	0.2903	0.08

Note: The error values in this table are not total telemetry errors since some error has been previously removed via the calibration coefficients.

*See text for an explanation of V_z.

**Before 1000-foot mark.

TABLE 5.15-10. CORRECTED CONDITIONS AT BURNOUT

Signal	Parameter
SR	27,850 feet
V_x	70.16 ft/sec
V_y	-4.03 ft/sec
V_z	425.3 ft/sec
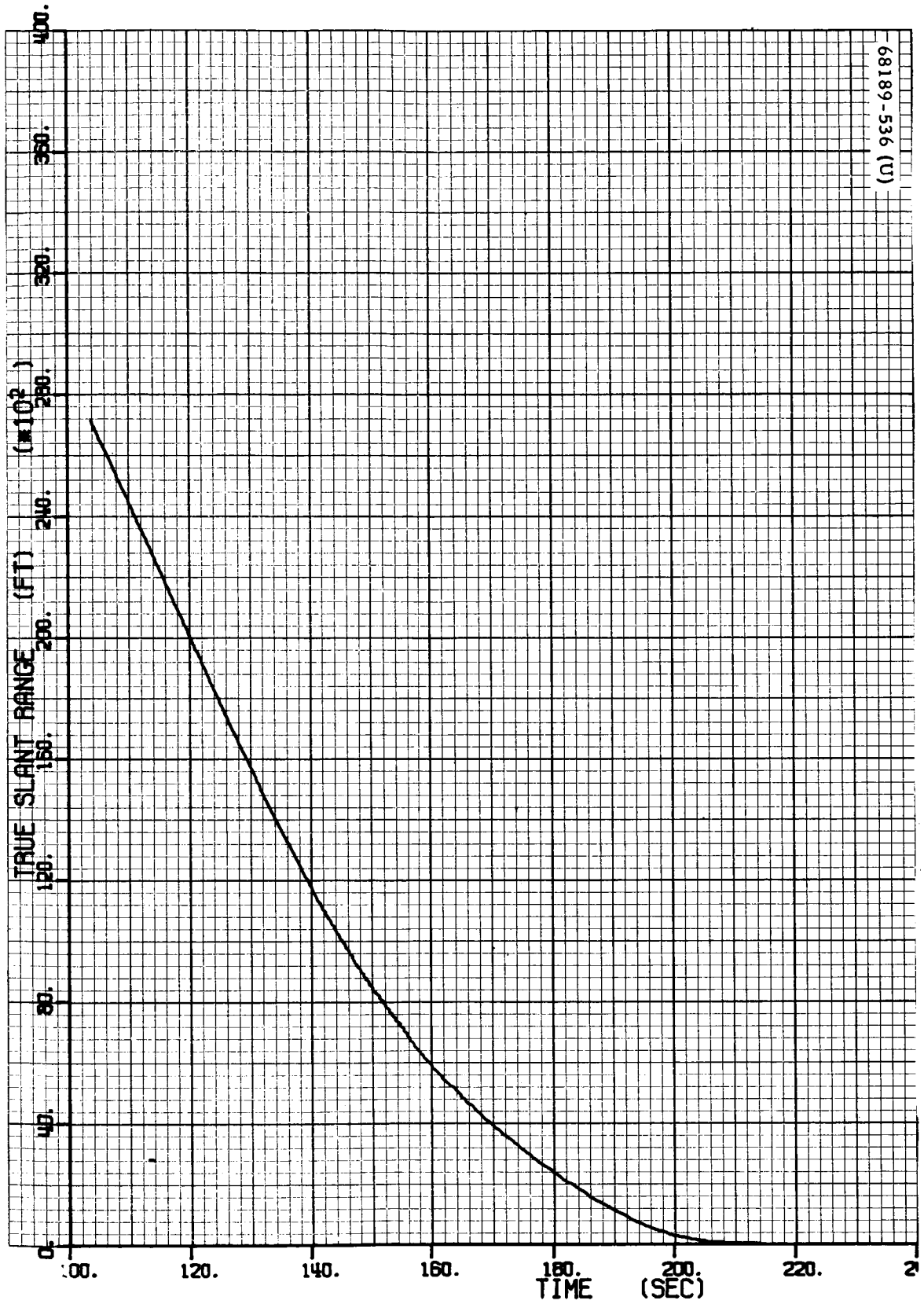
a) Best Slant Range Estimate, feet $\times 10^2$

Figure 5.15-11. Best Estimate Trajectory Parameters From
Six-Degree-of-Freedom Program
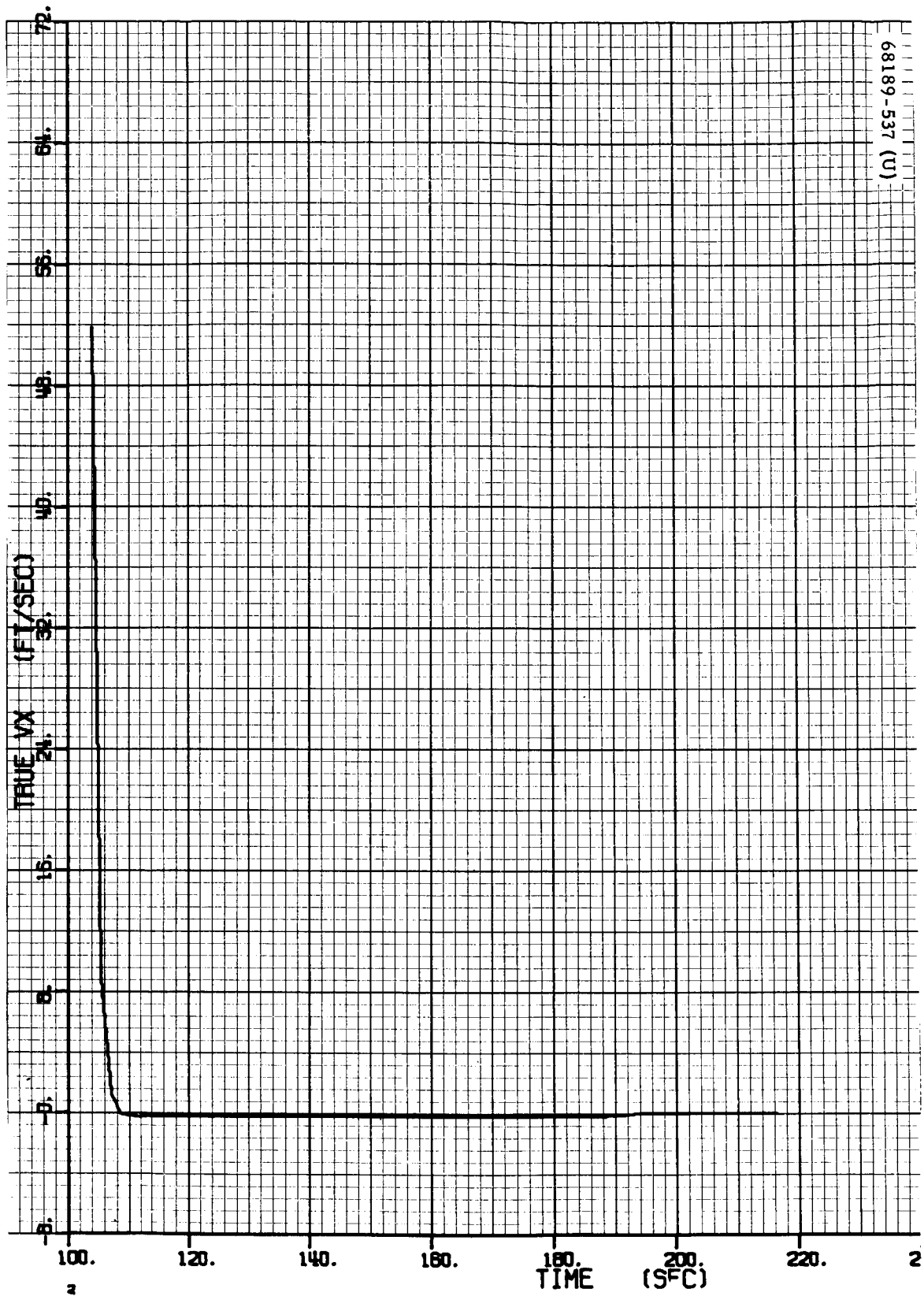
b) Best X Velocity Estimate, ft/sec

Figure 5.15-11 (continued). Best Estimate Trajectory Parameters
From Six-Degree-of-Freedom Program
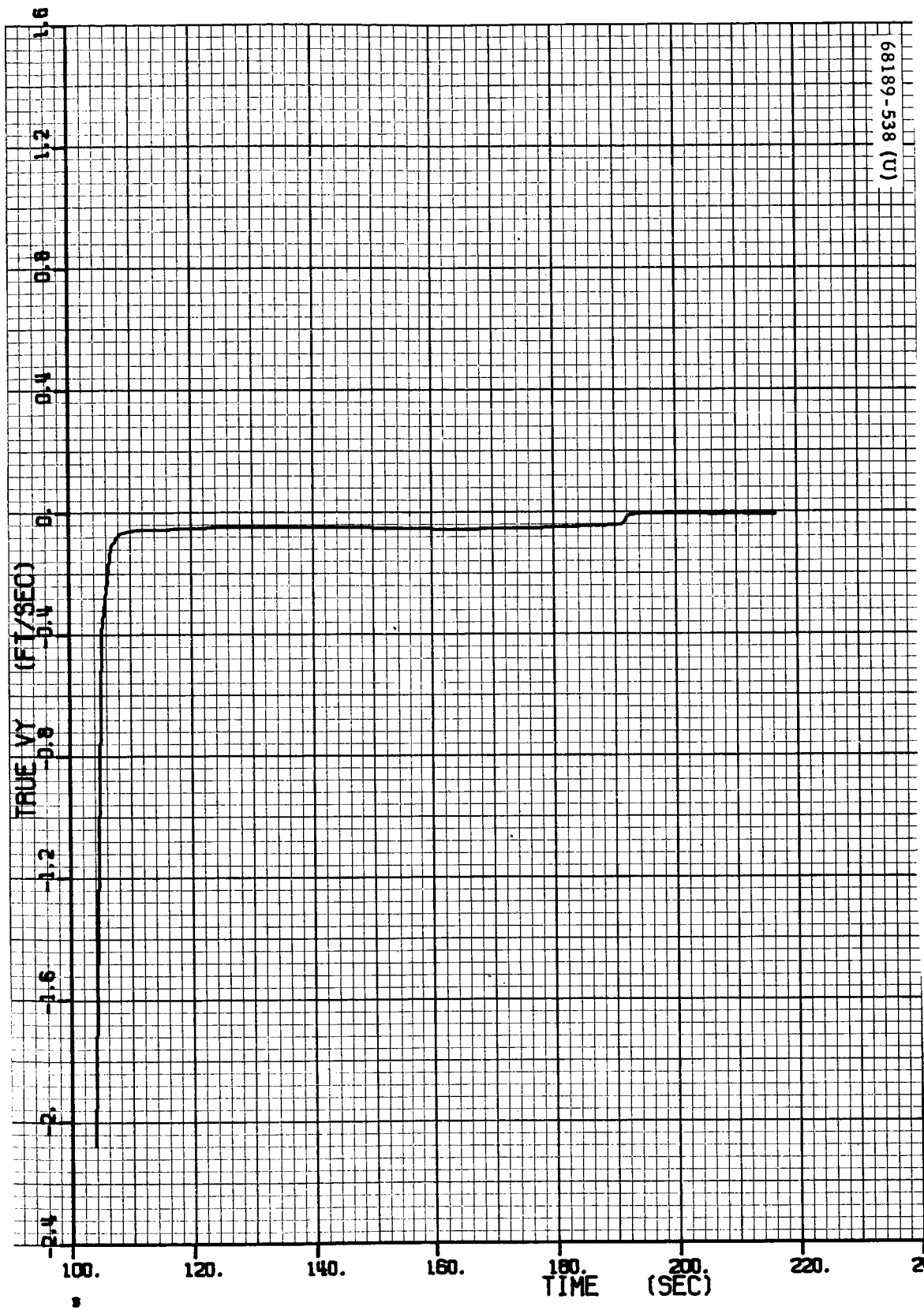
c) Best Y Velocity Estimate, ft/sec
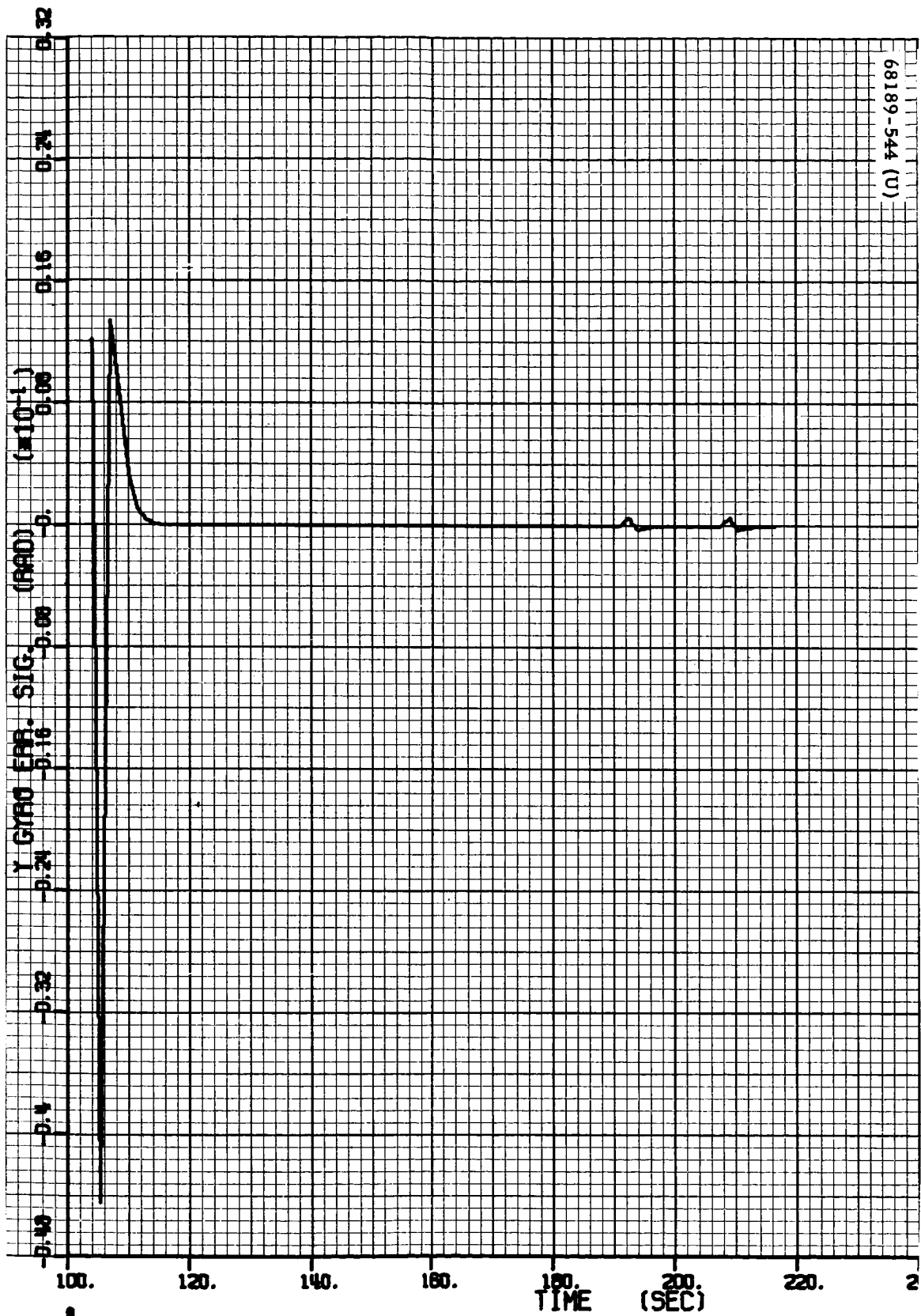
Figure 5.15-11 (continued).   Best Estimate Trajectory Parameters
From Six-Degree-of-Freedom Program
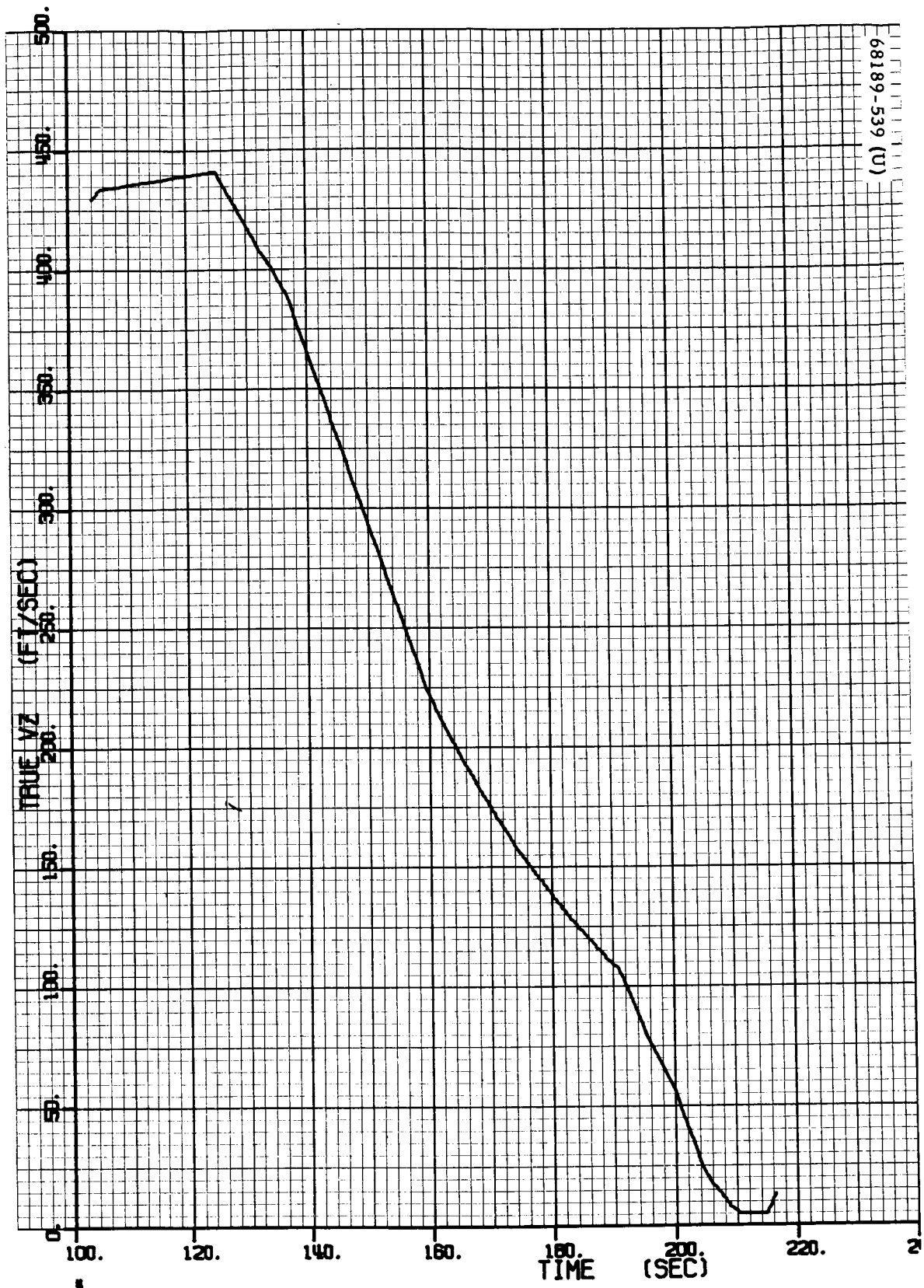
d) Best Z Velocity Estimate, ft/sec

Figure 5.15-11 (continued). Best Estimate Trajectory Parameters
From Six-Degree-of-Freedom Program
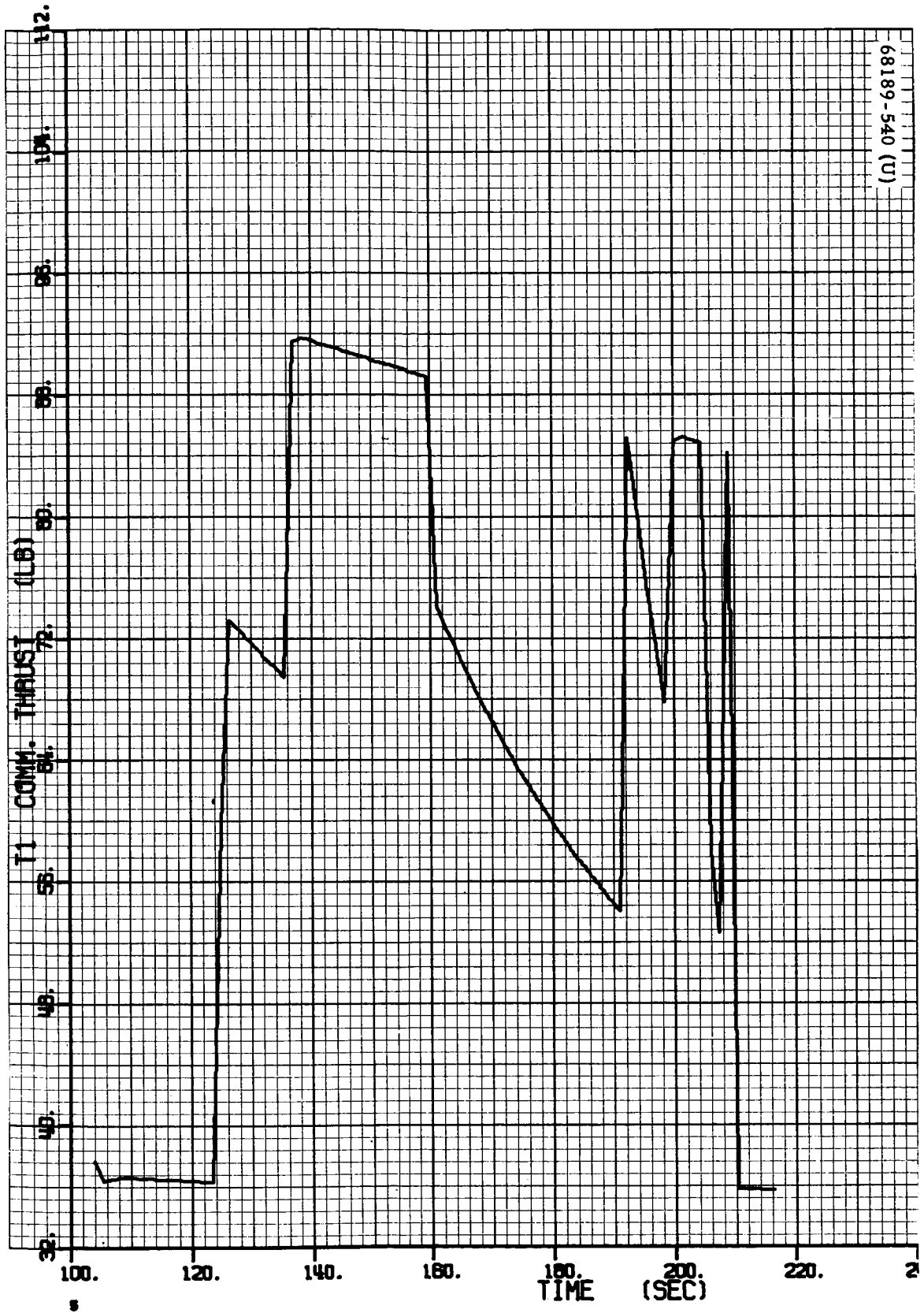
e) Best Vernier Engine 1 Thrust Command Estimate, pounds

Figure 5.15-11 (continued). Best Estimate Trajectory Parameters
From Six-Degree-of-Freedom Program
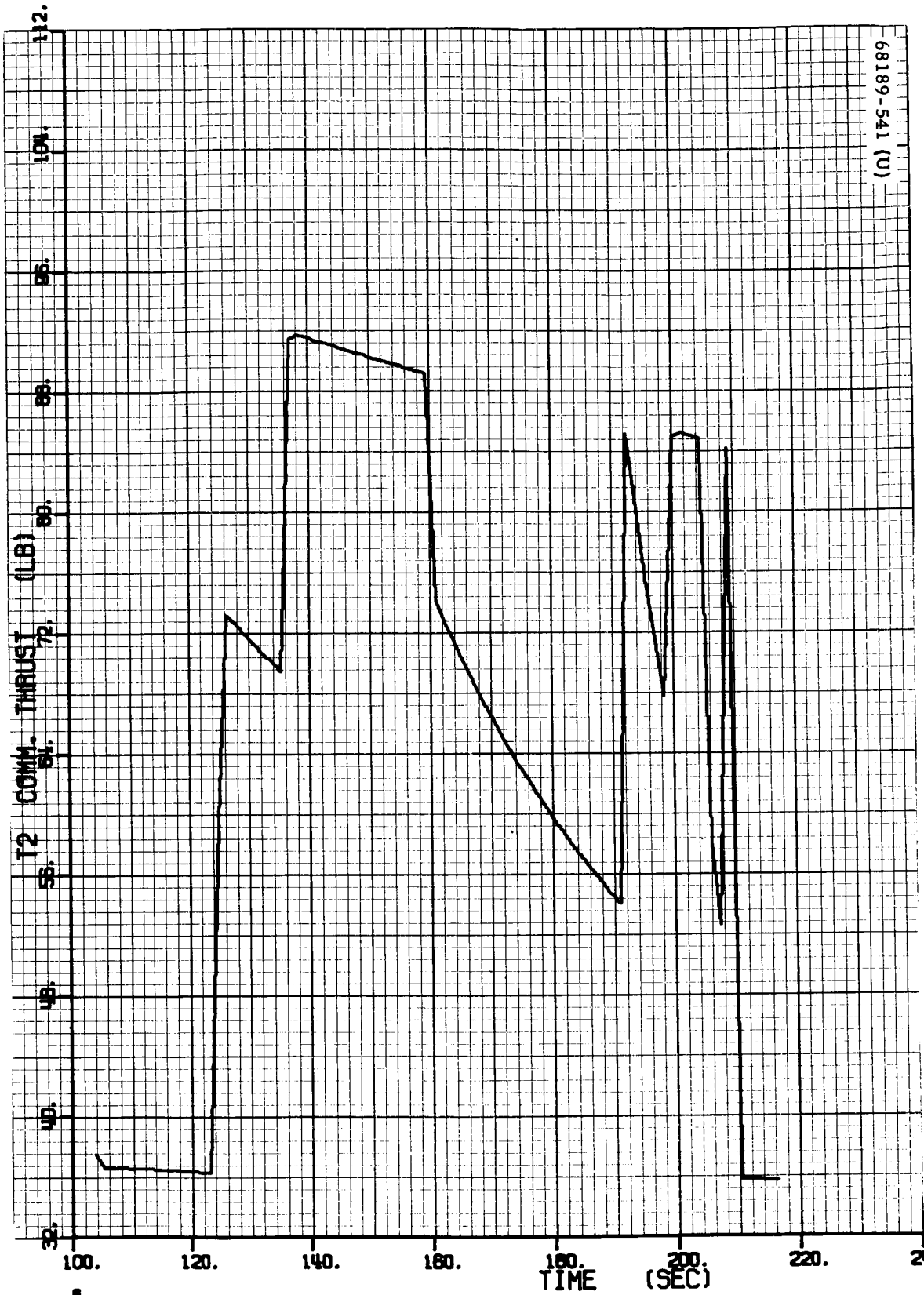
f) Best Vernier Engine 2 Thrust Command Estimate, pounds

Figure 5.15-11 (continued).   Best Estimate Trajectory Parameters
From Six-Degree-of-Freedom Program
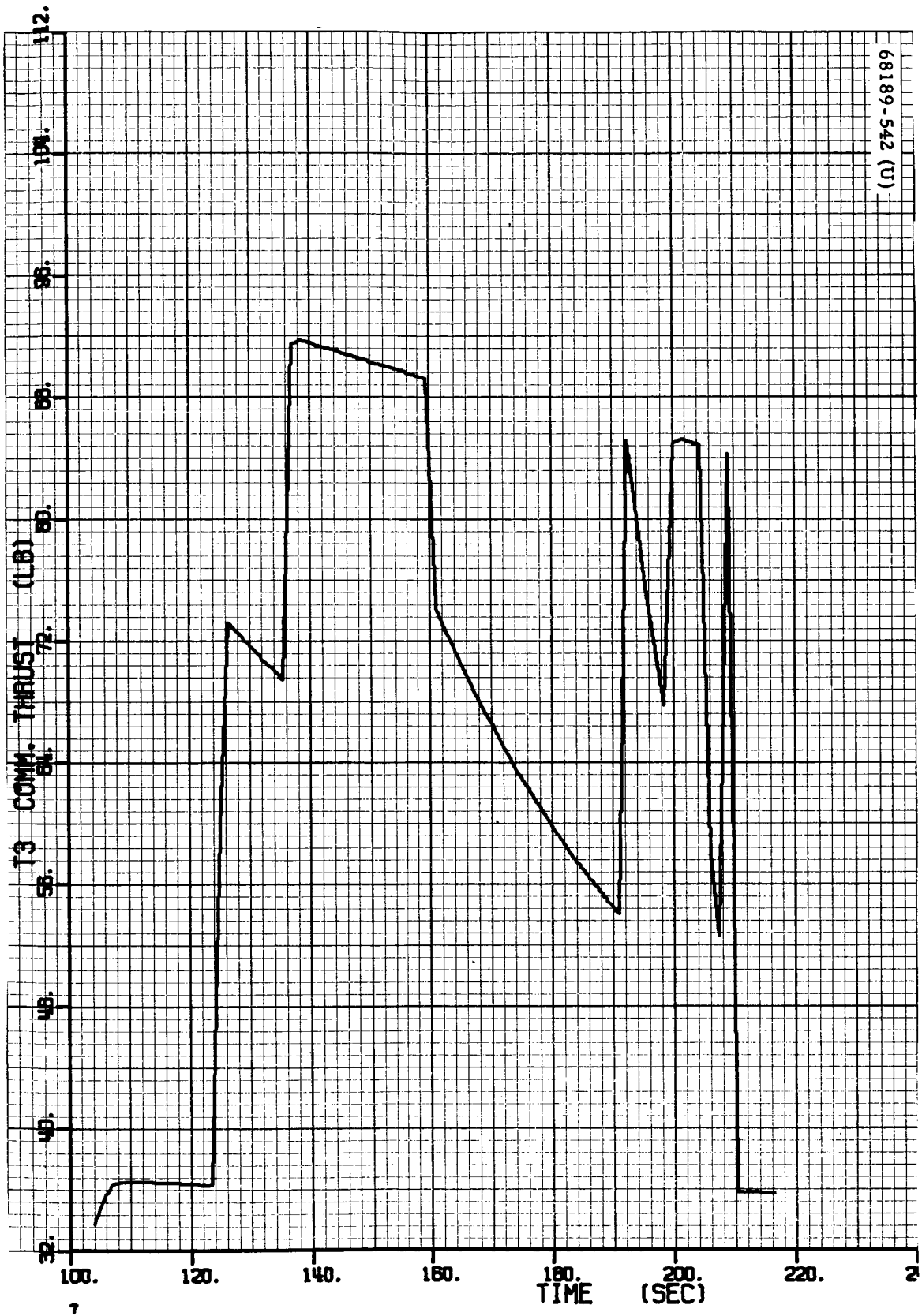
g) Best Vernier Engine 3 Thrust Command Estimate, pounds

Figure 5.15-11 (continued). Best Estimate Trajectory Parameters
From Six Degree-of-Freedom Program
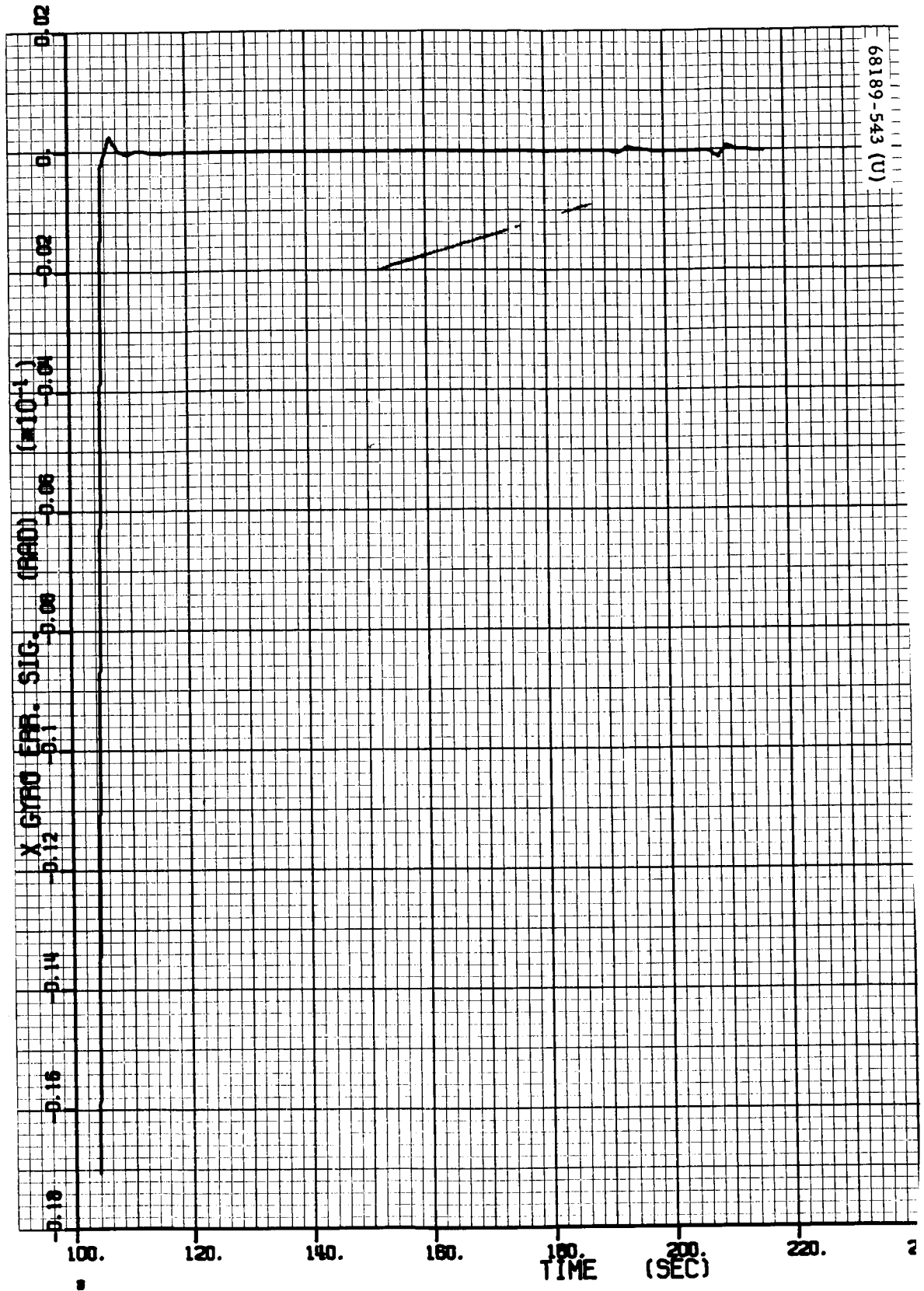
d) Best X Gyro Error Signal Estimate, degrees $\times 10^{-1}$

Figure 5.15-11 (continued).   Best Estimate Trajectory Parameters
From Six-Degree-of-Freedom Program

i) Best Y Gyro Error Signal Estimate, degrees × 10^{-1}

Figure 5.15-11 (continued). Best Estimate Trajectory Parameters
From Six-Degree-of-Freedom Program

data by rerunning the PREPRO program and exercising its bias and scale factor removal option. Figures 5.15-12a through 5.15-12i show the results of removing the bias and scale factor error values.

Most of the error values were very small, so the plots presented herein are almost undistinguishable from the uncorrected plots (Figures 5.15-8a through 5.15-8m). Close inspection shows obvious error removals from SR, V_y, φ_x, and φ_y, however.

The final plots (Figures 5.15-13a through 5.15-13h) in this section give the difference between the best estimate of trajectory parameters and the corrected telemetry parameters and, as such, should show zero-mean discrepancies between the two if the SEMBET adjustment is correct.

The ΔSR plot shows residual discrepancies of less than 100 feet, which represents excellent agreement. The $\Delta\varphi_x$, $\Delta\varphi_y$, ΔV_x, and ΔV_y plots are also very nearly zero-mean. A ΔV_z plot is not shown since the errors in V_z solved for by SEMBET were deduced to be not representative of any true error in the V_z signal and were therefore meaningless in the adjustment. The three thrust command difference plots (ΔT_1, ΔT_2, ΔT_3) point out an interesting fact. Note that in all three cases the mean is obviously non-zero, but note that the plotted data in the minimum-g phase (104 to 122 seconds) and in the saturated regions (138 to 158 seconds, and for a short period spanning 190 seconds) is very nearly zero-mean. The reason for the above behavior lies in the weighting scheme used by SEMBET. Whenever the data is noisy, its effect in determining the error values is proportionately disregarded. Therefore, as seen in the ΔT plots, SEMBET chose error source values that caused the best estimate of the trajectory to fit the telemetry values very closely in the regions of relative quiescence, letting the noisier regions fall more or less where they may. Another observation from the ΔT plots is that the data in the quiet regions does not quite exhibit a zero-mean, but still contains a slight, unexplained trend. It can be concluded from this that an error in the thrust commands did exist in the telemetry for which there is no exact representation in the SEMBET error model. The 1σ values attached to the thrust command bias and scale factor errors in Table 5.15-9 also point this out by indicating relatively high uncertainties in these errors. This residual error could be due to resistance changes in the torquing coils of the engines.

5.15.7   REFERENCES

1.   D. Bender, "SC-1 Event Times From TELTAB" IDC 2253.2/616, 11 July 1966.

5.15.8   ACKNOWLEDGMENTS

This section was compiled through the efforts of many individuals. In particular, Clinton Passey was responsible for development of the data processing system (operating on data tapes received from Saul Volansky)

used for the major portion of postflight analysis presented in this section. In addition, he is completely responsible for the trajectory reconstruction presented in subsection 5.15.6.3. Curt Spenny developed computer programs used in analyzing the retro accelerometer data. Edward White and David Bender contributed analysis and computer programs necessary for computation of retro phase velocity change through use of doppler and telemetered burnout velocity data. The spacecraft landing site location and retro case trajectory were analyzed by Vernon George. Other contributions in programming were made by Edward Kopitzke, Nancy Krupa, and Wendy Watson.
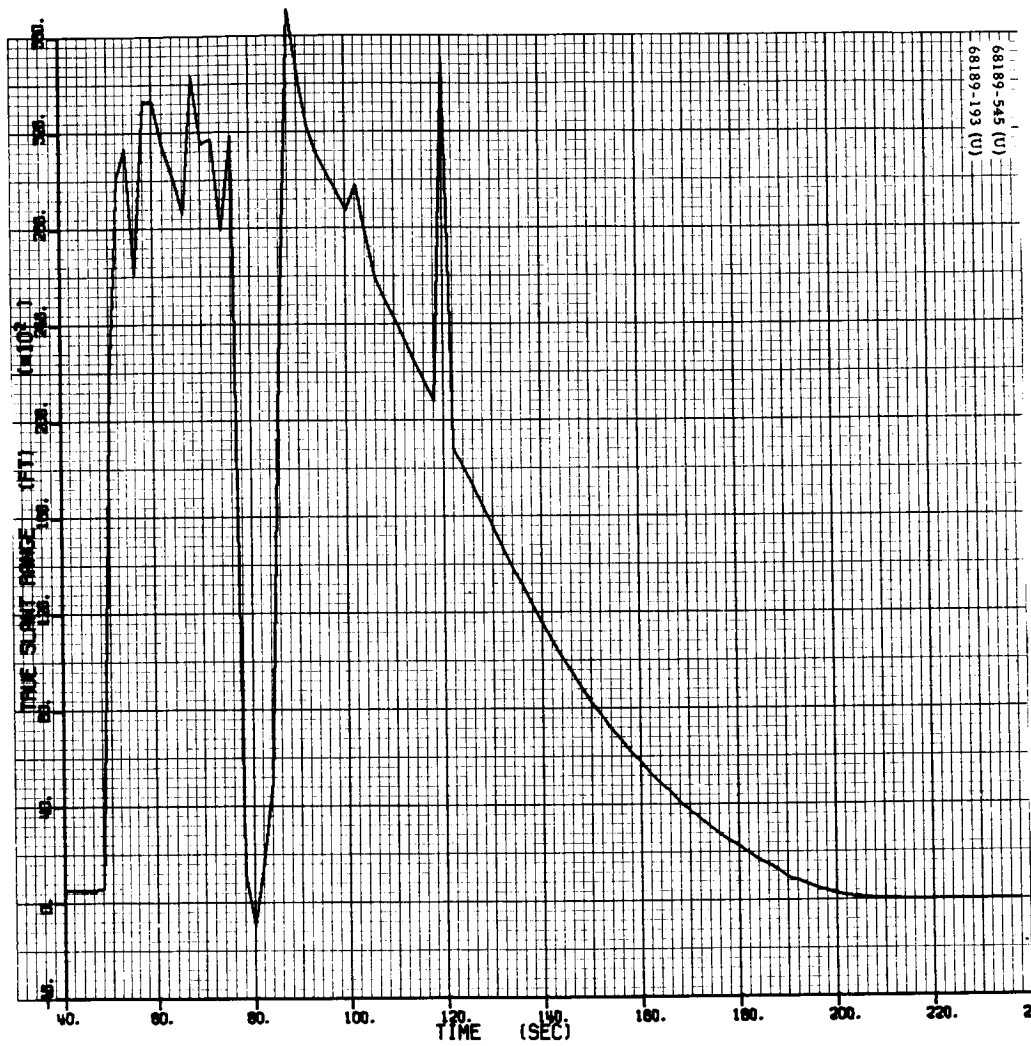
a)   Slant Range, feet $\times$ 10^2

Figure 5.15-12.   Telemetry Data Corrected by PREPRO
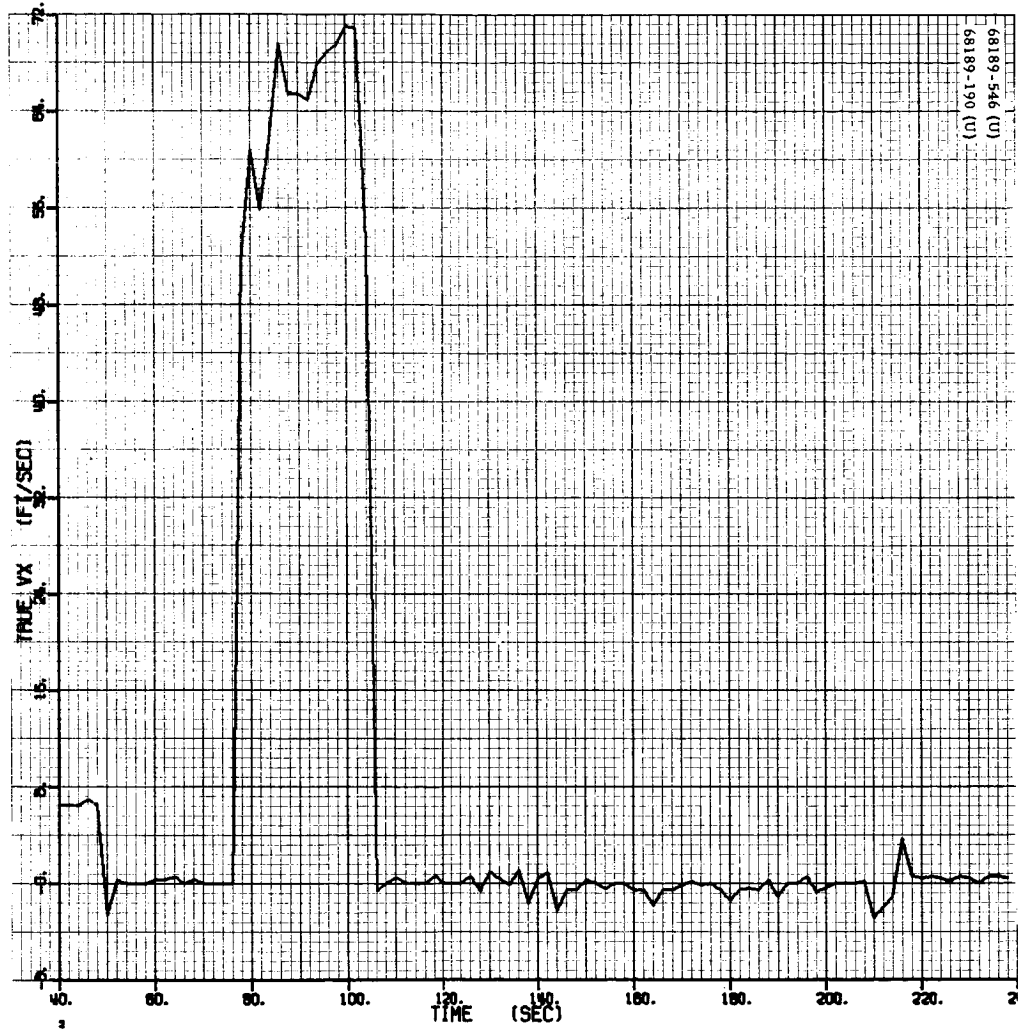
b) X Velocity, ft/sec

Figure 5. 15-12 (continued). Telemetry Data Corrected
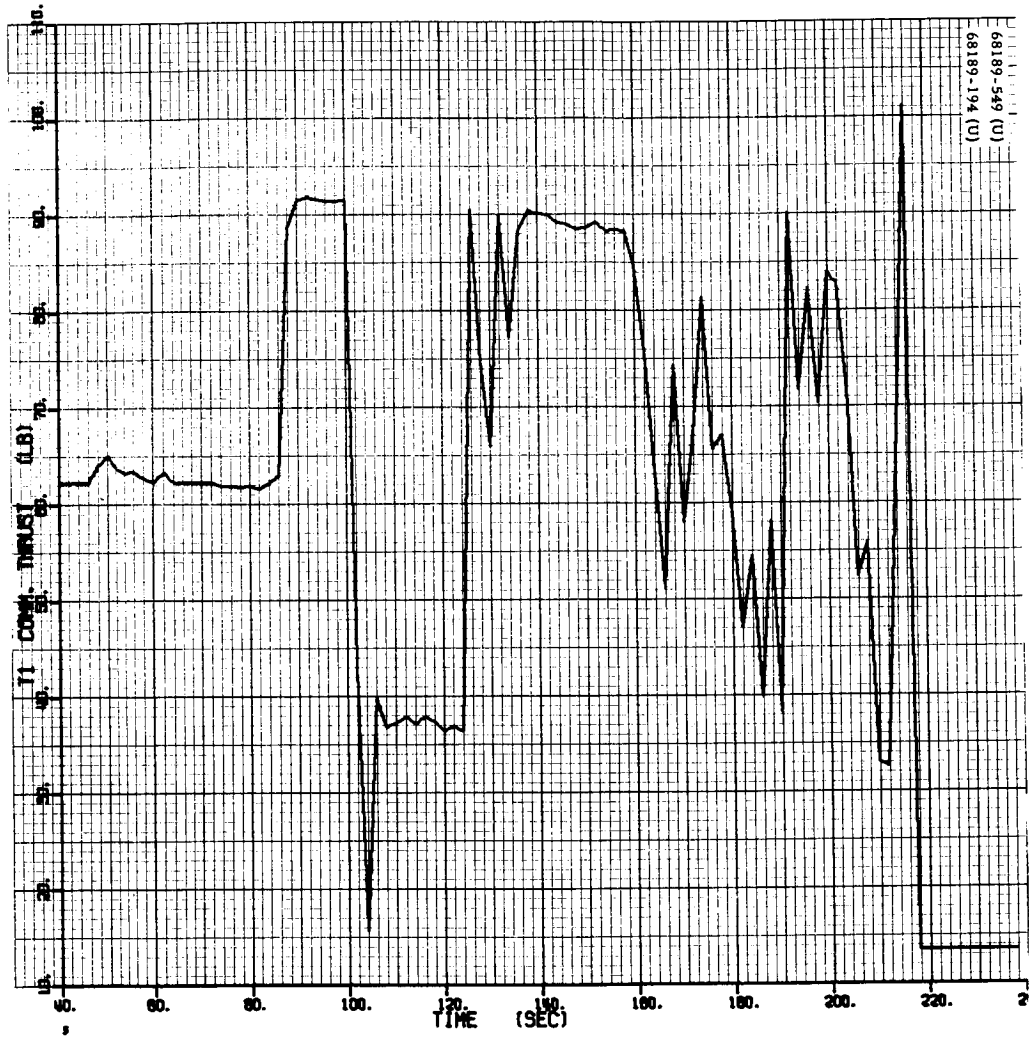by PREPRO
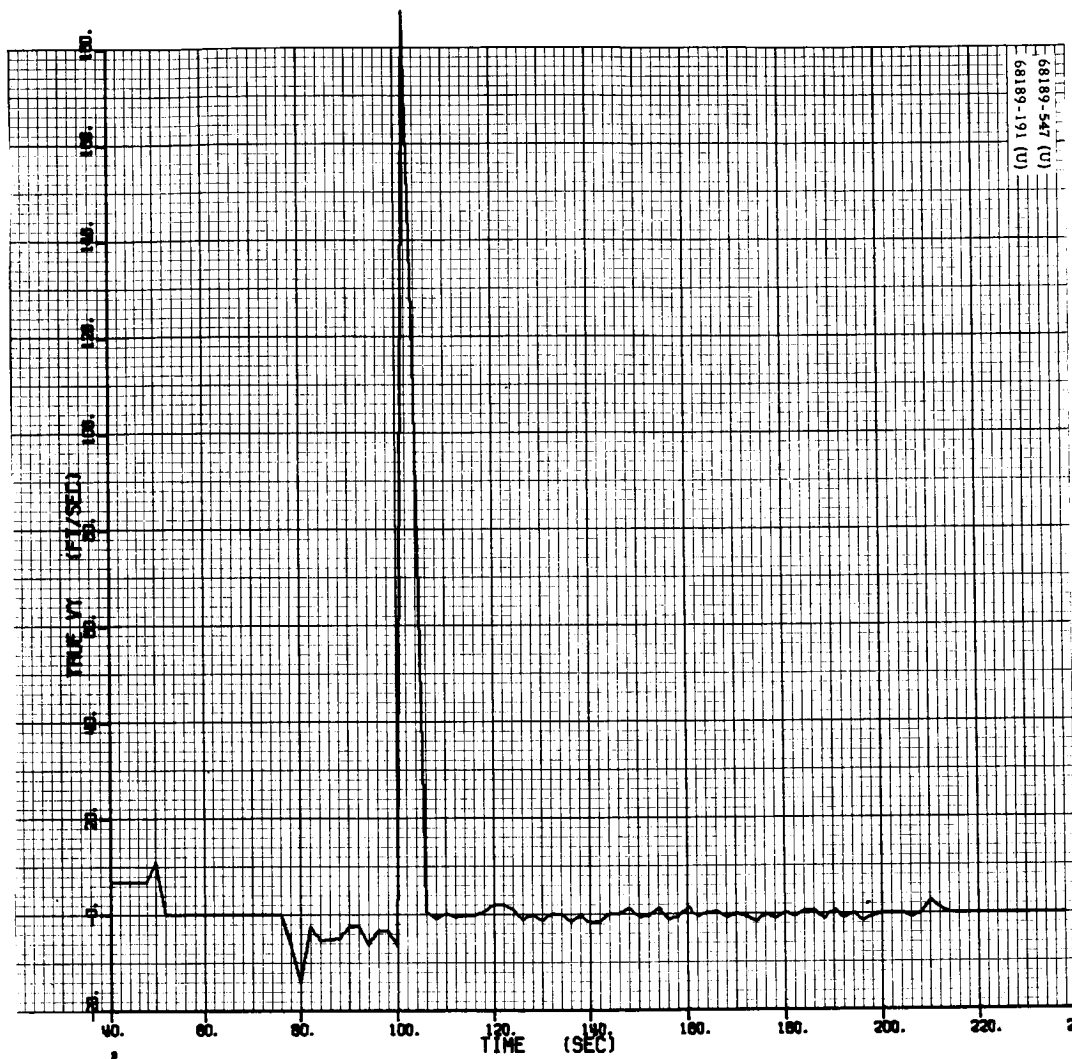
c) Y Velocity, ft/sec

Figure 5.15-12 (continued).   Telemetry Data Corrected
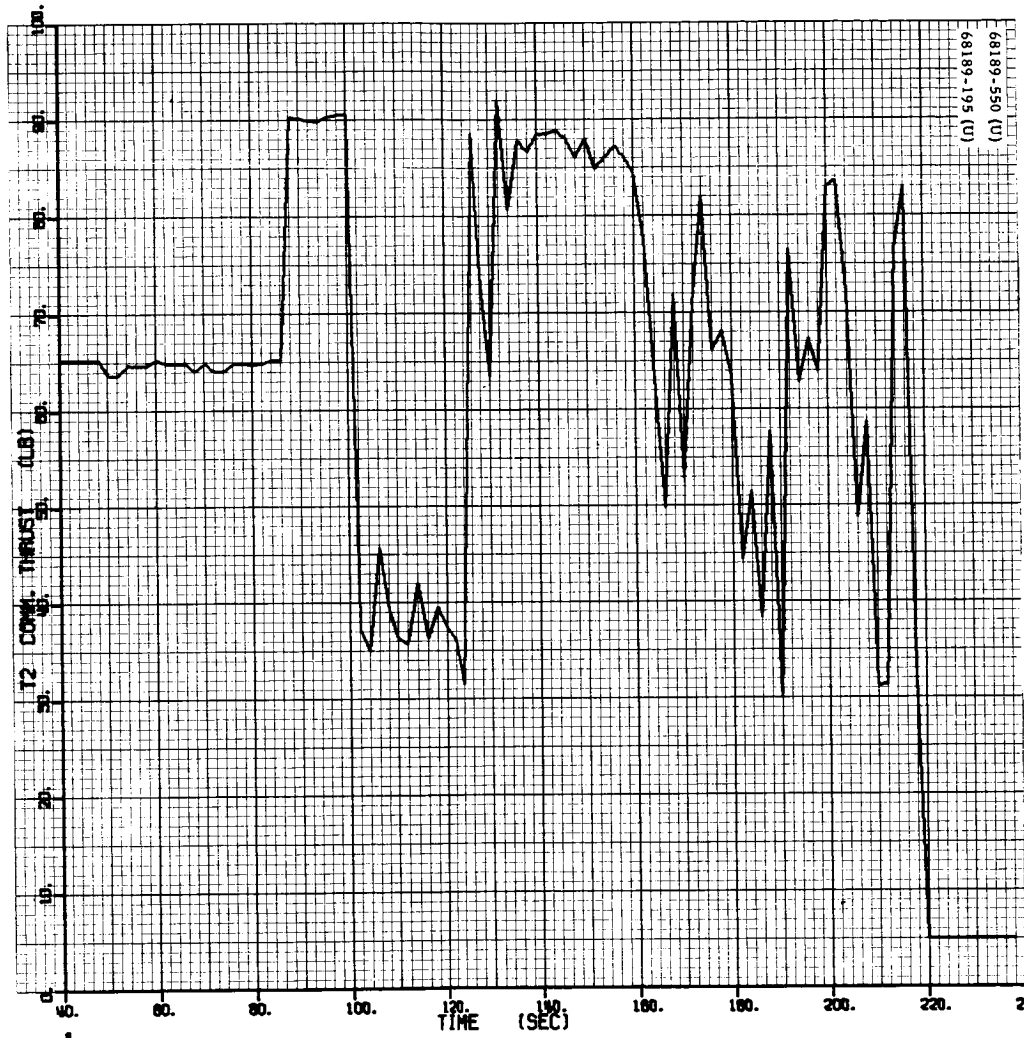by PREPRO
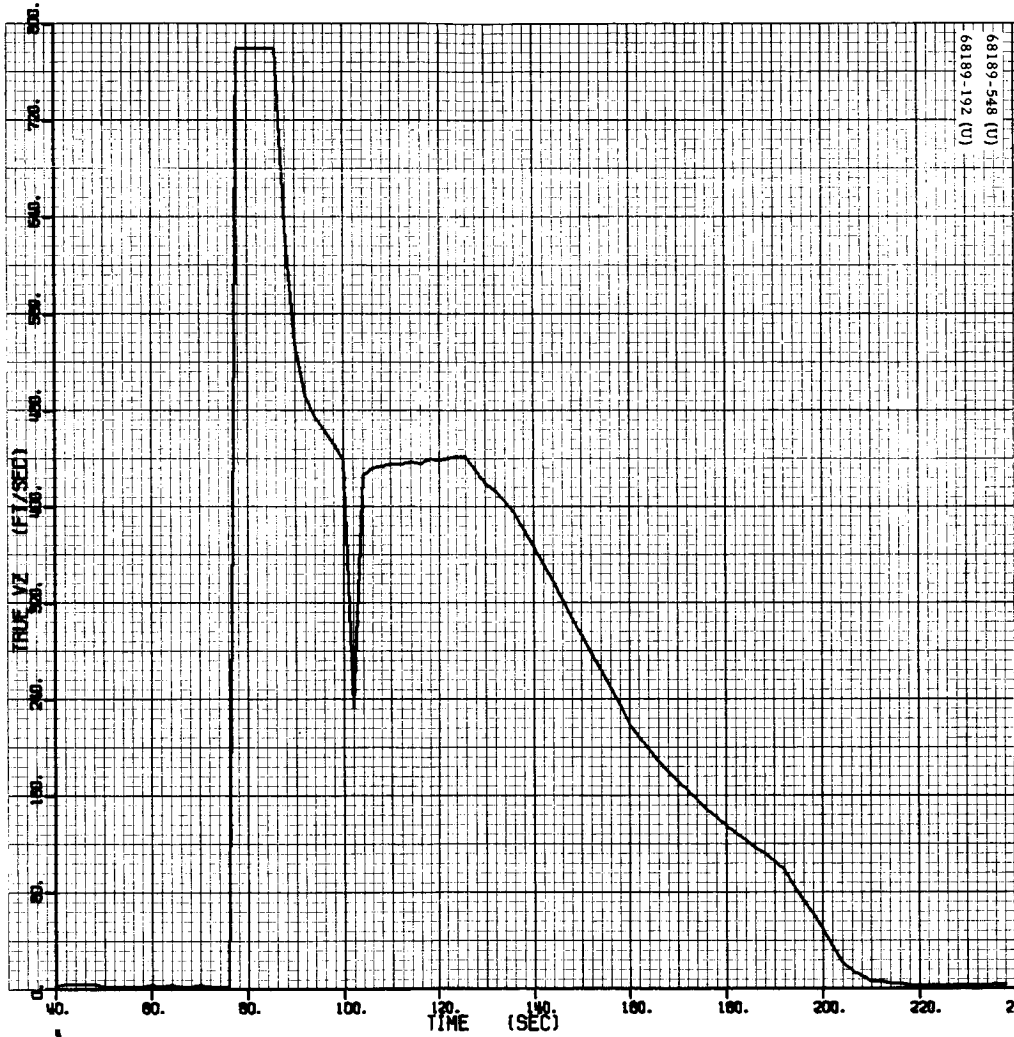
d) Z Velocity, ft/sec

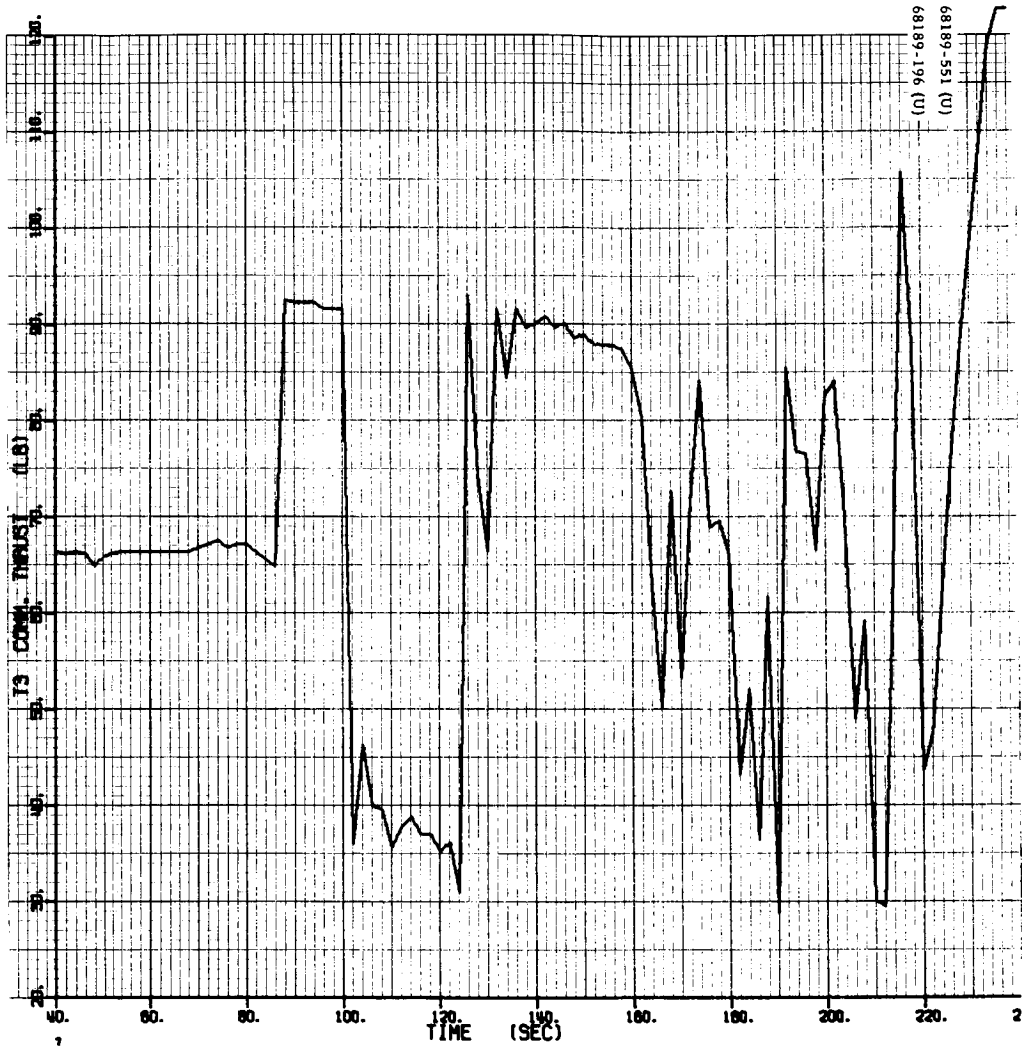Figure 5. 15-12 (continued). Telemetry Data Corrected
by PREPRO

e) Vernier Engine 1
Thrust Command, pounds

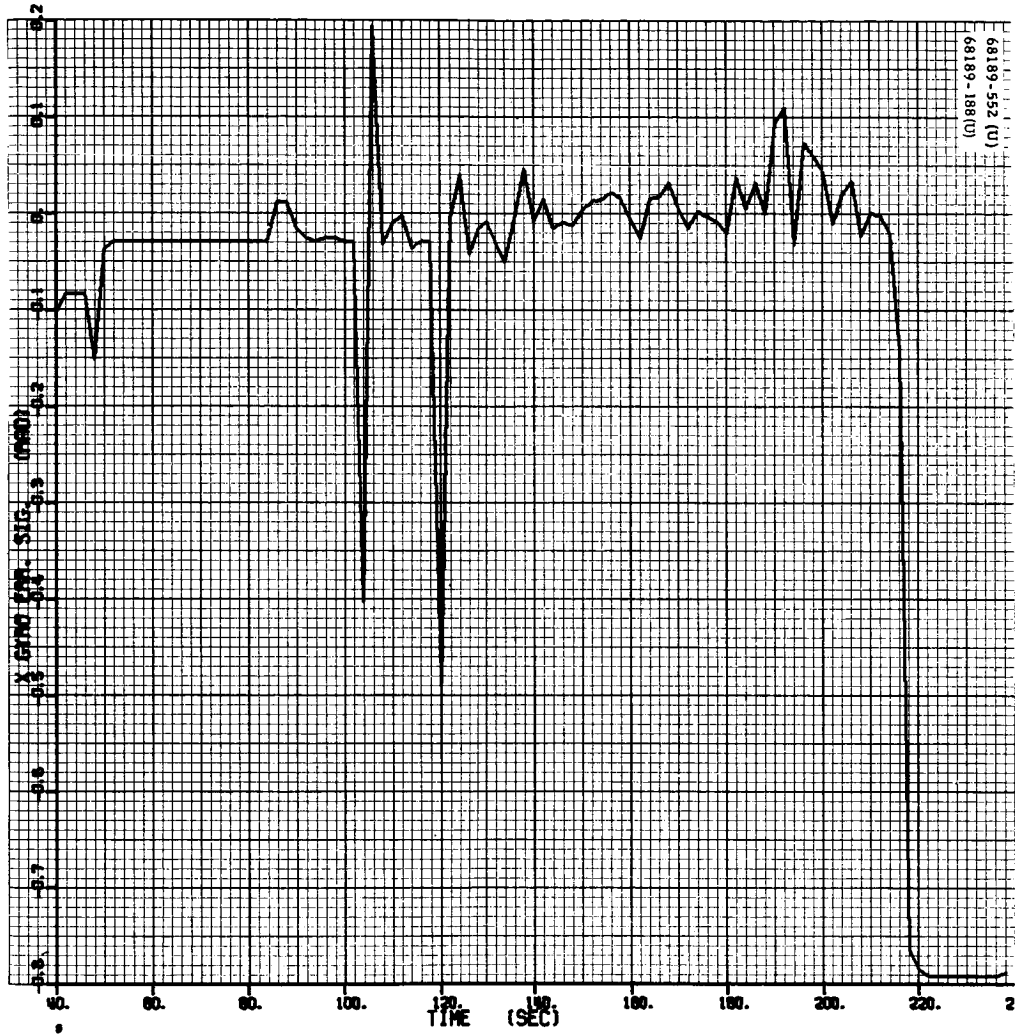Figure 5.15-12 (continued).   Telemetry Data Corrected
by PREPRO

f) Vernier Engine 2
Thrust Command, pounds

Figure 5.15-12 (continued). Telemetry Data Corrected
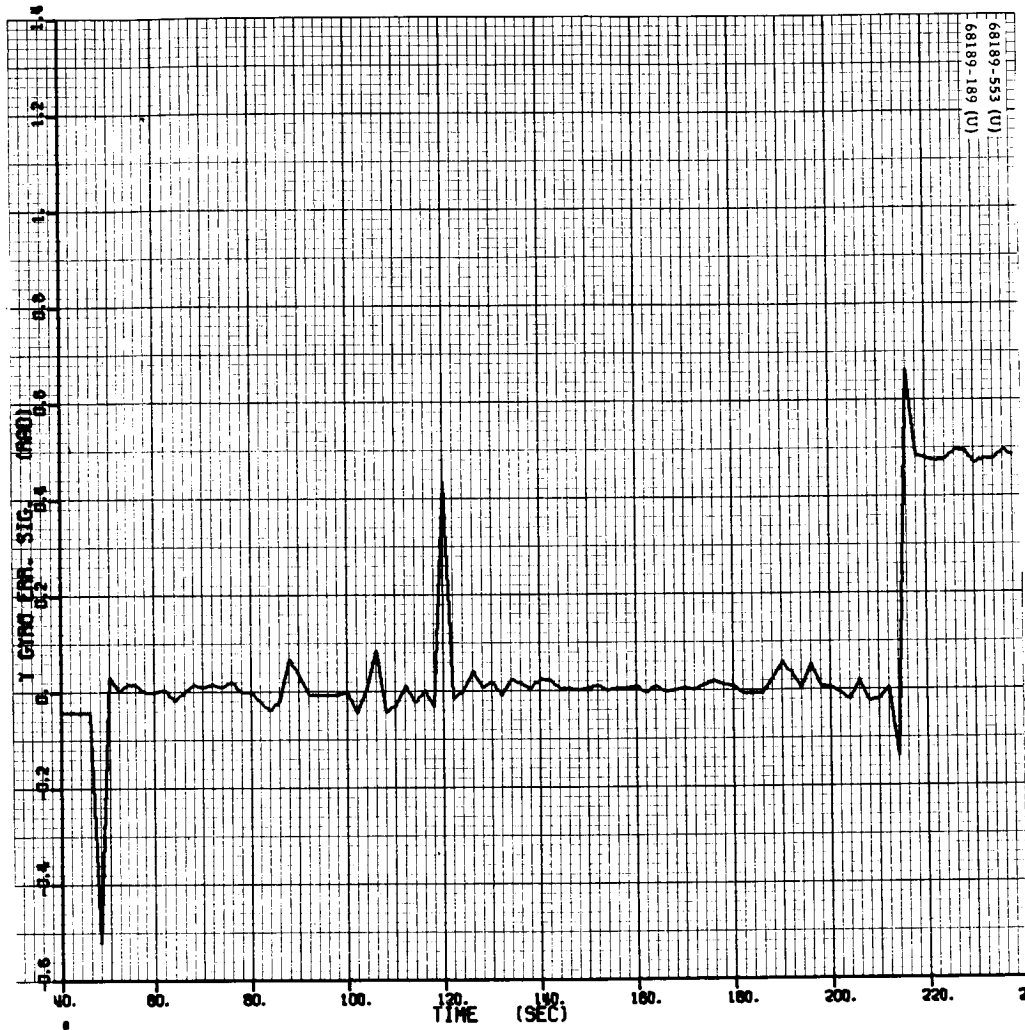by PREPRO

g) Vernier Engine 3
Thrust Commands, pounds

Figure 5.15-12 (continued). Telemetry Data Corrected
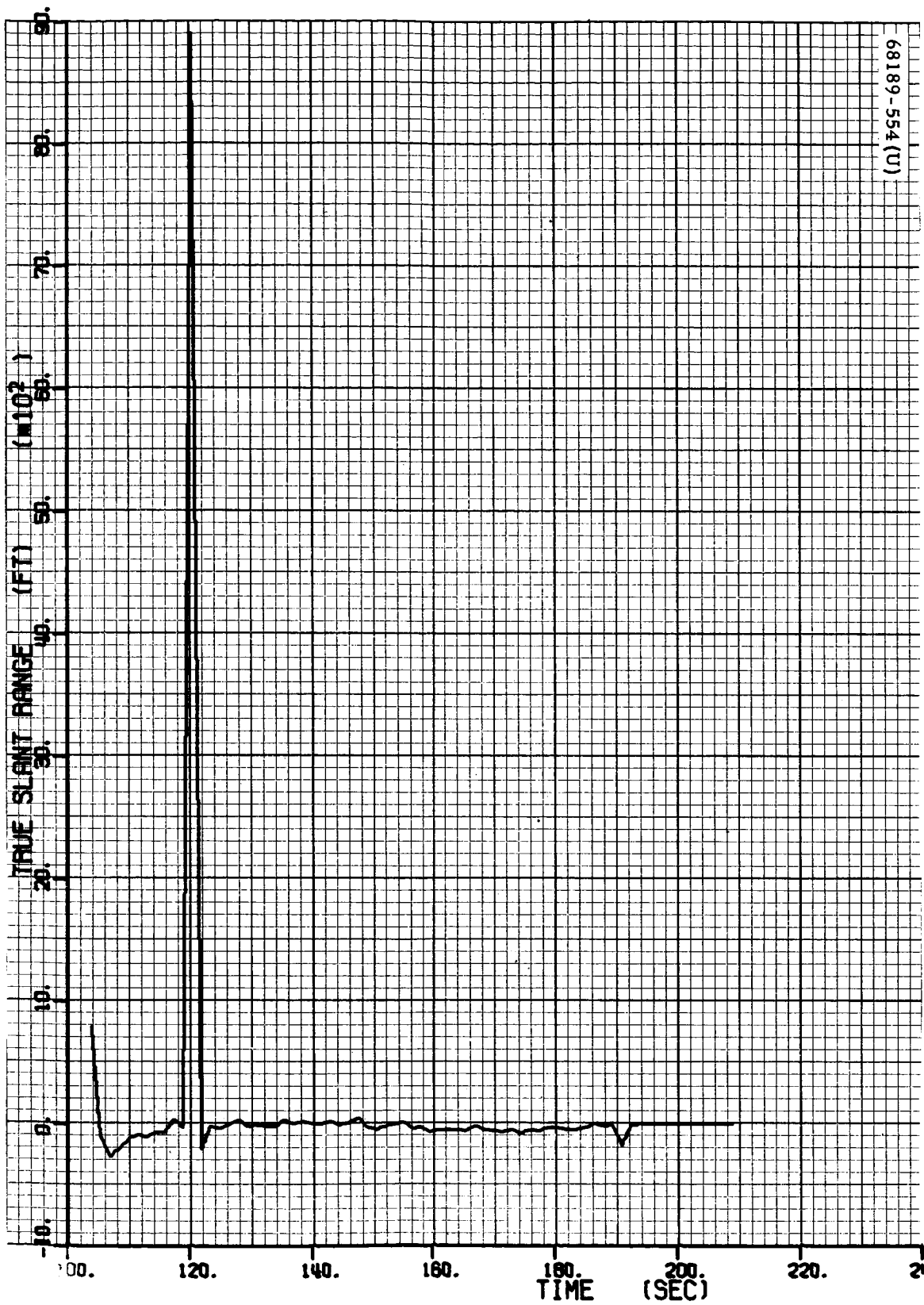by PREPRO

h) X Gyro
Error Signal, degrees

Figure 5.15-12 (continued). Telemetry Data Corrected
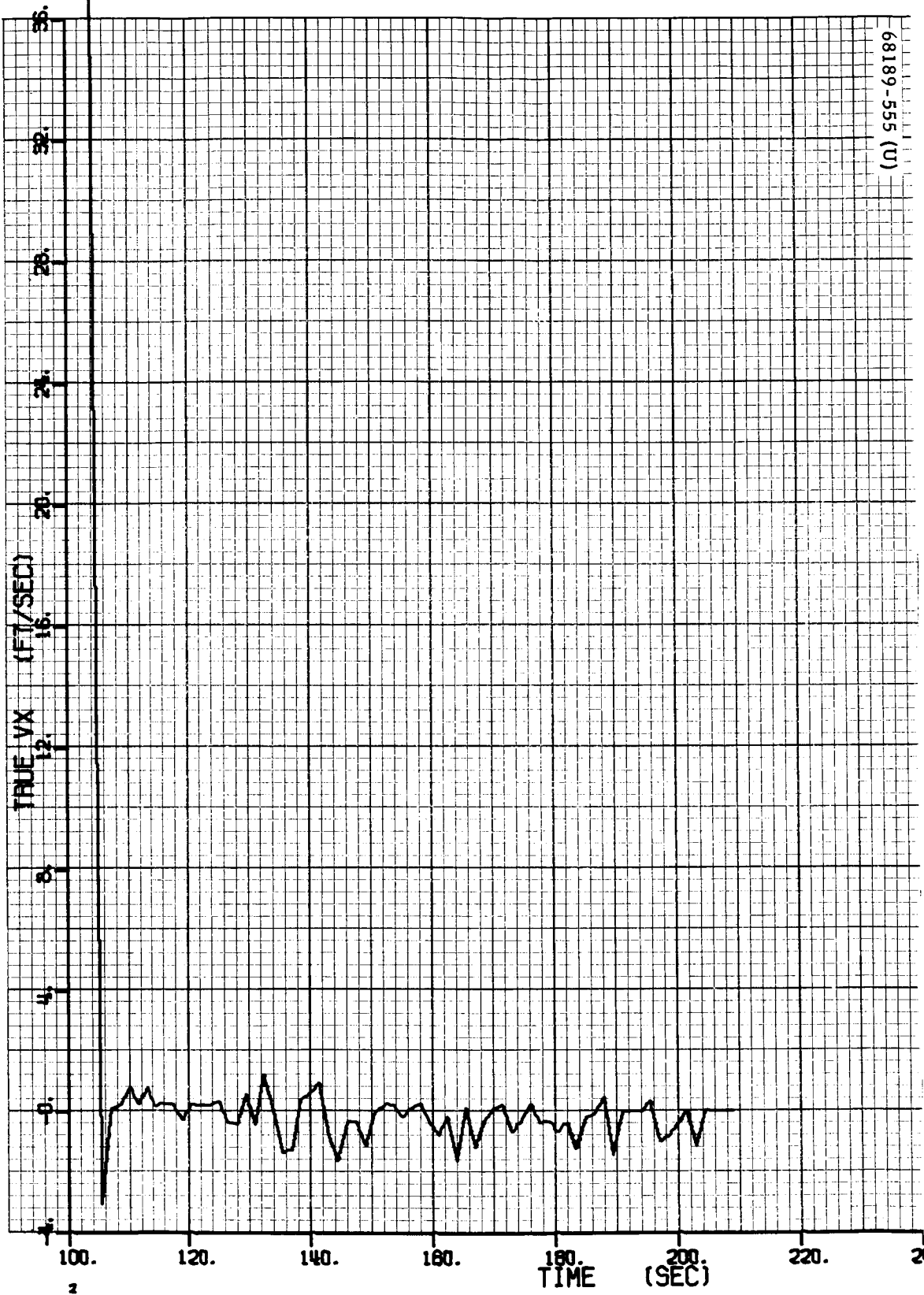by PREPRO

i) Y Gyro
Error Signal, degrees

Figure 5.15-12 (continued).   Telemetry Data Corrected
by PREPRO

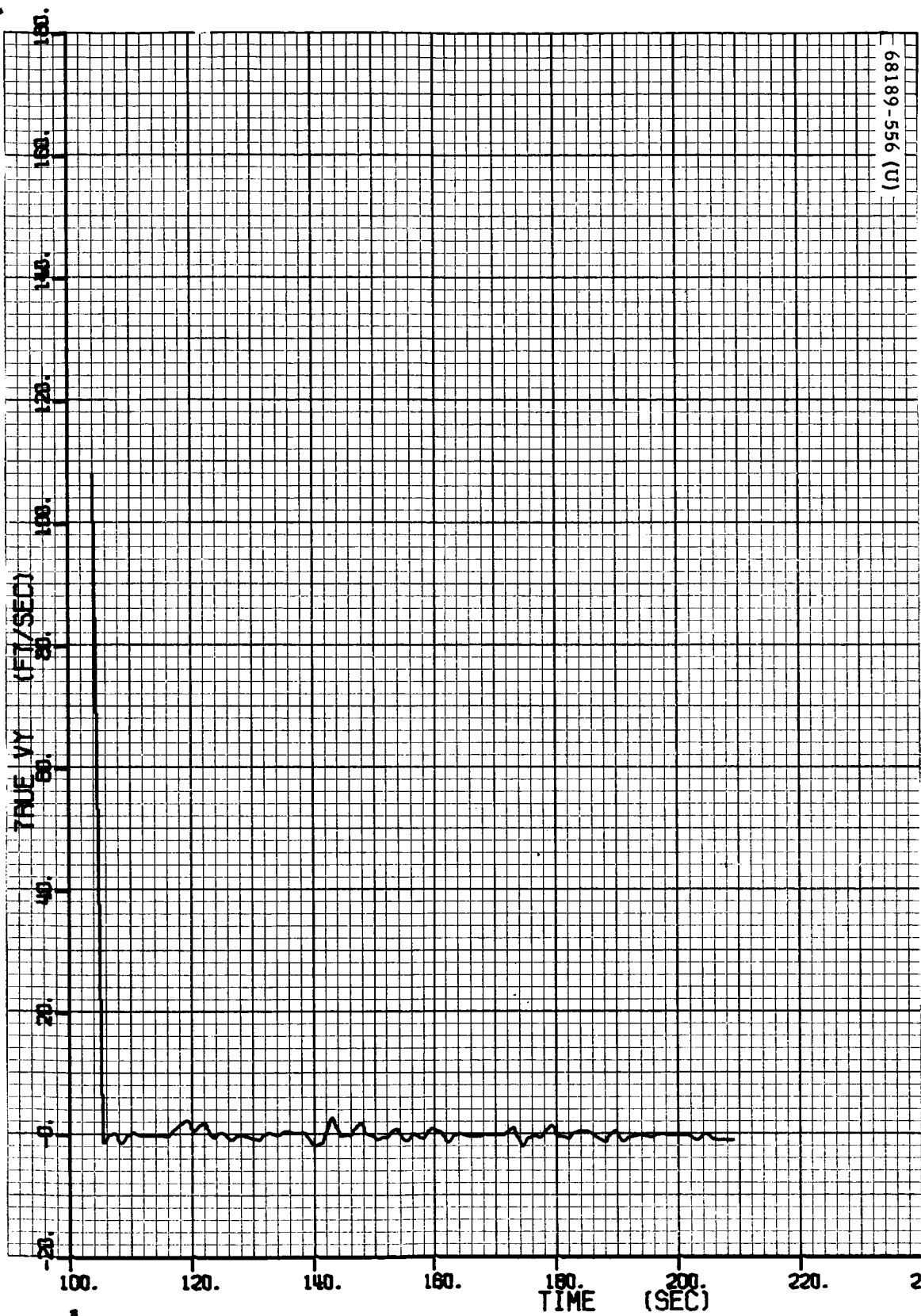a) Δ Slant Range (Final), feet x 10^2

Figure 5. 15-13.   Differences of Corrected Telemetry and Best
Estimate Trajectory Parameters

b) Δ X Velocity (Final), ft/sec

Figure 5.15-13 (continued). Differences of Corrected Telemetry
and Best Estimate Trajectory Parameters

c) Δ Y Velocity (Final), ft/sec

Figure 5.15-13 (continued). Differences of Corrected Telemetry
and Best Estimate Trajectory Parameters

d) Δ Vernier Engine 1 (Final), pounds

Figure 5.15-13 (continued).   Differences of Corrected Telemetry
and Best Estimate Trajectory Parameters

e) Δ Vernier Engine 2 (Final), pounds

Figure 5.15-13 (continued). Differences of Corrected Telemetry
and Best Estimate Trajectory Parameters

f) Δ Vernier Engine 3 (Final), pounds

Figure 5. 15-13 (continued). Differences of Corrected Telemetry
and Best Estimate Trajectory Parameters

5. 15-102

g) Δ X Gyro Error Signal (Final), degrees
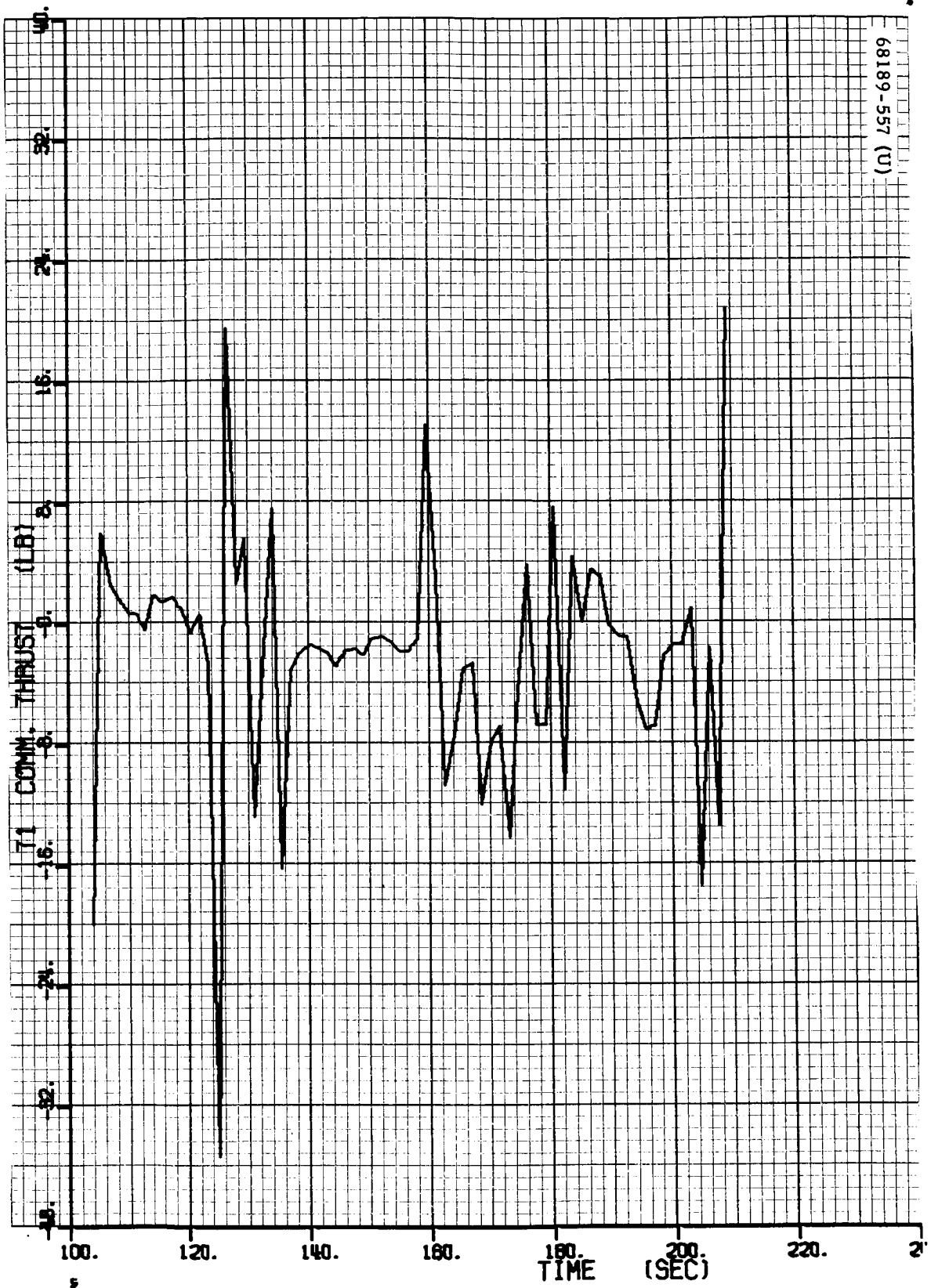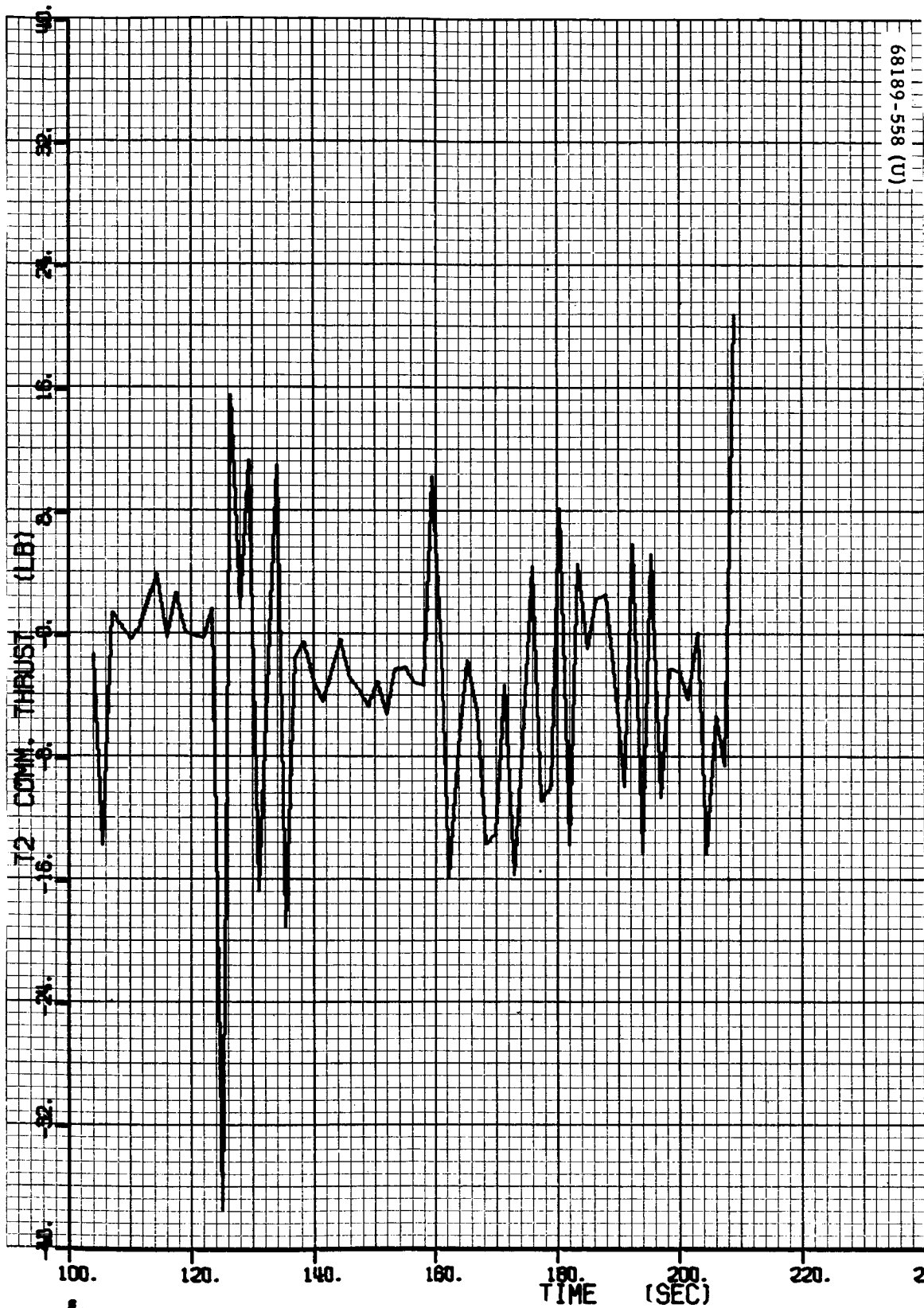
Figure 5. 15-13 (continued). Differences of Corrected Telemetry
and Best Estimate Trajectory Parameters

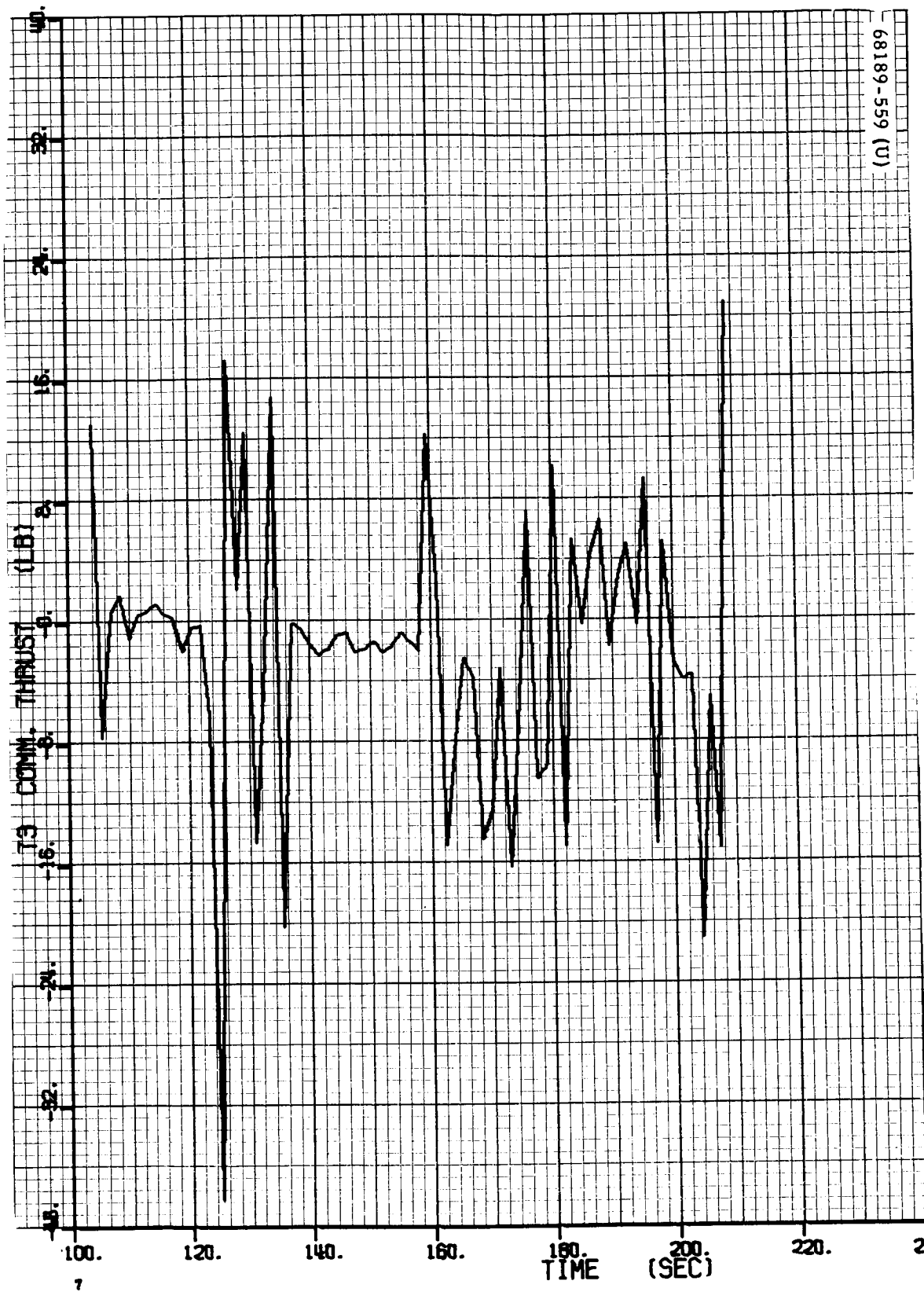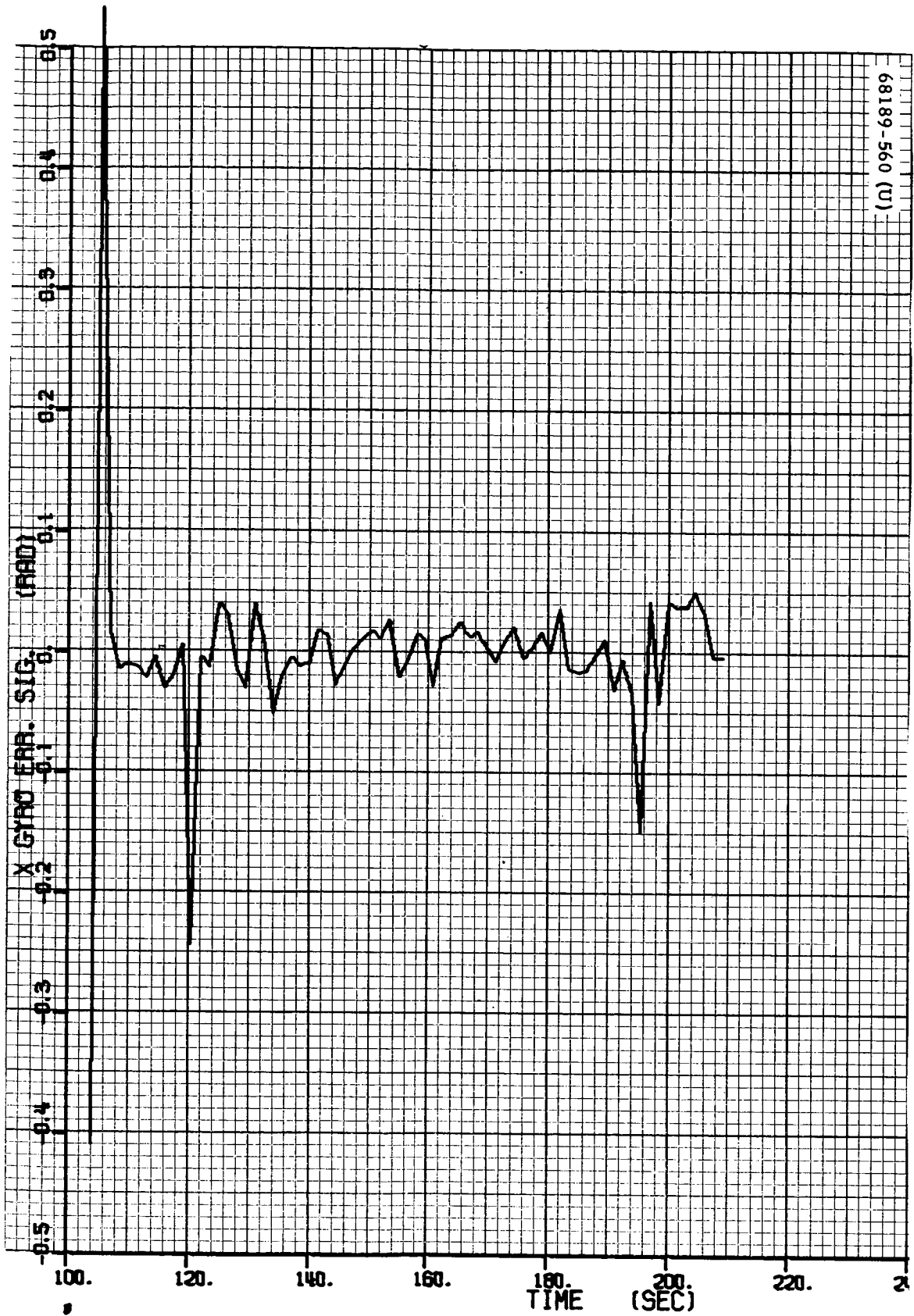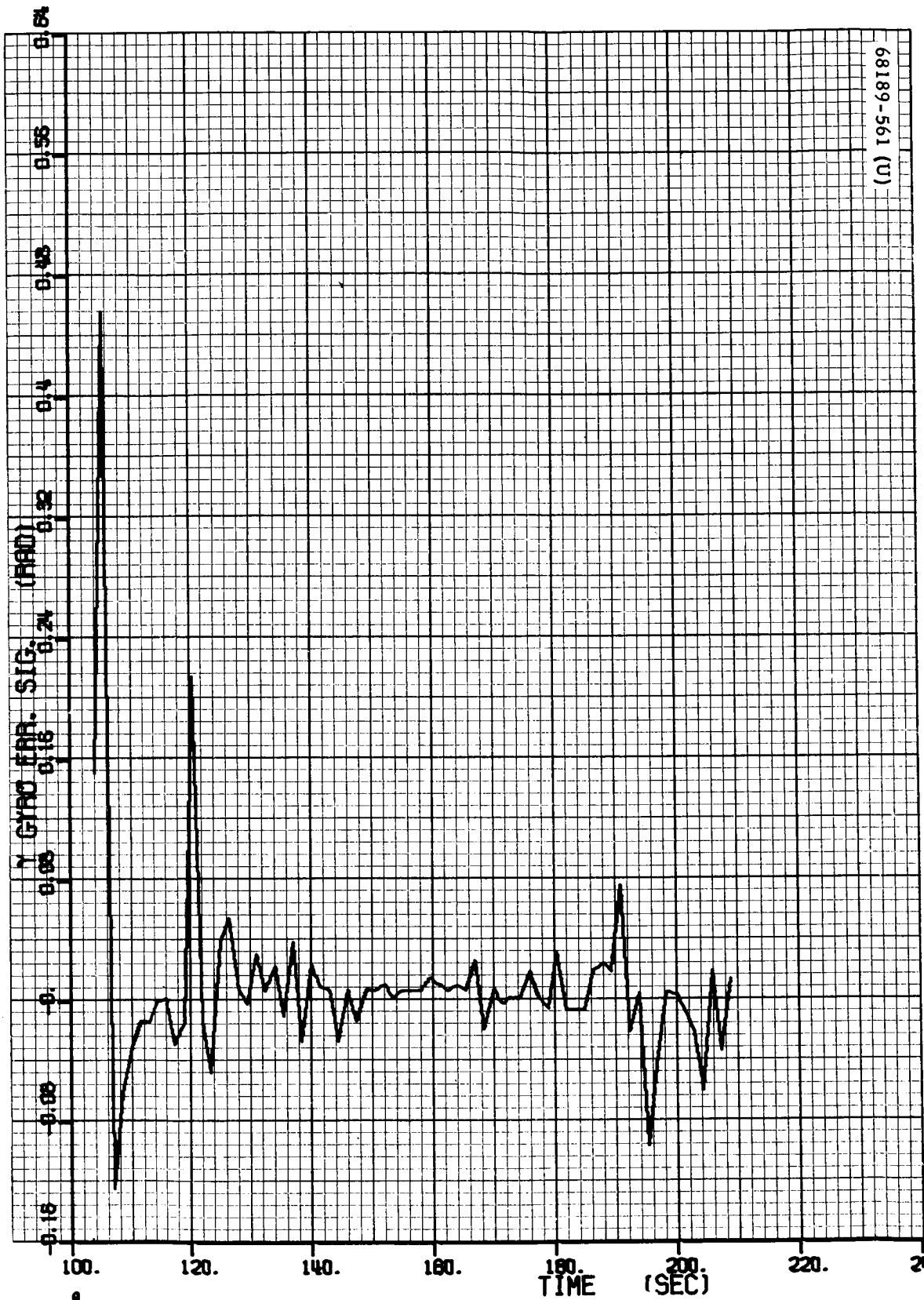h) Δ Y Gyro Error Signal (Final), degrees

Figure 5.15-13 (continued).   Differences of Corrected Telemetry
and Best Estimate Trajectory Parameters

5.16   RELIABILITY ANALYSIS

5.16.1   PERFORMANCE

Assessment of SC-1 performance from a reliability standpoint mainly concerns relevant failures and unit operating experience. As of this date, no TFR (failure mode) pertaining to the transit and lunar phases is considered relevant to reliability.*   TFRs that have been recorded during the two phases are listed in Table 5.16-1 with descriptions and current status. SC-1 unit operating experience is listed in Table 5.16-2 with unit part and serial number. The unit operating time and cycle was developed by translating commands transmitted to the spacecraft.

5.16.2   PERFORMANCE VERSUS PREDICTIONS

The predicted reliability for SC-1 equipment for the transit phase was 0.62, excluding the system interaction reliability factor, and 0.46 with the system interaction factor included. The growth pattern of SC-1 reliability estimates prior to launch is shown in Figure 5.16-1. These predictions assumed that nonstandard procedures would not be employed.

Although one mission attempt, whether successful or not, cannot in itself completely justify or vitiate prediction methods, the extent of the successful operation of SC-1 equipment during the transit phase indicates that a number of areas can reasonably be investigated for possible improvement in predictions and are discussed in the following paragraphs.

5.16.2.1   Reliability Math Model (Nonoperating Equipment)

Electronic equipment on SC-1 when in the nonoperating state is assumed to have a failure rate equal to 1/100 of the failure rate during its operating state, i.e.,

$$\lambda_{off} = 0.01 \lambda_{on}$$

This factor may be too high.

---

*"Reliability Relevant Failures," Hughes Aircraft Company, IDC 2258.2/328, 24 February 1966.

TABLE 5.16-1.   SC-1 TFR SUMMARY FOR FLIGHT AND
LUNAR PHASES

TFR Number	Descriptions	Status
18233	Telemetry signal M-1 did not indicate omnidirectional mechanism A extended at proper time.	Closed. Cause of failure is attributed to excessive friction at the pin puller/ mechanism interface and at the area of the mechanism pivot. Corrective action per ECRs 339301 (ECA 112733) and 33937 (ECA 112724) provide functional improvements such as addition of a boom "kick-out" spring, improved surface finishes, and improved lubrication of these surfaces. Retrofit of SC-2 has been completed.
27503	Extreme glare was present in various surveys of the moon's terrain in area where sun's image was visible to the camera's lens assembly entrance. In the worst case, approximately 50 percent of the camera format reached saturation (white level) when the survey was conducted in narrow angle. Of the full 360-degree survey capability of the television camera, approximately 130 degrees was not available.	Closed. The problem documented in this TFR arises from insufficient glare shielding of the TV survey camera lens and mirror assembly. A mirror hood redesign has been implemented for SC-5 and up (ECA 111769). This redesign accomplishes a reduction in glare angle susceptibility of 22.5 degrees. This is done within the framework of the elevation viewability specification limits such that celestial viewing capability will not be lost.
27504	Elevation potentiometer opened causing loss of all mirror assembly elevation position information.	Closed. The elevation readout potentiometer winding opened at a point corresponding to a mirror position approximately 15 degrees above the horizontal. This failure mode was verified during the mission because the elevation readout was essentially zero at higher mirror elevation steps and equaled the calibrate voltage at lower mirror elevation steps. Corrective action has been implemented for SC-5 and up as a result of ECAs 111769 and 112738 which incorporate potentiometers with niobium diselinide lubricant on pots for the mirror assembly and the lens assembly, respectively.
27505	The mirror assembly is intermittently failing to respond to step mirror up commands, thus, indicating possible mirror assembly binding.	Closed. The design solution is to incorporate niobium diselinide as a lubricant for the elevation potentiometer and use Lubeco 905 (HP-19 and HP-20) as the elevation gear lubricant. These changes are being implemented for SC-5 and up as a result of ECAs 111769 and 112738.

TABLE 5.16-2. SC-1 UNIT OPERATING TIME AND CYCLE DATA FOR FLIGHT AND LUNAR PHASES (DATA SOURCE: DSS TAPES)

Flight: Day 150, Hour 1500   Lunar: Day 153, Hour 0600
        Day 153, Hour 0600   Day 165, Hour 1200

Subsystem and Unit	Part Number	Serial Number	Time, Hours or Cycles	
			Flight	Lunar
Telecommunications				
Central command decoder	232000-5	1	62.9	294.2
Engineering signal processor	233350-7	2	5.0	40.3
Auxiliary engineering signal processor	264900-3	1	57.9	30.9
Signal processing auxiliary	232540-1	5	0.3	
Low data rate auxiliary	264875-2	5		
Omnidirectional antenna B	232400	6		
Omnidirectional mechanism A	287300	2	1	
Omnidirectional mechanism B	273880	2	1	
Central signal processor	232200-8	1	57.9	30.9
Transmitter A	263220-4	14		293.1
Transmitter B	263220-4	20	62.9	1.0
Receiver A	231900-3	13	62.9	294.2
Receiver B	231900-3	14	62.9	294.2
Low pass filter A	233466	9	62.9	294.2
Low pass filter B	233466	20	62.9	294.2
Telemetry buffer A	290780	11	62.9	294.2
Telemetry buffer B	290780	12	62.9	294.2
RF transfer switch	283984	14	1 cycle	6 cycles
SPDT RF swtich	283983	12	1 cycle	2 cycles
Television (for 10,316 frames)				
Survey camera	284312-3	12		36.4
Mirror				
Azimuth				6454 cycles
Elevation				6398 cycles
Focus				
In				6297 cycles
Out				6293 cycles
IRIS				6 cycles
Filter				26 cycles

Table 5.16-2 (continued)

Subsystem and Unit	Part Number	Serial Number	Time, Hours or Cycles	
			Transit	Lunar
Vehicle mechanisms				
Thermal sensors (total for 23)	988653		1446.7	6766.6
Thermal control and heater assembly A	232210-1	20	62.9	276.5
Thermal control and heater assembly B	232210-2	14	62.9	276.5
	238810			
Thermal switches (total for 14)	238811		943.5	4413.0
Thermal shell compartment A	263997		62.9	294.2
Thermal shell compartment B	230134		62.9	294.2
Spaceframe	264178	2	62.9	294.2
Landing gear 1	261278	3	1 cycle	
Landing gear 2	261279	2	1 cycle	
Landing gear 3	261280	3	1 cycle	
Footpad leg 1	263947			1 cycle
Footpad leg 2	263947			1 cycle
Footpad leg 3	263947			1 cycle
Crushable blocks				1 cycle each
Shock absorber leg 1	264300-1	4	1 cycle	1 cycle
Shock absorber leg 2	264300-1	7	1 cycle	1 cycle
Shock absorber leg 3	264300-1	8	1 cycle	1 cycle
Wiring harness compartment A	276951	5	62.9	294.2
Wiring harness compartment B	264094	1	62.9	294.2
Wiring harness basic bus 1	286473	4	62.9	294.2
Wiring harness basic bus 2	286398	1	62.9	294.2
Wiring harness antenna solar panel positioner	286417	4	0.16	1.9
Wiring harness auxiliary battery	264100	2	18.3	2.3
Wiring harness TV camera	276979	4		36.4
Wiring harness RF cabling			50.9	294.2
Wiring harness retro motor	286390	1	0.1	
Wiring harness battery cell voltage	3025155	3	62.9	294.2
Antenna solar panel positioner	287550	1		
Roll			495 cycles	4349 cycles
Solar			695 cycles	4747 cycles
Polar				4146 cycles
Elevation				451 cycles
Safety and arming devices (3)	293000	13	1 cycle each	
		14		
		15		

Table 5.16-2 (continued)

Subsystem and Unit	Part Number	Serial Number	Time, Hours or Cycles	
			Transit	Lunar
Propulsion				
Retro-rocket system	238612	A21-26	1 mission cycle	
Vernier engine 1	285063-1	545	1 mission cycle	
Vernier engine 2	285063-2	539	1 mission cycle	
Vernier engine 3	285063-3	541	1 mission cycle	
Electrical power				
Battery charge regulator	274100-3	11	62.9	294.2
Boost regulator	274200-96	12	62.9	294.2
Auxiliary battery control	273000-2	14	62.9	294.2
Main power switch	254112	4	63.0	294.2
Main battery	237900	49	62.9	294.2
Auxiliary battery	237921	44	18.3	2.3
Filter boost regulator	290060	11	62.9	294.2
Boost regulator filter assembly	284144	11	62.9	294.2
Solar panel	237760-3	1	62.9	294.2
Flight controls				
Flight control sensor group	235000-8	2		
Coast phase			62.9	0.2
Thrust phase			0.2	
Radar and guidance RADVS				
Signal data converter	232908-2	6	0.2	
Klystron power supply	232909	7	0.2	
Altitude-velocity sensor antenna	232910	3	0.2	
Velocity sensor antenna	232911-1	3	0.2	
Waveguide	232912	3	0.2	
Altitude marking radar	283827	12	0.2	
Roll actuator	235900-3	2	0.1	
Altitude jet leg 1	235700-2	3	5907 cycles	1 cycle
Altitude jet leg 2	235700-3	1	5907 cycles	1 cycle
Altitude jet leg 3	235700-2	2	5907 cycles	1 cycle
Secondary sun sensor	235450-1	1	59.2	
Pin pullers			13 cycles	
Pin-puller cartridges			13 cycles	

5.16.2.2 Reliability Math Model (Boost Vibration Effects)

Electronic equipment on SC-1 when in the boost period (vibration stress) is assumed to have an operating failure rate equal to 80 times the operating failure rate during nonboost periods, i.e.,

$$\lambda_{on\ boost} = 80\ \lambda_{on}$$

This factor may also be too high.

The predictions are based on the results of test data. It appears reasonable to question the possibility of "over stressing" and "over testing" the equipment since failure modes observed during testing did not occur during the transit mission.

5.16.2.3 Addition of Nonstandard Procedures to Model

The reliability predictions assumed that no nonstandard procedures would be employed. Those nonstandard procedures which have a high probability of being implemented during the mission should become part of the basic reliability math model.

5.16.3 FUTURE RELIABILITY PREDICTIONS

Reliability predictions for future spacecraft will include SC-1 transit and lunar phase unit experience where there are no significant design differences among units.
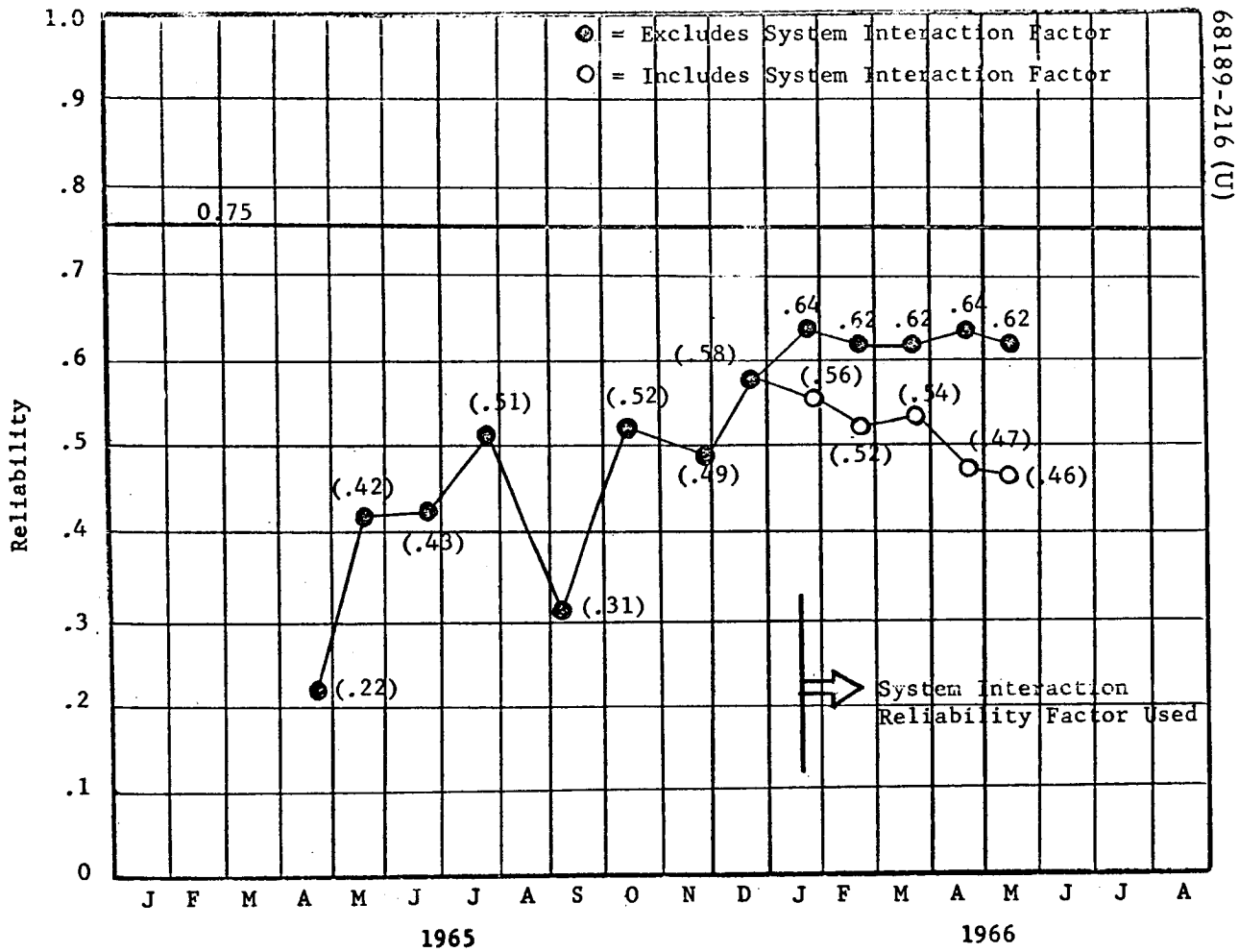
Figure 5. 16-1.   Surveyor I Reliability Estimate (Flight and Landing)